Development of Peptide-based Physical Gels for Various Applications

A Dissertation Submitted to the
Indian Institute of Technology Guwahati
As Partial Fulfillment for the Award of Degree of

DOCTOR OF PHILOSOPHY
IN
CHEMISTRY

Submitted by

Monikha Chetia

Roll No-176122039

Supervisor

Dr. Sunanda Chatterjee

Associate Professor

Department of Chemistry, Indian Institute of Technology, Guwahati,

Guwahati-781039

March 2024

Dedicated to

My Family

and All Friends

Declaration

I do hereby state that the research work presented in this thesis entitled ‘‘**Development of Peptide-based Physical Gels for Various Applications’’** has been carried out by me under the supervision of Dr. Sunanda Chatterjee, Associate Professor, during the period July 2017 to March 2024, at the Department of Chemistry, Indian Institute of Technology Guwahati (IITG), India. This work has not been submitted earlier to attain any other degree or diploma at any other Institution. Following the research ethics of reporting scientific observations, required acknowledgments have been made whenever the work is based on the findings of the other investigators.

Monikha Chetia

176122039

Certificate by the Supervisor

This is to certify that the thesis entitled "**Development of Peptide-based Physical Gels for Various Applications**," submitted by **Ms. Monikha Chetia** (Roll No. 176122039) for the award of Ph.D. degree to IIT Guwahati is absolutely based on her own research work under my supervision. This thesis or any part of it has not been submitted for any degree/ diploma or any academic award anywhere before.

Dr. Sunanda Chatterjee
Associate Professor
Department of Chemistry Indian Institute of Technology Guwahati
Contact: +91 361 258 3310 Fax: +91 361 258 2349
Email: sunanda.c@iitg.ac.i

Acknowledgment

The entire journey of my Ph.D. was undeniably about tasting boundless moments and opportunities. They have contented my past days with valuable learnings and shaped today with hopes for a promising tomorrow. This belief has been sprouted by collecting inspiration from many people I met on this journey. They have motivated, guided, and held my hands tightly whenever needed. This journey was never mine alone. Many people have contributed immensely and shared both the challenges and triumphs along with me. Old people remained a constant support, and new people became another family while stepping out beyond my comfort zone. These new people have taught me about the possibilities of making a family anywhere around the globe. I truly cherished IITG days from the beginning, and I greatly acknowledge the moment that I unlatched the door of the IITG campus to enroll in the Ph.D. program 6 years ago. It was the year 2017 when the PhD journey began, and I met all these amazing people whom I would like to acknowledge for their tireless support and presence.

One of the most rewarding aspects of my time at IIT Guwahati has been the opportunity to work under the guidance of **Dr. Sunanada Chatterjee**, Associate Professor in the Department of Chemistry. Without her constant support and endless encouragement, it would not have been impossible for me to complete this PhD journey. Her ever-ready smile and infectious enthusiasm constantly motivate me to keep moving forward. I am deeply grateful to her for allowing me to work under her expert supervision. I am also delighted to have the space and freedom provided by her to express my views. Apart from academic upliftment, she mentored me whenever difficulties knocked on my door. Her voracious love of traveling and trekking has taught me the importance of exploring places and meeting new people, while her appreciation for nature serves as a reminder of the beauty that surrounds us. I am grateful for meeting her.

I express my sincere gratitude to my doctoral committee members **Prof. Debapratim Das** (Chairperson) Professor, Department of Chemistry, IIT Guwahati; **Dr. Kalyan Raidongia**, Associate Professor, Department of Chemistry, IIT Guwahati; **Dr. Dipankar Srimani**, Associate Professor, Department of Chemistry, IIT Guwahati; and **Prof. Bhubaneswar Mandal**, Professor, Department of Chemistry, IIT Guwahati, for their support and valuable suggestions to improve the quality of work. I extend my gratitude to **Dr. Rajkumar Thummer** for facilitating the biological experiments conducted by his students for my research. I am also thankful to **Dr. Priyadarshi Satpati**, Associate Professor, Department of Biosciences and Bioengineering, IIT Guwahati, for his constant encouragement.

I am profoundly grateful to **Prof. Debapratim Das**, and my supervisor **Dr. Sunanda Chatterjee** for creating opportunities by conducting the weekly group meetings to learn new scientific areas and to improve presentation skills.

A special thanks to the Department of Chemistry, IIT Guwahati, and IIT Guwahati for providing all the instrumentation facilities for carrying out my research work, and for providing me with financial support. Also, my heartiest thanks to the Central Instruments Facility (CIF), IIT Guwahati, for providing all the necessary instrumental facilities.

I would like to express my deepest gratitude to my caring lab seniors, Dr. Karabi Roy, Dr. Gopal Pandit, and Dr. Swapna Debnath, and loving juniors Maitery Yadav, Jyoti Ganwar, whose support, encouragement, and advice have been invaluable throughout this journey. Their expertise, insights, and willingness to share knowledge have enriched my research experience immeasurably. A special thanks to Maitery for performing biological experiments for completing my work.

I am grateful to everyone in **Dr. Priyadarshi Satpati Sir's lab,** Dr. Abhishek Kumar Singh, Dr. Subhankar Ghosh, S. R. Vignesh, Pallav Sengupta, Ayesh Siddique, and Paramveer Yadav, for their constant help and support.

I extend my appreciation to Sumit Chaowdhory and Ritvika Kushwala for their help and for performing rheological experiments.

I would like to thank Chandrima Dey and Pradeep Kumar Sundaravadivelu for conducting the MTT assay experiment.

I am also grateful for the ongoing inspiration I receive from my kind seniors Sujan Kalita and Saurav Kalita, batch mates Bitan Sardar, Rupa Bai, Paresh Behera, Aragini Bhattacharya, Mihir Manna, Anjali Patel, and juniors Sukesh Shill, Manuranjan Konwar, Priyanka Adhikari, Dharmendra Adak, and Arindam Bikash Neog. Their help, encouragement, and consistently positive attitude have been invaluable.

I express my gratitude to the mess manager of the Subansiri hostel and the entire team for their dedicated work, consistently fulfilling our needs without a single complaint. Their kindness in providing food, even beyond the specified times, is truly commendable and greatly appreciated.

My journey at IITG would have felt incomplete without the companionship of my friends. They have been pillars of support, sources of encouragement, and providers of joy throughout my time here. I am truly fortunate to have friends like Arpita Shome, Shilpa Bhuyan, Saurav Bhowmick, Rakesh Mazumder, and Angana Borbora. Together, we have created countless cherished memories and shared much laughter. I am deeply thankful to my longstanding friends Bikash Sharma, Tushar Konch, and Aditya Bora for their unwavering support and presence in times of need throughout this Ph.D. journey. A heartfelt thank you goes out to my circle, Snigdha Deka, Nilavjyoti Sharma, Nayanjyoti Sharma, Anirban Basumatary, and Halim Hussain, for making IITG feel like home and standing by me as family. I extend sincere

appreciation to Hirakjyoti Basumatary for his steadfast support, which has consistently motivated and uplifted me, much like that of a brother.

To Swavalina Baruah, her unwavering presence and support since our college days have been a cornerstone of my journey. Her consistent encouragement has been a key motivator for me to persevere in life. To Nijara Konch, her steady care and support during challenging times have been invaluable, and I am deeply appreciative of the assistance she has provided whenever I needed it. To Rinkumoni Chaliha, Sarthak Chetia, Jimpi Gogoi, Priyanka Gogoi, and Bikashi Bora, I am truly grateful for their friendship and the unconditional support and encouragement they have offered over the years. I want to acknowledge my childhood friends, Kabyashree Phukan and Kasturi Phukan and thank them for their support and contributions to my life.

I want to give a special acknowledgment to Ankan Kumar Sarkar for his enthusiastic support throughout the completion of my thesis. His continual encouragement and presence have been an immense source of motivation for me throughout this journey.

And now I would like to express my heartfelt appreciation for the unconditional love and support of "MY FAMILY" throughout these years. Their eternal love, faith, and selfless sacrifices have shaped me with the enthusiasm and confidence necessary to pursue my goals. Additionally, my little nieces, *Prachi* and *Gloria*, bring abundant joy to my life, and their youthful exuberance serves as a constant reminder to maintain a youthful spirit. This journey also belongs to my uncles, aunts, and my lovely cousins.

I wholeheartedly thank all my teachers, from school to college, for not only teaching academic lessons but also helping me on my way to becoming a better human being. I conclude by expressing my gratitude to the Almighty and this beautiful Nature for assisting me in every possible manner to bring about this long-awaited achievement. **Thank you all!!**

Monikha

Abstract

Peptide-based supramolecular gels have versatile applicability in both biomedical and non-biomedical disciplines. Biocompatibility, biodegradability, low cytotoxicity, non-immunogenicity, and biological origin are some attributes that shape peptides to behave as advantageous soft materials. The ability to arrange themselves in secondary structures like β-sheets, α-helix, or tertiary structures renders peptides as potential building blocks for supramolecular architecture. Literature has already evidenced a wealth of remarkable progress in developing biomaterials made by peptide supramolecular gels. Even after decades of research in this area, the versatile nature of peptide gels still encourages scientist around the globe to explore the possibilities of their utility by modifying or designing new peptide sequences to create smart and advanced supramolecular gels.

In this thesis, with the advantages of peptide-based gel materials under consideration, an attempt has been made to design and synthesize small peptide molecule-based gels that can be utilized for both biomedical and non-biomedical sectors. Investigation of peptide self-assembly mechanisms to understand their gelation behavior was another important objective of our work. Primarily, we have developed small peptide-based gels (hydrogels/organogels) for utilizing them in varied applications including wastewater remediation, development of hybrid conducting material, encapsulation of quantum dots, and development of antimicrobial therapeutics. We have constituted purely physical gels, which are governed only by non-covalent interactions. The peptides used for the constitution of the gels vary from small hydrophobic and highly aromatic peptides to salt-tolerant and protease-resistant cationic antimicrobial lipopeptides. The developed hydrogels have been employed in diverse biomedical applications like drug release platform, adjuvant for potentiating antibiotics against resistant microbes and materials to prevent growth and propagation of biofilms. The organogels

on the other hand, have been employed for water remediation by removal of spilled oil and dyes, development of conducting material and immobilization cum stabilization of quantum dots. In addition to demonstrating their applications, we have characterized (thermostability, reversibility, mechanical stability, phase-selective gelation ability and morphology) these soft materials and investigated the mechanism of self-assembly/gelation in each of the systems through several spectroscopic and microscopic techniques. These studies would enable the better design of peptide-based physical gels in future.

Chapter 2:

This chapter detailed the design of four dipeptide molecules rich in aromatic moieties. All the peptides showed effective gelation abilities in a wide range of organic solvents. The obtained organogels were thermoreversible, phase-selective, and mechanically stable. Further, they were found to be useful in removing dyes from water, oil spill recovery, and fabrication of conducting gels. The mechanism of self-assembly was investigated thoroughly with the help of NMR, IR, PXRD, single crystal XRD, and fluorescence experiments, where it was established that hydrogen bonding and π-π interactions played key roles in the gelation process.

Chapter 3:

In this chapter, we have investigated the effect of the length of the spacer between the Phe residues of FF dipeptide on the self-assembly/gelation abilities of three analogs of FF dipeptide, namely, Boc-FLF-OMe, Boc-FLLF-OMe, and Boc-FLLLF-OMe. Here, a variable number of leucine amino acid residues were incorporated as a spacer in between the two Phe moieties. It was observed that all three peptides had similar kind of gelation properties in various organic solvents. All the organogels were thermoreversible, phase-selective, and mechanically stable. Further, one of the peptide oragonogelators (Boc-FLLF-OMe) was utilized for the immobilization and stabilization of CdSe/CdSe-ZnS quantum dots (QD). The gel matrix

successfully encapsulated the QDs, which not only resulted in the retention of their photo-physical properties, but also in an increase in the lifetime of their photo-physical properties.

Chapter 4:

This chapter probed six different cationic lipopeptides with different lengths of fatty acyl chains, C_8-C_{18}, to understand the effect of hydrophilic-hydrophobic balance on several properties of peptides such as gelation ability, secondary structure, cytotoxicity, salt-tolerance and protease-resistance of antimicrobial activity. The peptide with the longest fatty acyl chain, P18, was the most effective antimicrobial agent against both Gram-positive and Gram-negative bacterial strains, along with hydrogelation properties in a pH 7.4 buffer system. P18 was non-cytotoxic towards mammalian cells, non-hemolytic, proteinase K resistant, and salt tolerant in its antimicrobial potency. We established that the hydrophobic-hydrophilic balance, could play a crucial role in determining the properties of the peptides like gelation ability, antimicrobial activity, salt tolerant properties, and protease stability.

Chapter 5:

In this chapter, the concept of combination therapy was explored through the development of a composite antimicrobial hydrogel from the co-assembly of AMP P18, discussed in the earlier chapter, and antibiotic ciprofloxacin, which had the potential to prevent the biofilms formed by Methicillin-Resistant *Staphylococcus aureus* (MRSA). The new hybrid antimicrobial hydrogel had better antimicrobial activity and faster bactericidal effect than P18 hydrogel and the antibiotic alone. These antimicrobial hydrogels have also been scrutinized against MRSA resistance development tests, where no resistance occurred against them over 48 generations. At the same time, several folds of enhancement in MIC were found for the antibiotic ciprofloxacin.

Contents

L-Amino Acid with Abbreviations and Single Letter Codes

Amino Acid	Abbreviation	One letter code
Alanine	Ala	A
Valine	Val	V
Isoleucine	Ile	I
Leucine	Leu	L
Methionine	Met	M
Phenylalanine	Phe	F
Tyrosine	Tyr	Y
Tryptophan	Trp	W
Threonine	Thr	T
Serine	Ser	S
Asparagine	Asn	N
Glutamine	Gln	Q
Cysteine	Cys	C
Glycine	Gly	G
Proline	Pro	P
Arginine	Arg	R
Lysine	Lys	K
Histidine	His	H
Aspartic acid	Asp	D
Glutamic acid	Glu	E

Unnatural Amino Acids with Abbreviations

L-Phg: L Phenylglycine

Homo-Phe: Homo-phenylalanine

Abbreviations

AMP: Antimicrobial Peptide

UV: Ultraviolet

SCXRD: Single crystal X-ray diffraction

PXRD: powder X-ray diffraction

MALDI: matrix-assisted laser desorption/ionization

HRMS: Higher-resolution mass spectroscopy

FESEM: Field Emission Scanning Electron Microscopy

FETEM: Field Emission Transmission Electron Microscope

FTIR: Fourier Transform Infrared Spectroscopy

ESI-MS: Electrospray Ionization Mass Spectrometry

LC-MS: Liquid chromatography–mass spectrometry

Q-TOF: Quadrupole time-of-flight

CD: Circular Dichroism

NMR: Nuclear Magnetic Resonance

CCDC: Cambridge Structural Database accession number

TLC: Thin layer chromatography

J: Coupling constant

1D: One Dimension

2D: Two Dimension

MD: Molecular Dynamics

SPPS: Solid Phase Peptide Synthesis

HPLC: High Performance Liquid Chromatography

NMR: Nuclear Magnetic Resonance

CCDC: Cambridge Structural Database accession number

TLC: Thin layer chromatograph

J: Coupling constant

1D: One Dimension

2D: Two Dimension

MD: Molecular Dynamics

SPPS: Solid Phase Peptide Synthesis

HPLC: High Performance Liquid Chromatography

Boc: Tert-butoxycarbonyl

Fmoc: Fluorenylmethyloxycarbonyl

TFA: Trifluoroacetic acid

DNA: Deoxyribonucleic acid

RT: Room Temperature

THF: Tetrahydrofuran

HOBt: Hydroxybenzotriazole

PyBOP: Benzotriazole-1-yl-oxy-tris-pyrrolidino-phosphonium hexafluorophosphate

DMAP: 4-dimethylaminopyridine

DIC: *N, N′*-diisopropylcarbodiimide

DIPEA: *N, N*-diisopropylethylamine

DCM: Dichloromethane

D_2O: Deuterium Oxide

CH_3CN: Acetonitrile

$CHCl_3$: Chloroform

DCB: Dicholorobenzene

CV: Crystal Violet

RB: Rhodamine B

TFE: Tetrafluoroethylene

DMSO: Dimethylsulfoxide

NaCl: Sodium Chloride

$CaCl_2$: Calcium Chloride

mM: Millimolar

µM: Micromolar

E. coli: *Escherichia coli*

P. aeruginosa: *Pseudomonas aeruginosa*

K. pneumoniae: *Klebsiella pneumoniae*

S. aureus: *Staphylococcus aureus*

MRSA: Methicillin-resistant *S. aureus*

MDR: Multi-drug resistant

EtOH: Ethanol

EDC.HCl: N-(3-dimethylaminopropyl)-N′-ethylcarbodiimide hydrochloride

MeOH: Methanol

Fmoc-OSU: N-(9-Fluorenylmethoxycarbonyloxy) succinimide

ACN: Acetonitrile

CAC: Critical aggregation concentration

TIPS: Triisopropylsilane

$SOCl_2$: Thionyl chloride

LiOH: Lithium hydroxide

CaH_2: Calcium hydride

TPPI: Time-proportional phase incrementation

n-Buli: n-Butyl lithium

$NiCl_2$: Nickel chloride

H_2SO_4: Sulphuric acid

HCl: Hydrochloric acid

DBU: 1, 8-Diazabicyclo [5.4.0] undec-7-ene

$HCOONH_4$: Ammonium formate

K_2CO_3: Potassium carbonate

$NaHCO_3$: Sodium bicarbonate

Na_2SO_4: Sodium sulphate

RT: Room temperature

Chapter 1

Introduction

1.1. Molecular self-assembly

The term "molecular self-assembly" provides an incredible path for understanding the evolution of a broad range of exquisite architectures/arrangements existing in nature that arise from the spontaneous association of numerous constituents woven by diverse numbers of interactions. Our life itself depicts the inescapable importance of molecular self-assembly by creating multitudinous complex structures[1] like the organization of cell membrane through the usage of phospholipid self-assembly,[2] creation of DNA double helix specific hydrogen bonding pairs,[3] protein folding,[4] nucleic acid arrangements,[5-6] protein aggregates found in amyloid fibrils relevant to widely popular neurological abnormalities like Parkinson's, Alzheimer's diseases[7-8] and many others,[9-10] which are the basis of our existence. A complete living cell is found to be another wonderful platform for producing self-assembled structures by demonstrating different strategies.[11] Aside from living biological systems, the idea of assembled systems is found to exist everywhere. This includes large-scale phenomena like the formation of galaxies and planetary systems,[12] illustrating the hierarchical processes of the organization of galactic molecular gas, and their transformation into populations exhibiting diverse color, size, morphology etc., as evidenced in our universe.[13-15] All these diverse ranges of existing structures highlight the pervasive role of the supramolecular association. Hence, self-assembly can be defined as the process of the spontaneous association of available building blocks to form an ordered and stable arrangement from their randomly or separately distributed positions at any scale.[12,16] (Fig. 1.1) This suggests the possibility of fabrication of various well-defined and spontaneous supramolecular architectures with promising significance, through a bottom-up approach by utilizing the process of self-assembly.[17]

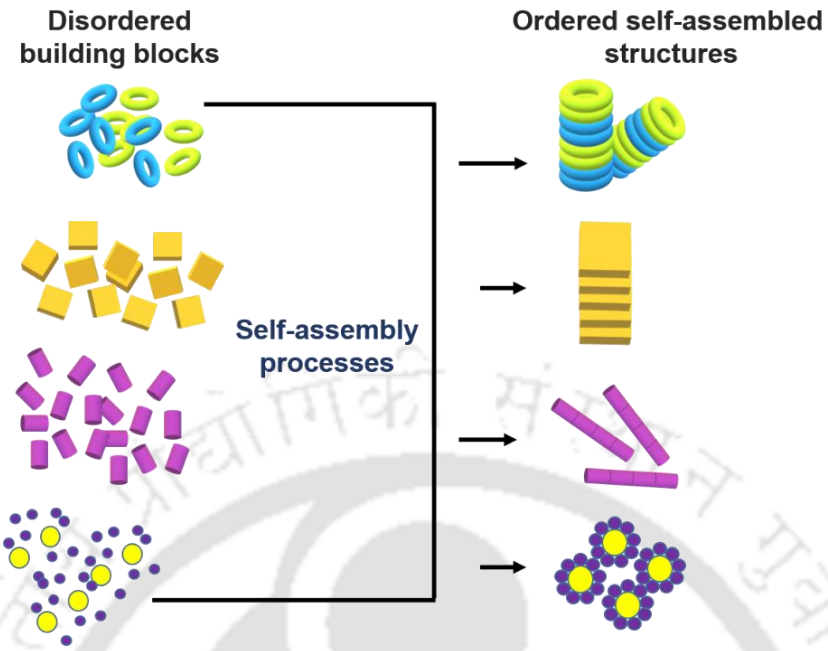

Fig. 1.1. Formation of ordered structures from various building blocks through the self-assembly process.

Also, it takes part in many aspects of applied disciplines by organizing molecular components and using various efficient interactions with several well-organized patterns.[18] Often, structures derived from the molecular self-assembly process are governed by non-covalent interactions namely hydrogen bonds, hydrophobic, van der Waals, ionic, and co-ordination bonds, though kinetically labile covalent bonds can also be utilized.[19] Understanding molecular self-assembly is essential as it offers the scope of designing hierarchical structures towards the advancement of functional materials.[20-21] As mentioned before, nature is the best example of utilizing the idea of self-assembly and giving uncountable structures necessary for survival.[22] By introducing the existing self-assembled structures from nature into synthetic systems, through mimicry and design, noble structures/materials with versatile application have taken birth.

In chemistry, molecular self-assembly is not a newly discovered concept; phenomena like the phase-separated polymer systems,[23] colloids formation,[24] molecular crystals arrangements,[25]

liquid bilayers,[26] self-assembled monolayers,[27] and also an association of ligand to a receptor[28] can be considered as types of self-assembly. Molecular self-assembly opens new direction for the creation of several ordered structures in wide range of size and shape with several useful applications.[29] Development of diverse array of structures with outstandingly advantageous features in both biological and non-biological domain of research is one of the greatest achievements of self-assembly processes.[30]

We, human beings, are constantly inspired by nature and its ways of constructing complex self-assembled structures. (Fig. 1.2) This inspires the innovation of new materials with sustainable benefits. One of the noteworthy accomplishments of perceiving inspiration from nature involves

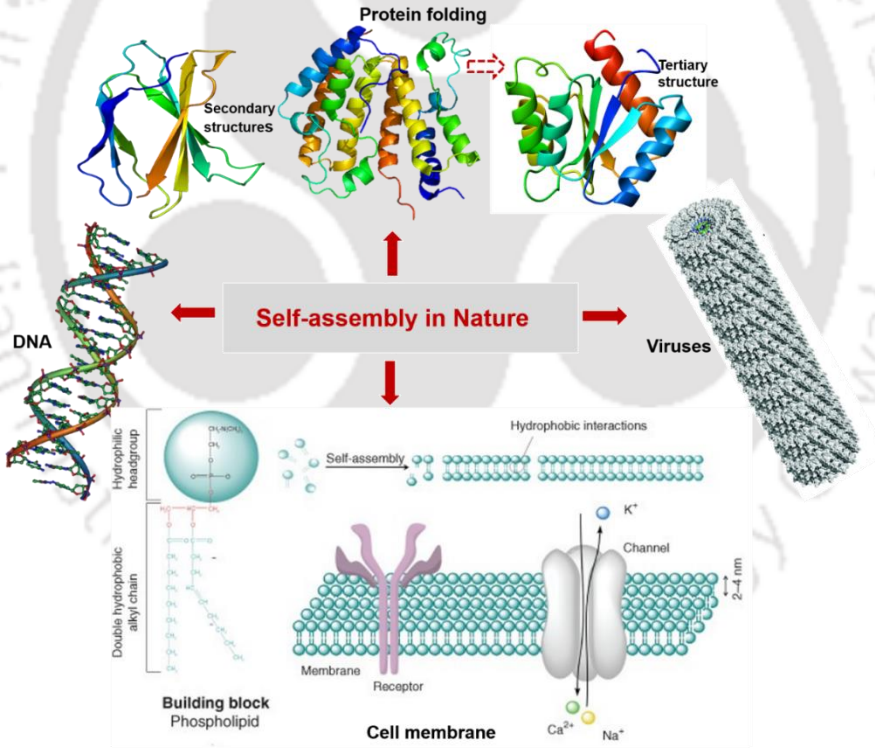

Fig. 1.2. Some self-assembled structures created by nature are proteins, DNA, viruses, cell membrane etc. (cell membrane part was adapted from the ref. 1 with permission, published by Wiley and Sons, DNA, virus structure were taken from wikibooks and micoop.com; protein folding was taken from protein library).

using biomolecules to design and create functional, dynamic, and reversible hierarchical structures on multiscale levels.[31-43] DNA, nucleic acids, lipids and peptides are some examples of biomolecules that have been widely exploited as essential elements for supramolecular architectures owing to their several advantages, including easy availability, ability for specific molecular recognition, scope of simple chemical and biological modification and biocompatibility for bottom-up fabrication.[44-49] In this regard, peptides have remarkable popularity for possessing versatile functionality, good biocompatibility, low immunogenicity, structural programmability, biological origin, chemical diversity, stability, robustness, easy synthesis, scalability, and cost-effectiveness.[31,50] The importance of secondary structures provided by natural peptide motifs have opened several ways to make new advanced materials by introducing β-sheets, helices and other conformations.[51] Thus, the fabrication of novel nano biomaterials can be explored by garnering knowledge from the naturally occurring peptides, designing de novo peptides with the desired properties and efficiency for targeted applications, and assembling them into supramolecular structures. Formation of intricate and improved supramolecular architectures have become possible by using peptides as building blocks of self-assembly by "bottom-up" approach.[52-56]

1.2. Peptide self-assembly

Peptides comprise of a varied composition of amino acids, including both natural and unnatural, and form a versatile group of constituents for the molecular self-assembly process.[57-58] The versatility of peptides emerges from their composition of amino acids with unique physico-chemical properties. Several functional groups carried by the side chains of the amino acids allow the peptides to undergo functionalization with other molecules. The presence of amide bond, possessing the ability to facilitate or stabilize the hydrogen bond formation, is another beneficial attribute that makes peptides potential building blocks. A couple of decades ago, components with

biological roots like nucleotides and amino acids were not regarded as advantageous constituents for materials engineering. However, this belief has altered in recent years with the advancement of synthetic and material science and other disciplines like genetic engineering, biotechnology etc.[56]Also, studies proved their better immunocompatibility and favorable pharmacokinetics. Widely acknowledged as biologically-inspired building blocks with attractive advantages, peptides have gained increasing attention in the development of several advanced materials and and the progression of diverse domains of research including biomedicine, nanotechnology and energy.[59-62] Moreover, peptide-based materials are useful as excellent nano-architectonics, to build intricate functional systems and devices, which can offer new avenues for mimicking biosystems.[63-67] Research activities on the development of peptide biomimetics have provided a wealth of new possibilities for the formation of various synthetic materials with comparable or improved functionality with respect to naturally occurring products.[1, 68-71]

1.2.1 Thermodynamics of peptide self-assembly

The process of peptide self-assembly describes a spontaneous thermodynamically and kinetically propelled phenomenon that results from the numerous intermolecular non-covalent interactions like π- π stacking, hydrophobic, hydrogen bonding, electrostatic, cation-π, and van der Waals interactions.[72] Their collective influence confirms the formation of final thermodynamically stable nanostructures. In addition, kinetic parameters like pH, temperature, counter ions, concentrations, and solvent environment can also remarkably influence the formation of nanostructures. The presence of selected kinetic parameters like change in pH, concentration, temperature, solvent composition, may confine the assembled structures in some metastable states.[73-76] But without the presence of the kinetic parameters, these metastable structures transform themselves into the thermodynamically favored state.[63] Also, many studies displayed the substantial contribution of

the kinetic parameters in influencing thermodynamic interactions among the peptide molecules along with their interactions with the solvent that are liable for peptide self-assembly.[77-84] Therefore, supramolecular processes are not limited to only thermodynamically controlled phenomena; there is always a competition between the assembly process of thermodynamically and kinetically controlled states. Building dynamic structures through supramolecular systems with desired properties is possible by understanding the ability to control possible transitions among kinetically trapped states and their pathways.[63]

1.2.2. Drivers in peptide self-assembly

Non-covalent interactions offer a significant contribution to the formation of nanostructures when peptide self-assembly occurs. (Fig. 1.3) Hydrophobic interactions, π- π stacking, hydrogen bonding, cation-π, electrostatic, and van der Waals interactions are some of the important non-

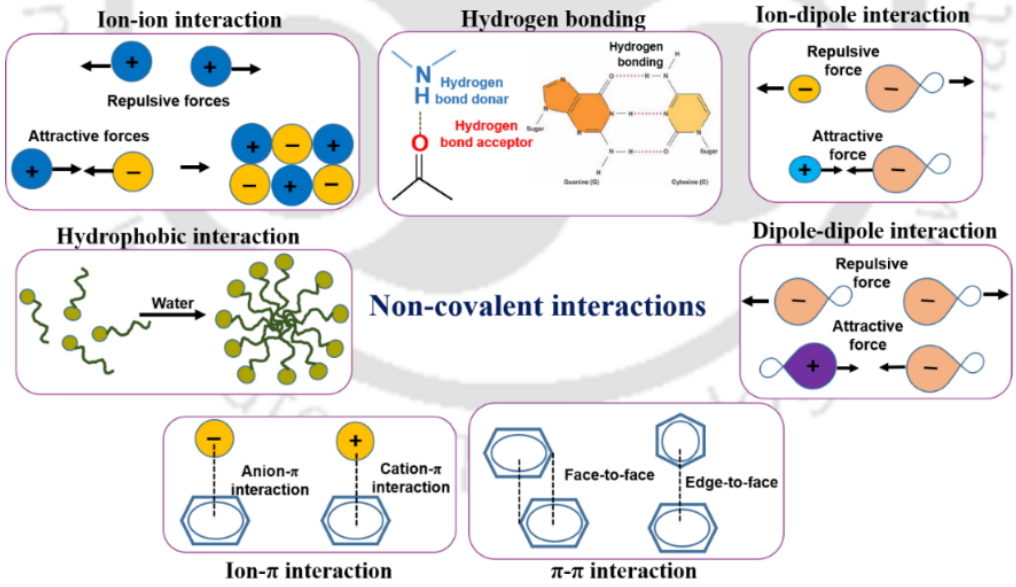

Fig. 1.3. Types of non-covalent interactions responsible for peptide self-assembly.

covalent interactions to promote peptide self-assembly.[72] However, regardless of the individual strengths, their combined effect is sufficient to initiate the self-assembly of building blocks to create well-ordered structures.[44,72] Moreover, the presence of various types of non-covalent interactions together is another approach for achieving stable self-assembled structures. For example, Stupp and his group have established a connection between the hydrogen bonding strength and hydrophobic attraction strength in the ‘‘phase diagram’’ of peptide amphiphiles with the help of molecular dynamics (MD) simulations.[85]

Apart from non-covalent interactions, peptide self-assembly can be regulated by the presence of external stimuli like temperature, light, sonication, heating, and internal stimuli, including redox reactions, solvent polarity, ionic strength, metal ions, pH, and enzymes (Fig. 1.4).[86-89a]

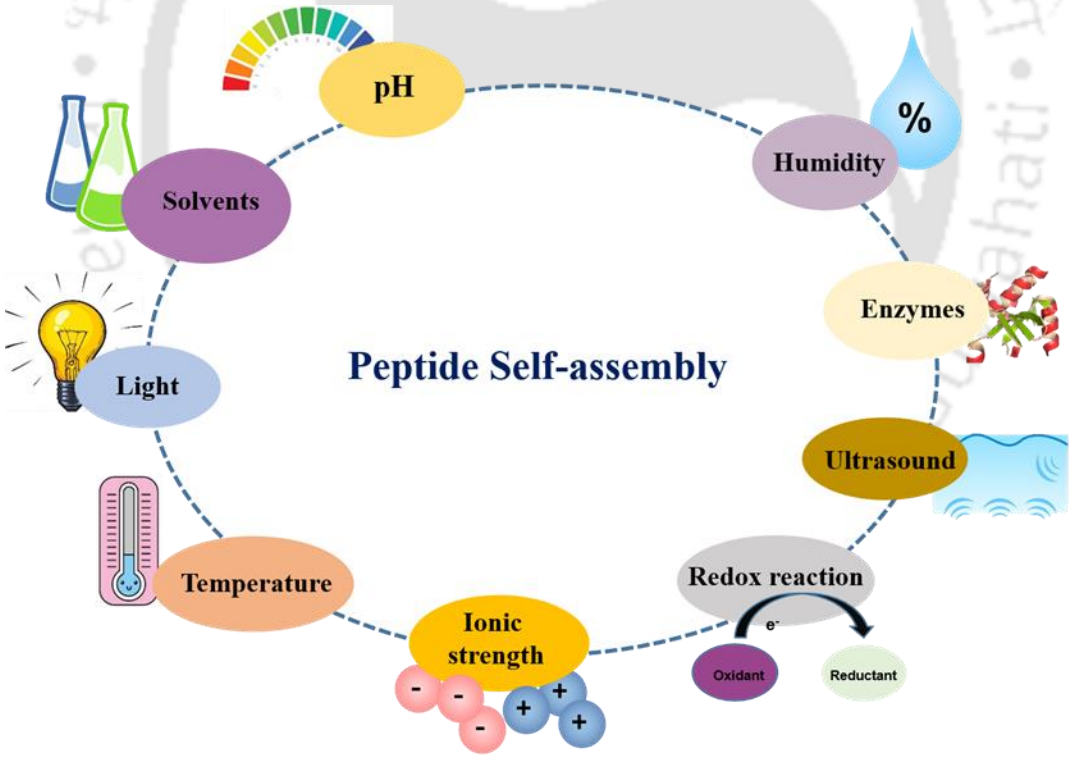

Fig. 1.4. Various stimuli that control peptide self-assembly.

The stimuli-responsive peptide self-assembly and their assembled structures are found to be highly advantageous for various medical applications under various physiological conditions. A pH-responsive KGSFSIQY-TYHVD peptide (KD) was designed for the formation of microcapsules through pH-induced self-assembly by Shimanovich *et al.* and utilized it for the controlled release of encapsulated cargos, including antibodies. At a low pH 6.5, the KD peptide was found to be in its monomeric state, but at a high pH of 8, it formed β-sheet nanofibrilar gel.[89b] Another group designed a redox-responsive peptide, selenopolypeptide, pSe-NapFFC-Glu conjugate by attaching a redox-responsive selenoether moiety to a short peptide NapFFC that can be used for delivery of anticancer drugs.[89c] Chibh *et al.* studied a novel disulfide containing dipeptide that had the ability to form nano assembly with the advantages of having S−S bonds that rendered the NPs (nanoparticles) to be redox-responsive. The free amino and carboxylic groups on the surface of the NPs facilitated their conjugation with drug molecules.[89d] These NPs were further derivatized with FA (folic acid) to increase the efficiency of cellular uptake, then loaded with DOX, to form FA-NPs-DOX. Subsequent reduction of the S−S bonds released the encapsulated DOX within the cancerous cells.

1.2.3. Nanostructures from peptide self-assembly

By utilizing the advantages of the versatility of peptides and exploitation of both non covalent interactions and external parameters, peptide self-assembly offers possibilities of generating various assembled structures including tubes,[90] filaments,[91]fibrils,[92] nanovesicles,[93] gels,[94] nanobelts,[95] nanoparticles[96] and rod like micelles.[97] Numerous types of peptide molecules have been designed and utilized for building diverse range of nanostructures. (Fig. 1.5) One of the most notable findings was the diphenylalanine (FF) peptide sequence, the core recognition motif of β-amyloid peptide in Alzheimer's disease. It has the outstanding potential to self-assemble into

discrete elongated tubular assemblies.[98-99] Other derivatives of diphenylalanine peptide were also known to form ordered aromatic dipeptides nano-structures (ADNS), like spheres, plates, tubes, and hydrogels.[100, 101, 102, 103a]

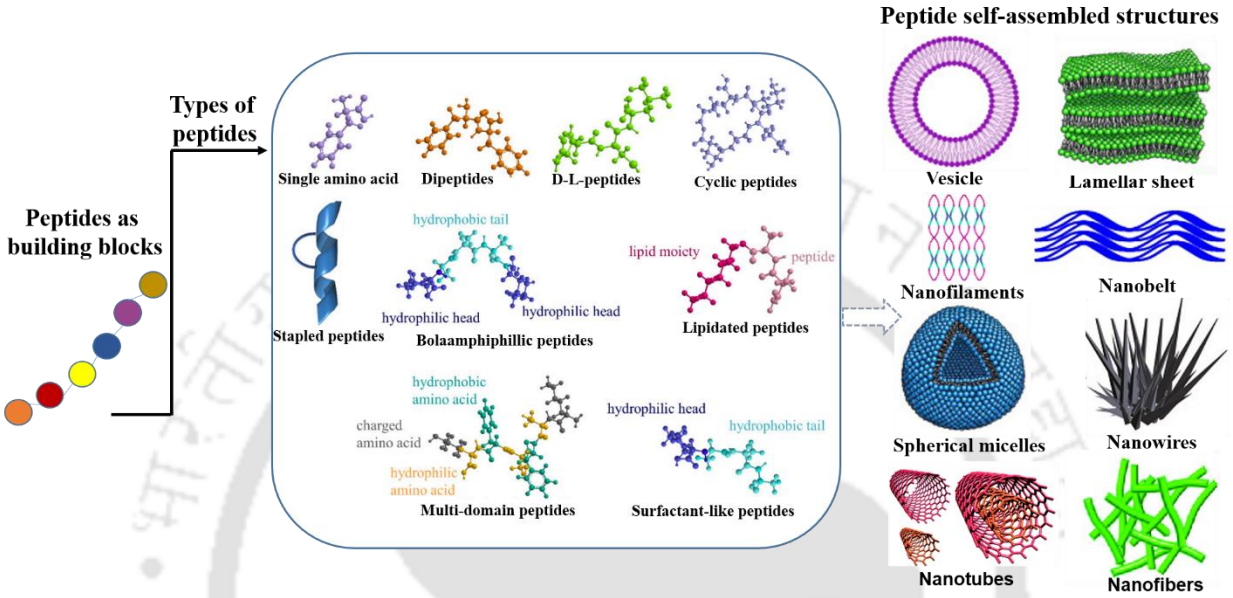

Fig. 1.5. Different classes of peptides forming a diverse range of nanostructures upon self-assembly. (One part of this Fig. adapted from ref. 103b with permission from Sara La Manna, International Journal of Molecular Sciences, Published by MDPI, 2021).

Literature has plenty of evidences of peptide based nanostructures for being used in broad array of biomedical applications such as drug release,[104] gene delivery,[105] tissue regeneration,[106] and also for non-biomedical applications like removal of toxic pollutants,[107] oil spill recovery,[108] fabrication of nanoclusters and nanoparticles[109] and other various applications.[110]

1.3. Supramolecular peptide gels

From these peptide self-assembled nanostructures, supramolecular gels are known to be one of the most intriguing outcomes in the emerging field of soft materials.[111,113] In general, gels are viscoelastic solid like materials with three dimensional fibrillar network that do not flow and have

the ability to stand without falling upon inverting the vial containing the gel.[112-113] This formation occurs from the entrapment of solvent within the solid 3D matrix provided by the cross linking of the polymeric strands of molecules by physical or chemical forces.[112] Further, gels can be subdivided into two classes depending upon the type of interaction they carry within the network. Chemical gels are stabilized by strong covalent cross-linking, while physical gels are stabilized through non-covalent interactions between the molecules.[114-115] Due to the strong covalent interactions chemical gels are irreversible, whereas weak non-covalent forces make physical gels reversible in nature.[112] Gels are also classified by considering the presence of solvents in hydrogels, where water entrapment occurs, and organogels, where organic solvents act as gelation medium. Further, two additional categories may be included in gel classification, namely xerogel, which is a solid formed after evaporation of the solvent at room temperature from a hydrogel or an organogel, and aerogel, which is described as dried gels formed upon solvent removal with the use of supercritical drying. Xerogels are highly porous with smaller pore sizes accompanied by larger surface area. Likewise, aerogels also possess high porosity and enormous surface area along with low apparent densities.[116-117]

1.3.1. Advantages of peptides as building block for Supramolecular gelation and mechanism

Several classes of biomolecules[118-123] and other synthetic organic molecules[124-126] are known to have the gelation ability (Fig. 1.6) and among them, peptides are considered one of the most attractive self-assembling units due to their relatively easy tailoring of structure and functions. They can generate highly porous gel systems with considerable mechanical stability.

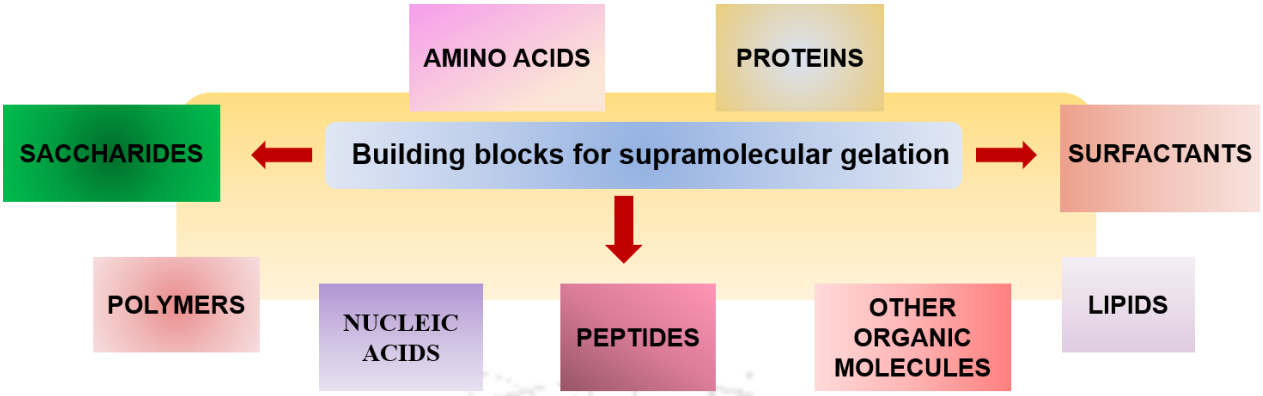

Fig. 1.6. Several classes of building blocks available for supramolecular gel formation.

Also, the possibility of their adjustable functions and biomimetic synthesis allow them to be used in advanced applications. Other properties like biocompatibility, low toxicity, easy functionality, and biodegradability are also added to the benefits of peptides as gelator molecules.[127-129] The ability to form secondary and tertiary structure, make peptides unique and versatile building blocks from the other self-assembling molecules. Also, another reason for peptides to appear as great choice for the development of supramolecular gels is the presence of a variety of functional groups encompassing donor-acceptor of hydrogen bond along with the flexibility in the modification of structures such as side chain functionality.[130-132]

Peptide supramolecular gel formation through self-assembly is a hierarchical process. Initially, the primary structure of selected peptide molecules tries to arrange themselves in some secondary structures like α- helices or β-sheet in solution, which further self-assemble into 2D aggregates by intermolecular non-covalent interactions and eventually form fibrils of nanoscale order under the favorable conditions. Thinner fibres gradually give rise to bundle of thicker fibers. These fibers again elongate themselves in a way that leads to a 3D fibrillar network, which may be considered as peptide gels with self-supporting properties[130, 133] (Fig. 1.7).

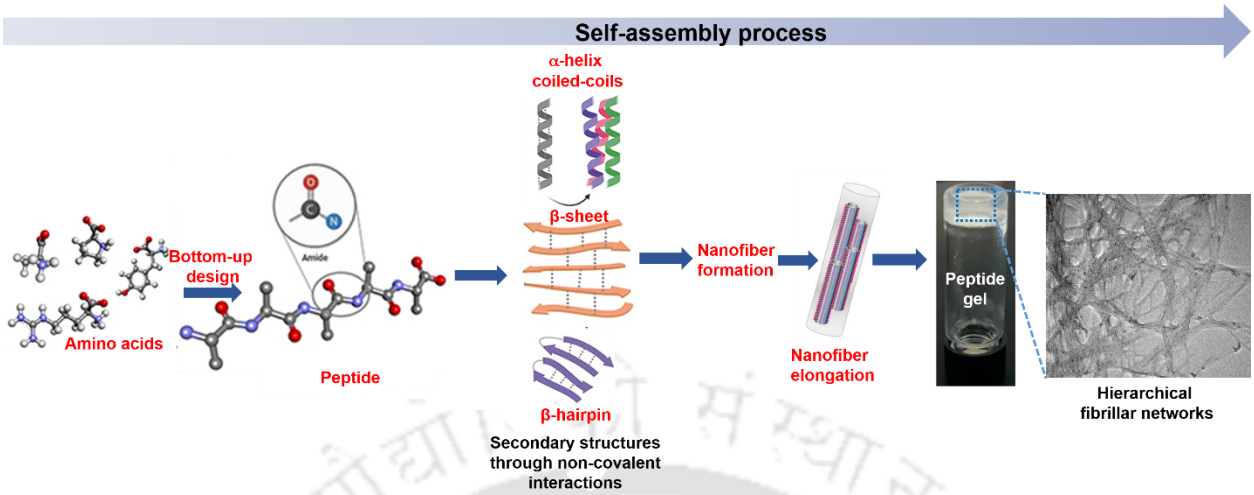

Fig. 1.7. Hierarchical formation peptide supramolecular gel. (Parts of the Fig were adapted from ref. 133b with permission from Taylor and Francis, 2020; ref. 202 with permission published by Wiley and Sons, 2018; ref 133c, Molecules, Published by MDPI, 2019).

1.3.2. Non-covalent interactions in supramolecular gelation

Like other self-assembly process, peptide supramolecular gelation is controlled by non-covalent forces. Hydrogen bonding is one of the essential interactions that can initiate gelation in peptide molecules.[134] There are many studies that have claimed the importance of hydrogen bonding in the formation of peptide gel. In this context, one previous study showed the role of intermolecular hydrogen bonding in self-assembly of cyclic dipeptide derivatives into nanofibres, nanoribbons and organogelation.[135] Another study revealed the organogelation of ferrocene-peptide through inter- versus intramolecular hydrogen bonding in the attached peptide chains.[136] Like hydrogen bonding, hydrophobic interaction is another important driver for peptide gelation. In the case of peptide amphiphiles, presence of both hydrophilic and hydrophobic parts utilize the hydrophobic interactions by arranging the hydrophobic domain in the core and hydrophilic chains remain exposed towards the external aqueous environment forming a hydrogel.[137-138] The balance between hydrophobic and hydrophilic parts is a crucial parameter for peptide gelation. To understand this balance, one study demonstrated the use of alkyl chains of variable length to a peptide sequence

Gly-Val-Lys-Gly-Asp-Lys-Gly-Asn-Pro-Gly-Trp-Pro-Gly-Ala-Pro derived from collagen protein. Excellent stability of the triple helix formed by this fragment was observed upon lipidation.[139] Díaz and coworkers established the importance of hydrophobic interaction in between hydrophobic amino acid residues by utilizing phenylalanine and its derivatives as potential low molecular weight gelators for the initiation of molecular aggregation and gelation process.[140a] Here, many groups introduced the concept of incorporating spacers between amino acids and other moieties to facilitate the process of gelation. For example, a series of three FF peptide mimetics was designed with both conformationally flexible and rigid spacers like 1,4-butadiene, m-xylene diamine, and m-diaminobenzene to investigate the effect of spacers in the gelation process. The study observed that the most flexible FF peptide mimetic with 1,4-butadiene spacer formed organogels in diverse organic solvents such as xylene, benzene, toluene, methanol, chlorobenzene, ethyl acetate, THF, and nitromethane by a heating-cooling technique. Comparatively rigid FF peptide mimetic with m-xylene diamine also formed organogels in benzene, toluene, xylene, chlorobenzene, methanol, ethanol, and nitromethane on heating-cooling. However, the most rigid FF peptide mimetic with m-diaminobenzene did not have the ability to form gels in all these solvents on heating-cooling and sonication, even at high concentrations.[140b] Additionally, the use of amino acid spacers, typically glycine, between "bulky" amino acids and other moieties (such as hydrophilic groups) has been shown to increase rotational flexibility and enhance gel formation. The study employed by the Stupp group established that an alkylated peptide amphiphile with three glycine residues as a linker had the ability to self-assemble into self-supporting gel at a lower pH for hydroxyapatite mineralization. Glycine was specifically chosen for this purpose to provide the hydrophilic head group of the peptide amphiphile flexibility from the more rigid cross-linked region.[140c] Other series of dipeptides protected with Fmoc group were

also investigated as hydrogelators, which established the role of hydrophobic effect in the gelation.[141-142]

π-π interaction in between planar aromatic rings is also a propellant for peptide self-assembly and gelation process.[143-144] Phenylalanine and tryptophan rich peptides are reported to self-assemble into hydrogels, which is greatly influenced by aromatic interactions.[145-147] Likewise, various N-protected amino acids attached with other aromatic groups such as fluorenylmethyloxycarbonyl (Fmoc) is also helpful for understanding the crucial role of π-π stacking for gelation. Hydrogelation of Fmoc FF dipeptides was found to be guided by aromatic π-π interactions along with hydrogen bonding.[145, 148] Apart from these interactions, electrostatic interaction is also found to be an important factor in the supramolecular gelation process. For example, one study claimed that the presence of additional electrostatic interaction between the negatively charged dipeptide Fmoc-FF and the positively charged poly-L-lysine could facilitate the process of hydrogel formation, with many desirable gel properties such as adjustable viscoelastic strength, shear thinning and self-healing properties.[149-150a]

These non-covalent interactions can be both intramolecular and intermolecular. Both have their specific roles to play in the gelation process. Interactions between different molecules are termed as intermolecular interactions, while those within the same molecule are termed as intramolecular interactions. For example, a peptide MAX1 with the sequence "VKVKVKVK^{D}PLPTKVKVKVKV-NH_2" was found to form a β-hairpin conformation through intramolecular hydrogen bonding. These β-hairpin peptides assembled via intermolecular interactions like hydrophobic interactions and hydrogen bonding into a three-dimensional hydrogel network.[150b] Another important study demonstrated that in a series of peptide amphiphiles, each peptide folded into a β-hairpin structure driven by intramolecular cation–π

interactions and intramolecular hydrogen bonds between two β strands. Then, the intermolecular interactions like the hydrophobic effect and hydrogen bond between individual peptide hairpins facilitated the growth of each fibril that subsequently self-assembled into a fibril-rich hydrogel.[150c]

1.3.3. Stimuli that can manipulate gelation process

Like other molecular self-assembly process, peptide gelation process has always been remarkable in taking advantages of both chemical and physical external stimuli, like changes in pH,[151] temperatures,[152-153] enzymatic transformation,[154] sonication,[155] presence of metal ions,[156] photo stimulation[157] and covalent bond formation.[158] An amphiphilic peptide, PEP-1 with strong hydrogel formation ability at pH 7.4 was found to be responsive towards pH change which led to the disruption of the secondary structure and the entanglement of fibrillar network under basic (pH 9.0 and 12.0) as well as acidic (pH 5.5) conditions.[159] Temperature also plays an important role in many cases of peptide gel formation, as in the formation of stable semi-transparent hydrogel by a peptide derivative CRB-FFFK-cyclen (CRB: chlorambucil, cyclen: a macrocyclic amine) via heating-cooling process.[160] Studies also showed the significant role of enzymes in promoting peptide self-assembly. To mimic the glycosylated micro-environment of the extracellular matrix, a novel glycopeptide based hydrogel formation was reported by Qi and co-workers, which was induced by the presence of an enzyme.[161a] Xu and his co-workers developed novel enzyme-instructed self-assembly (EISA) and hydrogelation where phosphonaphthyl (pNP) or phosphobiphenyl (pBP), acting as both the N-terminal capping group and the enzymatic trigger, of short peptides, resulting a alkaline phosphatase (ALP)-catalyzed gelation instantly.[161b] This study also revealed that distancing the phosphate trigger away from the peptide backbone likely favors fast enzymatic self-assembly, which could be a design strategy to combine EISA with other self-assembling molecules. Another study demonstrated that a protease can be used for reversed

hydrolysis to selectively trigger the self-assembly of peptide hydrogels.[161c] Proteases performed the reverse hydrolysis (i.e., peptide synthesis or reversed hydrolysis) to produce amphiphilic peptide hydrogelators that self-assembled to form nanofibrous structures. This approach of exploiting reverse hydrolysis with an enzyme had the benefit of forming no by-products other than an equivalent of water for each peptide bond. Likewise, a pH-responsive palmitoylated hexa peptide amphiphile (PA), C_{16}-VVAEEE, with hydrogelation ability, was found to be useful for cancer therapy. This study revealed that, in acidic pH, the self-assembled PA can selectively kill cancerous cells. The *vivo* results also supported the effectiveness of self-assembled PA in reducing tumor size, thereby inhibiting the growth of malignant cells in mice.[161d] Another group designed a UV-light responsive peptide 6-nitroveratryloxycarbonyl-diphenylalanine (Nvoc-FF) that possessed hydrogelation ability through aromatic hydrophobic group and was used for controlled release of the drug. To monitor the UV-light-triggered drug release phenomenon, insulin-fluorescein isothiocyanate (insulin-FITC) was chosen as the model of the hydrogel. Under UV light illumination, cleavage of the Nvoc group from the peptide was observed, leading to the disassembly of hydrogel and release of the drug molecules.[161e] Cao and his group developed a mixed thermo-reversible hydrogel by combining poly (N-isopropyl acrylamide (pNIPAM) and short peptide, I_3K, and utilized it for sustained and controlled release of an antibacterial peptide $G(IIKK)_3I\text{-}NH_2$. At lower temperatures, the antibacterial peptide was first encapsulated in the hydrogel by adding the solution in the sol phase and allowed to rise the temperature above 33 °C for gelation. Since the Tsol-gel was found to be around 33 °C, which is close to the body temperature, it opened up its potential as injectable hydrogel or injectable tissue engineering scaffolds using body temperature to induce hydrogel formation.[161f] Another important way to tweak peptide gelation is using sonication method. One study showed that the tripeptide Boc-Val-

Phe-Phe-OMe was found to form organogel having amyloid like fibril under the influence of sonication. Also, transformation of morphologies of peptides might be possible through sono-crystallization by applying ultrasound to generate more elongated fibers which further leads to the formation of hydrogels.[162] The idea of the presence of metal ions has also been used to promote gelation due to the interactions between the metal-gelator. Roy and coworkers established hydrogelation of a 20 residue β-hairpin peptide (VKVKVKV-CGPKEC-VKVKVKV-NH_2) in the presence of metal ions like Zn^{2+}, Pb^{2+}, Hg^{2+}.[163] Another study found the impact of the metal ions Cu^{2+}, Ni^{2+} and Co^{2+} on hydrogelation of histidine based dipeptide amphiphile due to their strong interactions with the histidine.[164] Another frequently used stimuli for driving self-assembly is light. Functionalization of gelators with photoresponsive chromophoric units makes them undergo changes like bond cleavage or bond formation in presence of light, that contributes towards the gelation process.[165-166] One study established that the photoresponsive supramolecular hydrogel formation was possible by combining azobenzene moiety with short peptide sequence.[167] Phenylalanine dipeptides protected by a light-sensitive ortho-nitrobenzyl derivative namely, Nvoc-FF (Nvoc: 6 nitroveratryloxycarbonyl) was also found to form photoresponsive hydrogels.[168]

Hofmeister effect, which defines the effect of the presence of relatively high amount of anions or cations on hydrophobic interaction of proteins/peptides in water also plays a significant role in peptide gelation. Presence of anions like sulfate or phosphate, known as kosmotropes, can reduce protein solubility due to their strong solvated form in water, enhancing the hydrophobic effect. But other more-polarizable ionic species known as chaotropes like iodide or sulfocyanide, can facilate protein solubilization by reducing the hydrophobic effect. The relevance of this effect in gelation of peptides has been investigated in several cases.[133,169-170] A bolaamphiphilic L-Valine derivative based hydrogel formation was found to be greatly influenced by the presence of different salts in

aqueous solution. They showed selective response towards ions of different salts which either improved or weakened the hydrogel. The reduced solubility of the gelator provided by kosmotropic anions like sulfate led to gel reinforcement and on the other hand, increased solubility encouraged by chaotropic species, such as perchlorate, led to gel weakening.[171] Ulijn and coworkers reported gel formation by enzymatic hydrolysis of the C-terminal methyl ester group of the dipeptides, where presence of salts affected the enzyme network that led to a change in the growth of the nanostructure.[170]

1.4. Design strategy and classes of peptide units used for gelation assembly

The design strategy of peptide sequences for inducing gelation is mostly based on their secondary structures like β-sheet, α-helix, β-hairpin, coiled-coil, and collagen triple helix.[172-177] Existing literature has a plethora of β sheet forming peptides undergoing hydrogelation.[178-180] Some studies claimed that peptide should have at least six residues for a stable β sheet conformation.[181-182] The relative stability of β-sheets compared to other secondary structures like alpha helix or random coil originates from the forces between the side-chains of neighboring amino acids and the solvation energies of side chains instead of hydrogen-bonding. These observations suggested some key parameters for designing β sheet forming peptides in solutions, which includes 1) cross-strand attractive forces including hydrogen-bonding, electrostatic, hydrophobic interactions between side-chains, 2) presence of lateral recognition between adjacent β-strands for promoting their self-assembly, preventing heterogeneous aggregated beta-sheet structures, and 3) strong adhesion of solvent to the surface of the tapes for regulating solubility. By considering these principles, Semenov and his group designed a set of two oligopeptides, DN1(11-residue long) and K24 (24 residue long) which formed semi-flexible, long, polymeric β sheet nanotapes in water and methanol.[183] Another frequently observed secondary structure in peptide hydrogels is β hairpin.

Schneider *et al.* designed a β hairpin forming twenty residue peptide by incorporating an intermittent tetrapeptide (-V^{D}PPT-) in between two β strands of complete sequence VKVKVKVK-V^{D}PPT KVKVKVKV-NH_2 to create type II β-turn structure. This peptide has the ability to form stimuli responsive hydrogels by intramolecular folding into a β hairpin conformation.[184] On the other hand, the use of α helical peptides is very limited to obtain supramolecular gels. Hartgerink and coworkers reported four 21 residues peptides which formed hydrogels under acidic pH by neutralization of the glutamic acid residues which were present in the peptide sequences to avoid the charge repulsion in the helices.[185-186]

Choosing amino acid residues and other moieties depending upon the requirements is also an important factor in designing different peptide gelators. There are several classes or designs of peptide units that are useful for promoting self-assembly and gelation process. They include amino acid derivatives,[187] dipeptides,[188] cyclic peptides,[189] amphiphilic peptides,[190] oligopeptides[191] and aromatic dipeptides[192] etc. All of the above have been widely utilized and modified for the generation of supramolecular 3D gel networks. Literature suggested that an amino acid derivative, N-lauroyl-L-alanine had the ability to show gelation in a range of non-polar organic solvent including both aromatic and aliphatic hydrocarbons.[193] Another study claimed the utility of Naphthalene group to functionalize dendrons composed of aspartic acid (Asp) and alanine (Ala) (Nap-G1 and Nap-G2) in the formation of organogels in cyclohexane and chloroform.[194] Further, Fmoc protection of Phe-Phe dipeptide was also reported for its gelation abilities by Gazit and his group.[141,145] Another group demonstrated a small series of functionalized dipeptides conjugated to an aromatic moiety at the N-terminus having gelation ability in DMSO/ water system.[188]

Peptide amphiphiles composed of both polar and hydrophobic regions constitute another important class of self-assembling building blocks that take part in developing supramolecular gels.[195]

Several gelator molecule design were based on peptide amphiphilic structures. (Fig. 1.8) A peptide amphiphile with a sequence $V_3A_3E_3$ and C16 alkyl chain at the N terminus was reported to form

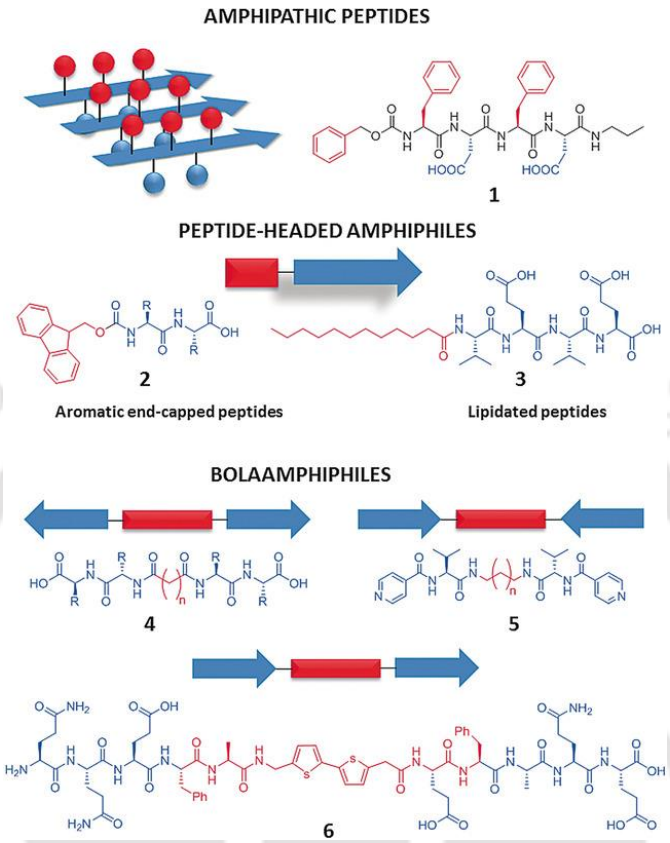

Fig. 1.8. Examples of peptide-based amphiphilic gelators (Adapted from ref. 133a with permission, published by Wiley and Sons, 2017).

gel in presence of HCl or $CaCl_2$.[190] Another peptide amphiphile containing $(VK)_5$ sequence and cysteine residue attached at its C-terminal by using a spacer, γ –aminobutyric acid was found to form a thixotropic hydrogel in basic pH through anti-parallel β-sheet formation.[196] Apart from these, bolaamphiphiles are another special class of amphiphiles formed by peptides, that have been extensively used for supramolecular assembly. These either have polar head groups at two ends of a lipid or have two hydrophilic heads connected by a hydrophobic region.[197-198] A peptide bolaamphiphile, HO–Tyr–Phe–Suc–Phe–Tyr–OH was reported to be triggered by a sequential

change in pH, for the hydrogelation.[199] Peptide headed amphiphiles which either have aromatic end capping or lipidation, are reported as gelator molecules.[200]

Cyclic peptides can also be utilized in developing peptide supramolecular gels. Montenegro and his group detailed about cyclic peptides being used for pH-triggered nanotube formation and fibrillation in confined aqueous droplets to give rise to viscoelastic hydrogels.[201] Perrier and coworkers studied a library of cyclic peptides with alternating D and L amino acids and their gelation properties by using various solvents, establishing important factors affecting both organogel and hydrogel formation. Hydrogels derived from the cyclic peptides containing two charged amino acid residues, either lysine or glutamic acid, were found to be pH responsive. The self-assembly process occurred through hollow nanotube formation by vertical stacking of cyclic peptides which further aggregated into larger fibers that entangled into a dense network and gave rise to hydrogel.[202] Besides these, amphiphilic peptide dendrimers are another class of peptides known to be a building blocks for supramolecular gelation.[203-204]

1.5. Peptide supramolecular gels for applications

The exploration of peptide molecules as building blocks for the development of supramolecular gelation systems provides us with beneficial advances in various fields. Over the last couple of decades, extensive exploration has been done by designing and modifying peptide sequences, that are capable of promoting assembly process via non-covalent interactions for the creation of functional materials. In soft material research, several successful approaches showed the importance of peptide based gels and their properties, that have encouraged further investigation for generating new biomaterials in the future. Literature confirmed that both peptide based organogels and hydrogels are helpful in various biomedical and non-biomedical applications.

1.5.1. Biomedical Applications

The vastness of supramolecular peptide gels in the biomedical platform exudes innumerable opportunities to resolve a diverse range of challenges (Fig. 1.9). They have been constantly

Fig. 1.9. Utilization of peptide supramolecular gels for various biomedical applications. (Parts of the Fig. were adapted from ref. 205 b with permission, published by American Chemical Society, 2020; ref. 205c with permission, published by MDPI, 2022; one part was adapted from ref. 205d).

exploited as sustainable nano biomaterials in many areas like combating microbes, drug release, gene delivery, membrane protein stabilization in 3D cell culture and tissue engineering and many other applications.

1.5.1.1. Antimicrobial applications

Antimicrobial resistance is one of the major concerns confronting the modern human society. Intrinsic resistance development in the microbes is augmented by overdose and improper use of antibiotics, and limited availability of new therapeutics.[205-208] To address this problem, antimicrobial peptides and their hydrogels can be an alternative option, presenting various advantages like slow/absence of resistance development by microbes, low toxicity, salt tolerance, and protease stability.[209-211] There are several studies on peptide hydrogels as antimicrobial agents reported in the literature. For example, a library of peptide amphiphiles of different fatty acyl chain lengths with the chemical formula [H_2N-$(CH_2)_n$CONH-Phe-CONHC_{12} where n=1-5, C_{12}= dodecylamine] was developed in the year of 2017 by Banerjee *et al.* This study revealed that only hydrogels of peptides having the longer fatty acyl chain were the most active antibacterial agents against both Gram-negative and Gram-positive bacteria like *E. coli*, *B. subtilis* and *S. aureus* respectively. This might be due to the effective interaction of longer alkyl chain with bacterial membranes, helping their disruption. Additionally, the hydrogels were proteolytically stable in presence of enzymes such as proteinase K and chymotrypsin.[212] In another study, a lysine-rich amphiphilic cationic peptide MAX1 was found to form a mechanically rigid hydrogel through β-sheet formation (Fig. 1.10 a). The bacterial membrane disruption was effected by the interaction in between cationic lysines on the surface of the fibrils, and negatively charged bacterial cell membrane. MAX1 hydrogel was active against ESKAPE pathogens including *E. coli*, *K. pneumonia*, *S. aureus, S. epidermidis* and *S. pyogenes*.[213] Literature evidenced that arginine is one of the most commonly found amino acids in many of the antimicrobial peptides.[214] Salick and his group developed an arginine based peptide MARG1 hydrogel based on the sequence of MAX1, where lysine residues were systematically replaced by arginine at positions 6 and 17. This newly

modified peptide MARG1 also contained lysine residues in a high porportions on its hydrophilic face. (Fig. 1.10 b) Therefore, the fibrils displayed a positively charged surface which had the ability to interact with the negatively charged bacterial membrane, providing antibacterial activity against MRSA.[215]

In another study, Veiga and coworkers demonstrated a peptide containing six arginine residues, EP6R, which showed the ability to adopt an amphiphilic β-hairpin conformation in buffer solution, and rapidly self-assembled into a hydrogel via β-sheet formation. PEP6R hydrogel exhibited antimicrobial potency against *S. aureus* and *E. coli* through membrane disruption mechanism. The reported hydrogel showed shear-thinning and injectable behavior (Fig. 1.10 c).[216] Again, Baral *et al*. reported a biocompatible and non-haemolytic dipeptide based hydrogel, with an outstanding antimicrobial potency against *E. coli* and *P. aeruginosa*.[217]

Many study suggested that peptides comprising of natural amino acids suffered from poor stability against proteolytic enzymes.[218] Therefore, to develop proteolytically stable peptide gels, Singh and coworkers designed α/γ hybrid peptides, Boc-D-Phe-γ4 -L-Phe-PEA (NH007) and Boc-L-Phe-γ4 -L-Phe-PEA (NH009) with high gelation abilities (Fig. 1.10 d). Both peptides were stable towards proteolytic enzymes and their gels were active against various bacterial pathogens including

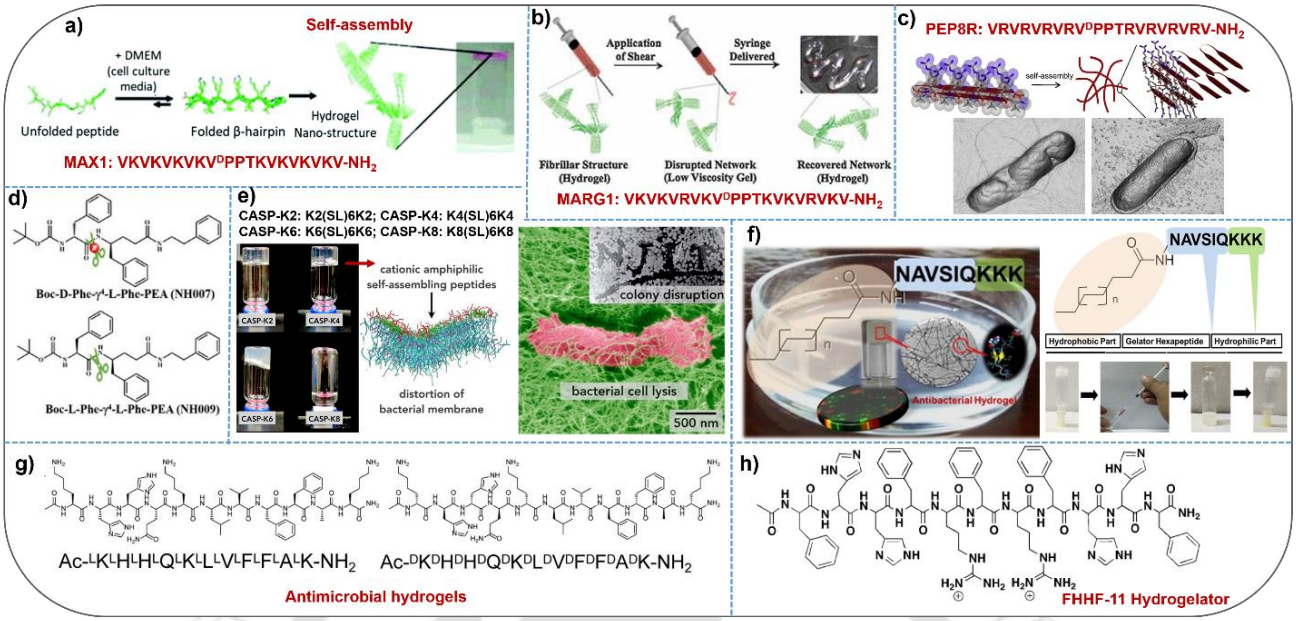

Fig. 1.10. Utilization of peptide-based supramolecular gels as antimicrobial agents: a) Antimicrobial MAXI nano-structured hydrogel and its self-assembly pattern (Adapted from ref. 213 with permission published by American Chemical Society, 2007). b) Replacement of lysine in MAX1 by arginine in MARGI, resulting in an injectable antimicrobial hydrogel that showed activity against MRSA (Adapted from ref. 215 with permission, published by Wiley and Sons, 2009). c) Amphiphilic arginine-rich peptide designed to self-assemble into β-sheet rich fibrils active against E. coli bacterial strain (Adapted from ref. 216 with the permission published by Elsevier, 2012) d) α/γ hybrid peptide hydrogels with proteolytical stability and active against both Gram-positive and Gram-negative bacteria (Adapted from ref. 219 a, published by American Chemical Society, 2018). e) Cationic amphiphilic peptides owing to hydrogelation ability and membrane-distrupting antimicrobial activity (Adapted from ref. 219 b with permission, published by American Chemical Society, 2019). f) Lipopeptide-based injectable antimicrobial hydrogel with biocompatibility and enzyme stability adapted from ref. 219c with permission, published by American Chemical Society, 2019). g) Antimicrobial hydrogels showing better activity with isomers adapted from ref. 219 d with permission, published by American Chemical Society, 2021). h) Structure of antimicrobial hydrogel (Adapted from ref. 219e).

B. subtilis, *S. aureus*, *P. aeruginosa*, and *E. coli.* They claimed that the improved stability was due to the presence of D-residue in α/γ hybrid peptide.[219a] Kumar and co-workers developed a class of cationic amphiphilic self-assembling peptides (CASP) that self-assembled to thixotropic hydrogels at physiological conditions (Fig. 1.10 e). It was observed that the nanofibers obtained from the

hydrogels have the antimicrobial potency towards *Pseudomonas aeruginosa* colonies with membrane disrupting mechanism.[219b] Another biocompatible lipopeptide, with lysine rich C-terminal was designed by Adak.*et.al.* (Fig. 1.10 f) The hydrogel was found to have antimicrobial potency against *S. aureus* and *E. coli* through the interaction with the bacterial membrane which was detrimental to membrane integrity. Also, enzymatic stability, non-cytotoxicity and non-haemolytic nature encouraged the hydrogel for its further applicability in biomedical field.[219c] Zang and co-workers reported the antimicrobial activity of D-peptide Ac-$^{D}K^{D}H^{D}H^{D}Q^{D}K^{D}L^{D}V^{D}F^{D}F^{D}A^{D}K$-NH2 (KKd-11) hydrogel in inhibition and eradication of biofilm and showed better activity compared to Ac-$^{L}K^{L}H^{L}H^{L}Q^{L}K^{L}L^{L}V^{L}F^{L}F^{L}A^{L}K$-NH2 (KK-11) (Fig. 1.10 g).[219d] A pH responsive hydrogel was obtained from the short peptide FHHF-11 due to changing degree of protonation of histidine residues that was employed against against both Gram-negative and Gram-positive bacteria (Fig. 1.10 h).[219e]

1.5.1.2. Tissue engineering

Peptide hydrogels are considered as immensely important biological scaffold exhibiting profound impact in the field of tissue engineering.[220-223] Also, hydrogels can hold high amount of water, offering the possibility of mimicking the 3D environment of cells. KLD12 peptide hydrogel with nanofibers of 3 orders of magnitude smaller than microfibers provided by most of the biopolymers, could function as a 3D scaffold for encapsulation of chondrocytes.[224] Lampe and coworkers studied a family of short, KYFIL pentapeptide based sequences which were capable of self-assembling into beta sheets, forming robust nanofibrous hydrogels that could encapsulate oligodendrocyte progenitor cells (OPCs), as well as promote proliferation and morphological process extension in OPCs.[225]

1.5.1.3. 3D Cell Culture

Recently, the use of self-assembling peptides with short sequences coupled with their functionalization has evolved rapidly for the advancement of new scaffolds for 3D cell culture.[226] One of earliest known peptide hydrogel called EAK16-II with amino acid sequence, AEAEAKAKAEAEAKAK and ability to retain beta sheet structure was found to be useful for 2D cell cultures including MG63, SH-SY5Y, HEK293, 3T3, HIT-T15, CEF, HFF, HepG2, Hela, and PC12 cells. But, soon this hydrogel was developed for 3D culture by mixing the suspension of cell/sucrose with the peptide solution to create cell encapsulated gel.[227-231] Based on EAK16, another peptide hydrogel RADA16 was designed which was utilized initially for 2D cell culture. Further, it was applied to a 3D ovarian cancer model to investigate the drug resistance as well as the cell invasion mechanism. The observed data suggested stronger resistance to anticancer agents like curcumin and paclitaxel in case of 3D compared to 2D cultures.[227-231] Combinations of some of the hydrogels formed from a series of Fmoc dipeptides consisting of four amino acid residues, alanine (Ala), leucine (Leu), glycine (Gly), and phenylalanine (Phe) were found to be stable and able to support cell culture of chondrocytes in two and three dimensions.[141] An amphiphilic peptide MAX8 (VKVKVKVK-V^{D}PPT-KVEVKVKV-NH_2) exhibiting the ability of forming beta hairpin hydrogel was reported to form a cell–gel construct by adding cells in serum-free medium to peptide, dissolved in HEPES buffer. MG63 cells have been successfully cultured and encapsulated within the MAX8 gel.[232] Another study demonstrated a small oligopeptide D-P1 ((Ac-D-Phe-D-Phe-D-Phe-Gly-D-Lys-OH) based hydrogel, that could be utilized as a scaffold for cell culturing and formation of cellular spheroids of HeLa cells. Additionally, D-P1 hydrogel was protease resistant and was nontoxic in nature.[233]

1.5.1.4. Delivery of therapeutic molecules

Conventional drug delivery systems are connected with numerous shortcomings such as poor solubility in water, quick biodegradation, inadequate oral availability, non-specificity, and unavoidable side effects.[234] To resolve these drug delivery related issues, advanced drug delivery systems with improved attributes need to be designed to maximize the drug efficacy.[235a] They should be biocompatiple, specific in their delivery, biodegradable, protective of the drug molecules from dilution and degradation, and able to release drugs in a controlled and sustained manner. Additionally, two very well-known adapted strategies for drug delivery are the covalent attachment and the physical combining of drug molecules with the carriers. Literature suggests that both methods have their own advantages and challenges.[235b, c] The covalent attachment describes a chemical bonding of the drug to a carrier molecule, which could be a nanoparticle, polymer,[235d] or macromolecule, and under specific physiological conditions such as pH,[235e] presence of an enzyme,[235f, b] etc., that bond can be cleaved to release the drug. These delivery methods allow for targeted drug release/controlled release with desirable pharmacokinetic and pharmacodynamic properties,[235d] good therapeutic efficacy,[235g] sustainability,[235h] and minimal systemic side effects.[253i] Also, covalent attachment can offer better stability and bioavailability to the drug molecules by minimizing their premature degradation.[235j] However, challenges like complex and laborious synthesis procedures, and inadequate release kinetics are also associated with this method.[235d] On the other hand, physical mixing is a very simple and versatile method that involves blending the drug with a carrier like hydrogels, liposomes, micelles, and polymeric nanoparticles without forming any covalent attachment.[235d, l] Due to its simplicity, it can be adapted for various drugs easily, offering faster development and easy formulation of different dosage forms, such as injections, or topical applications.[235k, m, d] However, in this method, there is a possibility of

undesirable drug release before reaching the target site, leading to reduced efficacy, low encapsulating efficiency, systemic side effects, stability issues in blood, and limited control over release.[235n] However, depending upon the nature of the drug to be delivered, requirements of the therapeutic application, and the target delivery site, the choice between these two strategies can be made. Peptide hydrogels have been found extremely promising as biomaterials for delivery of drugs in both ways. For example, a stable injectable hydrogel obtained from an ultrashort peptide containing α, β-dehydrophenylalanine, LeuΔPhe was displayed for entrapping and releasing mitoxantrone, an anticancer drug that significantly controlled tumor growth in an in-vivo mouse model.[236] Another injectable peptide hydrogel was designed based on KLD motif that was successfully utilized for controlled delivery of doxorubicin (DOX) or Smac-derived pro-apoptotic peptide (SDPP) for cancer therapy.[237] RADA16, was reported to have hydrogelation ability under physiological conditions and used to load the hydrophobic antitumor drug paclitaxel through the interaction between RADA16 and paclitaxel.[238] In another study, *in situ* gel forming self-assembling peptide, Ac-$(RADA)_4$-$CONH_2$, was developed as a biocompatible delivery system for the chemotherapeutic drug DOX and the anticancer agent curcumin that achieved localized chemotherapy of malignant brain tumors.[239] Tang and co-workers designed an octapeptide FEFEFKFK that self-assembled into antiparallel β-sheet rich fibres and formed hydrogel in water. It acted as a muco adhesive for the improved delivery of drugs (lidocaine and flurbiprofen) to local mucosal surfaces.[240] Apart from the delivery of drug molecules, peptide hydrogels have been employed for delivering proteins with benefits like high loading and improved protection to preserve stability. Additionally, limited mobility of proteins within the fibrillar network allowed their delivery to the targeted place efficiently without any degradation.[241] RADA16-I hydrogel was successfully utilized to encapsulate four proteins, bovine serum albumin (BSA), immunoglobulin

G (IgG) trypsin inhibitor, and lysozyme and release them at the desired site.[242a] A charged hexapeptide NH_2-WLVFFK-COOH (A1) was reported as noncytotoxic hydrogelator that have been used for sustainable of release various drugs, like ciprofloxacin, 5-fluorouracil, and two proteins namely lysozyme and bovine serum albumin (BSA). It was observed that there is no alteration in the activity of drugs after release. On the other hand, proteins have also showed complete retention of their secondary structure which signifies the applicability of the hydrogel as drug delivery therapeutics.[242b]

1.5.1.5. Biosensor

By definition, biosensor represents a device that detects chemical or biological reactions through the production of signals proportional to the amount of analyte present in the reaction. They have applicability in identifying disease-causing micro-organisms and pollutants, disease monitoring, drug discovery, etc.[243] In current years, peptide hydrogels have also been exploited as biosensor in various fields. The Fmoc–FF hydrogel was found to have the ability to perform as a biosensor by encapsulating enzymes (e.g. Glucose oxidase or horse radish peroxidase) and fluorescent nano particles like CdSe or CdTe quantum dots. These systems could efficiently detect analytes (phenolic compounds or glucose) by monitoring change in photophyscical properties of the hybridized quantum dots.[244] In another study, Yang and co-workers used Fmoc-Phe-Phe based hydrogel for enzyme-based electrochemical bio-sensing and cell monitoring purposes. The hydrogel acted as a host for peroxidase and showed the detection of H_2O_2 levels released from HeLa cells in *in vitro* conditions.[245] Miller and co-workers reported a self-assembling 3D peptide hydrogel which was utilized as a 3D solid support where oligonucleotides were immobilized and this prototype can be utilized to detect complementary sequences, with a detection limit of 22 pM.[246]

1.5.2. Non-biomedical applications

In the field of non-biomedical research, supramolecular peptide gels are found to be equally engaging as advanced soft materials (Fig.1.11). Their active participation in applications like environmental remediation, oil spill recovery, sensor development, catalysis etc. significantly influenced the field of material science.

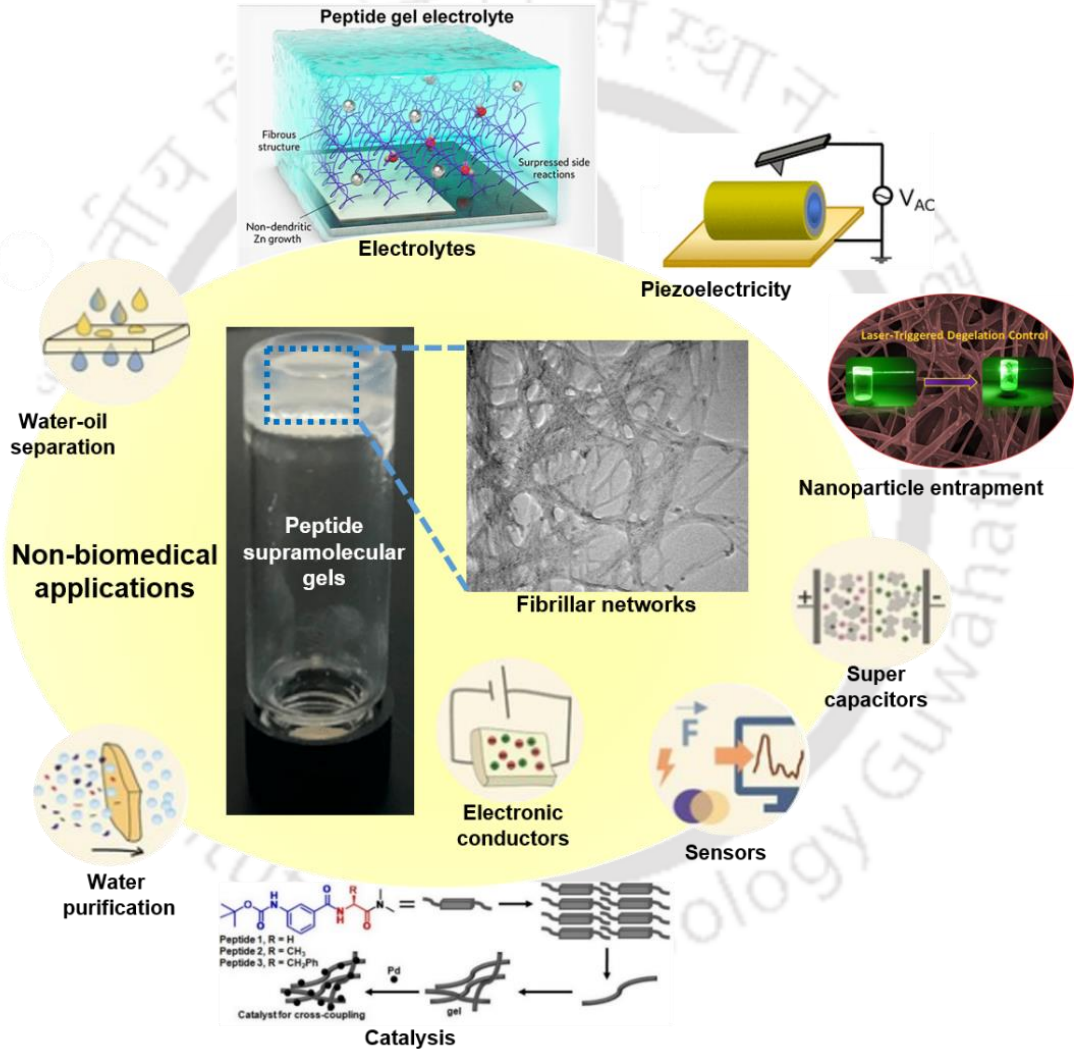

Fig. 1.11. Applicability of peptide supramolecular gels in various non-biomedical domain. (One part of the Fig. adapted from ref. 247 c; other parts were reproduced and modified from ref. 247 d with the permission, published by Wiley and Sons; and ref. 247 e published by American Chemical Society).

1.5.2.1. Peptide gels for water purification

Water pollution is one of the prime concerns that needs to addressed for healthy living. Several efforts have already been made toward combating the rapid damage of the water bodies. Toxic dyes, leaching of heavy metal ions such as mercury (Hg), cadmium (Cd), lead (Pb), and industrial waste are the main reasons behind this problem. The impact of dye effluents has been recognized as serious risk on the immune system and reproductive systems, along with potential genotoxicity and cardiotoxicity.[247] Heavy metal like mercury is considered neurotoxic and can cause lipid peroxidation, mitochondrial damage, microtubule destruction, and accumulation of neurotoxic molecules such as glutamate, aspartate, and serotonin.[247a, 248] On the other hand, lead exposure can induce many adverse effects on the human body by influencing reproductive, renal and central nervous, and hematopoietic systems through the elevation of oxidative stress. The non-biodegradable nature of lead makes it more threatening to the environment.[247] Peptide based supramolecular gels mainly from low molecular weight gelators have become popular new generation biomaterials water remediation. Ray *et al.* claimed that a bolaamphiphile consisting of phenylalanine and a centrally located oligomethylene group formed hydrogels in the presence of sonication and divalent metal salts within pH range of 6.5-7. This pH-responsive metallohydrogel could efficiently remove various toxic dyes such as pyrene (a non-ionic dye), naphthol blue black (an anionic dye) and crystal violet (a cationic dye), and from waste water (Fig. 1.12 a).[249] A family of dipeptides comprised of nonpolar aromatic/aliphatic amino acid residues and variable alkyl chain length starting from C-12 to C-16 were utilized for the formation of thermoreversible organogels through the balanced hydrogen bonding and van der Waals interaction. Further, they established that these organogels can be put in waste water management application due to their property of absorbing dyes including crystal violet, rhodamine 6G from water.[250]

Schneider and his group utilized a twenty residue peptide (VKVKVKVCGPKECVKVKVKV-NH_2) for the formation hydrogel in the presence of heavy metal ions, Cd^{2+}, Hg^{2+} , Zn^{2+}, or Pb^{2+}, and mono methyl arsonous acid (Fig. 1.12 b) The responsive nature of the peptide due to complexation with ions led to subsequent folding of the peptide into an amphiphilic β hairpin that rapidly self-assembled into fibrillar network through β-sheet formation.[251] Another study evidenced gelation ability of a small dipeptide composed of N-(tert-butoxycarbonyl)pentafluoro-L-phenylalanine and O-benzyl-L-tyrosine methyl ester in a mixture of solvent systems. They claimed that presence of water was crucial for gelation in polar protic solvent. On the hand, diesel, kerosene, and petroleum ether were found to be important for gelation in aromatic solvents. The gelation ability of this dipeptide has further widened its applicability in oil spill recovery (Fig. 1.12 c).[252] One report claimed a novel triphenylalanine based hydrogel with low gelation concentration and time-dependent self-shrinking property by repelling water molecules, as an easy and effective way of removing toxic heavy metal ions (Pb^{2+}) and toxic organic dyes such as Brilliant blue and Methylene blue from water. Also, reusability and higher absorption capacity were the advantageous qualities of this hydrogel which made it a cheaper material for waste water treatment.[253] In 2014, Das and his group reported an amphiphilic peptide based low molecular weight organogelator comprising of tetra butyloxy carbonyl protected L-phenylalanine, L-lysine and 6-amino caproic acid with gelation ability in a wide range of aromatic and aliphatic solvents through the involvement of non-covalent interactions like π–π, hydrophobic, hydrogen bonding, and van der Waals interactions.[254] These organogels were found to be phase selective and thermo-reversible in nature and their corresponding xerogel had an excellent efficiency of eliminating toxic dyes from water within a short period of time. Another peptide hydrogelator with the sequence FmocFFGGGY was developed for removal of dyes like congo red, methyl violet,

bromocresol green, rhodamine b, coomassie brilliant blue G-250, and xylenol orange from water exhibiting adsorption effectiveness of more than 80%.[255] Chatterjee and her group designed dicyclohexyl urea (DCU) derivatives of amino acids Fmoc-Phe-DCU (M1), Fmoc-Phg-DCU (M2) and Fmoc-Gaba-DCU (M3) for the first time for developing low molecular weight gelators. They were found to form thermoreversible, phase selective, and mechanically robust gels in a variety organic solvents. Further, obtained organogels have been employed in the water remediation application as efficient and recyclable organic dye absorbents.[256a] The same group again reported two charge complementary peptides A1 (NH_2-WLVFFK-COOH) and A2 (NH_2-WLVFFE-COOH) which were utilized to initiate co-assembly and to form a cooperative hydrogel, through electrostatic interaction aided by hydrophobic, aromatic interactions and hydrogen bonding. The self-assembled and co-assembled hydrogels both were efficient in removal of different kinds of toxic metal ions (Hg^{2+}, Pb^{2+}, Co^{2+}, and Ni^{2+}) and organic dyes (neutral, cationic, and anionic) from a mixture of contaminated water. Also, they were capable of detecting peptides arsenic in its most toxic (III/V) oxidation states.[256b]

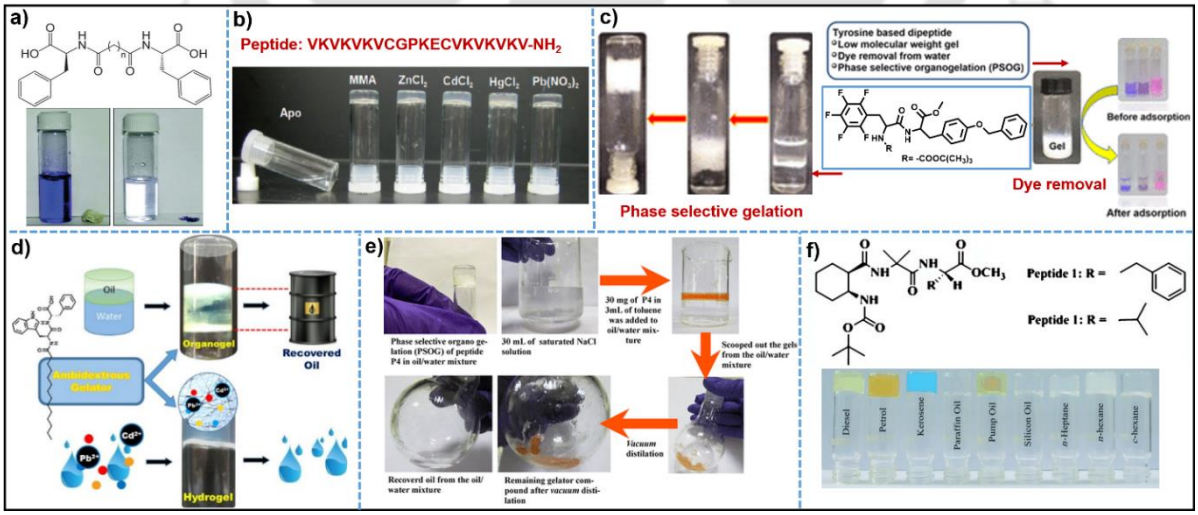

Fig. 1.12. Implementation of peptide-based supramolecular gels for water remediation: a) Dye removal by tyrosine-based low molecular weight peptide organogels. (Adapted from ref. 249 with the permission published by American Chemical Society, 2007) b) Hydrogelation of peptide in the

presence of metal ions (Adapted from ref. 251 with the permission published by Royel Society of Chemistry, 2012). c) Removal of crystal violet dye from water (Adapted from ref. 252, 2019) d) Utilization of ambidextrous peptide gelator removal of metal ion and oil spill recovery (Adapted from ref. 262 with permission published by American Chemical Society, 2020) e) Oil spill recovery by using peptide hybrid gels (Adapted from ref. 263 with permission published by American Chemical Society, 2019). f) Gelation abilities of peptides in various oils (Adapted from ref. 264 with permission, published by Wiley and Sons, 2014).

Apart from dyes and metal ions, oil spillage is another major cause of water pollution. It has been reported that the spilled oil remained in the water and finally accumulated on the sea bottom, thus endangering the whole marine ecosystem.[257-259] Low molecular weight peptide-based gels have been popular for their utility in oil spill recovery. Most of them are phase selective in nature and thus have the ability to form gel selectively in the oil layer from the oil water biphasic mixture. Further, the gel part can be removed easily leaving the clean water behind.[260-261] Banerjee and his coworkers reported a dipeptide amphiphile containing tryptophan and a myristyl chain which could selectively form organogels in fuel oil, petrol, diesel, and kerosene from a mixture of salt water and oil within a few seconds. The gel material was found to be reusable multiple times without compromising its activity showing its utility in environmental remediation (Fig. 1.12 d).[262] Another class of short hybrid dipeptides containing conformationally flexible new β(O)-δ5-amino acids were reported for being divergent supramolecular gelators and were further explored for recovery of oil spills(Fig. 1.12 e).[263] A terminally protected peptide, Boc-cis-ACHC-Aib-Phe-OMe (cis-ACHC=cis-2 aminocyclohexanecarboxylic acid), was designed and utilized for the development of self-supporting organogels in various organic solvents and oils. Also, this organogel exhibited phase selective behavior, which made it capable of entrapping organic or oil layers selectively over the aqueous layer suggesting its usefulness for oil spill recovery (Fig. 1.12 f).[264]

1.5.2.2. Catalysis

Catalysis is the another field of research where peptide supramolecular gels have gathered recognition due to their catalytic activity in wide range of reactions. Several peptides-based gels are already reported as catalytic materials. Banerjee and his group designed a histidine based peptide amphiphile connected with C13 fatty acyl chain and N-histidyl N′-myristry ethyl amine that could form hydrogel in the presence of Fe^{3+} and Hg^{2+} ions separately in aqueous dispersions at pH 6.6. The reported hydrogel was found to have catalytic activity towards ester hydrolysis of p-nitrophenyl esters of acetyl, n-butyl and n-octyl esters (n = 3, 4, 8).[265] Another study, showed that hydrolysis of a model ester 2, 4-dinitrophenyl acetate (DNPA) was possible on the surface of nanofibres formed by a peptide amphiphile based gel system. The rate of hydrolysis obtained by the use of ordered nanofibers was higher compared to catalysts in solution and in spherical aggregates.[266] Hydrogels formed from a series of short peptides having the sequence $(FE)_n$ or $(EF)_n$ with L-proline at their N terminus were found to be catalytically active towards aldol reaction. The non-assembling or non-aggregated analogues lacked in showing catalytic activity in solution, suggesting the importance of catalytic activity of short self-assembling peptides in water.[267] Besides these examples, a lot of studies are available claiming the catalysis activity of peptide hydrogels.[268-269]

1.5.2.3. Template for Nanofabrication

The exploration of peptide self-assembly and utilization of gel matrix as templates have provided useful advancements in the progress of nanofabrication.[270] One study revealed that fabrication of luminescent CdS nanoparticles was achieved with the support of the gel nanofiber network obtained from a pH responsive thermoreversible hydrogel made up of self-assembling short synthetic tri peptides, Boc-Phe-X-Phe-OH (Boc=tert-butoxycarbonyl; X=Val, Leu or Phe). This

fabrication did not alter the dimension of the CdS nanoparticles in the nanofibrillar gel network, but showed a significant blue shift in the emission spectrum suggesting the tuning of optoelectronic properties was possible without any deformation of nanoparticles in such hybrid systems.[271] Another study established a method for the shape controlled synthesis of gold nanoparticles *in situ* within the low molecular gel template derived from tryptophan-based dipeptide amphiphiles. This synthesis was carried out without any external capping agent or reducing agents and various shapes like decahedral, octahedral, sheet, and wire were successfully modulated.[272] Further, amino acid (tryptophan/tyrosine) based amphiphilic hydrogelators was explored for *in situ* synthesis of silver nanoparticle (AgNP) within their assemblies without use of any stabilizing agent. These newly developed soft nanocomposites showed antimicrobial potency against both Gram-positive and Gram-negative bacteria.[273] Another nano fabrication was obtained from a tripeptide containing an oligo methylene group in presence of citric acid, where the induced hydrogel was used for the *in situ* formation of gold and silver nanoparticles. The nano-hybrid system containing peptide fibers and silver nanoparticle was proven to be useful as catalyst in the conversion of nitro aromatics to the corresponding aromatic amines with recyclability properties.[274]

1.5.2.4. Sensors

The applicability of peptide gels in the area of sensing is well established. In developing sensors for detecting various analytes, biomolecules like peptides have emerged as a promising platform.[275] A fluorescent hydrogel obtained from two dipeptide amphiphiles conjugated with pyrene at the C-terminus (TGM-82) and the N-terminus (TGM-83) via bicomponent antiparallel beta sheet co-assembly, was recognized with the ability to detect toxic nitro explosives including nitrophenol, trinitrobenzene and trinitrotoluene. The selective and sensitive detection was facilitated by the sandwich like interaction of nitroaromatics within the hydrogel matrix.[276] A poly

aspartate peptide based nano fibrous hydrogel was developed for naked eye detection of Cu^{2+} ions with a detection limit of 0.01 mg/L in water. Also, the hydrogel was highly selective towards Cu^{2+} in the presence of other ions and could display a colorimetric response upon alteration of pH.[277] Another efficient, economically viable and reusable fluorescent hydrogel derived from a histidine containing bolaamphiphilic peptide joined with naphthalenediimide was designed by Banerjee and co-workers for the detection of hazardous volatile acid and base vapors such as HCl, H_2SO_4, TFA, HCOOH, acetic acid and basic ammonia vapor. Based on that they demonstrated a paper strip method that exhibited "turn on" fluorescence in the presence of hazardous acid vapors and "turn off" fluorescence in ammonia vapor suggesting a promising sensor.[278] Das *et. al.* reported peptide/carbon dot composite xerogel for p-xylene vapor sensing with a detection limit of 50 ppm where the peptide fibres helped in gaining semicoductivity and carbon dots strengthened the sensitivity.[279] The same group developed another small peptide PyFFK based sensor for Picric acid with detection limits of 115.24 ppt and 22.91 ppb, in solution and gel respectively.[280]

1.5.2.5. Energy harvesting

Most of the materials used in organic electronics and light harvesting suffer from the poor organization between the molecules, impacting the long range charge delocalization and transport. In this regard, self-assembling peptides can afford enhanced ordering to these materials due to β-sheet forming ability, hydrogen bonding, hydrophobic interaction along with other non-covalent interactions.[133, 281] A known chromophore Perylenebisimide (PBI) was functionalized with peptide that formed nanostructures showing high photoconductivity due to the generation of highly stable radical anion in air and in the presence of water.[282] Again, functionalization of electron donor tetrathiaful-valene(TTF) with C-terminal amidated peptide was found to form highly ordered nanofibers with improved conductivity upon doping with electron acceptors, like iodine or

tetracyano-p-quinodimethane(TCNQ).[283] Also, thiophene-based peptide nano fibers were evaluated for hybrid electron and proton transport throght varying the humidity level which effected a change in the conductance value.[284]

All these reports detailed above highlight the importance of supramolecular peptide gels in developing biomaterials for myriad biomedical and non-biomedical applications.

1.6. Aims of this thesis

1. Design and synthesis of small peptide-based gelators
2. Development of small peptide-based organo/hydrogels and their characterization
3. Mechanistic study to understand the gelation process
4. Employing the developed gels in various applications like

a. Water remediation (Removal of oil and dyes from water)

b. Development of conducting materials

c. Stabilization of the Quantum dots

d. Development of antimicrobial hydrogels to inhibit MRSA biofilms

e. Development of hydrogels as a drug delivery platform

5. Investigation of the role of "hydrophobic-hydrophilic balance" in manipulating several properties of the designed peptides

References

1. Mendes, A. C.; Baran, E. T.; Reis, R. L.; Azevedo, H. S. Self-assembly in nature: using the principles of nature to create complex nanobiomaterials. *WIREs Nanomed Nanobiotechnol*. **2013**, *5*, 582-612.

2. Derek Marsh, D. Thermodynamics of phospholipid self-assembly. *Biophys. J.* **2012**, *102*, 1079–1087.

3. Dragan, A. I.; Crane-Robinson, C.; P. L. Privalov, P. L. Thermodynamic basis of the α-helix and DNA duplex. *Eur Biophys J*. **2021**, *50*, 787–792.

4. Kim, N. H.; Choi, H.; Shahzad, Z. M.; Ki, H.; Lee, J.; Chae, H.; Kim, Y. H. Supramolecular assembly of protein building blocks: from folding to function. *Nano Convergence* **2022,** 9, 1-17.

5. Krissanaprasit, A.; Key, C. M.; Pontula, S.; LaBean. T. H. Self-assembling nucleic acid nanostructures functionalized with aptamers. *Chem. Rev.* **2021**, *121*, 13797-13868.

6. Rich, A. Molecular structure of the nucleic acids. *RMP* **1959**, *31*, 191-200.

7. Scanlon, S.; Aggeli, A. Self-assembling peptide nanotubes. *Nano Today* **2008**, *3*, 22-30.

8. Hamley, I. W. Peptide fibrillization. *Angew. Chem. Int. Ed.* **2007**, *46*, 8128–8147.

9. Liu, Z.; Qiao, J.; Niu, Z. W.; Wang, Q. Natural supramolecular building blocks: from virus coat proteins to viral nanoparticles *Chem. Soc. Rev.* **2012**, *41*, 6178–6194.

10. Kushner, D. J. Self-assembly of biological structures. *Bacteriol. Rev*. **1969**, *33*, 302-345.

11. Dergham, M.; Lin, S.; Geng, J. Supramolecular self-assembly in living cells. *Angew. Chem. Int. Ed*. **2022**, *61*, 1-11.

12. Whitesides, G. M.; Mila Boncheva, M. Beyond molecules: Self-assembly of mesoscopic and macroscopic components *PNAS* **2002**, *99*, 4769-4774.

13. White, S. D. M.; Rees, M. J. Core condensation in heavy halos: a two stage theory for galaxy formation and clustering. *Mon. Not. R. astr. Soc.* **1978**, *183*, 341-358.

14. Blanton, M. R.; Moustakas, J. Physical properties and environments of nearby galaxies. *Annu. Rev. Astron. Astrophys*. **2009**, *47*, 159-210.

15. Guo, Y. The assembly of galaxies over cosmic time. Ph.D. Dissertation, University of Massachusetts Amherst, 2012, https://doi.org/10.7275/ndgc-f089. https://scholarworks.umass.edu/open_access_dissertations/642.

16. G. M. Whitesides and B. Grzybowski, Self-assembly at all scales. *Science* **2002**, *295*, 2418-2421.

17. Busseron, E.; Ruff, Y.; Moulin, E.; Giuseppone, N. Supramolecular self-assemblies as functional nanomaterials. *Nanoscale* **2013**, *5*, 7098-7140.

18. Cravotto, G.; Cintas, P. Molecular self-assembly and patterning induced by sound waves. The case of gelation. *Chem. Soc. Rev*. **2009**, *38*, 2684–2697.

19. Gale, P. A.; Steed, J. W. Supramolecular chemistry: from molecules to nanomaterials, ed. Wiley-VCH Verlag GmbH & Co. KGaA, Weinheim, 2012.

20. Wang, A.; Huang, J.; Yan, Y. Hierarchical molecular self-assemblies: construction and advantages. *Soft Matter* **2014**, *10*, 3362–3373.

21. Kim. H. J.; Kim. T.; Lee, M. Responsive nanostructures from aqueous assembly of rigid-flexible block molecules. *Acc. Chem. Res*. **2011**, *44*, 72– 82.

22. Liu, Y.; Wang, Q.; Li, F.; Ling, D. Nature-inspired supramolecular assemblies for precise biomedical imaging and therapy. *Acta Pharm Sin B.* **2022**, *12*, 4008-4010.

23. Thomas, E. L. The ABCs of self-assembly. *Science* **1999**, *286*, 1307.

24. Evans, D. F.; Wennerstrom, H. The colloidal domain: where physics, chemistry, biology, and technology meet; Wiley, New York, 1999.

25. Desiraju, G. R. Crystal Engineering: The Design of Organic Solids; Elsevier, New York, 1989.

26. Jones, M. N.; Chapman, D. Micelles, monolayers, and biomembranes; Wiley-Liss, New York, 1995.

27. Kumar, A.; Abbott, N. A.; Kim, E.; Biebuyck, H. A.; Whitesides, G. M. Patterned self-assembled monolayers and meso-scale phenomena. *Acc. Chem. Res*. **1995**, *28*, 219–226.

28. Bongrand, P. Ligand-receptor interactions. *Rep. Prog. Phys*. **1999**, *62*, 921–968.

29. Yadav, S.; Sharma, A. K. S.; Kumar, P. Nanoscale self-assembly for therapeutic delivery. *Front. Bioeng. Biotechnol*. **2020**, *8*, 1-24.

30. Lombardo, D.; Calandra, P.; Pasqua, L.; Magazù, S. Self-assembly of organic nanomaterials and biomaterials: the bottom-up approach for functional nanostructures formation and advanced applications. *Materials* **2020**, *13*, 1048.

31.Yuan, C.; Li, S.; Zou, Q.; Ren, Y.; Yan, X. Multiscale simulations for understanding the evolution and mechanism of hierarchical peptide self-assembly. *Phys. Chem. Chem. Phys*. **2017**, *19*, 23614-23631.

32. Liu, K.; Kang, Y.; Ma, G.; Mohwald, H.; Yan, X. Molecular and mesoscale mechanism for hierarchical self-assembly of dipeptide and porphyrin light-harvesting system. *Phys. Chem. Chem. Phys*. **2016**, *18*, 16738-16747.

33. Aggeli, A.; Nyrkova, I. A.; Bell, M.; Harding, R.; Carrick, L.; McLeish, T. C.; Semenov, A. N.; Boden, N. Hierarchical self-assembly of chiral rod-like molecules as a model for peptideβ-sheet tapes, ribbons, fibrils, and fibers. *Proc. Natl. Acad. Sci. U. S. A.* **2001**, *98*, 11857−11862.

34. Yang, L.; Tan, X.; Wang, Z.; Zhang, X. Supramolecular polymers: historical development, preparation, characterization, and functions. *Chem. Rev.* **2015**, *115*, 7196-7239.

35. Jia, Y.; Li, J. Molecular assembly of schiff base interactions: construction and application. *Chem. Rev.* **2015**, *115*, 1597-1621.

36. Zou, Q.; Zhang, L.; Yan, X.; Wang, A.; Ma, G.; Li, J.; Mohwald, H.; Mann, S. Multifunctional porous microspheres based on peptide porphyrin hierarchical co-assembly. *Angew. Chem., Int. Ed.* **2014**, *53*, 2366–2370.

37. Liu, K.; Xing, R.; Chen, C.; Shen, G.; Yan, L.; Zou, Q.; Ma, G.; Mçhwald, H.; Yan, X. Peptide-induced hierarchical long-range order and photocatalytic activity of porphyrin assemblies. *Angew. Chem. Int. Ed*. **2015**, *54*, 500-505.

38. Chang, R.; Zhao, L.; Xing, R.; Li, J.; Yan, X. Functional chromopeptide nanoarchitectonics: molecular design, self-assembly and biological applications. *Chem. Soc. Rev*. **2023**, *52*, 2688-2712.

39. Liu, K.; Kang, Y.; Ma, G.; Mohwald, H.; Yan, X. Molecular and mesoscale mechanism for hierarchical self-assembly of dipeptide and porphyrin light-harvesting system *Phys. Chem*. *Chem. Phys*. **2016**, *18*, 16738–16747.

40. Chen, C.; Liu, K.; Li, J.; Yan, X. Functional architectures based on self-assembly of bio-inspired dipeptides: Structure modulation and its photoelectronic applications. *Adv. Colloid Interface Sci*. **2015**, *225*, 177-193.

41. Abbas, M.; Zou, Q.; Li, S.; Yan, X. Self-assembled peptide- and protein-based nanomaterials for antitumor photodynamic and photothermal therapy. *Adv. Mater.* **2017**, *29*, 1605021.

42. Brito, A.; Kassem, S.; Reis, R. L.; Ulijn, R. V.; Pires, R. A.; Pashkuleva, I. Carbohydrate amphiphiles for supramolecular biomaterials: Design, self-assembly, and applications. *Chem*. **2021**, *7*, 2943-2964.

43. Zou, Q.; Liu, K.; Abbas, M.; Yan, X. Peptide-modulated self-assembly of chromophores toward biomimetic light-harvesting nanoarchitectonics. *Adv. Mater*. **2016**, *28*, 1031–1043.

44. Yan, X.; Zhua, P.; Li, J. Self-assembly and application of diphenylalanine-based nanostructures. *Chem. Soc. Rev*. **2010**, *39*, 1877–1890.

45. He, Q.; Duan, L.; Qi, W.; Wang, K.; Cui, Y.; Yan, X.; Li. J. Microcapsules containing a biomolecular motor for atp biosynthesis. *Adv. Mater*. **2008**, *20*, 2933–2937.

46. Ko, S. H.; Su, M.; Zhang, C.; Ribbe, A. E.; Jiang, W.; Mao, C. Synergistic self-assembly of RNA and DNA molecules. *Nat. Chem.* **2010**, *2*, 1050-1055.

47. Barbee, M. H.; Wright, Z. M.; Allen, B. P.; Taylor, H. F.; Patteson, E. F.; Knight, A. S. Protein-mimetic self-assembly with synthetic macromolecules. *Macromolecules* **2021**, *54*, 3585−3612.

48. Yamada, N.; Ariga, K.; Naito, M.; Matsubara, K.; Koyama, E. Regulation of β-sheet structures within amyloid-like-sheet assemblage from tripeptide derivatives. *J. Am. Chem. Soc*. **1998**, *120*, 12192–12199.

49. Zhang, S. Fabrication of novel biomaterials through molecular self-assembly. *Nat. Biotechnol*. **2003**, *21*, 1171–1178.

50. Gazit, E. Self-assembled peptide nanostructures: the design of molecular building blocks and their technological utilization. *Chem. Soc. Rev*. **2007**, *36*, 1263–1269.

51. Pochan, D.; Scherman, O. Introduction: molecular self-assembly. *Chem. Rev*. **2021**, *121*, 13699-13700.

52. Bromley, E. H. C.; Channon, K.; Moutevelis, E.; Woolfson, D. N. Peptide and protein building blocks for synthetic biology: from programming biomolecules to self-organized biomolecular systems. *ACS Chem. Biol*. **2008**, *3*, 38-50.

53. Davis, M. E.; Hsieh, P. C. H.; Takahashi, T.; Song, Q.; Zhang, S.; Kamm, R. D.; Grodzinsky, A. J.; Anversa, P.; Lee, R. T. Local myocardial insulin-like growth factor 1 (IGF-1) delivery with biotinylated peptide nano fibers improves cell therapy for myocardial infarction. *Proc. Natl. Acad. Sci. U. S. A.* **2006**, *103*, 8155– 8160.

54. Yan, X.; He, Q.; Wang, K.; Duan, L.; Cui, Y.; Li, J. Transition of cationic dipeptide nanotubes into vesicles and oligonucleotide delivery. *Angew. Chem. Int. Ed.* **2007**, *46*, 2431-2434.

55. Zhao, X.; Nagai, Y.; Reeves, P. J.; Kiley, P.; Khorana, H. G.; Zhang, S. Designer short peptide surfactants stabilize G protein-coupled receptor bovine rhodopsin. *Proc. Natl. Acad. Sci. U. S. A.* **2006**, *103*, 17707–17712.

56. Zhao, X.; Pan, F.; Xu, H.; Yaseen, M.; Shan, H.; Hauser, C. A. E.; Zhang, S.; Lu, J. R. Molecular self-assembly and applications of designer peptide amphiphiles. *Chem. Soc. Rev*. **2010**, *39*, 3480–3498.

57. Sinha, N. J.; Langenstein, M. G.; Pochan, D. J.; Kloxin, C. J.; Saven, J. G. Peptide design and self-assembly into targeted nanostructure and functional materials. *Chem. Rev.* **2021**, *121*, 13915−13935.

58. Santis, E. D.; Ryadnov. M. G. Peptide self-assembly for nanomaterials: the old new kid on the block *Chem. Soc. Rev*. **2015**, *44*, 8288-8300.

59. Rusiecka, I.; Gągało, I.; Kocić, I. Cell-penetrating peptides improve pharmacokinetics and pharmacodynamics of anticancer drugs. *Tissue barriers* **2022**, *10*, e1965418.

60. a) Hauser, C. A. E.; Zhang, S. Peptides as biological semiconductors. *Nature* **2010**, *468*, 516–517.

b) Kholkin, A.; Amdursky, N.; Bdikin, I.; Gazit, E.; Rosenman, G. Strong piezoelectricity in bioinspired peptide nanotubes. *ACS Nano* **2010**, *4*, 610–614.

61. Rajagopal, K.; Schneider, J. P. Self-assembling peptides and proteins for nanotechnological applications. *Curr. Opin. Struct. Biol.* **2004**, *14*, 480–486.

62. Ulijn, R. V.; Woolfson, D. N. Peptide and protein based materials in 2010: from design and structure to function and application. *Chem. Soc. Rev*. **2010**, *39*, 3349–3350.

63. Wang, J.; Liu, K.; Xinga, R.; Yan, X.; Peptide self-assembly: thermodynamics and kinetics. *Chem. Soc. Rev.* **2016**, *45*, 5589-5604.

64. Aono, M.; Ariga, K. The way to nanoarchitectonics and the way of nanoarchitectonics. *Adv. Mater*. **2016**, *28*, 989–992.

65. Ariga, K. Minami, K.; Ebara, M.; J. Nakanishi, J. What are the emerging concepts and challenges in NANO? Nanoarchitectonics, hand-operating nanotechnology, and mechanobiology. *Polym. J.* **2016**, *48*, 371-389.

66. Ariga, K.; Ji, Q.; Nakanishi, W.; Hill, J. P.; Aono, M.; Nanoarchitectonics: a new materials horizon for nanotechnology. *Mater. Horiz.* **2015**, *2*, 406-413.

67. Nakanishi, W.; Minami, K.; Shrestha, L. K.; Ji, Q.; Hill, J. P.; Ariga, K. Bioactive nanocarbon assemblies: Nanoarchitectonics and applications. *Nano Today* **2014**, *9*, 378-394.

68. Levin, A.; Hakala, T. A.; Schnaider, L.; Bernardes, G. J. L.; Gazit, E.; Knowles, T. P. J. Biomimetic peptide self-assembly for functional materials. *Nat. Rev. Chem.* **2020**, *4*, 615-634.

69. Cui, Y.; Kim, S. N.; Naik, R. R.; McAlpine, M. C. Biomimetic peptide nano sensors. *Acc. Chem. Res.* **2012**, *45*, 696-704.

70. Bromley, E. H. C.; Channon, K.; Moutevelis, E.; Woolfson, D. N. Peptide and protein building blocks for synthetic biology: from programming biomolecules to self-organized biomolecular systems. *ACS Chem. Biol.* **2008**, *3*, 38-50.

71. Wei, G.; Su, Z.; Reynolds, N. P.; Arosio, P.; Hamley, I. W.; Gazit, E.; Mezzenga. R. Self-assembling peptide and protein amyloids: from structure to tailored function in nanotechnology. *Chem. Soc. Rev.* **2017**, *46*, 4661-4708.

72. Gao, Y.; Wang, L.; Zhang, X.; Zhou, Z.; Shen, X.; Hu, H.; Sun, R.; Tang, J. Advances in self-assembled peptides as drug carriers. *Pharmaceutics* **2023**, *15*, 482.

73. Cui, H.; Muraoka, T.; Cheetham, A. G.; Stupp, S. I. Self-assembly of giant peptide nanobelts. *Nano Lett.* **2009**, *9*, 945–951.

74. T. J. Moyer, J. A. Finbloom, F. Chen, D. J. Toft, V. L. Cryns and S. I. Stupp, ph and amphiphilic structure direct supramolecular behavior in biofunctional assemblies. *J. Am. Chem. Soc*. **2014**, *136*, 14746-14752.

75. Korevaar, P. A.; Newcomb, C. J.; Meijer, E. W.; Stupp S. I., Pathway selection in peptide amphiphile assembly. *J. Am. Chem. Soc.* **2014**, *136*, 8540–8543.

76. Hamley, I. W.; Dehsorkhi, A.; Castelletto, V.; Furzeland, S.; Atkins, D.; Seitsonen, J.; Ruokolainen, J. Reversible helical unwinding transition of a self-assembling peptide amphiphile. *Soft Matter* **2013**, *9*, 9290-9293.

77. A. Dehsorkhi, A.; Castelletto, V.; Hamley, I. W. Self-assembling amphiphilic peptides. *J. Pept. Sci*. **2014**, *20*, 453-467.

78. Nellas, R. B.; Johnson, Q. R.; Shen, T. Solvent-induced α- to 3_{10}-helix transition of an amphiphilic peptide. *Biochemistry* **2013**, *52*, 7137-7144.

79. Qin, L.; Duan, P.; Xie, F.; Zhang, L.; and Liu, M. A metal ion triggered shrinkable supramolecular hydrogel and controlled release by an amphiphilic peptide dendron. *Chem. Commun.* **2013**, *49*, 10823-10825.

80. Sun, Y.; Qian, Z.; Guo, C.; Wei, G. Amphiphilic peptides A6k and V6k display distinct oligomeric structures and self-assembly dynamics: A combined all-atom and coarse-grained simulation study. *Biomacromolecules* **2015**, *16*, 2940-2949.

81. Cheng, H.; Cheng, Y. J.; Bhasin, S.; Zhu, J. Y.; Xu, X. D.; Zhuo, R. X.; Zhang, X. Z. Complementary hydrogen bonding interaction triggered co-assembly of an amphiphilic peptide and an anti-tumor drug. *Chem. Commun.* **2015**, *51*, 6936-6939.

82. Sukthankar, P.; Whitaker, S. K.; Garcia, M.; Herrera, A.; Boatwright, M.; Prakash, O.; Tomich, J. M. Thermally induced conformational transitions in nascent branched amphiphilic peptide capsules. *Langmuir* **2015**, *31*, 2946–2955.

83. Micklitsch, C. M.; Medina, S. H.; Yucel, T.; Nagy-Smith, K. J.; Pochan, D. J.; Schneider. J. P. Influence of hydrophobic face amino acids on the hydrogelation of β-hairpin peptide amphiphiles. *Macromolecules* **2015**, *48*, 1281–1288.

84. Zhou, P.; Deng, L.; Wang, Y.; Lu, J. R.; Xu, H. Different nanostructures caused by competition of intra- and inter-β-sheet interactions in hierarchical self-assembly of short peptides. *Colloid Interface Sci.* **2016**, *464*, 219–228.

85. Tsonchev, S.; Niece, K. L.; Schatz, G. C.; Ratner, M. A.; Stupp, S. I. Phase diagram for assembly of biologically-active peptide amphiphiles. *J. Phys. Chem. B* **2008**, *112*, 441-447.

86. Wang, C.; Fu, L.; Hu, Z.; Zhong, Y. A mini-review on peptide-based self-assemblies and their biological applications. *Nanotechnology* 2**021**, *33*, 062004.

87. Zhou, Y.; Li, Q.; Wu, Y.; Li, X.; Zhou, Y.; Wang, Z.; Liang, H.; Ding, F.; Hong, S.; Steinmetz, N. F.; Cai, H. Molecularly stimuli-responsive self-assembled peptide nanoparticles for targeted imaging and therapy. *ACS Nano* **2023**, *17*, 8004-8025.

88. Qi, G. B.; Gao, Y. J.; Wang, L.; Wang, H. Self-assembled peptide-based nanomaterials for biomedical imaging and therapy. *Adv. Mater*. **2018**, *30*, 1703444.

89. a) Wang, A.; Huang, J.; Yan, Y. Hierarchical molecular self-assemblies: construction and advantages. *Soft Matter* **2014**, *10*, 3362–3373. b) Shimanovich, U.; Levin, A.; Eliaz, D.; Michaels, T.; Toprakcioglu, Z.; Frohm, B.; de Genst, E.; Linse, S.; Åkerfeldt, K. S.; Knowles, T. P. J. pH-responsive capsules with a fibril scaffold shell assembled from an amyloidogenic peptide. *Small* **2021**, *17*, 2007188. c) Yao, Q.; Wu, G.; Hao, H.; Lu, H.; Gao, Y. Redox-mediated reversible supramolecular assemblies driven by switch and interplay of peptide secondary structures. *Biomacromolecules* **2021**, *22*, 2563−2572. d) Chibh, S.; Kour, A.; Yadav, N.; Kumar, P.; Yadav, P.; Chauhan, V. S.; Panda, J. J. Redox-responsive dipeptide nanostructures toward targeted cancer therapy. *ACS Omega* **2020**, *5*, 3365−3375.

90. Xu H.; Wang Y.; Ge X.; Han S.; Wang S.; Zhou P.; Shan H.; Zhao X.; Lu, J. R. Twisted nanotubes formed from ultrashort amphiphilic peptide i3k and their templating for the fabrication of silica nanotubes. *Chem. Mater.* **2010**, *22*, 5165–5173.

91. Lashuel, H. A.; LaBrenz, S. R.; Woo, L.; Serpell, L. C. S.; Kelly, J. W. Protofilaments, filaments, ribbons, and fibrils from peptide mimetic self-assembly: implications for amyloid fibril formation and materials science. *J. Am. Chem. Soc*. **2000**, *122*, 5262-5277.

92. Deng, M.; Yu, D.; Hou, Y.; Wang, Y. Self-assembly of peptide-amphiphile C12-aβ (11-17) into nanofibrils. *J. Phys. Chem. B* **2009**, *113*, 8539-8544

93. Matsumoto, K.; Vaughn, M.; Bruce, B. D.; Koutsopoulos, S.; Zhang, S. Designer peptide surfactants stabilize functional photosystem-i membrane complex in aqueous solution for extended time. *J. Phys. Chem. B.* **2009**, *113*, 75-83.

94. Zhou, M.; Smith, A. M.; Das, A. K.; Hodson, N. W.; Collins, R. F.; Ulijn, R. V.; Gough, J. E. Self-assembled peptide-based hydrogels as scaffolds for anchorage dependent cells. *Biomaterials* **2009**, *30*, 2523-2530.

95. Yongxin Li, Y.; Linyin Yan, L.; Kai Liu, K.; Juan Wang, J.; Anhe Wang, A.; Shuo Bai, S.; Xuehai Yan, X. Solvothermally mediated self-assembly of ultralong peptide nanobelts capable of optical waveguiding. *Small* **2016**, *12*, 19, 2575-2579.

96. Liu, L.; Xu, K.; Wang, H.; Tan, P. K. J.; Fan, W.; Venkatraman, S. S.; Li, L.; Yang, Y. Y. Self-assembled cationic peptide nanoparticles as an efficient antimicrobial agent. *Nat. Nanotechnol.* **2009**, *4*, 457-463.

97. Missirlis, D.; Khant, H.; Tirrell, M. Biochemistry Mechanisms of Peptide Amphiphile Internalization by SJSA-1 Cells *in Vitro*. *Biochemistry* **2009**, *48*, 3304-3314.

98. Reches, M.; Gazit, E. Casting metal nanowires within discrete self-assembled peptide nanotubes. *Science* **2003**, *300*, 625–627.

99. Gorbitz, C. H. The structure of nanotubes formed by diphenylalanine, the core recognition motif of Alzheimer's β-amyloid polypeptide. *Chem. Commun.* **2006**, 2332-2334

100. Reches, M.; and Gazit, E. Designed aromatic homo-dipeptides: formation of ordered nanostructures and potential nanotechnological applications. *Phys. Biol*. **2006**, *3*, S10–S19.

101. Reches, M.; Gazit, E. Self-assembly of peptide nanotubes and amyloid-like structures bycharged-termini-capped diphenylalanine peptide analogues. *Isr. J. Chem*. **2005**, *45*, 363–371.

102. Tang, C.; Ulijn, R. V.; Saiani, A. Effect of glycine substitution on fmoc-diphenylalanine self-assembly and gelation properties. *Langmuir* **2011**, *27*,14438-14449.

103. a) Adler-Abramovich, L.; Gazit, E. The physical properties of supramolecular peptide assemblies: from building block association to technological applications. *Chem. Soc. Rev*. **2014**, *43*, 6881-6893.

b) Manna, S. L.; Natale, C. D.; Valentina Onesto, V.; Marasco, D. Self-assembling peptides: from design to biomedical applications. *Int. J. Mol. Sci.* **2021**, *22*, 12662.

104. Fan, T.; Yu, X.; Shen, B.; Sun, L. Peptide self-assembled nanostructures for drug delivery applications. *J. Nanomater*. **2017**, 1-16. doi.org/10.1155/2017/4562474.

105. McCarthy, H. O.; McCaffrey, J.; McCrudden, C. M.; Zholobenko, A.; Ali, A. A.; McBride, J. W.; Massey, A. S.; Sreekanth Pentlavalli, S.; Chen, K. H.; Cole, G.; Loughran, S. P.; Dunne, N. J.; Donnelly, R. F.; Kett, V. L.; Robson, T. Development and characterization of self-assembling nanoparticles using a bio-inspired amphipathic peptide for gene delivery. *J. Controlled Release* **2014,** *189*, 141–149.

106. Stile, R. A.; Healy, K. E. Thermo-responsive peptide-modified hydrogels for tissue regeneration. *Biomacromolecules* **2001**, *2*, 1, 185–194.

107. Adhikari, B.; Palui, G.; Banerjee, A. Self-assembling tripeptide based hydrogels and their use in removal of dyes from waste-water. *Soft Matter* **2009**, *5*, 3452–3460.

108. Yang, X.; Xie, Y.; Wang, Y.; Qi, W.; Huang, R.; Su, R.; He, Z. Self-assembled microporous peptide-polysaccharide aerogels for oil–water separation. *Langmuir* **2018**, *34*, 36, 10732-10738.

109. Adhikari, B.; Banerjee, A. Short-peptide-based hydrogel: a template for the in situ synthesis of fluorescent silver nanoclusters by using sunlight. *Chem. Eur. J*. **2010**, *16*, 13698-13705.

110. Li, T.; Lu, X. M.; Zhang, M. R.; Hu, K.; Li, Z. Peptide-based nanomaterials: Self-assembly, properties and applications. *Bioact. Mater.* **2022**, *11*, 268-282.

111. Cai, Y.; Zheng, C.; Xiong, F.; Ran, W.; Zhai, Y.; Zhu, H. H.; Wang, H.; Li, Y.; Zhang, P. Recent progress in the design and application of supramolecular peptide hydrogels in cancer therapy. *Adv. Healthc. Mater.* **2021**, *10*, 2001239.

112. Sangeetha, N. M.; Maitra, U. Supramolecular gels: functions and uses. *Chem. Soc. Rev.* **2005**, *34*, 821-836.

113. Mondal, S.; Sujoy Das, S.; Nandi, A. K. A review on recent advances in polymer and Peptide hydrogels. *Soft Matter* **2020**, *16*, 1404-1454.

114. An, Y.; Solis, F. J.; Jiang, H. A thermodynamic model of physical gels. *J. Mech. Phys. Solids* **2010**, *58*, 2083–2099.

115. Ahn, S-K.; Kasi, R. M.; Kim, S. C.; Sharmaa, N.; Zhou, Y. Stimuli-responsive polymer gels. *Soft Matter* **2008**, *4*, 1151–1157.

116. Nayak, A. K.; Das. B. Introduction to polymeric gels, Editor(s): Kunal Pal, Indranil Banerjee, In Woodhead Publishing Series in Biomaterials, Polymeric Gels, Woodhead Publishing, 2018, 3-27, ISBN 9780081021798.

117. Pierre, A. C.; Pajonk, G. M. Chemistry of aerogels and their applications. *Chem. Rev*. **2002**, *102*, 4243−4265.

118. Frith, W.J.; Donald, A.M.; Adams, D.J.; Aufderhorst-Roberts, A. Gels formed from amino-acid derivatives, their novel rheology as probed by bulk and particle tracking rheological methods. *J. Nonnewton. Fluid Mech.* **2015**, *222*, 104-111.

119. Scott Banta, S.; Ian R. Wheeldon, I. R.; Mark Blenner, M. Protein engineering in the development of functional hydrogels. *Annu. Rev. Biomed. Eng*. **2010**, *12*, 167-186.

120. Xiong, X.; Zhou, C.; Wu, C.; Zhu, G.; Chen, Z.; Tan, W. Responsive DNA-based hydrogels and their applications. *Macromol. Rapid Commun.* **2013**, *34*, 1271–1283.

121. Wang, W.; Wang, H.; Ren, C.; Wang, J.; Tan, M.; Shen, J.; Yang, Z.; Wang, P. G.; Wang, L. A saccharide-based supramolecular hydrogel for cell culture. *Carbohydr. Res.* **2011**, *346*, 1013-1017.

122. Diaferia, C.; Netti, F.; Ghosh, M.; Sibillano, S.; Giannini, C.; Morelli, G.; Adler-Abramovich, L.; Accardo, A. Bi-functional peptide-based 3d hydrogel-scaffolds. *Soft Matter* **2020**, *16*, 7006-7017.

123. a) Silvaa, A.C.; Amaral, M.H.; González-Mirac, E.; Santos, D.; Ferreira, D.; Solid lipid nanoparticles (SLN)-based hydrogels as potential carriers for oral transmucosal delivery of Risperidone: Preparation and characterization studies. *Colloids Surf. B* **2012**, *93*, 241–248.

b) Wang, D.; Chen, H.; Song, B.; Yan, T.; Zhai, Z.; Pei, X.; Cui, Z. Supramolecular hydrogels with chiral nanofibril structures formed from β-cyclodextrin and a rosin-based amino acid surfactant. *Agric. Food Chem*. **2020**, *68*, 37, 10056-10062.

c) Appel, E. A.; Barrio, J. D., Loh, X. J.; Scherman, O. A. Supramolecular polymeric hydrogels. *Chem. Soc. Rev*. **2012**, *41*, 6195-6214.

124. Kumar, P.; Kadam, M. M.; Gaikar, V. G. Low molecular weight organogels and their application in the synthesis of cds nanoparticles. *Ind. Eng. Chem. Res.* **2012**, *51*, 15374−15385.

125. Jia, W.; Yuan, C.; Wang, F.; Liu, J.; Qin, M.; Yan, X.; Feng. C. Deciphering the structure-property relationship in coumarin-based supramolecular organogel materials. *Colloids Surf. A* **2020,** *597*, 124744.

126. Xue, P.; Boqi Yao, B.; Wang, P.; Gong, P.; Zhang, Z.; Lu. R.; Strong fluorescent smart organogel as a dual sensing material for volatile acid and organic amine vapors. *Chem. Eur. J.* **2015**, *21*, 17508-17515.

127. a) Yan Wang, Y.; Zhang, W.; Gong, C.; Liu, B.; Li, Y.; Wang, L.; Su, Z.; Wei, G. Recent advances in the fabrication, functionalization, and bioapplications of peptide hydrogels. *Soft Matter* **2020**, *16*, 10029-10045.

b) Jung, J. P.; Gasiorowski, J. Z.; Collier, J. H. Fibrillar peptide gels in biotechnology and biomedicine. *J. Pept. Sci.* **2010**, *94*, 49-50.

128. Anika M. Jonker, A. M.; Löwik, D. W. P. M.; Hest, J. C. M. V. Peptide and protein-based hydrogels. *Chem. Mater*. **2012**, *24*, 759−773.

129. Wang, J., Yan, X. (2018). Peptide-based hydrogels/organogels: assembly and application. In: Li, B., Jiao, T. (eds) Nano/Micro-structured materials for energy and biomedical applications. Springer, Singapore. https://doi.org/10.1007/978-981-10-7787-6-6.

130. Dasgupta, A.; Mondal, J. H.; Das, D. Peptide hydrogels. *RSC Adv*. **2013**, *3*, 9117-9149.

131. Sutton, S.; Campbell, N. L.; Cooper, A. I.; Kirkland, M.; Frith, W. J.; Adams, D. J. Controlled release from modified amino acid hydrogels governed bymolecular size or network dynamics. *Langmuir* **2009**, *25*, 10285–10291.

132. Ryan, D. M. R.; Anderson, S. B.; Nilsson, B. L. The influence of side-chain halogenation on the self-assembly and hydrogelation of Fmoc-phenylalanine derivatives. *Soft Matter* **2010**, *6*, 3220-3231.

133. a) Singh, N.; Kumar, M.; Miravet, J. F.; Ulijn, R. V.; Escuder, B. Peptide-based molecular hydrogels as supramolecular protein mimics. *Chem. Eur. J.* **2017**, *23*, 981-993.

b) Castillo-Díaz, L. A.; Ruiz-Pacheco, J. A.; Elsawy, M. A.; Reyes-Martinez, J. E.; Enríquez-Rodríguez, A. I. Self-assembling peptides as an emerging platform for the treatment of metabolic syndrome. *Int. J. Nanomed.* **2020**, *15*, 10349-10370.

c) Falcone, N.; Shao, T.; Rashid, R.; Kraatz. H-B.; Enzyme entrapment in amphiphilic myristyl-phenylalanine hydrogels. *Molecules* **2019**, *24*, 2884.

134. In-situ gelling polymers for biomedical applications. Xian Jun Loh Editor, ISSN 2196-8861 ISSN 2196-887X (electronic) ISBN 978-981-287-151-0 ISBN 978-981-287-152-7 (eBook) DOI 10.1007/978-981-287-152-7 Library of Congress Control Number: 201494949.

135. Manchineella, S.; Govindaraju, T. Hydrogen bond directed self-assembly of cyclic dipeptide derivatives: gelation and ordered hierarchical architectures. *RSC Advances* **2012**, *2*, 5539-5542.

136. Adhikari, B.; Singh, C.; Shah, A.; Lough, A. J. L.; Kraatz, H-B. Amino acid chirality and ferrocene conformation guided self-assembly and gelation of ferrocene-peptide conjugates. *Chem. Eur. J.* **2015**, *21*, 11560 -11572.

137. Fu, I. W.; Markegard, C. B.; Chu, B. K.; Nguyen, H. D. Role of hydrophobicity on self-assembly by peptide amphiphiles via molecular dynamics simulations. *Langmuir* **2014**, *30*, 7745-7754.

138. Rouse1, C. K.; Adam D. Martin, A. D.; Christopher J. Easton, C. J.; Thordarson, P. A Peptide Amphiphile organogelator of polar organic solvents. *Sci. Rep.* **2017**, *7*, 43668. DOI: 10.1038/srep43668

139. Yu, Y-C.; Tirrell, M.; Fields, G. B. Minimal lipidation stabilizes protein-like molecular architecture. *J. Am. Chem. Soc*. **1998**, *120*, 39, 9979-9987.

140. a) Das, T.; Häring, M.; Haldar, D.; Díaz, D. D. Phenylalanine and derivatives as versatile low-molecular weight gelators: design, structure and tailored function. *Biomater. Sci*. **2018**, *6*, 38-59.

b) Joseph Ibukun, O. J.; Gumtya, M. Singh, S.; Shit, A.; Haldar, D. Effect of the spacer on the structure and self-assembly of FF peptide mimetics. *Soft Matter* **2023**, *19*, 3215-3221.

c) Hartgerink, J. D.; Beniash, E.; Stupp, S. I. Self-assembly and mineralization of peptide amphiphile nanofibers. *Science* **2001**, *294*, 1684-1688.

141. Jayawarna, V.; Ali, M.; Jowitt, T. A.; Miller, A. F.; Saiani, A.; Gough, J. E.; Ulijn, R. V. Nanostructured hydrogels for three-dimensional cell culture through self-assembly of fluorenylmethoxycarbonyl-dipeptides. *Adv. Mater.* **2006**, *18*, 611-614.

142. Adams, D. J.; Mullen, L. M.; Berta, M.; Chen, L.; Frith, W. J. Relationship between molecular structure, gelation behaviour and gel properties of Fmoc-dipeptides. *Soft Matter* **2010**, *6*, 1971-1980.

143. Gazit, E. A possible role for -stacking in the self-assembly of amyloid fibrils. *FASEB Journal* **2002**, *16*, 77-83.

144. Fleming, S.; Ulijn, R. V. Design of nanostructures based on aromatic peptide amphiphiles *Chem. Soc. Rev.* **2014**, ***43***, 8150-8177.

145. Mahler, A.; Reches, M.; Rechter, M.; Cohen, S.; Gazit, E., Rigid, Self-assembled hydrogel composed of a modified aromatic dipeptide. *Adv. Mater.* **2006**, *18*, 1365- 1370.

146. Yan, X.; Zhu, P.; Li, J., Self-assembly and application of diphenylalanine-based nanostructures. *Chem. Soc. Rev*. **2010**, *39*, 1877-1890.

147. Zhang, J.; Liu, S.; Li, H.; Tian, X.; Li, X. Tryptophan-based self-assembling peptides with bacterial flocculation and antimicrobial properties. *Langmuir* **2020**, *36*, 11316–11323.

148. Jayawarna1, V.; Smith, A.; Gough, J. E.; Ulijn, R. V Three-dimensional cell culture of chondrocytes on modified di-phenylalanine scaffolds. *Biochem. Soc. Trans.* **2007**, *35*, 535-537.

149. Joyner, K.; Taraban, M. B.; Feng, Y.; Yu, Y. B. An interplay between electrostatic and polar interactions in peptide hydrogels. *Peptide Science* **2012**, *100*, 174-183.

150. a) Xing, R.; Li, S.; Zhang, N.; Shen, G.; Möhwald, H.; Yan, X. Self-assembled injectable peptide hydrogels capable of triggering antitumor immune response. *Biomacromolecules* **2017**, *18*, 3514-3523.

b) Ozbas, B.; Kretsinger, J.; Rajagopal, K.; Schneider, J. P. and Pochan, D. J. Salt-triggered peptide folding and consequent self-assembly into hydrogels with tunable modulus. *Macromolecules* **2004**, *37*, 7331-733710.

c) Chen, S.; Li, Z.; Zhang, C.; Wu, X.; Wang, W.; Huang, Q.; Chen, W.; Shi, J.; Yuan, D. Cation–π interaction trigger supramolecular hydrogelation of peptide amphiphiles. *Small* **2023**, *19*, 2301063.

151. Raza, F.; Zhu, Y.; Chen, L.; You, X.; Zhang, J.; Khan, A.; Khan, M. W.; Hasnat, M.; Zafar, H.; Wu, J.; Ge, L. Paclitaxel-loaded pH responsive hydrogel based on self-assembled peptides for tumor targeting. *Biomater. Sci.* **2019**, *7*, 2023-2036.

152. Vegners, R.; Shestakova, I.; Kawinsh, I.; Euell, R. M.; Janmey, P. A. Use of a gel-forming dipeptide derivative as a carrier for antigen presentation. *J. Pept. Sci.* **1995**, *1*, 371-378.

153. Huang, R.; Wang, Y.; Qi, W.; Su, R.; He, Z. Temperature-induced reversible self-assembly of diphenylalanine peptide and the structural transition from organogel to crystalline nanowire. *Nanoscale Res. Lett.* **2014**, *9*, 653.

154. Toledano, S.; Williams, R. J.; Jayawarna, V.; Ulijn, R. V. Enzyme-triggered self-assembly of peptide hydrogels via reversed hydrolysis. *J. Am. Chem. Soc.* **2006**, *128*, 1070-1071.

155. Pan, S.; Luo, S.; Li, S.; Lai, Y.; Geng, Y.; He, B.; Gu, Z. Ultrasound accelerated gelation of novel L-lysine based hydrogelators. *Chem. Commun*. **2013**, *49*, 8045—8047.

156. Micklitsch, C. M. Knerr, P. J.; Branco, M. C.; Nagarkar, R.; Pochan, D. J.; Schneider, J. P. Zinc-triggered hydrogelation of a self-assembling β-hairpin peptide. *Angew. Chem. Int. Ed*. **2011**, *50*, 1577 -1579.

157. Li, X.; Gao, Y.; Kuang, Y.; Xu, B. Enzymatic formation of a photoresponsive supramolecular hydrogel. *Chem. Commun*. **2010**, *46*, 5364-5366.

158. Bowerman, C. J.; Nilsson, B. L. A Reductive trigger for peptide self-assembly and hydrogelation. *J. Am. Chem. Soc*. **2010**, *132*, 9526–9527.

159. Ghosh, G.; Barman, R.; Sarkar, J.; Suhrit Ghosh, S.; pH-Responsive biocompatible supramolecular peptide hydrogel. *J. Phys. Chem. B* **2019**, *123*, 5909-5915.

160. Guoa, Q.; Liub, Y.; Mua, G.; Yanga, L.; Wangb, W.; Liu, J.; Liu, J. A Peptide-drug hydrogel to enhance anti-cancer activity of chlorambucil. *Biomater. Sci*. **2020**, *8*, 5638-5646.

161. a) Qi, J.; Yan, Y.; Cheng, B.; Deng, L.; Shao, Z.; Sun, Z.; Li, X. Enzymatic formation of an injectable hydrogel from a glycopeptide as a biomimetic scaffold for vascularization. *ACS Appl. Mater. Interfaces* **2018**, *10*, 6180−6189.

b) Yia, M.; Guoa, J.; Hea, H.; Tana, W.; Harmonb, N.; Ghebreyessus, K.; Xu, B. Phosphobisaromatic motifs enable rapid enzymatic self-assembly and hydrogelation of short peptides. *Soft Matter* **2022**, *17*, 8590-8594.

c) Toledano, S.; Williams, R. J.; Jayawarna, V.; Ulijn, R. V. Enzyme-Triggered Self-Assembly of Peptide hydrogels via reversed hydrolysis. *J. Am. Chem. Soc*. **2006**, *128*, 1070-1071.

d) Yamamoto, S.; Nishimura, K.; Morita, K.; Kanemitsu, S.; Nishida, Y.; Morimoto, T.; Aoi, T.; Tamura, A.; Maruyama, T. Microenvironment pH-induced selective cell death for potential cancer

therapy using nanofibrous self-assembly of a peptide amphiphile. *Biomacromolecules* **2021**, *22*, 2524−2531.

e) Roth-Konforti, M. E.; Comune, M.; Halperin-Sternfeld, M.; Grigoriants, I.; Shabat, D.; Adler-Abramovich, L. UV Light-responsive peptide-based supramolecular hydrogel for controlled drug delivery. *Macromol. Rapid Commun*. **2018**, *39*, 1800588.

f) Cao, M.; Wang, Y.; Hu, X.; Gong, H.; Li, R.; Cox, H.; Zhang, J.; Waigh, T. A.; Xu, H.; Lu, J. R. Reversible thermoresponsive peptide PNIPAM hydrogels for controlled drug delivery. *Biomacromolecules* **2019**, *20*, 3601-3610.

162. Maity, S.; Kumar, P.; Haldar, D. Sonication-induced instant amyloid-like fibril formation and organogelation by a tripeptide. *Soft Matter* **2011**, *7*, 5239–5245.

163. Knerr, P. J.; Branco, M. C.; Nagarkar, R.; Pochan, D. J.; Schneider, J. P. Heavy metal ion hydrogelation of a self-assembling peptide via cysteinyl chelation. *J. Mater. Chem*. **2012**, *22*, 1352-1357.

164. Sharma, P.; Kaur, H.; Roy, S. Inducing differential self-assembling behaviour in ultrashort peptide hydrogelators using simple metal salts. *Biomacromolecules* **2019**, *20*, 2610-2624.

165. Yagai, S.; Karatsu, T.; Kitamura, A. Photocontrollable self-assembly. *Chem. Eur. J.* **2005**, *11*, 4054-4063

166. Dey, A.; Biradha, K. Photochemical reactions in supramolecular assemblies of gels: dimerizations and polymerizations via pericyclic reactions. *Isr. J. Chem*. **2018**, *58*, 1-14.

167. Huang, Y.; Qiu, Z.; Xu, Y.; Shi, J.; Lina, H.; Zhang, Y. Supramolecular hydrogels based on short peptides linked with conformational switch. *Org. Biomol. Chem*. **2011**, *9*, 2149-2155.

168. Roth-Konforti, M. E.; Comune, M.; Halperin-Sternfeld, M.; Grigoriants, I.; Shabat, D.; Adler-Abramovich, L. UV Light–responsive peptide-based supramolecular hydrogel for controlled drug delivery. *Macromol. Rapid Commun.* **2018**, 1800588.

169. Paterov, J.; Rembert, K. B.; Heyda, J.; Kurra, Y.; Okur, H. I.; Liu, W. R.; Hilty, C.; Cremer, P. S.; Jungwirth, P. Reversal of the Hofmeister series: specific ion effects on peptides *J. Phys. Chem. B* **2013**, *117*, 8150-8158.

170. Roy, S.; Javid, N.; Sefcik, J.; Halling, P. J.; Ulijn, R. V. Salt-induced control of supramolecular order in biocatalytic hydrogelation. *Langmuir* **2012**, *28*, 16664-16670.

171. Nebot, V. J.; Ojeda-Flores, J. J. Smets, J.; Fernandez-Prieto, S.; Escuder, B.; Miravet, J. F. Rational design of heat-set and specific-ion-responsive supramolecular hydrogels based on the Hofmeister effect. *Chem. Eur. J.* **2014**, *20*, 14465-14472.

172. Petka, W. A.; Harden, J. L.; McGrath, K. P.; Wirtz, D.; Tirrell, D. A. Reversible hydrogels from self-assembling artificial proteins. *Science* **1998**, *281*, 389–392.

173. Wang, C.; Stewart, R. J.; Kopecc˘ek, J. Hybrid hydrogels assembled from synthetic polymers and coiled-coil protein domains. *Nature* **1999**, *397*, 417–420.

174. Potekhin, S. A.; Melnik, T. N.; Popov, V.; Lanina, N. F.; Vazina, A. A.; Rigler, P.; Verdini, A. S.; Corradin, G.; Kajava, A. V. De-Novo design of fibrils made of short α-helical coiled coil peptides. *Chem. Biol.* **2001**, *8*, 1025–1032.

175. Dong, H.; Paramonov, S. E.; Hartgerink, J. D. Self-assembly of α-helical coiled coil nanofibers. *J. Am. Chem. Soc.* **2008**, *130*, 13691–13695.

176. Gribbon, C.; Channon, K. J.; Zhang, W. J.; Banwell, E. F.; Bromley, E. H. C.; Chaudhuri, J. B.; Oreffo, R. O. C.; Woolfson, D. N. Magicwand: A single, designed peptide that assembles to stable, ordered α-helical fibers. *Biochemistry* **2008**, *47*, 10365–10371.

177. O'Leary, L. E. R.; Fallas, J. A.; Bakota, E. L.; Kang, M. K.; Hartgerink, J. D. Multi-hierarchical self assembly of a collagen mimetic peptide from triple helix to nanofibre and hydrogel. *Nat. Chem.* **2011**, *3*, 821–828.

178. Wychowaniec, J. K.; Smith, A. M.; Ligorio, C.; Mykhaylyk, O. O.; Miller, A. F.; Saiani, A. Role of sheet-edge interactions in β-sheet self-assembling peptide hydrogels. *Biomacromolecules* **2020**, *21*, 6, 2285–2297.

179. Kim, S.; Kim, J. H.; Lee, J. S.; Park, C. B. β-sheet-forming, self-assembled peptide nanomaterials towards optical, energy, and healthcare applications. *Small* **2015**, *11*, 3623-3640.

180. Aggeli, A.; Bell, M.; Carrick, L. M.; Fishwick, C. W. G.; Harding, R.; Mawer, P. J.; Radford, S. E.; Strong, A. E.; Boden, N. pH as a Trigger of peptide β-sheet self-assembly and reversible switching between nematic and isotropic phases. *J. Am. Chem. Soc.* **2003**, *125*, 9619-9628.

181. Krejchi, M. T.; Atkins, E. D. T.; Waddon, A. J.; Fournier, M. J.; Mason, T. L.; Tirell, D. A. Chemical sequence control of β-sheet assembly in macromolecular crystals of periodic polypeptides. *Science* **1994**, *265*, 1427-1432.

182. Osterman, D. G.; Kaiser, E. T. Design and characterization of peptides with amphiphilic β-strand structures. *J. Cell. Biochem.* **1985**, *29*, 57-72.

183. Aggeli, A.; Bell, M.; Boden, N.; Keen, J. N.; McLeish, T. C. B.; Nyrkova, I.; Radford, S. E.; Semenov, A. Engineering of peptide β-sheet nanotapes. *J. Mater. Chem.* **1997**, *7*, 1135–1145.

184. Schneider, J. P.; Pochan, D. J.; Ozbas, B.; Rajagopal, K.; Pakstis, L.; Kretsinger, J. Responsive hydrogels from the intramolecular folding and self-assembly of a designed peptide. *J. Am. Chem. Soc.* **2002**, *124*, 15030–15037.

185. Dong, H., Paramonov, S. E., and Hartgerink, J. D. Self-assembly of α-helical coiled coil nanofibers. *J. Am. Chem. Soc*. **2008**, *130*, 13691–13695.

186. Mehrban, N.; Zhu, B.; Tamagnini, F.; Young, F. I.; Wasmuth, A.; Hudson, K. L.; Thomson, A. R.; Birchall, M. A.; Randall, A. D.; Song, B.; Woolfson, D. N. Functionalized α-helical peptide hydrogels for neural tissue engineering. *ACS Biomater. Sci. Eng.* **2015**, *1*, 6, 431-439.

187. Pal, A.; Dey, J. Water-induced physical gelation of organic solvents by n-(n-alkylcarbamoyl)-L-alanine amphiphiles. *Langmuir* **2011**, *27*, 3401–3408.

188.Fuentes-Caparrós, A. M.; McAulay, K.; Rogers, S. E.; Dalgliesh, R. M.; Adams, D. J. On the mechanical properties of n-functionalised dipeptide gels. *Molecules* **2019**, *24*, 3855. doi:10.3390/molecules24213855.

189. Zhu, J.; Tang, C.; Kottke-Marchant, K.; Marchant, R. E. Design and synthesis of biomimetic hydrogel scaffolds with controlled organization of cyclic rgd peptides. *Bioconjugate Chem.* **2009**, *20*, 333–339.

190. Greenfield, M. A.; Hoffman, J. R.; De la Cruz, M. O.; Stupp, S. I. Tunable mechanics of peptide nanofiber gels. *Langmuir* **2010**, *26*, 3641–3647.

191. Taraban, M. B.; Ramachandran, S.; Gryczynski, I.; Gryczynski, Z.; Trewhella, J.; Yu. Y. B. Effects of chain length on oligopeptide hydrogelation. *Soft Matter* **2011**, *7*, 2624-2631.

192. Yang, Z.; Liang, G.; Xu, B. Supramolecular hydrogels based on β-amino acid derivatives. *Chem. Commun.* **2006**, *7*, 738–740.

193. Bhattacharya, S.; and Krishnan-Ghosh, Y. First report of phase selective gelation of oil from oil/water mixtures. Possible implications toward containing oil spills. *Chem. Commun.* **2001**, 185-186. DOI: 10.1039/b007848o.

194. Kuang, G. C.; Teng, M. J.; Jia, X. R.; Chen, E. Q.; Wei, Y. Polymorphism of amino acid-based dendrons: from organogels to microcrystals. *Chem. Asian J.* **2011**, *6*, 1163-1170.

195. Dasgupta, A.; Das, D. Designer peptide amphiphiles: self-assembly to applications. *Langmuir* **2019**, *35*, 10704-10724.

196. Dowari, P.; Pramanik, B.; Das, D. pH and secondary structure instructed aggregation to a thixotropic hydrogel by a peptide amphiphile. *Bull. Mater. Sci.* **2020**, *43*, 1-7.

197. Diegelmann, S. R.; Gorham, J. M.; Tovar, J. D. One-dimensional optoelectronic nanostructures derived from the aqueous self-assembly of pi-conjugated oligopeptides. *J. Am. Chem. Soc.* **2008**, *130*, 13840.

198. Miravet, J. F.; Escuder, B. Pyridine-functionalised ambidextrous gelators: towards catalytic gels. *Chem. Commun.* **2005**, 5796-5798.

199. Maity, I.; Rasale, D. B.; Das, A. K. Exploiting a self-assembly driven dynamic nanostructured library. *RSC Adv.* **2013**, *3*, 6395–6400.

200. a) Ma, M.; Kuang, Y.; Gao, Y.; Zhang, Y.; Gao, P.; Xu, B. Aromatic-aromatic interactions induce the self-assembly of pentapeptidic derivatives in water to form nanofibers and supramolecular hydrogels. *J. Am. Chem. Soc*. **2010**, *132*, 2719;

b) Cui, H.; Cheetham, A. G.; Pashuck, E. T.; Stupp, S. I. Amino acid sequence in constitutionally isomeric tetrapeptide amphiphiles dictates architecture of one-dimensional nanostructures. *J. Am. Chem. Soc*. **2014**, *136*, 12461.

c) Fleming, S.; Ulijn, R. V. Fmoc-modified amino acids and short peptides: simple bio-inspired building blocks for the fabrication of functional materials. *Chem. Soc. Rev.* **2014**, *43*, 8150.

d) Tao, K.; Levin, A.; Adler-Abramovich, L.; Gazit, E. Fmoc-modified amino acids and short peptides: simple bio-inspired building blocks for the fabrication of functional materials. *Chem. Soc. Rev.* **2016**, *45*, 3935-3953.

201. Méndez-Ardoy, A.; Granja, J. R.; Montenegro, J. pH-Triggered self-assembly and hydrogelation of cyclic peptide nanotubes confined in water micro-droplet. *Nanoscale Horiz.* **2018**, *3*, 391-396.

202. Shaikh, H.; Rho, J. Y.; Macdougall, L. J.; Gurnani, P.; Lunn, A. M.; Yang, J.; Huband, S.; Mansfield, E. D. H.; Peltier, R.; Perrier, S. Hydrogel and organogel formation via hierarchical self-assembly of cyclic peptides nanotubes. *Chem. Eur. J.* **2018**, *24*, 19066-19074.

203. Duan, P.; Qin, L.; Zhu, X.; Liu, M. Hierarchical self-assembly of amphiphilic peptide dendrons: evolution of diverse chiral nanostructures through hydrogel formation over a wide pH range. *Chem. Eur. J.* **2011**, *17*, 6389 – 6395.

204. Spitzer, D.; Marichez, V.; Formon, G. J. M.; Besenius, P.; Hermans, T. M. Surface-assisted self-assembly of a hydrogel by proton diffusion. *Angew. Chem. Int. Ed.* **2018**, *57*, 11349-11353.

205. a) Munita, J. M.; Arias C. A. Mechanism of antibiotic resistance. *Microbiol. Spectr.* **2016**, *4*, 0016-2015.

b) Chen, J.; Peng, Q.; Peng, X.; Han, L.; Wang, X.; Wang, J.; Zeng, H. Recent advances in mechano-responsive hydrogels for biomedical applications. *ACS Appl. Polym. Mater.* **2020**, *2*, 1092−1107.

c) Bordbar-Khiabani, A.; Gasik, M. Smart hydrogels for advanced drug delivery systems. *Int. J. Mol. Sci.* **2022**, *23*, 3665.

d) Kulkarni, N.; Rao, P.; Jadhav, G. S.; Kulkarni, B.; Kanakavalli, N.; Kirad, S.; Salunke, S.; Tanpure, V. Sahu, B. Emerging role of injectable dipeptide hydrogels in biomedical applications. *ACS Omega* **2023**, *8*, 3551−3570.

206. Hiltunen, T.; Virta, M.; Laine, A. L. Antiboitic resistance in the wild: an eco-evolutionary perspective. *Philos Trans R Soc Lond B Biol Sci.* **2017**, *372*, 1712.

207. Khoury, A. E.; Lam, K.; Ellis, B.; Costerton, J. W. Prevention and control of bacterial infections associated with medical devices. *ASAIO J*. **1992**, *38*, 174−178.

208. Ventola, C. L. The antibiotic resistance crisis. *P T*. **2015**, *40*, 277–283.

209. Mor, A.; Nicolas, P. The NH_2-terminal alpha-helical domain 1-18 of dermaseptin is responsible for antimicrobial activity. *J. Biol. Chem*. **1994**, *269*, 1934-1939.

210. Li, W.; Separovic, F.; Brien-simpson, O.; Wade, J. D. Chemically modified and conjugated antimicrobial peptides against superbugs. *Chem. Soc. Rev.* **2021**, *50*, 4932-73.

211. Gan, B. H.; Gaynord, J.; Rowe, S. M.; Deingruber, T.; Spring, D. R. The multifaceted nature of antimicrobial peptides: current synthetic chemistry approaches and future directions. *Chem Soc. Rev*. **2021**, *50*, 7820-7880.

212. Nandi, N.; Gayen, K.; Ghosh, S.; Bhunia, D.; Kirkham, S.; Sen, S.K.; S. Ghosh, S.; Hamley, I.W.; Banerjee, A. Amphiphilic peptide-based supramolecular, noncytotoxic, stimuli-responsive, hydrogels with antibacterial activity. *Biomacromolecules* **2017**, *18*, 3621–3629.

213. Salick, D.A.; Kretsinger, J. K.; Pochan, D.J.; Schneider, J.P. Inherent antibacterial activity of a peptide-based β-hairpin hydrogel. *J. Am.Chem. Soc.* **2007**, *129*, 14793-14799.

214. David I. Chan, Elmar J. Prenner, Hans J. Vogel. Tryptophan and arginine-rich antimicrobial peptides: Structures and mechanisms of action. *Biochim. Biophys. Acta* **2006**, *1758*, 1184-1202.

215. Salick, D. A.; Pochan, D. J.; Schneider, J. P. Design of an injectable β-hairpin peptide hydrogel that kills methicillin-resistant *Staphylococcus aureus*. *Adv Mater*. **2009**, *21*, 4120-4123.

216. Veiga, A.S.; Sinthuvanich, C.; Gaspar, D.; Franquelim, H.G.; Castanho, M.; Schneider, J.P. Arginine-rich self-assembling peptides as potent antibacterial gels. *Biomaterials* **2012**, *33*, 8907–8916.

217. Baral, A.; Roy, S.; Ghosh, S.; Merino, D.H.; Hamley, I.W.; Banerjee, A. A Peptide-based mechano-sensitive, proteolytically stable hydrogel with remarkable antimicrobial properties. *Langmuir* **2016**, *32*, 1836.

218. Musaimi, O. A.; Lombardi, L.; Williams, D. R.; Albericio, F. Strategies for improving peptide stability and delivery. *Pharmaceuticals* **2022**, *15*, 1283.

219. a) Malhotra, K.; Shankar, S.; Rai, R.; Singh, Y. Broad-spectrum antibacterial activity of proteolytically stable self-assembled αγ-hybrid peptide gels. *Biomacromolecules*. **2018**, *19*, 782-792.

b) Sarkar, B.; Siddiqui, Z.; Nguyen, P. K.; Dube, N.; Fu, W.; Park, S.; Jaisinghani, S.; Paul, R.; Kozuch, S. D.; Deng, D.; Iglesias-Montoro, P.; Li, M.; Sabatino, D.; Perlin, D. S.; Zhang, W.; Mondal, J.; Kumar. V. A. Membrane-disrupting nanofibrous peptide hydrogels. *ACS Biomater. Sci. Eng.* **2019**, *5*, 4657−4670.

c) Adak, A.; Ghosh, S.; Gupta, V.; Ghosh, S. Biocompatible lipopeptide-based antibacterial hydrogel. *Biomacromolecules* **2019**, *20*, 1889−1898.

d) Guo, Z.; Wang, Y.; Tan, T.; Ji, Y.; Hu, J.; Zhang, Y. Antimicrobial D-peptide hydrogels. *ACS Biomater. Sci. Eng.* **2021**, *7*, 1703−1712.

e) Edirisinghe, D. I. U.; D'Souza, A.; Ramezani, M.; Carroll, R. J.; Chicón, Q.; Muenzel, C. L.; Soule, J. S.; Monroe, M. B. B.; Patteson, A. E.; Makhlynets, O. V. Antibacterial and cytocompatible pH-responsive peptide hydrogel. *Molecules* **2023**, *28*, 4390.

220. Koutsopoulos, S.; Zhang, S. Long-term three-dimensional neural tissue cultures in functionalized self-assembling peptide hydrogels, Matrigel and Collagen I. *Acta Biomater*. **2013**, *9*, 5162–5169.

221. Ghosh, M.; Halperin-Sternfeld, M.; Grinberg, I.; Adler-Abramovich, L. Injectable alginate-peptide composite hydrogel as a scaffold for bone tissue regeneration. *Nanomater.* **2019**, *9*, 497.

222. Dou, X. Q.; Feng. C. L. Amino acids and peptide-based supramolecular hydrogels for three-dimensional cell culture. *Adv. Mater.* **2017**, *29*, 1604062.

223. Castillo Diaz, L. A.; Elsawy, M.; Saiani, A.; Gough, J. E.; Miller, A. F. Osteogenic differentiation of human mesenchymal stem cells promotes mineralization within a biodegradable peptide hydrogel. *J. Tissue Eng.* **2016**, *7*, 1–15.

224. Kisiday, J.; Jin, M.; Kurz, B.; Hung, H.; Semino, C.; Zhang, S.; Grodzinsky, A. J. Self-assembling peptide hydrogel fosters chondrocyte extracellular matrix production and cell division: Implications for cartilage tissue repair. *Proc. Natl. Acad. Sci. U. S. A.* **2002**, *99*, 9996–10001.

225. Tang, J. D.; Mura, C.; and Lampe, K. J. A stimuli-responsive, pentapeptide, nanofiber hydrogel for tissue engineering. *J. Am. Chem. Soc.* **2019**, *141*, 4886-4899.

226. Worthington, P.; Pochan, D. J.; Langhans, S. A. Peptide hydrogels-versatile matrices for 3D cell culture in cancer medicine. *Front. Oncol*. **2015**, *5*, 1.

227. Yang, Z.; Zhao, X. A 3D model of ovarian cancer cell lines on peptide nanofiber scaffold to explore the cell-scaffold interaction and chemothera- peutic resistance of anticancer drugs. I*nt. J. Nanomed.* **2011**, *6*, 303–10.

228. Zhang, S.; Gelain, F.; Zhao, X. Designer self-assembling peptide nanofiber scaffolds for 3D tissue cell cultures. *Semin. Cancer Biol.* **2005**, *15*, 413–20.

229. Zhang, S.; Lockshin, C.; Herbert, A.; Winter, E.; Zuotin, R. A. a putative Z-DNA binding protein in Saccharomyces cerevisiae. *EMBO J*. **1992**, *11*, 3787–96.

230. Zhang, S.; Holmes, T. C.; DiPersio, C. M, Hynes, R. O.; Su, X.; Rich, A. Self-complementary oligopeptide matrices support mammalian cell attachment. *Biomaterials* **1995**, *16*, 1385–93.

231. Luo, Z.; Yue, Y.; Zhang, Y.; Yuan, X.; Gong, J.; Wang, L. Designer D-form self-assembling peptide nanofiber scaffolds for 3-dimensional cell cultures. *Biomaterials* **2013**, *34*, 4902–13.

232. Yan, C.; Mackay, M. E.; Czymmek, K.; Nagarkar, R. P.; Schneider, J. P.; Pochan, D. J. Injectable solid peptide hydrogel as cell carrier: effects of shear flow on hydrogel and cell payload. *Langmuir* **2012**, *28*, 6076–6087.

233. Restua, W. K.; Yamamoto, S.; Nishidaa, Y.; Ienagab, H.; Aoib, T.; Maruyama, T. Hydrogel formation by short D-peptide for cell-culture scaffolds. *Mater. Sci. Eng. C* **2020**, *111*, 110746.

234. Su, C. W.; Chiang, C. S.; Li, W. M.; Hu, S. H.; Chen, S. Y. Multifunctional Nanocarriers for simultaneous encapsulation of hydrophobic and hydrophilic drugs in cancer treatment. *Nanomed.* **2014**, *9*, 1499–1515.

235. a) Rosler, A.; Vandermeulen, G. W. M.; Klok, H. A. Advanced drug delivery devices via self-assembly of amphiphilic block copolymers. *Adv. Drug Deliv. Rev.* **2001**, *53*, 95–108.

b) West, K. R.; Otto, S. Reversible covalent chemistry in drug delivery. *Curr. Drug Deliv. Technol.* **2005**, 2, 123-160.

c) Al-Hilal, T. A.; Alam. F.; Byun, Y. Oral drug delivery systems using chemical conjugates or physical mixing. *Adv. Drug Deliv. Rev.* **2013**, *65*, 845-864.

d) Ulbrich, K.; Holá, K.; Šubr, V.; Bakandritsos, A.; Tuček, J.; Zbořil, R. Targeted drug delivery with polymers and magnetic nanoparticles: covalent and noncovalent approaches, release control, and clinical studies. *Chem. Rev.* **2016**, *116*, 5338-5431.

e) Mu, Y.; Gong, L.; Peng, T.; Yao, J.; Lin, Z. Advances in pH-responsive drug delivery systems. *Open Nano* **2021**, *5*, 1000031.

f) Shahriari, M.; Zahiri, M.; Abnous, K.; Taghdisi, S. M.; Ramezani, M.; Alibolandi, M. Enzyme responsive drug delivery systems in cancer treatment. *J. Controlled Release* **2019**, *308*, 172-189.

g) Vargason, A. M.; Anselmo, A. C.; Mitragotri, S. The evolution of commercial drug delivery technologies. *Nat. Biomed. Eng.* **2021**, *5*, 951-967.

h) Nabipour, H.; Hu, Y. Sustainable drug delivery systems through green nanotechnology in Nano engineered biomaterials for advanced drug delivery, *Elsevier* 2020.

i) Manzari, M. T.; Shamay, Y.; Kiguchi, H.; Rosen, N.; Scaltriti, M.; Heller, D. A. Targeted drug delivery strategies for precision medicine. *Nat. Rev. Mat.* **2021**, *6*, 351-370.

j) Li, F.; Mahato, R. I. Bioconjugate therapeutics: current progress and future perspective. *Mol. Pharmaceutics* **2017**, *14*, 1321-1324.

k) Dada, S. N.; Babanyinah, G. K.; Tetteh, M. T.; Palau, V. E.; Walls, Z. F.; Krishnan, K.; Croft, Z.; Khan, A. U.; Liu, G.; Wiese, T. E.; Glotser, E.; Mei, H. Covalent and noncovalent loading of doxorubicin by folic acid-carbon dot nanoparticles for cancer theranostics. *ACS Omega* **2022**, *7*, 23322-23331.

l) Lin, R.; Cui, H. Supramolecular nanostructures as drug carriers. *Curr. Opin. Chem. Eng*. **2015**, *7*, 75-83.

m) Gao, Y.; Wang, L.; Zhang, X.; Zhou, Z.; Shen, X.; Hu, H.; Sun, R.; Tang, J. Advances in self-assembled peptides as drug carriers. *Pharmaceutics* **2023**, *15*, 1-20. n) Liu, P.; Chen, G.; Zhang, J. A review of liposomes as a drug delivery system: current status of approved products, regulatory environments, and future perspectives. *Molecules* **2022**, *27*, 1372.

236. Thota, C. K.; Yadav, N.; Chauhan, V. S. A novel highly stable and injectable hydrogel based on a conformationally restricted ultrashort peptide. *Sci. Rep.* **2016**, *6*, 31167.

237. Yishay-Safranchika, E.; Golana, M.; David, A. Controlled release of doxorubicin and Smac-derived pro-apoptotic peptide from self-assembled KLD-based peptide hydrogels *Polym. Adv. Technol.* **2014**, *25*, 539–544.

238. Liu, J.; Zhang, L.; Yang, Z.; Zhao, X. Controlled release of paclitaxel from a self-assembling peptide hydrogel formed in situ and antitumor study in vitro. *Int. J. Nanomed.* **2011**, 6, 2143–2153.

239. Karavasili, C.; Panteris, E.; Vizirianakis, I. S.; Koutsopoulos, S.; Fatouros, D. G. Chemotherapeutic delivery from a self-assembling peptide nanofiber hydrogel for the management of glioblastoma. *Pharm. Res.* **2018**, *35*, 166.

240. Tang, C.; Miller, A. F.; Saiani, A. Peptide hydrogels as muco adhesives for local drug delivery. *Int. J. Pharm*. **2014**, *465*, 427–435.

241. Yi Li, Y.; Feihu Wang, F.; Honggang Cui, H. Peptide-based supramolecular hydrogels for delivery of biologics. *Bioeng. Transl. Med.* **2016**, *1*, 306-322.

242. a) Koutsopoulos, S.; Unsworth. L. D.; Nagai, Y.; Zhang, S. Controlled release of functional proteins through designer self-assembling peptide nanofiber hydrogel scaffold. *Proc. Natl. Acad. Sci. U. S. A.* **2009**, *106*, 4623– 4628.

b) Roy, K.; Pandit, G.; Chetia, M.; Sarkar, A. K.; Chowdhury, S.; Bidkar, A. P.; Chatterjee, S. Peptide hydrogels as platforms for sustained release of antimicrobial and antitumor drugs and proteins. *ACS Appl. Bio Mater.* **2020**, *3*, 6251–6262.

243. Bhalla, N.; Jolly, P.; Formisano, N.; Estrela. P. Introduction to biosensors. *Essays Biochem*. **2016**, *60*, 1-8.

244. Kim, J. H.; Lim, S. Y.; Nam, D. H.; Ryu, J.; Ku, S. H.; Park, C. B. Self-assembled, photoluminescent peptide hydrogel as a versatile platform for enzyme-based optical biosensors. *Biosens. Bioelectron*. **2011**, *26*, 1860–1865.

245. Lian, M.; Chen, X.; Lu, Y.; Yang, W. Self-assembled peptide hydrogel as a smart biointerface for enzyme-based electrochemical biosensing and cell monitoring. *ACS Appl. Mater. Interfaces* **2016**, *8*, 25036-25042.

246. King, P. J. S.; Saiani, A.; Bichenkova, E. V.; Miller, A. F. A de novo self-assembling peptide hydrogel biosensor with covalently immobilised DNA-recognising motifs. *Chem. Commun.* **2016**, *52*, 6697-6700.

247. a) Jaishankar, M.; Tseten, T.; Anbalagan, N.; Mathew, B. B.; Beeregowda, K. N. Toxicity, mechanism and health effects of some heavy metals. *Interdiscip. Toxicol.* **2014**, *7(2)*, 60–72.

b) Flora, G.; Gupta, D.; Tiwari, A. Toxicity of lead: A review with recent updates. *Interdiscip Toxicol.* 2012, 5, 47–58.

c) Chowdhury, S. R.; Nandi, S. K.; Haldar, D. Proof of Concept: Interface of recyclable organogels with embedded palladium nanoparticles catalyzing suzuki–miyaura coupling in water at room temperature. *ACS Omega* **2022**, *7*, 21566-21573

d) Kuzina, M. A.; Kartsev, D. D.; Stratonovich, A. V.; Levkin, P. A. Organogels versus hydrogels: advantages, challenges, and applications. *Adv. Funct. Mater.* **2023**, *33*, 2301421.

e) Erdogan, H.; Sakalak, H.; Yavuz, M. S.; Demirel, G. Laser-triggered degelation control of gold nanoparticle embedded peptide organogels. *Langmuir* **2013**, *29*, 6975−6982.

248. Patrick, L. Mercury toxicity and antioxidants: Part 1: role of glutathione and alpha-lipoic acid in the treatment of mercury toxicity. *Altern. Med. Rev*. 2002, 7, 456-471.

249. Ray, S.; Das, A.K.; Banerjee, A. pH-Responsive, Bolaamphiphile-based smart metallo-hydrogels as potential dye-adsorbing agents, water purifier, and vitamin B12 carrier. *Chem. Mater*. **2007**, *19*, 1633-1639.

250. S. Debnath, S.; Shome, A.; S. Dutta, S.; Das, P.K. Dipeptide-based low-molecular-weight efficient organogelators and their application in water purification. *Chem. Eur. J.* **2008**, *14*, 6870–6881.

251. Knerr, P.J.; Branco, M.C.; Nagarkar, R.; Pochan, D.J.; Schneider, J.P. Heavy metal ion hydrogelation of a self-assembling peptide via cysteinyl chelation. *J. Mater. Chem*. **2012,** *22*, 1352–1357.

252. Majumder, L.; Chatterjee, M.; Bera, K.; Maiti, N. C.; Banerji, B. Solvent-assisted tyrosine-based dipeptide forms low-molecular weight gel: preparation and its potential use in dye removal and oil spillage separation from water. *ACS Omega* **2019**, *4*, 14411-14419.

253. Basak, S.; Nandi, N.; Paul, S.; Hamley, I.W.; Banerjee, A. A tripeptide-based self-shrinking hydrogel for waste-water treatment: removal of toxic organic dyes and lead (Pb^{2+}) ions. *Chem. Commun.* **2017**, *53*, 5910.

254. Kar, T., Mukherjee, S.; Das, P. K. Organogelation through self-assembly of low-molecular-mass amphiphilic peptide. *New J. Chem.* **2014**, *38*, 1158-1167.

255. Li, Y.; Wang, L.; Removing organic dyes by a small peptide hydrogel. *Chem. Lett.* **2016**, *45*, 1253–1255.

256. a) Roy, K.; Ghosh, S.; Chetia, M.; Satpati, P.; Chatterjee, S. Dicyclohexylurea derivatives of amino acids as dye absorbent organogels and anion sensors. *Org. Biomol. Chem*. **2019**, *17*, 3026-3039. b) Roy, K.; Chetia, M.; Sarkar. A. K.; Chatterjee, S. Co-assembly of charge complementary peptides and their applications as organic dye/heavy metal ion (Pb^{2+}, Hg^{2+}) absorbents and arsenic(III/V) detectors. *RSC Adv.* **2020,** *10*, 42062-42075.

257. Schrope, M.; Deep wounds. *Nature* **2011**, *472*, 152–154.

258. Oil Spills R de la Huz, M Lastra, and J Lo´ pez & 2011 Elsevier B.V, 2011, 251-255, Encyclopedia of Environmental Health.

259. Schrope, M. A. Scientist at the centre of the spill: Vernon Asper was one of the first researchers in the Gulf of Mexico to study the oil gushing out from the BP well. But it has not all been smooth sailing. *Nature* **2010**, *466*, 680–684.

260. Li, J.; Huo, Y.; Zeng, H.; Combinatorial identification of a highly soluble phase-selective organogelator with high gelling capacity for crude oil gelation. *J. Mater. Chem. A.* **2018**, *6*, 10196-10200.

261. Chen, J.; Boott, C. E.; Lewis, L.; Siu, A.; Debasi, R. A.; Carta, V.; Fogh, A. A.; Kurek, D. Z.; Wang, L.; MacLachlan, M. J.; Hum., G. Amino acid-containing phase-selective organogelators: a waterbased delivery system for oil spill treatment. *ACS Omega* **2020**, *5*, 18758—18765.

262. Mondal, B.; Bairagi, D.; Nandi, N.; Hansda, B.; Das, K. S.; Edwards-Gayle, C. J. C.; Castelletto, V.; Hamley, I. W.; Banerjee. A.; Peptide-based gel in environmental remediation: removal of toxic organic dyes and hazardous Pb^{2+} and Cd^{2+} ions from wastewater and oil spill recovery. *Langmuir* **2020**, *36*, 12942-12953.

263. Reja, R. M.; Patel, R.; Kumar, V.; Jha, A.; Gopi, H. N. Divergent supramolecular gelation of backbone modified short hybrid δ-peptides. *Biomacromolecules* **2019**, *20*, 1254-1262.

264. Konda, M.; Maity, I.; Rasale, D. B.; Das. A. K. A new class of phase-selective synthetic β-amino acid based peptide gelator: from mechanistic aspects to oil spill recovery. *ChemPlusChem*. **2014**, *79*, 1482-1488.

265. Gayen, K.; Basu, K.; Bairagi, D.; Castelletto, V.; Hamley, I. W.; Banerjee, A. An amino acid based metallo-hydrogel that acts like an esterase. *ACS Appl. Bio Mater.* **2018**, *1*, 1717-1724.

266. Guler, M. O.; Stupp. S. I. A Self-assembled nanofiber catalyst for ester hydrolysis. *J. Am. Chem. Soc*. **2007**, *129*, 12082-12083.

267. Tena-Solsona, M.; Nanda, J.; Daz-Oltra, S.; Chotera, A.; Ashkenasy, G.; Escuder, B. Emergent catalytic behavior of self-assembled low molecular weight peptide-based aggregates and hydrogels. *Chem. Eur. J.* **2016**, *22*, 6687-6694.

268. Garcia, A. M.; Kurbasic, M.; Kralj, S.; Melchionnaa, M.; Marchesan, S. Biocatalytic and thermoreversible hydrogel from a histidine containing tripeptide. *Chem. Commun*. **2017**, *53*, 8110-8113.

269. Mazzier, D.; Carraro, F.; Crisma, M.; Rancan, M.; Toniolo, C.; Moretto, A. A terminally protected dipeptide: from crystal structure and self-assembly, through co assembly with carbon-based materials, to a ternary catalyst for reduction chemistry in water. *Soft Matter* **2016**, *12*, 238-245.

270. Bellotto, O.; Cringoli, M. C.; Perathoner, S.; Fornasiero, P.; Marchesan, S. Peptide gelators to template inorganic nanoparticle formation. *Gels* **2021**, *7*, 14.

271. Palui, G.; Nanda, J.; Ray, S.; Banerjee, A. Fabrication of luminescent cds nanoparticles on short-peptide-based hydrogel nanofibers: tuning of optoelectronic properties. *Chem. Eur. J.* **2009**, *15*, 6902-6909.

272. Mitra, R. N.; Das, P. K. In situ preparation of gold nanoparticles of varying shape in molecular hydrogel of peptide amphiphiles. *J. Phys. Chem. C.* **2008**, *112*, 8159–8166.

273. Shome, A.; Dutta, S.; Maiti, S.; Das, P. K. In situ synthesized Ag nanoparticle in self-assemblies of amino acid based amphiphilic hydrogelators: development of antibacterial soft nanocomposites. *Soft Matter* **2011**, *7*, 3011–3022.

274. Banerjee, A.; Paul, S.; Basu, K.; Das, K. S. Peptide-based hydrogel as a scaffold for in situ synthesis of metal nanoparticles: catalytic activity of the nano-hybrid system. **2018**, *4* 882-887.

275. Sun, X.; Wang, Y.; Lei, Y.; Fluorescence based explosive detection: from mechanisms to sensory materials. *Chem. Soc. Rev.* **2015**, *44*, 8019.

276. Madhu, C.; Roy, B.; Makam, P.; Govindaraju, T. Bicomponent β-sheet assembly of dipeptide fluorophores of opposite polarity and sensitive detection of nitro-explosives. *Chem. Commun.* **2018**, *54*, 2280-2283.

277. Zhanga, C.; Wanb, L. Y.; Wua, S.; Wua, D.; Qina, X.; Kob, F. A reversible colorimetric chemosensor for naked-eye detection of 2 copper ions using poly (aspartic acid) nanofibrous hydrogel. *Dyes Pigm*. **2015**, *123*, 380-385.

278. Gayen, V. K.; Kingshuk Basu, K.; Nandi, N.; Das, K. S.; Merino, D. H.; Hamley, I. W.; Banerjee. A. A self-assembled peptide-appended naphthalene diimide: a fluorescent switch for sensing volatile acid and basic. *ChemPlusChem.* **2019**, *84*, 1673-1680.

279. Singha, S.; Neogi, S.; Pramanik, B.; Das, S.; Dasgupta, A.; Ghosh, R.; Das, D. Ultra-fast, highly sensitive and selective detection of p-xylene at room temperature by peptide hydrogel based composite material. *ACS Appl. Polym. Mater*. **2019**, *1*, 2267–2272.

280. Pramanik, B.; Singha, N.; Das, D. Sol, gel, and paper-based detection of picric acid at femtogram level by a short peptide gelator. *ACS Appl. Polym. Mater*. **2019**, *1*, 833–843.

281. Ardoña, H. A. M.; Tovar. J. D. Peptide π-Electron conjugates: organic electronics for biology? *Bioconjugate Chem.* **2015**, *26*, 2290–2302.

282. Draper, E. R.; Walsh, J. J.; McDonald, T. O.; Zwijnenburg, M. A.; Cameron, P. J.; Cowan, A. J.; Adams, D. J. Air-stable photoconductive films formed from perylene bisimide gelators. *J. Mater. Chem. C.* **2014**, *2*, 5.

283. Nalluri, S. K. M.; Shivarova, N.; Kanibolotsky, A. L.; Zelzer, M.; Gupta, S.; Frederix P. W. J. M.; Skabara, P. J.; Gleskova, H.; Ulijn, R. V. Conducting nanofibers and organogels derived from the self-assembly of tetrathiafulvalene-appended dipeptides. *Langmuir* **2014**, *30*, 12429.

284. Amit, M.; Appel, S.; Cohen, R.; Cheng, G.; Hamley, I. W.; Ashkenasy, N. Hybrid proton and electron transport in peptide fibrils. *Adv. Funct. Mater*. **2014**, *24*, 5873.

Chapter 2

Self-Assembly and Multifunctionality of Peptide Organogels: Oil Spill Recovery, Dye Absorption and Synthesis of Reduced Graphene Oxide Incorporated Conducting Biomaterials

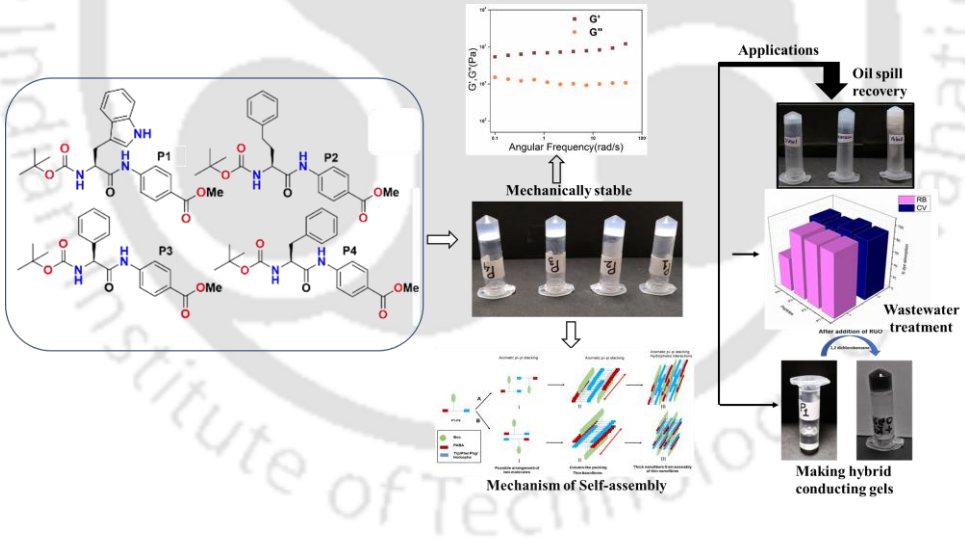

RSC Adv. **2020**, *10*, 5220-5233

2.1. Introduction

Low molecular weight supramolecular gels (LMWG) are an important class of materials that can encapsulate large amounts of solvents in mesh-like entangled structures resulting from the ordered hierarchical arrangement of individual molecules.[1-4] Many of them are known to have phase-selective gelation properties. Such phase-selective gelation is highly desirable in oil spill recovery[5], which is a major source of water pollution, creating a tremendous environmental hazard for marine ecosystems.[6] Additionally, these gel-based soft materials offer an appealing alternative for removing dyes from contaminated water due to their high water permeability, large surface area for adsorption, and simplicity of use and reusability.[7-17] Therefore, the LMWG has opened up its utility in water remediation to a great extent. As the literature suggested, peptides can be one of the most fascinating gelator molecules for water remediation owing to their easy synthesis, biocompatibility, and multifunctionality.[18]

Another important usefulness of peptide-based gels is observed in developing hybrid materials. In this context, graphene is well known for making hybrid materials, and its derivatives with inorganic/polymeric materials are highly conducting. Graphene containing hybrid materials have been put to interesting applications, including renewable energy conversion/storage devices, supercapacitors, electroresponsive systems, electrocatalysis, optoelectronic devices, electromagnetic interference shielding etc.[19-30] In a number of studies, graphene and its derivatives have also been incorporated into peptide organogels. Peptide-based hybrid materials become moderately conducting in nature upon insertion of graphene or its derivates.[31-33]

Therefore, focusing on the development of environmental friendly biomaterials like peptide-based LMWG, we have designed four dipeptides, P1-P4, containing aromatic moieties for studying their self-assembly and generating materials with multiple applications.

The building blocks of P1-P4 were chosen such that their self-assembly would be guided by aromatic and hydrophobic interactions. The mechanism of self-assembly of P1-P4 was established using various spectroscopic and microscopic experiments. Interestingly, all the peptides were capable of forming gels in a variety of organic solvents and in fuels like petrol, diesel, and kerosene, which made them ideal materials to be used for oil spill recovery. All the organogels studied here were excellent adsorbents for cationic dyes. RGO was incorporated into peptide organogels to generate conducting biomaterials. Generating environmentally friendly materials with directed self-assembly, which are equipped with multiple applications is of considerable interest and is the main focus of our study.

2.2. Experimental section

2.2.1. Materials procured

All amino acids, L-Phe, L-Trp, PABA, L-Phg, L-HomoPhe, all solvents, di-t-butyl dicarbonate, *N*, *N*′-Dicyclohexylcarbodiimide (DCC), sodium hydroxide,1-hydroxybenzotriazole (HOBt), and thionyl chloride were all purchased from Spectrochem, Merck and Rankem. CDCl3 and DMSO-d6 solvents were obtained from Sigma Aldrich. Dyes CV and RB were purchased from Spectrochem. Fuels like kerosene, diesel and petrol were obtained from Bharat petroleum gas station. Graphite powder was purchased from Asbury carbons.

2.2.2. Synthesis of Peptides

All peptides were synthesized by racemization free, fragment condensation technique based traditional solution phase methodology. The N-termini of the amino acids were protected by Boc group using $(Boc)_2O$ while the C-termini were protected as methyl ester. Peptide couplings were done using DCC and HOBt as coupling reagents. All the compounds were purified by column

chromatography using silica gel (100-200 mesh size) as stationary phase and hexane/ethyl acetate as eluent. Finally, purity of dipeptides was confirmed by analytical HPLC with >95% (Appendix, Fig. A2.1-A2.4), and characterized by mass spectrometry (Appendix, Fig. A2.5- A2.8), ^{1}H NMR (Appendix, Fig. A2.9-A2.12).

2.2.3. Gelation experiments

To check the ability of P1-P4 to form gel in different solvents, weighed 1mg amount of the purified compounds (P1-P4) were taken in micro centrifuge tubes and 500 µL of different solvents were added to them. Samples were heated in a heating block at temperatures ranging from 60°*C*- 100 °C and subsequently cooled to room temperature. Gel was formed within 10-15 minutes which was stable to inversion of the micro centrifuge tube.

For making the RGO incorporated P1 organogel (RGO-P1), the freshly prepared RGO (1mg, 0.2wt %) was added to 500 µL 1,2-DCB solution of peptide P1 at its MGC. The mixture was sonicated until a homogeneous suspension of RGO in the peptide was obtained. This was further heated at 100°C for 15 mins, followed by vortexing for 10 sec. Upon cooling the mixture, black coloured organogel formed within another 5-10 mins. Hybrid organogels were formed with varying amounts of RGO.

2.2.4. Determination of the gel-to-sol transition temperature

The gel-to-sol transition temperature (T_{gel}) of the organogels from single peptides and RGO-peptide hybrid organogel were determined by placing the gel containing vial in an oil bath and raising the temperature of the bath at the rate of 1°C /minute. The temperature was monitored using a thermometer. The (T_{gel}) was defined as the temperature at which the gel melted and started to flow.

2.2.5. Phase selective gelation

Peptides P1-P4 at their MGC were added to mixtures of 500 µL each of organic and aqueous solvents. The mixture was vortexed for 2 minutes to yield a homogeneous suspension, heated at 60-100°C and subsequently cooled. Gels were selectively formed from the organic solvents within 10-15 mins.

2.2.6. Rheology

The viscoelastic properties of self-assembled and RGO incorporated hybrid organogels were determined by rheology studies using Anton Paar MCR102 Rheometer equipped with a 20 mm parallel-plate measuring system at 25 °C. 1.0 w/v% pristine organogels of P1-P4 in 1,2-DCB and 1wt% RGO incorporated in RGO-P1 was used for the study. A strain sweep test was performed over a range from 0.1-100% strain at a fixed oscillatory frequency of 1 rad/s. Furthermore, the mechanical strength of the organogels were determined from the oscillatory test, *i.e*. frequency sweep (with the frequency ranging from 1-100 rad/s), which was carried out under a fixed strain. Rheological experiments measure two parameters; storage modulus (G′) and loss modulus (G″). A defining measure of gelation process is having a higher value of G′ than G″ which are essentially independent of frequency.

2.2.7. FESEM

FESEM images reported in this study were obtained on a FESEM Sigma Zeiss microscope. A drop of the solution of P1-P4 in 1,2-DCB was casted on a silicon wafer and was allowed to dry for a few hours under vacuum before imaging. For studying the morphology of the pristine organogels P1-P4 and hybrid gel RGO-P1, small pieces of the organogel were casted on the silicon wafer and allowed to dry under vacuum before imaging.

2.2.8. FT-IR

FT-IR spectroscopy measurements were recorded on a Spectrum Two Perkin Elmer FT-IR Instrument using KBr pellets. Measurements were performed on both powdered samples and on the xerogels (obtained from organogels of 1,2-DCB) for P1-P4. Lyophilized peptides obtained post-purification were used as powdered samples. Measurements were also performed on xerogels of P1 (obtained from organogel in kerosene) and RGO-P1(obtained from organogel in 1,2-DCB). Xerogels were prepared by keeping organogels in the desicator under vaccum condition. After 3-4 days it visibly became a white, dry and solid mass. This solid mass was powdered was used for making KBr pellets in the FT-IR analysis.

2.2.9. NMR experiments

NMR experiments were performed on a 600 MHz and 400MHz Bruker NMR spectrometer. ^{1}H NMR experiments were performed in DMSO-d_6 for routine characterization of the molecule. Concentration dependent ^{1}H NMR (5 mM, 6.86 mM (MGC), 9 mM and 13 mM for P1; 2mM, 3mM, 4.8mM(MGC) and 7mM for P2) was recorded for the peptides P1 and P2 in $CDCl_3$ at ambient temperature. DMSO titration of P1 and P2 was performed by addition of increasing concentrations (0.5% to 10%) of DMSO-d_6 in $CDCl_3$ at ambient temperature.

2.2.10. Fluorescence

To gain an insight into the role of aromatic π-π stacking in the self-assembly of P1, concentration dependent fluorescence experiment was performed by monitoring the intrinsic fluorescence of the amino acid Trp on a Fluoromax-4 spectrophotometer. Samples of different concentrations of P1 were prepared in THF and their fluorescence emission was monitored keeping the fluorescence excitation wavelength fixed at 280 nm.

2.2.11. pXRD

Wide angle X-ray diffraction analysis was done on a Bruker D2 Phaser X Ray diffractometer (Cu-Kα radiation, λ=1.5406 Å) and a Rigaku Smartlab X Ray diffractometer with (Cu-Kα radiation, λ=1.540 Å) for both the powdered samples (P1-P4) (as obtained post lyophilization) and the xerogels obtained from drying the organogels (described above) of (a) individual peptides (P1-P4) grown from 1,2-DCB, (b) P1 in kerosene and (c) RGO-P1 hybrid organogel obtained from 1,2-DCB.

2.2.12. Crystallization and X-ray crystallography

Single crystals were obtained from peptides P2 and P4 in MeOH-H_2O solvent systems. Intensity data was collected with Mo-Kα radiation (λ=0.71073 Å) by a Bruker APEX-2 CCD diffractometer. Data was processed using the Bruker SAINT package. The structure solution and refinement were performed by SHELX2016.

2.2.13. Dye absorption studies

Into the preformed gels obtained from self-assembly of the individual peptides P1-P4, aqueous solution of dyes namely crystal violet (CV) and rhodamine b (RB) was added and allowed to stand for 24 h at RT, after which the amount of unabsorbed dye in the supernatant was checked by monitoring the UV of the supernatant aqueous solution and calculating the concentration from a standard curve of the dye (Appendix, Fig. A2.13). The amount of dye loaded in the gel and the dye loading efficiency was then calculated as follows:

Dye loaded = (Initial dye - Unabsorbed dye)

Loading efficiency: (Dye loaded/Initial dye) X 100

2.2.14. Recyclability of the Organogels for dye absorption

To the dye absorbed organogels, diethyl ether was added and was left for 24 h. The dye was released into the ether medium and the gel became colorless once more. The ether layer was removed and after another round of ether wash, the gel was reused for the second cycle of dye absorption studies. Such studies were carried out for 3 subsequent cycles and the efficiency of the dye absorption was estimated in each cycle.

2.2.15. Synthesis of RGO

2.2.15.1. Preparation of graphene oxide

Graphene oxide (GO) was synthesized following the modified Hummers' method.[34] 1g of graphite powder was added to 50 mL of concentrated sulphuric acid taken in a conical flask while maintaining the temperature between 0-5° C followed by the addition of 6g potassium permanganate (KMnO4) to the above mixture under constant stirring. The conical was then transferred to a water bath where it was maintained at 35° C for 2 hours. In the next step the conical flask was again transferred to an ice bath where 100 ml of DI water was slowly added under vigorous stirring. Lastly 8 ml of hydrogen peroxide (H_2O_2) was added to this diluted mixture to obtain a yellow coloured slurry, which was washed with 20% HCl followed by acetone until the pH increased above 5. The as obtained GO powder was then dispersed in DI water. Formation of GO was characterized by PXRD and Ramananalysis (Appendix, Fig. A2.14 a, A2.15 a and A2.16 a).

2.2.15.2. Preparation of reduced graphene oxide

100 ml of 0.5 mg/ml of GO dispersion in water was taken in a reagent bottle and heated at about 70 °C followed by addition of 3 ml liquid ammonia and 40 µL of hydrazine hydrate. The resultant

mixture turned blackish in colour and was further heated for another 30 minutes to obtain the reduced graphene oxide. Formation of RGO was confirmed by PXRD, Raman, FETEM ana EDX analysis (Appendix, Fig. A2.14 b, A2.15 a, b and A2.16 b)

2.2.16. Conductivity determination of RGO-peptide hybrid organogels

Two copper wires were inserted into the RGO-P1(with different amounts of RGO) hybrid organogel and were connected to the sourcemeter (Keithley 2450 model). A potential of -1 to +1 was applied, and the conductivity measurements (i.e. current-voltage (I-V) characteristics) were performed.

2.3. Results and discussions

2.3.1. Design strategy and gelation studies of peptides

We synthesized four dipeptides Boc-Trp-PABA-OMe (P1), Boc-homoPhe-PABA-OMe (P2), Boc-Phg-PABA-OMe (P3) and Boc-Phe-PABA-OMe (P4) (Fig. 2.1 a) using standard solution based peptide synthesis strategy, purified using column chromatography and characterized with analytical HPLC, ESI-MS and ^{1}H NMR (Appendix, Fig. A2.1-A2.12). All the four dipeptides were terminally protected and contained an aromatic delta amino acid residue PABA. The second amino acid residue (Trp, Homo-Phe, Phg, Phe) was aromatic in nature.

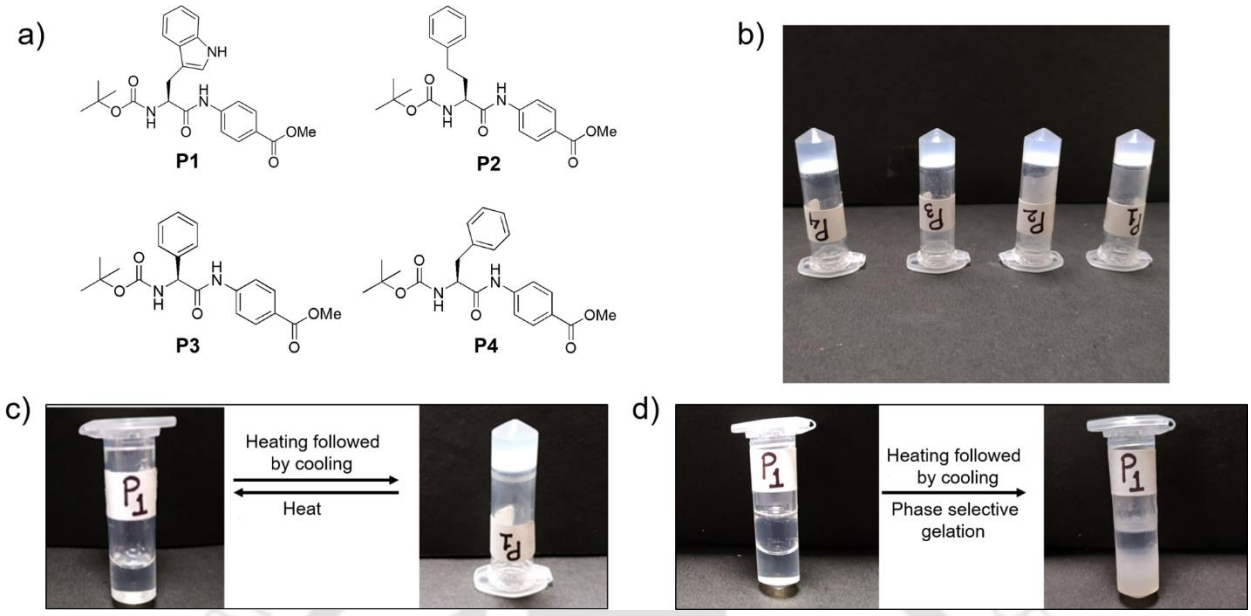

Fig. 2.1. (a) Chemical structures of LMWG P1-P4, (b) Gels formed in 1,2-DCB by P1-P4 (c) Thermoreversibility of the organogel formed by P1 in 1,2-DCB and (d) Phase selective gelation of P1 in 1,2-DCB in presence of water.

The design of building blocks intended to facilitate self-assembly using aromatic interactions and hydrophobic interactions. Homologs of Phe namely Phg, Homo-Phe were used for understanding the role of the length of side chain on the assembly of the peptides.

All the dipeptides readily formed phase selective, thermoreversible gels in various organic solvents like chloroform, THF, 1,2-dichlorobenzene, etc. (Fig. 2.1 b, c, d Table 2.1) and in fuels like kerosene, diesel and petrol upon heating and subsequent cooling. The minimum gelation concentration of the peptides depended on the solvents but generally lied in between 0.2-0.4 w/v% (Table 2.1). Thermal stability of the peptides was studied from the T_{gel} which lied in the range of 30-80°C. As the gels were translucent and most thermostable in 1,2-DCB, further characterization of the organogels were done in this solvent.

Table 2.1. Gelation properties of peptides P1-P4. OG: Opaque Gel, TNS: Translucent Gel, S: Soluble

Solvents	P1 State/MGC(%w/v)/T_{gel}(ºC)	P2 State/MGC(%w/v)/T_{gel}(°C)	P3 State/MGC(%w/v)/T_{gel}(ºC)	P4 State/MGC(%w/v)/T_{gel}(ºC)
Chloroform	OG/0.20/52	OG/0.20/50	OG/0.30/32	OG/0.20/45
1,2 DCB	TNS/0.4/69	TNS/0.30/62	TNS/0.40/78	TNS/0.40/76
Toluene	Transparent/0.20/50	Transparent/0.20/63	Transparent/0.25/75	Transparent/0.10/62
Benzene	Transparent/0.25/52	Transparent/0.20/57	Transparent/0.20/56	Transparent/0.30/51
THF	OG/0.35/55	OG/0.20/70	OG/0.35/40	OG/0.20/40
Chlorobenzene	Transparent/0.35/50	Transparent/0.20/47	Transparent/0.35/71	TNS/0.40/43
ACN	S	-	S	S
Dioxane	S	-	S	S
DMF	S	-	S	-
Ethanol	S	S	S	S
DMSO	S	S	S	S
Methanol	S	-	S	S
n-heptane	-	S	-	-

2.3.2. Morphological study

Self-assembled morphology P1-P4 in 1,2-DCB in the solution and gel state was studied using Field Emission Scanning microscopy (FESEM) (Fig. 2.2). Apparently, the morphology of P1 in the solution and in the gel state (Fig. 2.2) looked different. The morphology of P1 was nano fibrous in the solution state while it looked like densely packed continuous matrix in the gel state.

Morphology of the peptides P2 and P3 in solution and gel state were same with slight variations. Peptide P4 formed fibrous entangled morphology both in the solution and in gel state, with a denser mesh in the later. The subtle differences in the morphology of P1-P4 could be attributed to the varying chains of the amino acids present in them.

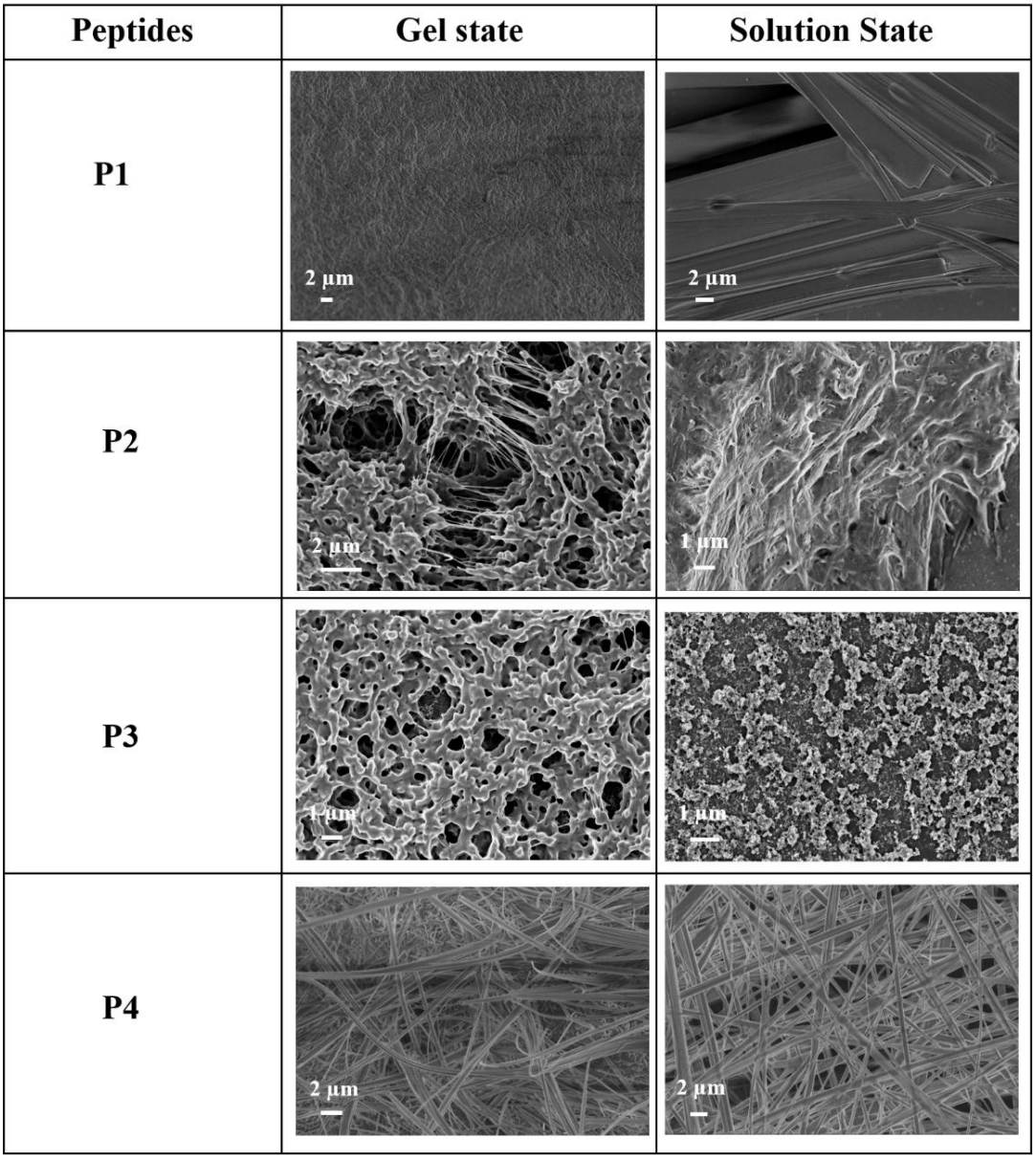

Fig 2.2. FESEM images of P1, P2, P3 and P4 in 1,2-DCB in both solution state and gel state.

2.3.3. Rheology

The mechanical strength and the stability of the organogels derived from self-assembly of the individual peptides were studied by rheology. The storage modulus (G´) and the loss modulus (G´´) were measured as a function of different parameters like angular frequency and strain sweep. For this study, gels were formed from P1-P4 in 1,2-DCB at 1.0% w/v. In strain sweep experiment, where the storage modulii (G´) and the loss moduli (G´´) for the four organogels were plotted as a function of % strain (0.1-100%) (Fig. 2.3 a, b, c, d), it was found that G´ was higher than G´´ till a particular strain (Linear viscoelastic region (LVR), γ = 0.1% for P1-P4).

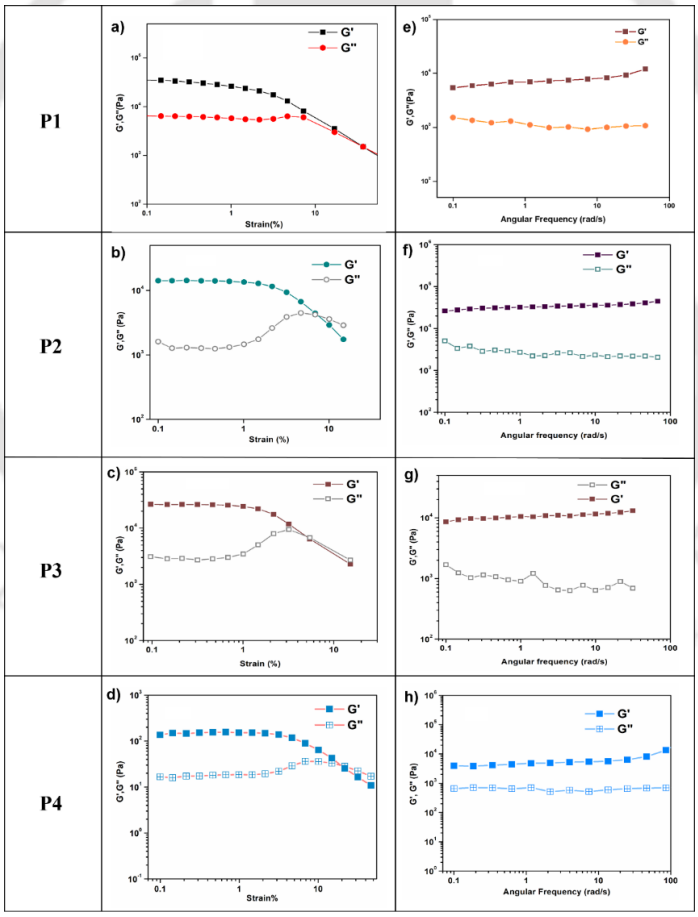

Fig. 2.3. Rheology profile of organogels. a), b), c), d) strain dependence and e), f), g), h) Frequency dependence of the dynamic storage moduli (G′) and the loss moduli (G″) of organogel from P1-P4 in 1,2-DCB at 2 % w/v.

In the angular frequency sweep experiment performed at a constant strain of 0.1% at 25°C, for all the four organogels, the G′ was found to be dominating over G″ till about 100 rad/s (Fig. 2.3 e, f, g, h). Also, G′ and G″ were found to be independent of angular frequency, in the region 1-100 rad/s which indicated the formation of stable organogels. The storage modulii of all the organogels were of the order of $\geq 10^4$ Pa, in the frequency sweep experiment which indicated a considerable mechanical strength of all the organogels.

2.3.4. Non-covalent interactions in promoting the self-assembly

The peptides were designed to be hydrophobic and rich in aromatic moieties. Thus aromatic π-π interactions and hydrophobic interactions were expected to be the key non covalent forces driving self-assembly (see the sections 1.2.2. and 1.3.2). Peptide backbones are rich in hydrogen bond donor and acceptor groups and hence hydrogen bonding might be another important factor aiding self-assembly. The following experiments were performed to identify the key interactions driving the assembly process.

2.3.4.1. Fluorescence studies

The intrinsic fluorescence of tryptophan residue was used to study the role of aromatic π-π stacking interactions in the self-assembly of peptide P1. Fig. 2.4 a shows the fluorescence emission spectra of P1 in THF at various concentrations (0.1 mM-7mM). The emission maxima of tryptophan at 325 nm was steadily quenched upon increasing the concentration of the peptide. This might be attributed to the stacking of the tryptophan moieties with progressive self-assembly upon increasing the concentration of the peptide.[35 a, b, c] A prominent excimer peak was observed at 455 nm which got quenched upon increasing the concentration of the peptide. Usually increasing peptide concentration, leads to more excimer formation, which is accompanied by increase in the intensity of the excimer fluorescence peak. P1 contained two types of aromatic moieties, the indole

ring from Trp and the aromatic backbone of the PABA amino acid. If the self-assembly of P1 led to stacking of these two different moieties, then exciplex would be formed instead of excimer. Fluorescence intensity for the exciplex might quench with the increase in the concentration of exciplex.[35 d] Thus this experiment clearly proved that in the case of P1, aromatic π-π stacking interactions played an important role and suggested that the stacking occurred between the Trp side chains and the aromatic ring of PABA.

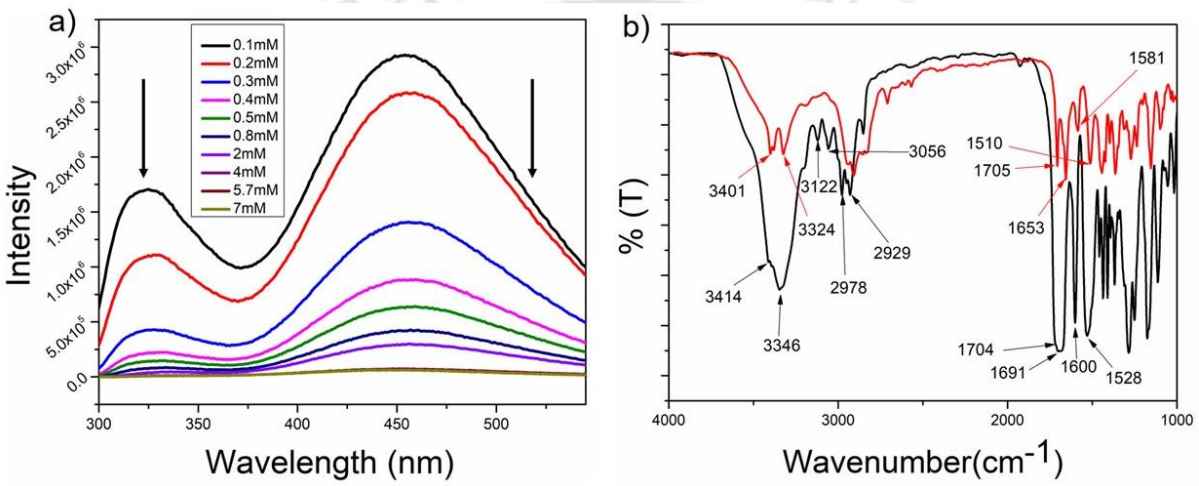

Fig. 2.4. a) Concentration dependent tryptophan fluorescence spectra for P1 in THF (λ_{ex} at 280 nm) and b) Superimposed FT-IR spectrum of P1 in powdered (black) and xerogel state (red).

As the peptides P2-P4 were structurally very similar to P1, it might be assumed that aromatic stacking played an important role in their self-assembly as well.

2.3.4.2. FT-IR

Fig. 2.4 b shows the superposition of the FT-IR spectra recorded for the powder and xerogel samples from 1,2-DCB for P1. There were two distinct peaks observed at 3414 and 3346 cm^{-1} in powdered form of P1 for non-hydrogen bonded and hydrogen bonded NHs respectively, which shifted to 3401 and 3324 cm^{-1} respectively, in the xerogel indicating increased hydrogen bonding in the xerogel state. However, presence of two peaks indicated existence of both hydrogen bonded

and non-hydrogen bonded NHs. The CO stretching frequency shifted from 1691 cm^{-1} in the powdered form to 1653 cm^{-1} in the xerogel form suggesting that the backbone conformation of the P1 was not β sheet like. In the case of P2-P4 (Fig. 2.5), a broad peak was observable in the NH stretching region at around 3420-3430 cm^{-1} for the xerogel, indicating the presence of non-hydrogen bonded backbone NHs.

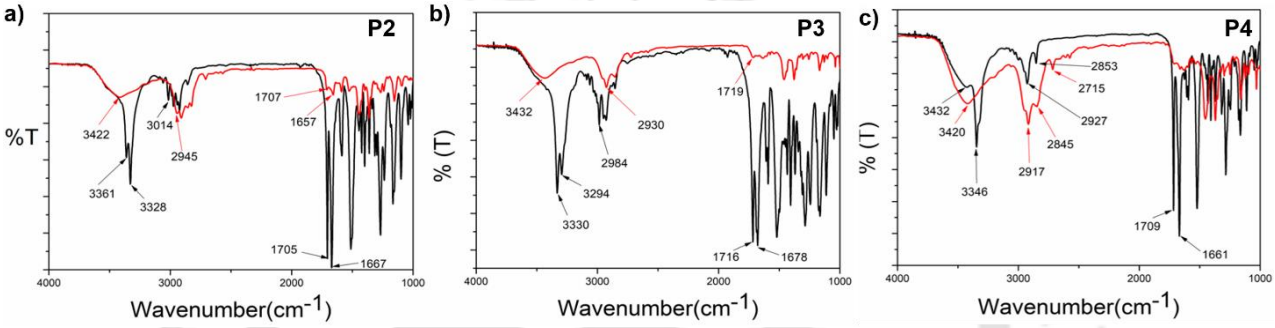

Fig. 2.5. Superimposition of the FT-IR spectra of a) P2, b) P3 and (c) P4 in their powder (black) and xerogel state (red).

Lack of any peak at around 3200 cm^{-1} suggested absence of hydrogen bonded amide protons in these systems in the self- assembled state. The amide I peaks in P2-P4 did not indicate typical β-sheet kind of conformation. Presence of hydrogen bonding status of the amide protons was further studied using NMR spectroscopy.

2.3.4.3. NMR

The role of intermolecular hydrogen bonds in driving the self-assembly was probed by monitoring the NH chemical shifts of P1 and P2 in $CDCl_3$ at concentrations, below, above and at their minimum gelation concentration (Fig. 2.6 a, b). For both the peptides, none of the NH protons

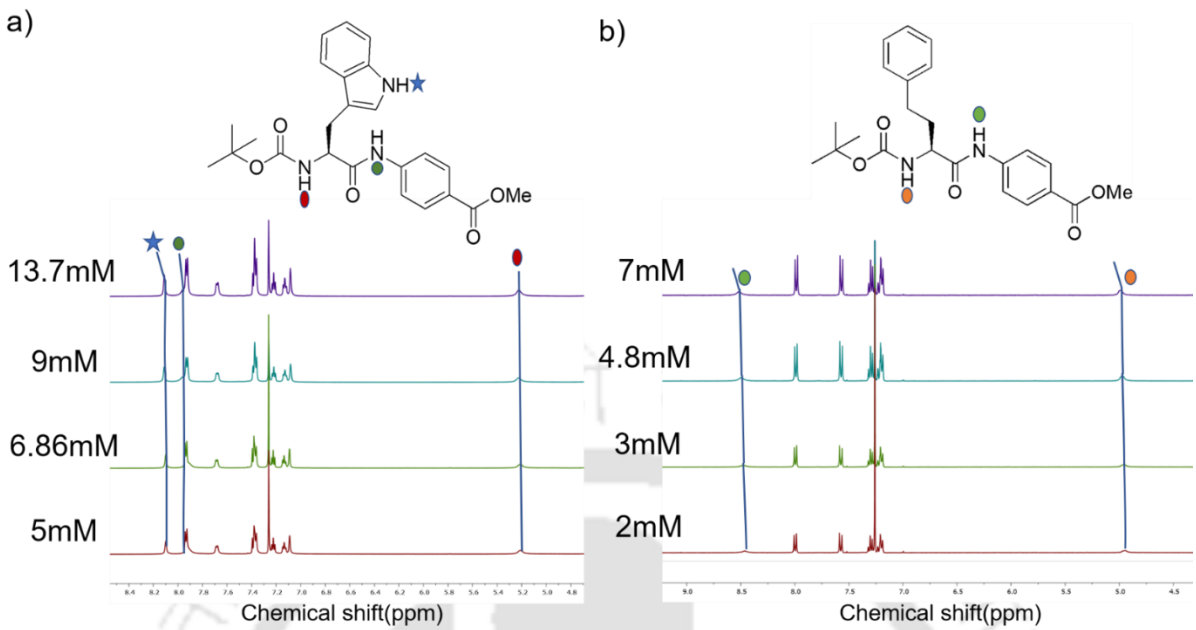

Fig. 2.6. NH region of the stacked ^{1}H NMR spectra of the peptides (a) P1 and (b) P2 in $CDCl_3$ at different concentrations which are lower, equal and higher than the MGC of the solution.

showed any change in their chemical shifts over the entire concentration range indicating that there was no change in the hydrogen bonded state of the backbone amide protons over the concentration range in which the study was performed. Further, to understand the hydrogen bonded state of the amide protons, DMSO titration experiment of P1 and P2 were performed (Fig. 2.7 a, b). For P1, it was seen that the NH of tryptophan did not show any change in the chemical shift value, suggesting it to be hydrogen bonded while the NH of PABA residue and the indole NH showed considerable change in their chemical shift values suggesting that they were solvent exposed or non-hydrogen bonded. This corroborated the observation from FT-IR experiments of P1 in xerogel state, where there was presence of both hydrogen bonded as well as non-hydrogen bonded NHs. Aromatic protons showed a striking upfield shift upon addition of DMSO-d_6 to the $CDCl_3$ solution

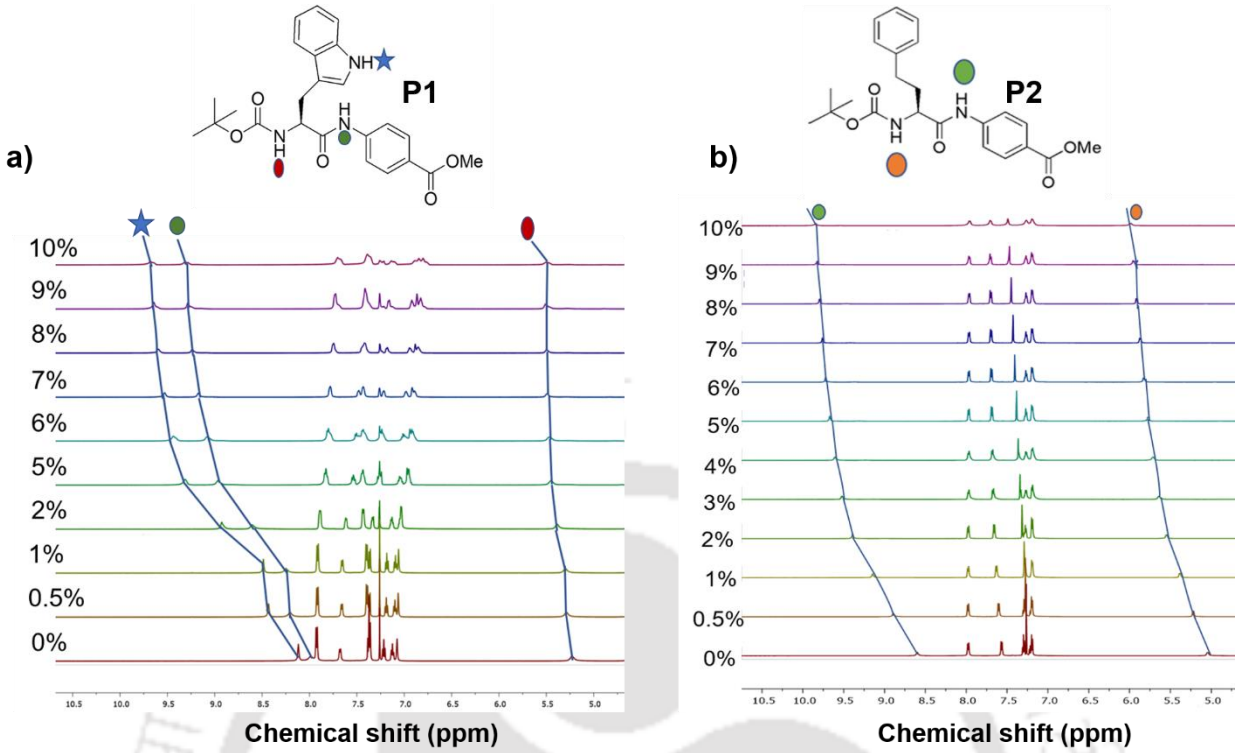

Fig. 2.7. Stacked NH region of the ^{1}H NMR spectrum obtained upon addition of increasing amounts of DMSO-d_6 to the $CDCl_3$ solution of a) P1 and b) P2.

of P1. Addition of increasing amounts of DMSO-d_6 disrupted the self-assembly thus changing the electronic environment of the aromatic protons, which got shielded. This was an indirect proof of the fact that stacking of aromatic moieties played an important role in the self-assembly of P1. In the case of P2, NHs of both the amino acid residues were solvent exposed or non-hydrogen bonded, supporting the FT-IR data where only a broad peak corresponding to non-hydrogen bonded NHs was observed.

Thus in summary, the hydrogen bonding pattern in P1 was slightly different from that in P2-P4. Hydrogen bonding did not seem to be play a crucial role in the self-assembly process of P2-P4 unlike in P1.

2.3.4.4. pXRD

Information on the molecular packing of the peptides P1-P4 in gel state was obtained upon performing pXRD experiments (Fig. 2.8). The XRD pattern for the P1 xerogel was ordered unlike

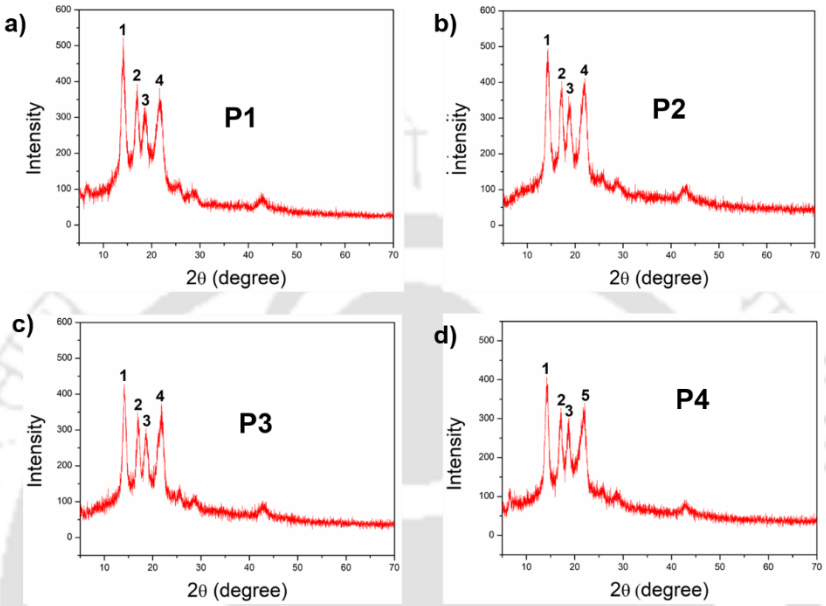

Fig. 2.8. PXRD of xerogels of peptides a) P1, b) P2, c) P3 and d) P4.

its powdered form (Fig. 2.9). The wide angle pXRD patterns for P1-P4 xerogels showed similar periodic diffraction patterns which indicated presence of similar ordered arrangement in all the xerogels. In the peptide xerogels P1-P4 peaks were observed at d values of 6.25 Å (2θ = 14.12), 5.19 Å (2θ = 17.04), 4.75 Å (2θ = 18.64) and 4.10 Å (2θ = 21.60) (Table 2.2) . The ideal centroid to centroid distance in π-π stacked aromatic systems is about 4 Å. The distance of 4.20 Å present in all the xerogels might be attributed to the distance in between the aromatic moieties of the gelator molecules present in the system. This again indicated that aromatic π-πinteractions were crucial for self-assembly and was present in all the xerogel systems. Peak at around 4 Å was absent in the XRD of the powdered samples of P1, P3 and P4 indicating lack of aromatic π-π interactions in the powdered form of the peptides.

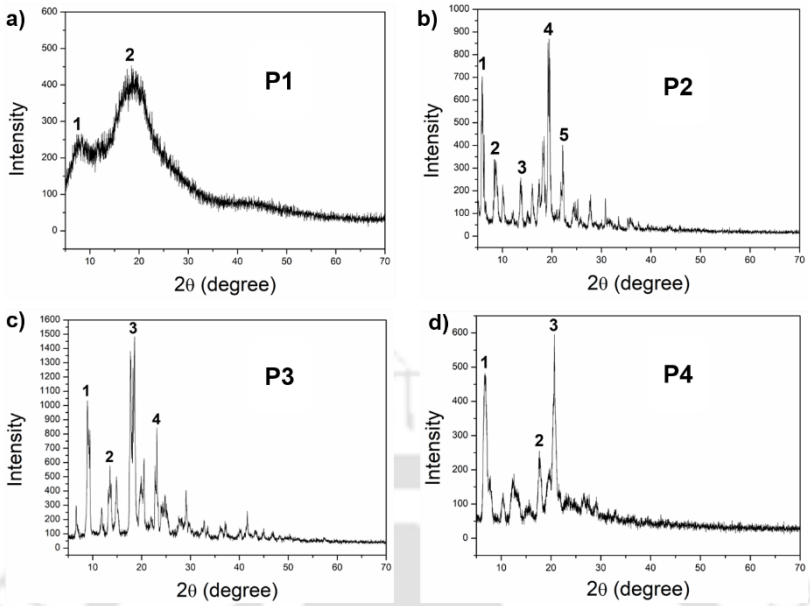

Fig. 2.9. PXRD of peptides in powdered state. (a) P1, (b) P2 (c) P3 and (d) P4.

Table 2.2: Interplaner distances in the xerogels obtained from PXRD.

Xerogels	Peak 1		Peak 2		Peak 3		Peak 4	
	2θ (degree)	d(Å)	2θ (degree)	d(Å)	2θ (degree)	d(Å)	2θ (degree)	d(Å)
P1 (DCB)	14.121	6.265	17.041	5.191	18.641	4.754	21.601	4.109
P2 (DCB)	14.321	6.179	17.181	5.154	18.901	4.689	22.041	4.028
P3 (DCB)	14.121	6.265	16.861	5.252	18.641	4.754	21.841	4.064
P4 (DCB)	14.241	6.212	17.161	5.162	18.841	4.704	22.061	4.024

RGO-P1 hybrid (DCB)	14.199	6.232	17.081	5.18501	18.652	4.751	21.993	4.037
P1 (Kerosene)	17.093	5.185	18.690	4.7428	21.88	4.0579	25.645	3.4695

2.3.4.5. Crystal structures of P2 and P4

Structure of peptides P2 and P4 were elucidated from the single crystal X-ray analysis (Table 2.3). Crystals were grown from the MeOH-H_2O system by slow evaporation of solvent at room temperature.

Table 2.3. Crystallographic parameters of P2 and P4

Parameters	P2	P4
Molecular formula	C_{23} H_{28} N_2 O_5	C_{22} H_{26} N_2 O_5
Formula weight	412.47	398.45
Crystal system	Monoclinic	Monoclinic
Crystallizing solvent	Methanol/H_2O	Methanol/H_2O
Space group	I 2 (5)	C 2 (5)
a/Å	20.281(9)	27.13(2)
b/Å	5.226(3)	5.227(4)
c/Å	22.662(10)	15.424(12)
α/°	90	90
β/°	105.39(5)	105.46(4)
γ/°	90	90
V/ Å^3	2316(2)	2108(3)
Z	4	4
Density/g cm^{-3}	1.183	1.255
Molecules/asym.unit	1	1
R1	0.0829	0.1036
wR2	0.1971	0.2240
CCDC No.	1961451	1961450

The backbone of both the peptides P2 and P4 were kinked at the Cα carbon of the alpha amino acid residue (Fig. 2.10 and Fig. 2.11, Table 2.4). There were no intramolecular hydrogen bonds present in both the peptides. We could not obtain crystals for the peptides P1 and P3, but as the

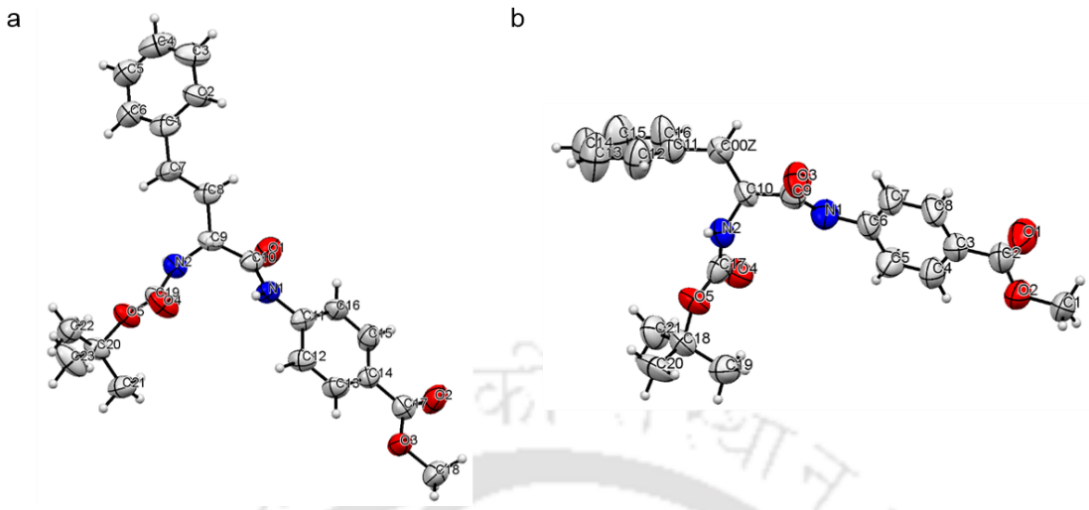

Fig. 2.10. ORTEP diagram for peptide (a) P2 and (b) P4 with ellipsoid of 50% probability as obtained in the crystals grown from slow evaporation of MeOH-H_2O.

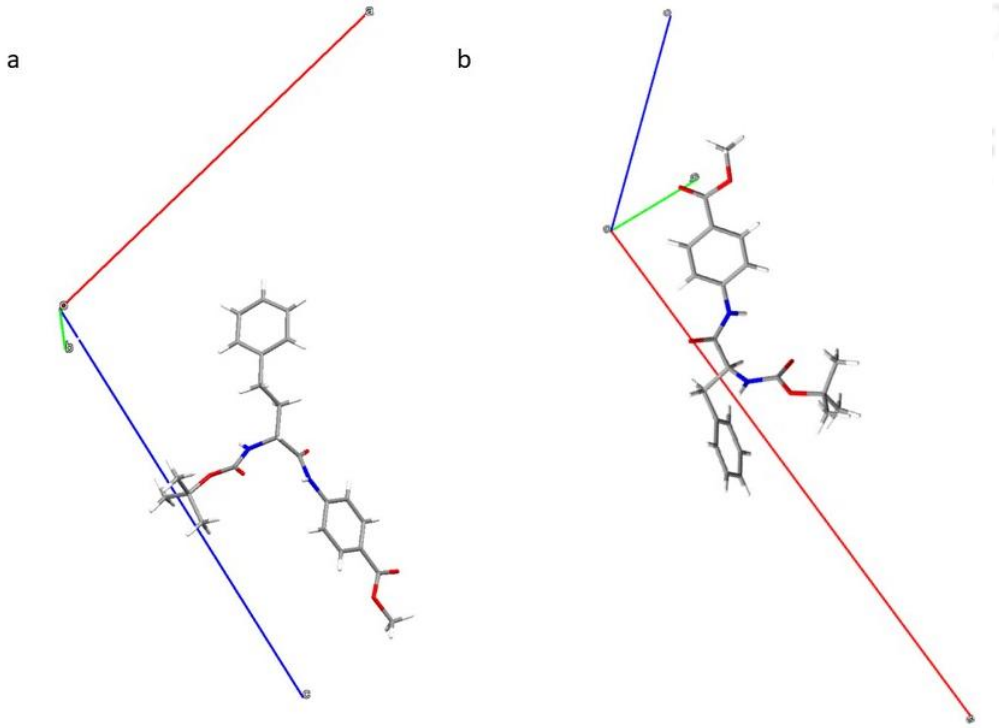

Fig. 2.11. Asymmetric unit cell in the crystals of (a) P2 and (b) P4.

Table 2.4. Torsion angles (deg) for the peptides of P2 and P4.

Peptide	Residue	ϕ	θ_1	θ_2	θ_3	ψ
P2	HPhe PABA	95.83 30.06	178.55	1.41	179.36	89.48 180.0
P4	Phe PABA	-98.44 -35.70	-177.73	2.35	-179.25	92.06 178.54

back bone of all the molecules were same, we could assume that similar backbone conformation was present in P1 and P3 as well. P2 and P4 did not have a β sheet like conformation which explained the absence of any characteristic peak in the amide I region in the FT-IR spectrum of xerogels. Fig. 2.12 showed the packing in crystals for P2 and P4 respectively. Packing in both the systems were fairly similar. For both the peptides, pairs of molecules packed togather and such pairs stacked to form column like structures. In case of P2, Boc groups of the two individual molecules in a pair faced each other. The aromatic rings of PABA came close together while the aromatic groups of Homo-Phe stuck out in opposite directions. In P4, the packing of a pair of molecules was a bit different with the Boc groups of one molecule pointing away from the other and the Phe side chain of one molecule stacking with the Phenyl ring in the backbone of PABA of the other molecule. Both in P2 and P4, pairs of molecules self-assembled to form columnar structures primarily through aromatic stacking interactions, hydrophobic interactions and weak hydrogen bonded interactions (C=O----H-N bond distance of about 2.2 Å, Table 2.5).

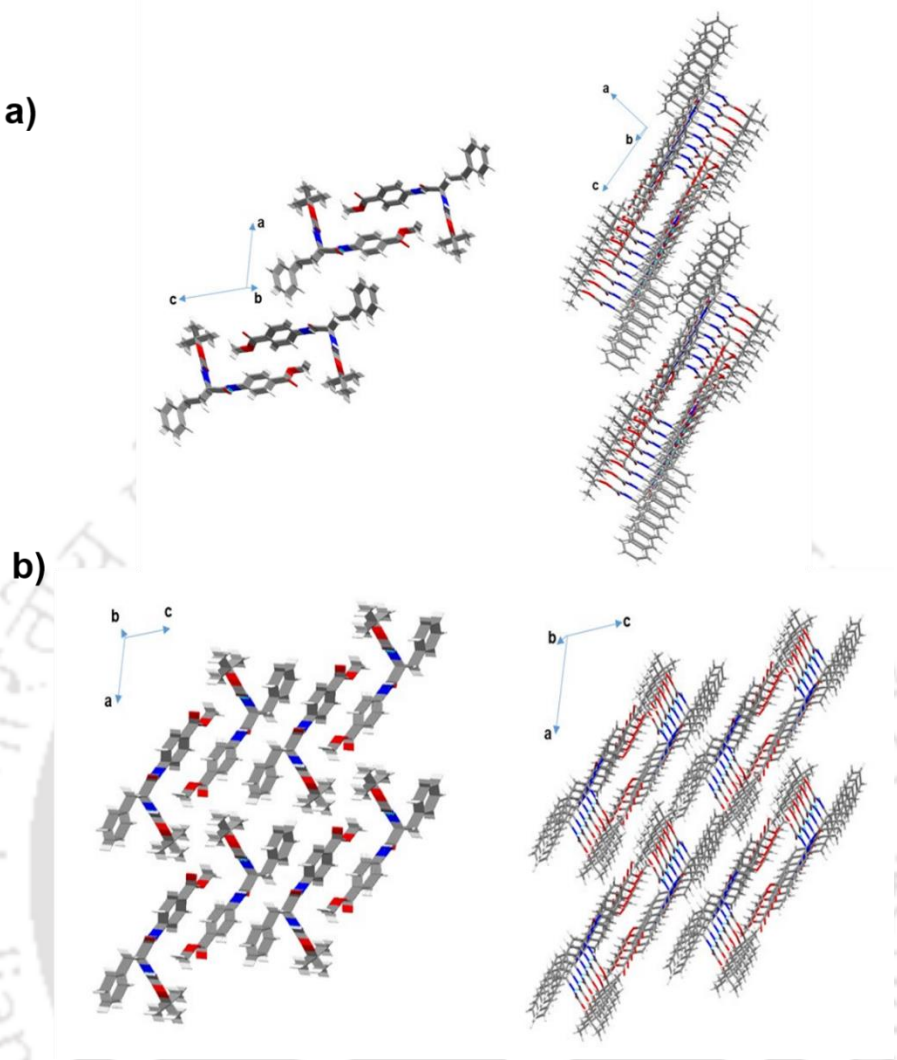

Fig. 2.12. Packing in the crystals of a) P2 and b) P4.

Table 2.5. Intermolecular H-bond parameters for peptides P2 and P4.

Peptide	Donor (N)	Acceptor (O)	N----O (Å)	H----O (Å)	<N-H----O (deg)
P2	N1 (PABA) N2'(HPhe)	O1'(HPhe) O4 (Boc-CO)	3.027 3.086	2.259 2.269	148.90 158.46
P4	N1 (PABA) N2'(Phe)	O3'(Phe) O4 (Boc-CO)	3.034 3.040	2.265 2.217	149.40 159.77

2.3.4.6. Mechanism of self-assembly

Fig. 2.13 summarizes the mechanism of self-assembly of the LMWG P1-P4. Molecules assembled primarily through aromatic π-π stacking and hydrophobic interactions. π-π stacking might occur in between same or different aromatic moieties.

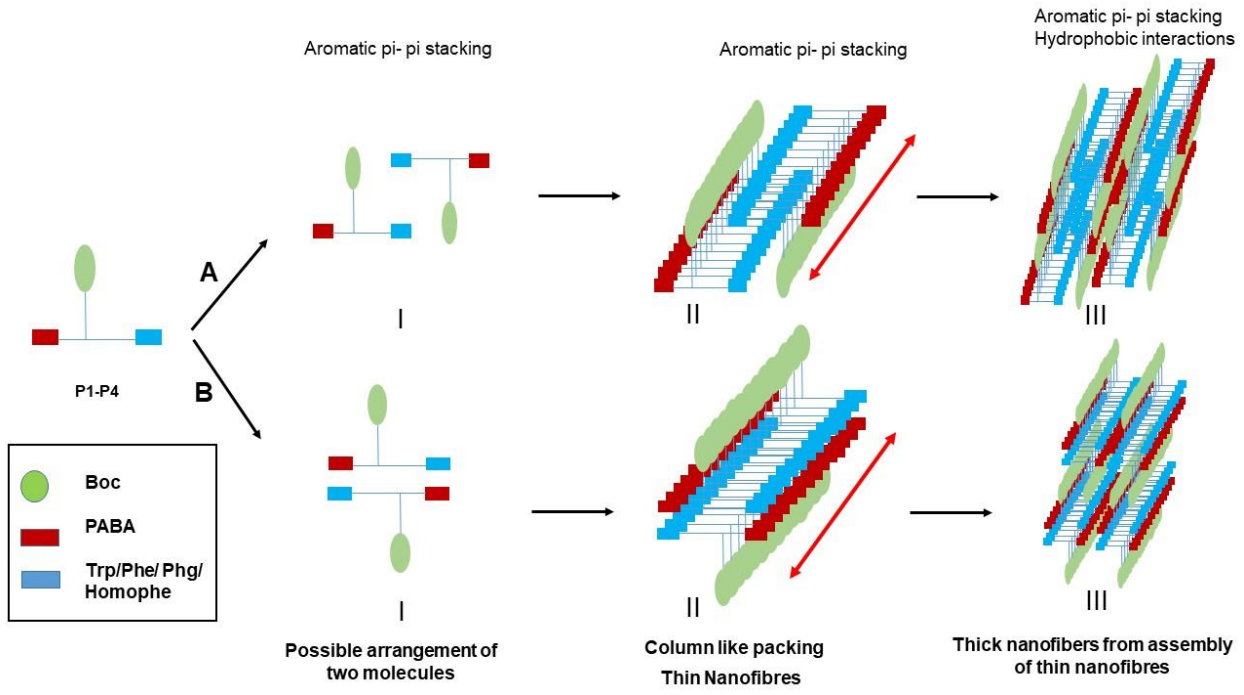

Fig. 2.13. Self-assembly mechanism of P1-P4. Formation of thin nanofibers through columnar-like packing mainly driven by aromatic π-π stacking. Thin nano-fibers further self-assemble into thick nanofibers.

Though all the molecules contained ample hydrogen bond donors and acceptors in the backbone, yet there seemed to be absence of hydrogen bonding in the self- assembled system as evidenced from the FT-IR and NMR studies. While P2-P4 completely lacked hydrogen bonding, P1 contained both hydrogen bonded and non-hydrogen bonded NH's. In the crystals of P2 and P4, weak hydrogen bonds (2.2Å) were present which helped in the crystal packing. Closer approach of the molecules to yield stronger hydrogen bonding might be absent in the crystals to minimize

associated unfavorable van-der-Waals interactions. In the supramolecular packing arrangement in the organogels, presence of solvent molecules further weakened the hydrogen bonds to the limit of non-existence. Thus it was clear that mere presence of hydrogen bonding groups did not ensure hydrogen bonding to be one of the driving forces in the self-assembly of any system. Instead, the assembly of molecules exploited only those parameters which were sufficient to give rise to a thermodynamically favored system. In this case, the aromatic π-π stacking interactions and the hydrophobic interactions were sufficient to create and sustain a thermodynamically favorable self-assembly. There might be subtle differences in the self-assembly of the molecules P1-P4, depending on the side chains of the first amino acid residue. However, the global arrangement of the molecules was similar as evidenced from the pXRD experiments. The backbone conformation of the peptides was kinked at the Cα carbon atom preventing the formation of β sheets as evidenced from the FT-IR studies. The molecules stacked on top of each other initiating unidirectional self-assembly, giving rise to column like structures with fibrous morphology. Many of such thin fibers assembled together due to favorable hydrophobic interactions forming thicker fibers that were seen in the FESEM experiments.

Careful observation indicated that P1-P4 formed gel in several less polar organic solvents like toluene, chloroform, dichlorobenzene etc. in contrast to more polar organic solvents like ethanol, DMSO etc. This seemed to be logical that the non-polar solvents were better accommodated in the entangled network formed by the hydrophobic peptides P1-P4. As the solvents were non-polar and there was no evidence of hydrogen bonding obtained from FTIR and NMR, it might be concluded that the only interaction of the peptides with the solvents was of hydrophobic origin.

2.3.5. Oil spill recovery

Peptides P1-P4 phase selectively formed gels in fuels like kerosene, petrol and diesel. (Fig. 2.14 a, Table 2.6).

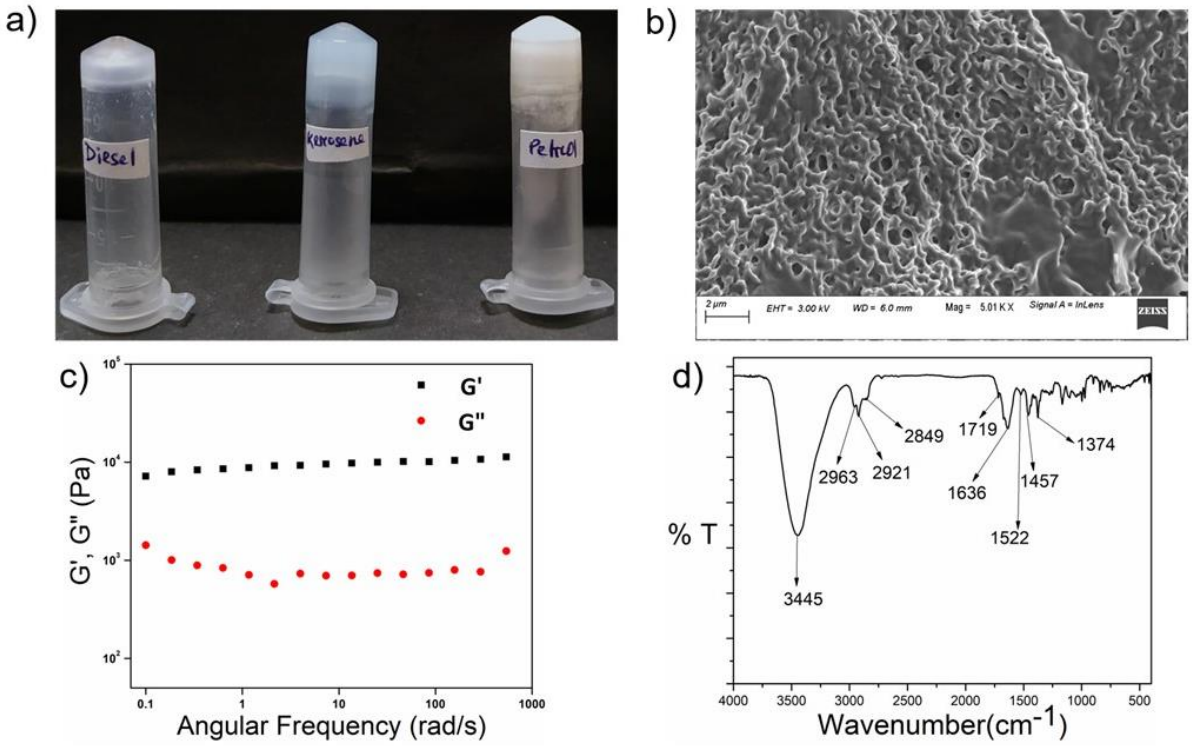

Fig. 2.14. (a) Gels formed by P1 in kerosene, diesel and petrol. (b) FESEM image of P1 organogel in kerosene. (c) Frequency dependence of the dynamic storage moduli (G′) and the loss moduli (G″) of organogel from P1 in kerosene at 1 % w/v. (d) FT-IR of xerogel of P1 in kerosene.

Table 2.6. Gelation ability of P1 in different fuels.

P1	MGC(w/v)	T_{gel}
Kerosene	0.6%	91º C
Petrol	1.5%	75º C
Diesel	1.5%	84º C

The gels had fibrous morphology as seen from FESEM (Fig. 2.14 b) and were mechanically robust (Fig. 2.14 c). In the frequency sweep experiment, the G′ was greater than the G″ throughout the

entire range of the experiment. G′ had value in the order of 10^4-10^5 which suggested that the gels were robust in nature (Fig. 2.14 c). Backbone conformation of the peptide in the xerogel state was probed using FT-IR (Fig. 2.14 d). Though the Amide I peak in the xerogel of P1 in kerosene at 1636 cm^{-1} lied in the antiparallel β sheet region, observation of peak at 3445 cm^{-1}, indicated the presence of non-hydrogen bonded amide protons in the system, which countered the presence of β sheet like conformation. pXRD of P1 xerogel in kerosene showed similar peak pattern and hence interplaner distances as observed for the xerogels of P1 obtained from other organic solvents (Fig. 2.15 a).

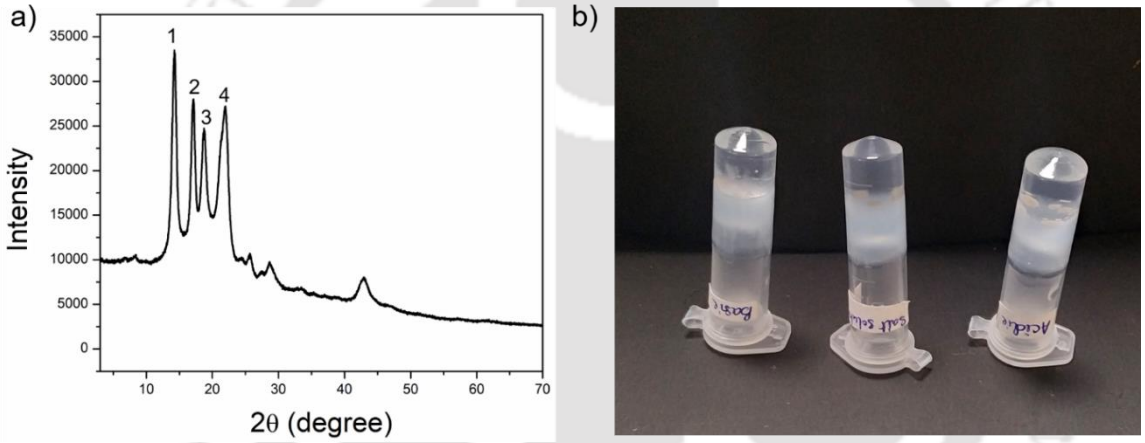

Fig. 2.15. a) PXRD of P1 xerogel in kerosene. b) Phase selective gelation of P1 in kerosene in the presence of acidic, salt solution and basic solution.

This indicated identical arrangement of the molecules in both the cases. Also, we have tested gelation in the presence of acidic, basic and saline aqueous medium and they formed gels upon being heated and cooled subsequently (Fig. 2.15 b).

Summarizing all the above, the mode of self-assembly of P1 in kerosene seemed identical to that in other organic solvents. About 70% of kerosene could be easily recovered upon vacuum distillation of the P1 organogel in kerosene. Facile recovery of the fuel in addition to the gelation

ability of the peptides in presence of variable pH and salt conditions render them as potential candidates for addressing oil spill recovery.

2.3.6. Dye absorption

Organic dye pollutants in the water bodies is one of the major raising concerns for the modern civilization. The organogels obtained from P1-P4 in the present study were checked for their dye absorption abilities. As the peptides were rich in aromatic moieties and hence electrons, they might be good candidates for absorption of cationic dyes (Fig. 2.16-17).

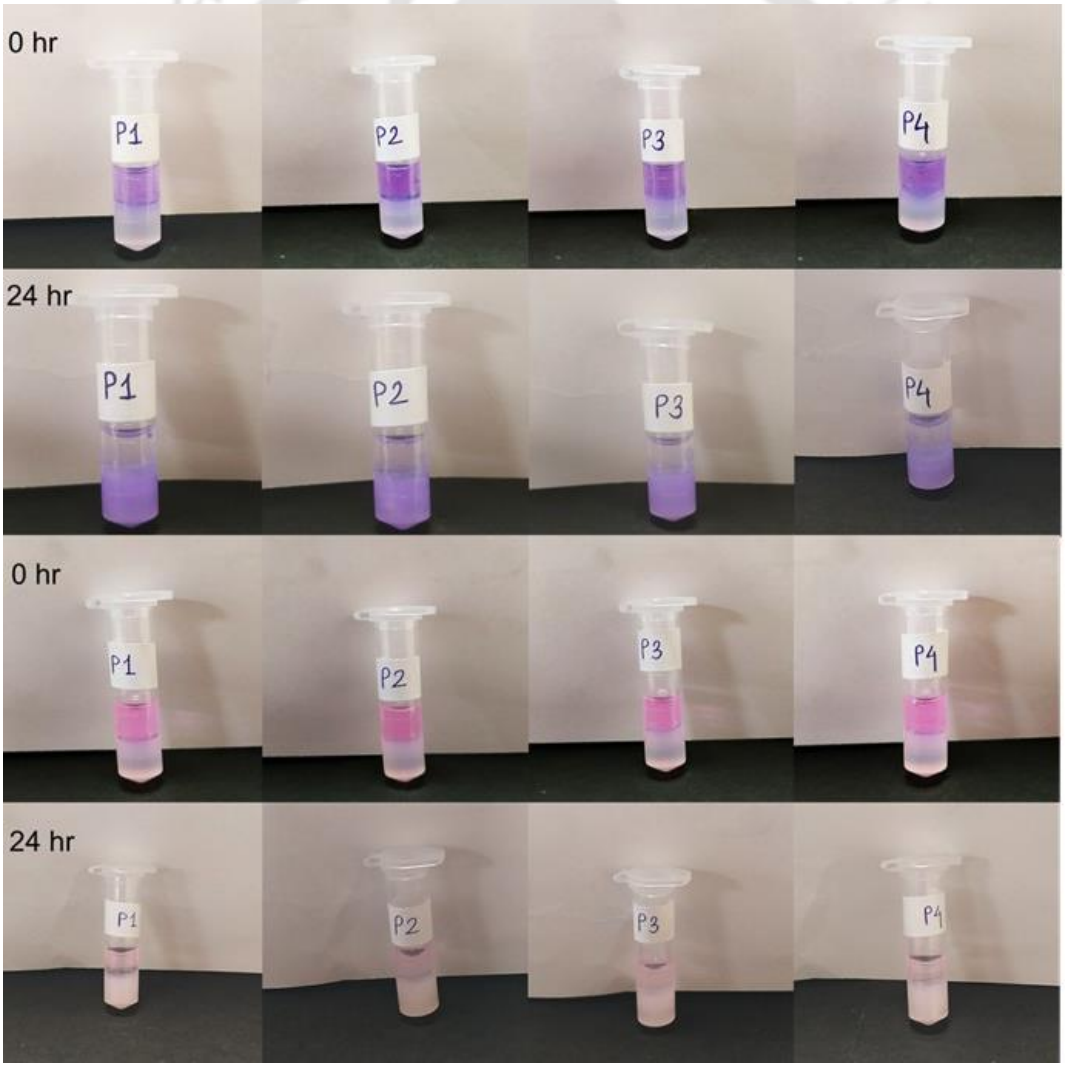

Fig. 2.16. Absorption of cationic dyes CV and RB by organogels P1-P4.

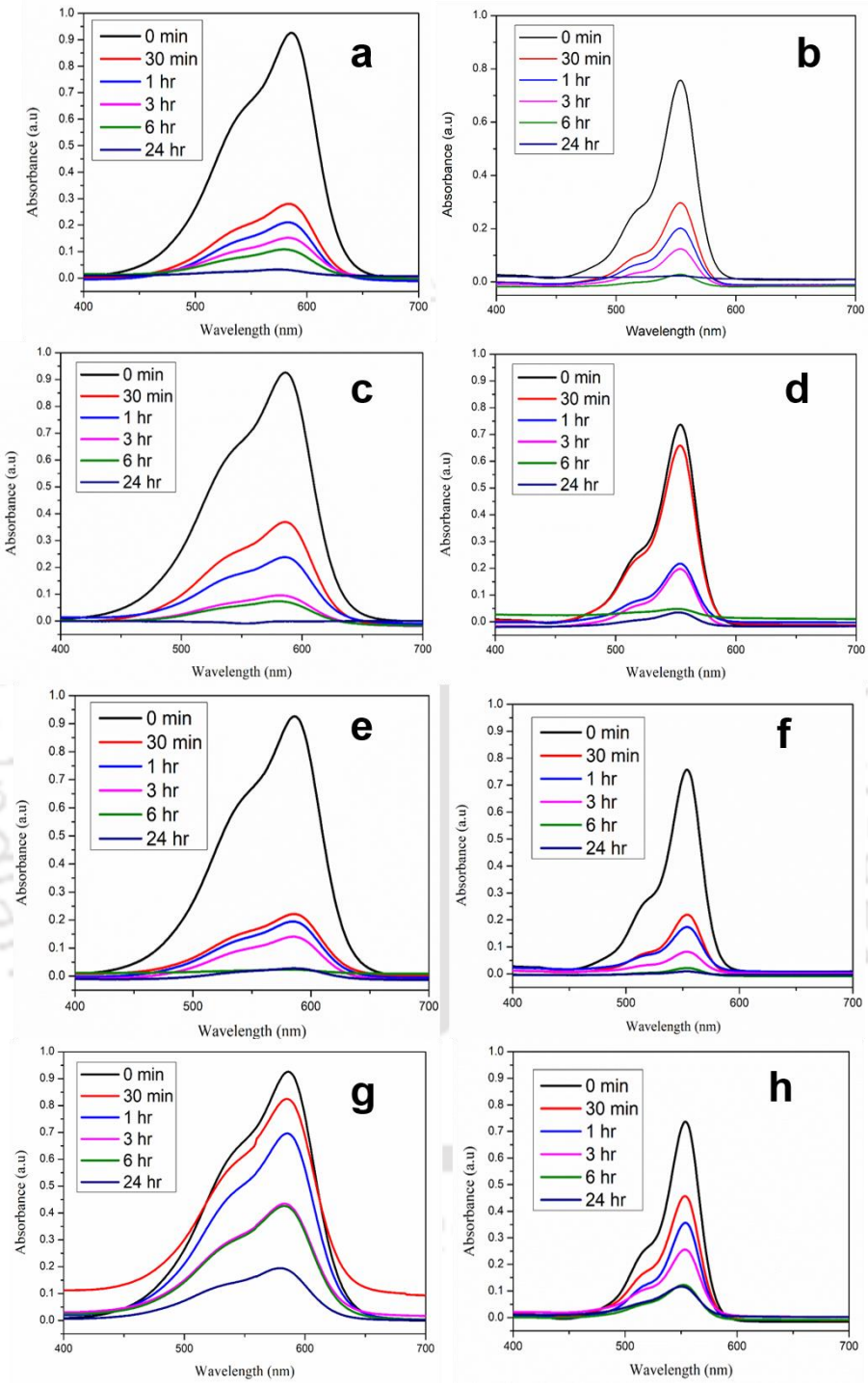

Fig. 2.17. Absorption of dyes by organogels P1-P4 studied by UV spectroscopy. Time dependent absorption spectra of the supernatant solution containing CV (a, c, e, g) and RB (b, d, f, h) incubated with organogels formed by P1-P4 respectively in 1,2-DCB.

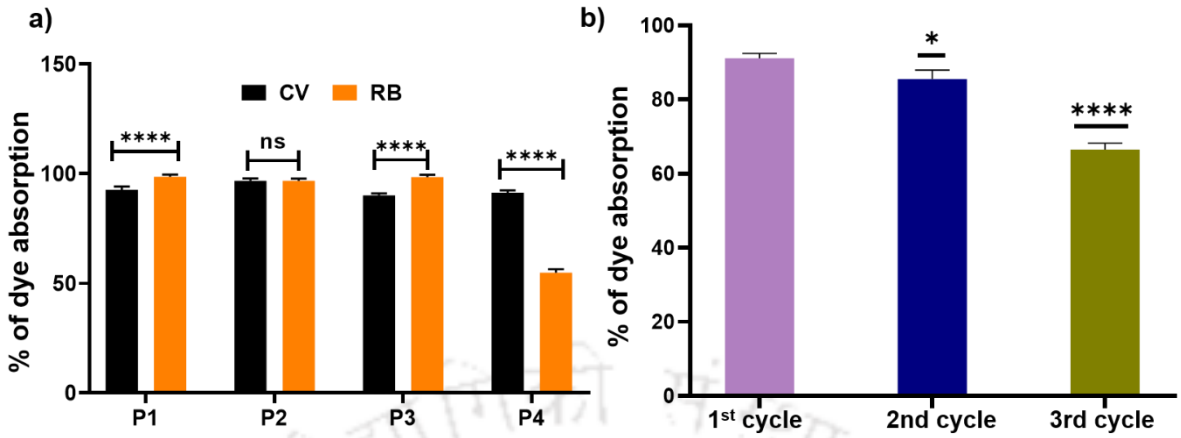

Fig. 2.18. Dye absorption by the organogels P1-P4 in 1,2-DCB. The bar diagram represents the efficiency of (a) absorption of cationic dyes CV and RB by organogels P1-P4 and (b) CV absorption in the subsequent cycles by organogels from P1. The data represents the mean of N=3 experiments (*p< 0.05, **p< 0.01, ***p< 0.001, ****p< 0.0001) via two-way analysis of variance (ANOVA) with Sidak's multiple comparison test for plot a and unpaired t-test for plot b).

Most of the organogels showed high efficiency (≥ 90%) of absorption of representative cationic dyes crystal violet (CV) and rhodamine b (RB) (Fig. 2.18a, Table 2.7). Organogel P4 showed relatively less efficiency in the absorption of RB.

Table 2.7. Dye absorption efficiencies of the organogels P1-P4.

Gelators	CV(%)	RB(%)
P1	92.94	98.57
P2	95.66	97.70
P3	89.00	99.60
P4	91.87	53.55

2.3.6.1. Reusability of the organogel for dye absorption

For commercial use as dye absorbents in the purification of water, the organogels should be reusable. The dyes were released in diethyl ether medium in over 24 h and the original organogels were recovered. The organogels from P1-P4 were tested for three consecutive cycles. Fig. 2.18 b indicates the decreasing loading capacity of CV by P1 organogel in three subsequent cycles.

2.3.7. RGO incorporated organogels

For fabricating conducting organogels, we incorporated RGO into organogels from P1-P4. Reduced graphene oxide is conducting in nature unlike the graphene oxide. As the peptides P1-P4 were rich in aromatic amino acid residues, the incorporation of RGO into the gel was anticipated to be facilitated by aromatic π-π stacking interactions. All the peptides formed organogels in the presence of RGO at their MGC in 1,2-DCB (Fig. 2.19 a). RGO containing peptide organogels were thermoreversible in nature. The RGO doped organogels were thermostable in nature and their T_{gel} were in the same range as that of the native gels. Different amounts of RGO were incorporated into P1 organogel. In the present study, we have incorporated a maximum of 1.2 wt % of RGO in the hybrid gels without destroying the gelation ability of the peptide gelator molecules. Attempts to load higher percentages of RGO in these organogels led to precipitation of RGO and formation of inhomogeneous material.

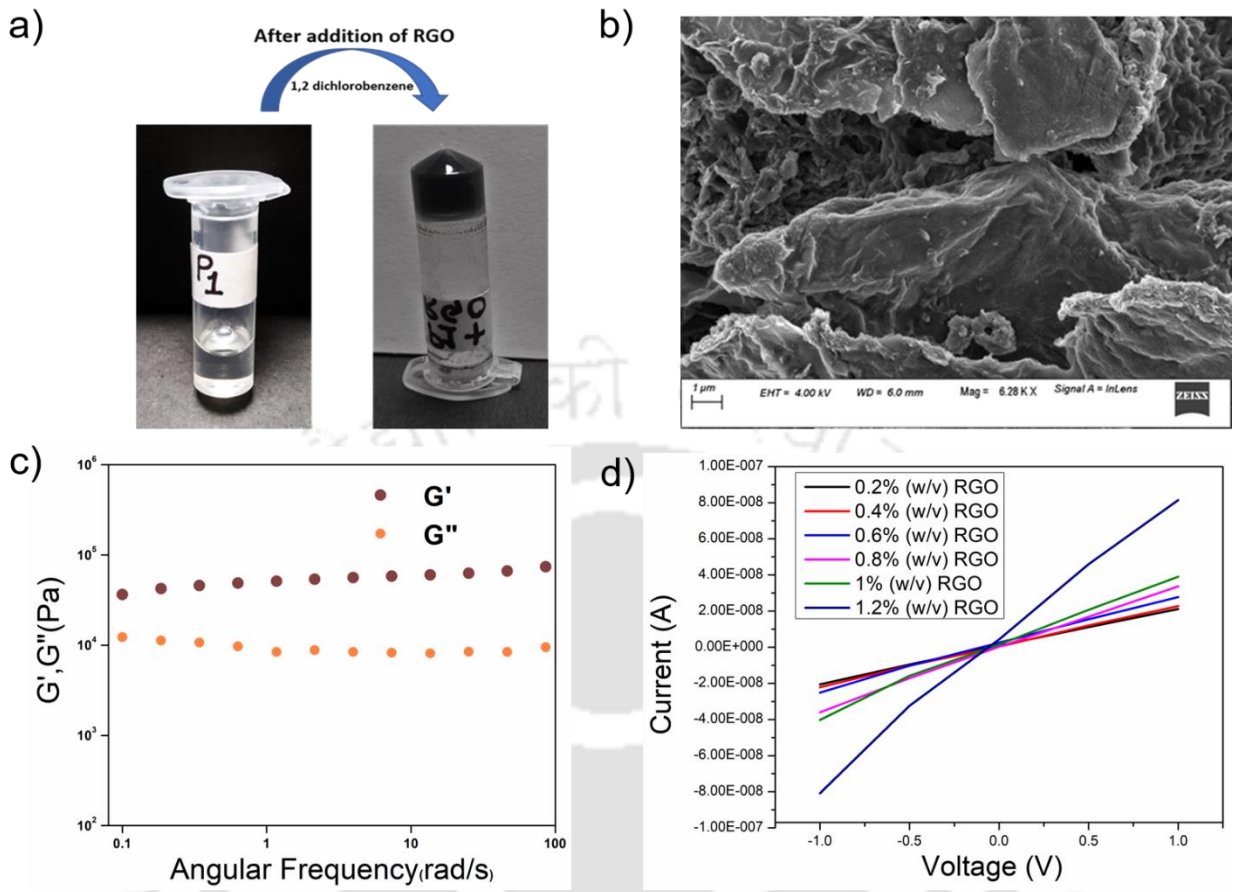

Fig. 2.19. (a) Reduced graphene oxide incorporated hybrid organogel RGO-P1. (b) FESEM image of RGO-P1 hybrid organogel. (c) Frequency dependence of the dynamic storage moduli (G′) and the loss moduli (G″) of RGO-P1 hybrid organogel (1wt%) in 1,2-DCB. (d) I-V curve showing the conductivity of hybrid organogels upon RGO incorporation.

To probe the morphology, FESEM was performed on P1-RGO organogel. Fig. 2.19 b showed the presence of both the RGO nanosheets and the peptide fibres in the hybrid RGO-P1 organogels containing 1wt% of RGO. The RGO nanosheets were clearly visible with the peptide fibrous network dispersed on its surface indicating a good interaction in between the components of the hybrid organogel system. As the peptides were hydrophobic and contained considerable amount of aromatic moieties in them, a good interaction with the RGO, rich in aromatic components might be anticipated in the hybrid organogel. The viscoelastic properties of RGO-P1 xerogel was probed

by rheological studies. Studies were performed on RGO-P1 hybrid organogels containing 1wt % of RGO (Fig. 2.19 c). In the frequency sweep experiment, the value of G′ was greater than G″ throughout the experimental limit indicating that the hybrid organogels were "solid like" similar to the native gel. Interestingly, the values of G′ and G″ increased 10 folds in the case of RGO-P1 containing 1wt % of RGO in comparison to the native gel. This meant that the incorporation of RGO enhanced the rigidity of the gel. This might be attributed to the favorable interaction in between the peptide nanofibers and the RGO sheets.

Graphene is known for its highly conducting nature. Oxidation of graphite to graphene oxide changes some carbons to sp^3, thus destroying the conductivity of the material. RGO on the other hand, once again becomes conducting in nature, though not as good as graphene. Upon incorporation of RGO into the organogels, the hybrid materials became conducting in nature. There are lots of studies in the literature where hybrid materials containing graphene and its derivatives have been used for energy conversion and storage.[19-23] Most of these hybrid materials are of inorganic nature and have high conductivity. There are fewer examples of peptide based materials containing graphene and its derivatives.[31-33] Though, peptide based hybrid materials are less conducting in nature compared to their inorganic counterparts, they are interesting as they might find applications in biomedical applications/devices owing to their biocompatibility. Fig. 2.19 d shows the I-V curves obtained from the hybrid organogel RGO-P1 containing different amounts of RGO in them. The conductivity of the RGO doped organogels increased proportionately to the amount of RGO in them. Homogeneous gels could not be prepared beyond insertion of 1.2 w/v% of RGO, hence they were not considered for conductivity studies.

To understand the backbone conformation of the peptide molecules in the hybrid organogel RGO-P1, FT-IR was performed on the xerogel containing 1wt % RGO (Fig. 2.20 a). The NH stretching

frequency was observed at 3421 cm^{-1}, which indicated the presence of non-hydrogen bonded NHs in the hybrid xerogel much like the scenario of the pristine xerogels made from peptides alone. The Amide I stretching peak was observed at 1667 cm^{-1}, similar to that obtained from the xerogel containing the peptide alone. Thus the backbone conformation of the peptides was identical both in the pristine and in RGO-P1 xerogel. pXRD data obtained from the RGO-P1 xerogel was similar to that obtained from pristine xerogel indicating that the solid state arrangement of the molecules was the same in both the hybrid and the pristine organogel systems (Fig. 2.20 b).

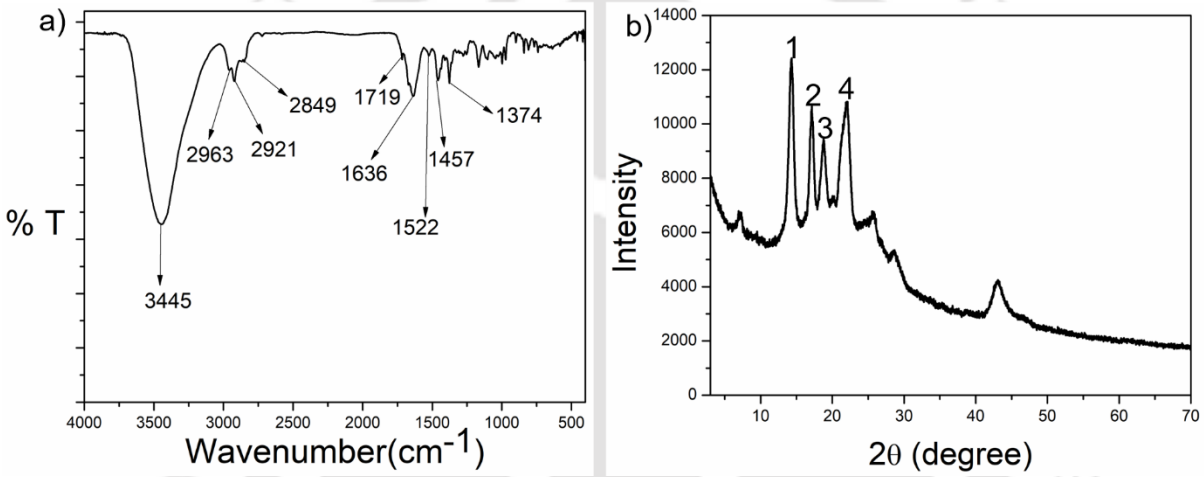

Fig. 2.20. a) FT-IR of RGO-P1 hybrid xerogel and b) PXRD of RGO-P1 hybrid organogel.

Summing it all up, insertion of RGO in the peptide organogel did not disrupt the self-assembly pattern that was present in the only peptide system. The backbone conformation, solid state packing etc. remained unaltered upon insertion of RGO. From the FESEM images, it was evident that both RGO and the peptides retained their distinct morphologies. Hence the mode of coassembly might be considered as "orthogonal" in this case. Favorable aromatic interactions in between the peptides and the RGO might result in increased rigidity in the system.

2.4. Conclusions

Small gelator peptides rich in aromatic moieties were designed in this work which readily formed phase selective, thermoreversible, mechanically robust organogels in a large variety of organic solvents and in fuels like kerosene, diesel and petrol. Phase selective gelation ability of P1-P4 in petroleum fuels in various pH and saline conditions render these organogels as potential materials for controlling marine oil spills. Aromatic π-π stacking and hydrophobic interactions were the driving force for the assembly process while, hydrogen bonding played a trivial role in some systems and was completely absent in others. All the four organogels, obtained from P1-P4 were excellent dye absorbents and potential materials to be used in water purification. RGO was incorporated into the peptide organogels to yield hybrid organogels which were conducting in nature. Hybrid organogels were more rigid than the native peptide gels and their conductivity was proportional to the RGO content of the organogel. Hence with rational design of the structural components in the LMWG, self-assembly might be directed to yield materials which are economically viable, recyclable and can be utilized for multiple applications.

Despite the numerous advantages of our organogels, further explicit study is required to apply them effectively in real-world water remediation issues. Since this study involved only a laboratory-scale synthesis of the peptides, therefore scaling up to an industrial level is necessary for being performed on a larger platform. Additionally, the synthesis process needs to become greener for long-term sustainability with the use of alternative coupling reagents and solvents. Moreover, we have tested the efficiency of organogels in water remediation only with a limited selection of dyes and oils. Therefore, future research should explore their effectiveness with other possible toxic dyes, metal ions, oils and real samples collected from polluted water bodies.

2.5. References

1. P. Dastidar, P. Supramolecular gelling agents: can they be designed? *Chem. Soc. Rev.* **2008**, *37*, 2699.

2. Sangeetha, N. M.; Maitra, U. Supramolecular gels: functions and uses. *Chem. Soc. Rev.* **2005**, *34*, 821.

3. Yu, G.; Yan, X.; Han, C.; Huang, F. Characterization of supramolecular gels. *Chem. Soc. Rev*. **2013**, *42*, 6697.

4. Bera, S.; Haldar, D. A rechargeable self-healing safety fuel gel. *J. Mater. Chem. A* **2016**, *4*, 6933.

5. Lim, J. Y. C.; Goh, S. S.; Liow, S. S.; Xue, K.; Loh; X. J. Molecular gel sorbent materials for environmental remediation and wastewater treatment. *J. Mater. Chem. A* **2019**, *7*, 18759-18791.

6. Schrope, M.; Deep Wounds. *Nature* **2011**, *472*, 152–154.

7. Wood, D. M.; Greenland, B. M.; Acton, A. L.; Rodríguez-Llansola, F.; Murray, C. A.; Cardin, C, J.; Miravet, J. F.; Escuder, B.; Hamley, I, W.; Hayes, W. pH-Tunable Hydrogelators for Water Purification: Structural Optimisation and Evaluation. *Chem. Eur. J.* **2012**, *18*, 2692.

8. Rodríguez-Llansola, F.; Escuder, B.; Miravet, J. F.; Hermida-Merino, D.; Hamley, I. W.; Cardin, C. J.; Hayes, W. Selective and highly efficient dye scavenging by a pH-responsive molecular hydrogelator. *Chem. Commun*. **2010**, *46*, 7960.

9. Basak, S.; Nandi, N.; Paul, S.; Hamley, I. W.; Banerjee, A. A tripeptide-based self-shrinking hydrogel for waste-water treatment: removal of toxic organic dyes and lead (Pb^{2+}) ions. *Chem. Commun*. **2017**, *53*, 5910.

10. Adhikari, B.; Palui, G.; Banerjee, A. Self-assembling tripeptide based hydrogels and their use in removal of dyes from waste-water. *Soft Matter* **2009**, *5*, 3452.

11. Ray, S.; Das, A. A.; Banerjee, A. pH-responsive, bolaamphiphile-based smart metallo-hydrogels as potential dye-adsorbing agents, water purifier, and vitamin B12 carrier *Chem. Mater*. **2007**, *19*,1633.

12. Okesola, B. O.; Smith, D. K. Versatile supramolecular pH-tolerant hydrogels which demonstrate pH-dependent selective adsorption of dyes from aqueous solution. *Chem. Commun*. **2013**, *49*, 11164.

13. Chakraborty, P.; Roy, B.; Bairi, P.; Nandi, A. K. Improved mechanical and photophysical properties of chitosan incorporated folic acid gel possessing the characteristics of dye and metal ion absorption. *J. Mater. Chem*. **2012**, *22*, 20291.

14. Sengupta, S.; Mondal, R. A novel gel-based approach to wastewater treatment–unique one-shot solution to potentially toxic metal and dye removal problems. *J. Mater. Chem. A* **2014**, *2*, 16373.

15. Chakrabarty, A.; Maitra, U.; Das, A. D. Metal cholate hydrogels: versatile supramolecular systems for nanoparticle embedded soft hybrid materials. *J. Mater. Chem*. **2012**, *22*, 18268.

16. Cheng, N.; Hu, Q.; Guo, Y.; Wang, Y.; Yu, L. Efficient and selective removal of dyes using imidazolium-based supramolecular gels. *ACS Appl. Mater. Interfaces* **2015**, *7*, 10258.

17. Debnath, S.; Shome, A.; Dutta, S.; Das, P. K. Dipeptide-based low-molecular-weight efficient organogelators and their application in water purification *Chem. Eur. J*. **2008**, *14*, 6870.

18. Basu, K.; Nandi, N.; Mondal, B.; Dehsorkhi, A.; Hamley, I. W.; Banerjee, A. Peptide-based ambidextrous bifunctional gelator: Applications in oil spill recovery and removal of toxic organic dyes for waste water management. *Interface Focus* **2017**, *7*, 20160128.

19. Huang, X.; Qi, X.; Boey, F.; Zhang, H. Graphene-based composites. *Chem. Soc. Rev.* **2012**, *41*, 666.

20. Maiti, U. N.; Lim, J.; Lee, K. E.; Lee, W. J.; Kim, S. O. Three-dimensional shape engineered, interfacial gelation of reduced graphene oxide for high rate, large capacity supercapacitors. *Adv. Mater.* **2014**, *26*, 615-619.

21. Yang, C.; Liu, Z.; Chen, C.; Shi, K.; Zhang, L.; Ju, X.-J.; Wang, W.; Xie, R.; Chu, L.-Y. Reduced graphene oxide-containing smart hydrogels with excellent electro-response and mechanical properties for soft actuators. *ACS Appl. Mater. Interfaces* **2017**, *9*, 15758-15767.

22. Kumar, R.; Singh, R. K.; Alaferdov, A. V.; Moshkalev, S. A. Rapid and controllable synthesis of Fe3O4 octahedral nanocrystals embedded-reduced graphene oxide using microwave irradiation for high-performance lithium-ion batteries. *Electrochim. Acta* **2018**, *281*, 78-87.

23. Kumar, R.; da Silva, E. T. S. G.; Singh, R. K.; Savu, R.; Alaferdov, A. V.; Fonseca, L. C.; Carossi, L. C.; Singh, A.; Khandka, S.; Kar, K. K.; Alves, O. L.; Kubota, L. T.; Moshkalev, S. A. Microwave-assisted synthesis of palladium nanoparticles intercalated nitrogen doped reduced graphene oxide and their electrocatalytic activity for direct-ethanol fuel cells. *J. Colloid Interface Sci.* **2018**, *515*, 160-171.

24. Kumar, R.; Singh, R. K.; Singh, D. P.; Vaz, A. R.; Yadav, R. R.; Rout, C. S.; Moshkalev, S. A. Synthesis of self-assembled and hierarchical palladium-CNTs-reduced graphene oxide composites for enhanced field emission properties. *Mater. Des.* **2017**, *122*, 110-117.

25. Kumar, R.; Sahoo, S.; Joanni, E.; Singh, R. K.; Tan, W. K.; Kar, K. K.; Matsuda, A. Recent progress in the synthesis of graphene and derived materials for next generation electrodes of high performance lithium ion batteries. *Prog. Energy Combust. Sci.* **2019**, *75*, 100786.

26. Kumara, R.; Joanni, E.; Singh, R. K.; Singh, D. P.; Moshkalev, S. A. Recent advances in the synthesis and modification of carbon-based 2D materials for application in energy conversion and storage. *Prog. Energy Combust. Sci.* **2018**, *67*, 115-157.

27. Vedhanarayanan, B.; Babu, B.; Shaijumon, M. M.; Ajayaghosh, A. Exfoliation of reduced graphene oxide with self-assembled π-gelators for improved electrochemical performance. *ACS Appl. Mater. Interfaces* **2017**, *9*, 19417-19426.

28. Kuwahara, R. Y.; Oi, T.; Hashimoto, K.; Tamesue, S.; Yamauchi, T.; Tsubokawa, N. Easy preparation of graphene-based conducting polymer composite via organogel. *Colloid Polym. Sci.* **2015**, *293*, 1635-1645.

29. Adhikari, B.; Biswas, A.; Banerjee, A. Graphene oxide-based hydrogels to make metal nanoparticle-containing reduced graphene oxide-based functional hybrid hydrogels. *ACS Appl. Mater. Interfaces* **2012**, *4*, 5472-5482.

30. Kumar, R.; Macedo Jr, W. C.; Singh, R. K.; Tiwari, V. S.; Constantino, C. J. L.; Matsuda, A.; Moshkalev, S. A. Nitrogen–sulfur co-doped reduced graphene oxide-nickel oxide nanoparticle composites for electromagnetic interference shielding. *ACS Appl. Nano Mater.* **2019**, *2*, 4626-4636

31. Adhikari, B.; Nanda, J.; Banerjee, A. Pyrene-containing peptide-based fluorescent organogels: inclusion of graphene into the organogel. *Chem. Eur. J.* **2011**, *17*, 11488-11496.

32. Adhikari, B.; Banerjee, A. Short peptide-based hydrogels: incorporation of graphene into the hydrogel. *Soft Matter* **2011**, *7*, 9259- 9266

33. Han, T. H.; Lee, W. J.; Lee, D. H.; Kim, J. E.; Choi, E.-Y.; Kim, S. O. Peptide/graphene hybrid assembly into core/shell nanowires. *Adv. Mater.* **2010**, *22*, 2060-2064.

34. Deka, P.; Verma, V. K.; Chandrasekaran, A.; Neog, A. B.; Bardhan, A.; Raidongia, K.; Subbiah. S. Performance of novel sericin doped reduced graphene oxide membrane for FO based membrane crystallization application. *J. Membr. Sci.* **2022**, *660*, 120884.

35. a) Maity, I.; Mukherjee, T. K.; Das, A. K. Photophysical study of a π-stacked β-sheet nanofibril forming peptide bola amphiphile hydrogel. *New J. Chem.* **2014**, 3*8*, 376-385.

b) Das, A. K.; Hirst, A. R.; Ulijn, R. V. Evolving nanomaterials using enzyme-driven dynamic peptide libraries (eDPL). *Faraday Discuss*. **2009**, *143*, 293–303.

c) Pandit, G.; Roy, K.; agarwal, U.; chatterjee, S. Self-assembly mechanism of a peptide-based drug delivery vehicle. *ACS Omega* **2018**, *3*, 3143–3155.

d) Liang, J. X.; Nguyen, Q. L.; Matsika, S. Exciplexes and conical intersections lead to fluorescence quenching in π-stacked dimers of 2-aminopurine with natural purine nucleobases. *Photochem. Photobiol. Sci.* **2013**, *12*, 1387-1400.

Chapter 3

Fabrication of Thermoreversible CdSe/CdSe-ZnS Quantum Dots Doped Hybrid Peptide Organogels

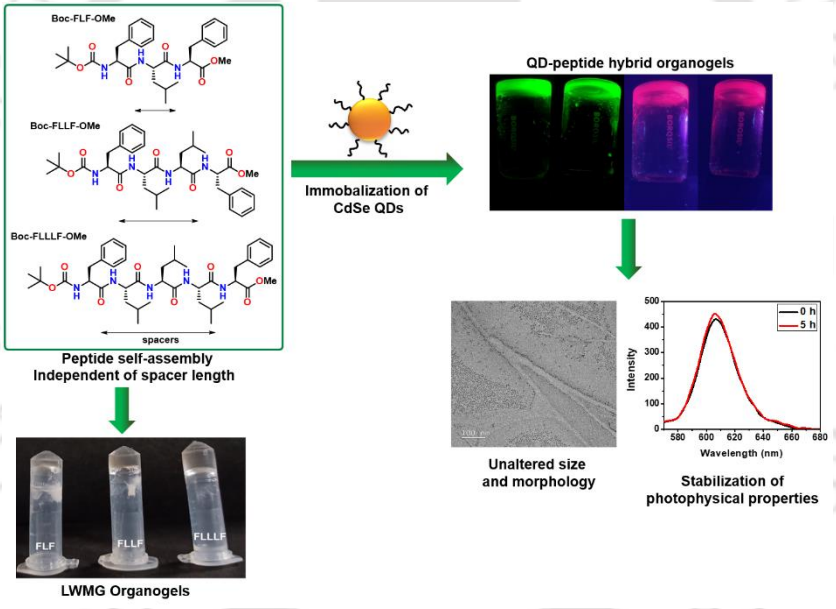

3.1. Introduction

Diphenylalanine (FF) is known to be the smallest self-assembling peptide motif as evidenced from the existing literature.[1] In addition to being identical to the core recognition motif of the β-amyloid polypeptide,[2] which is responsible for Alzheimer's disease, the FF unit has been utilized to create numerous hierarchical structures like elongated tubular assemblies,[3] fibrillar networks,[4] spheres,[5] plates[6] etc. Apart from several other assemblies, the FF dipeptide and its derivatives are famous for their ability to form LMWG several organic solvents like toluene, chloroform, benzene, chlorobenzene, etc., very efficiently.[7-10] The presence of the Phe amino acid residue facilitates π-π interactions through phenyl rings, which makes its derivatives good gelators in various solvents.[11] Exploiting this property, it has been possible to modify the FF motif to generate desired assemblies by incorporating various groups in between the Phe amino acid residues,[12] connecting other molecules,[13] or by simply varying the protecting groups at the termini.[14] Haldar and coworkers studied a series of FF peptidomimetics with conformationally rigid and flexible spacers, two of which were found to form stimuli-responsive organogels in a wide range of solvents, including methanol.[12] Over the past few decades, these LMWG-based biomaterials derived from FF units have extensively been studied as potential candidates for designing of soft materials, such as hybrid nanomaterials.[15-16]

On the other hand, fluorescent organogels developed by entrapping various nanoparticles, are important owing to their potential applications in optoelectronic devices and sensors. The fibrillar gel network provides stability and proper organization to the metallic nanoparticles.[17] Inorganic luminescent nanoparticles, QDs, have been gaining increased attention in the recent times, due to their size-dependent emission spectra along with broad excitation, narrow emission, and high photoluminescence efficiencies.[18] Till now, QDs have been vastly used in many research areas

like biology,[19] analytical[20] and material chemistry.[21] The most commonly used QDs are usually composed of CdSe that has a luminescent core.[22] Also, the presence of an inorganic shell with higher band gap such as zinc sulphide (ZnS) shell, can reduce the surface defects and also enhance the quantum yield of the QDs.[23] Most of these QDs are capped by trioctylphosphine oxide and octadecylamine. The organic ligands help to disperse the QDs in different organic solvents. However, over time, even in the presence of these ligands, the Cd core is oxidized, and this leads to the leaching of Cd from the QD surface. This eventually results in QD aggregation and quenching of their luminescent properties.[24] Thus, incorporation of these QDs into microenvironments such as low molecular weight gels for enhancement of their stability, has become an active area of research in recent times.[18, 25] This approach is not only important in designing and studying the properties of the hybrid QD-gel materials but also in stabilization of the QD core in absence/presence of ZnS shell, by reduction of the aggregation and enhancement of the photostability of the QDs. These hybrid structures are held together predominately by π-π interactions.

Reports claimed that FF peptide-based organogels are suitable alternatives for encapsulation and stabilization of QDs.[26] Li and co-workers described the preparation of hybrid organogels by mixing CdSeS nanocrystals with FF dipeptide molecules in a gelling solution. The resulting FF dipeptide organogel was found to be capable of encapsulating QDs with retained photoluminescence (PL), offering an effective method of protection of QDs from oxidation and improvement of the stability of the QDs. However, reports of the prevention of QDs from oxidation-based fluorescence quenching by peptide-based gels are limited. Groups of Banerjee and Gopi incorporated CdS nanoparticles into self-assembled structures obtained from peptide hydrogel and organogel-based systems.[27-28]

In this work, we wanted to probe if the physical proximity of the two Phe residues in the di-Phe moiety was necessary for its remarkable and versatile assembling nature. To investigate this, we designed three different peptides based on Boc-FF-OMe (FF), namely Boc-FLF-OMe (FLF), Boc-FLLF-OMe (FLLF) and Boc-FLLLF-OMe (FLLLF), by incorporating variable number of hydrophobic amino acid residues leucine (L, Leu), as spacers in between the two phenylalanine residues, and compared their self-assembly patterns/gelation abilities with the parent dipeptide. We investigated if these organogels were effective for encapsulating and stabilizing the QDs. FLLF organogel was found to efficiently encapsulate both green and red CdSe QDs in presence/absence of ZnS shells, and greatly stabilize the QDs by retaining their luminescence properties and preventing them from undergoing oxidative fluorescence-quenching.

3.2. Experimental section

3.2.1. Materials procured

All of the amino acids, coupling reagents 1-Ethyl-3-(3dimethylaminopropyl) carbodiimide hydrochloride (EDC.HCl) and 1-hydroxybenzotriazole (HOBt) were purchased from GL Biochem (Shanghai, China). Dioxane, Trifluoroacetic acid (TFA), HPLC grade acetonitrile and methanol were obtained from Merck. Di-tert-butyl dicarbonate (Boc), thionyl chloride ($SOCl_2$) *N*, *N*′-diisopropylethylamine (DIPEA), calcium hydride, lithium hydroxide (LiOH) and other chemicals were purchased from Sigma-Aldrich. Methanol and dichloromethane were dried using magnesium turnings and calcium hydride (CaH_2), respectively. All reagents for peptide synthesis were used as received without further purification. Column chromatography was done using silica gel (60-120/100-200 mesh size) as stationary phase and hexane/ethyl acetate as eluent. Thin layer chromatography (TLC) was performed using TLC Silica Gel 60 F254 and visualized by UV light, or stained with iodine vapor and $KMnO_4$ solution.

3.2.2. General procedure of peptide synthesis and purification

All peptides were synthesized through conventional solution phase chemistry using a fragment condensation strategy, involving a 1+1, 1+2, 2+2 and 2+3 coupling in the final step for di, tri, tetra and pentapeptides, respectively. Tert-Butyloxycarbonyl (Boc) was used for N-terminus protection, and the C-terminus was protected as a methyl ester. Peptide coupling was mediated by EDC.HCl and HOBt. Deprotection of Boc group was achieved by TFA in DCM (1:1), and the methyl group was removed by saponification using LiOH in mixture of methanol and water (2:1).

Crude peptides were purified by reverse-phase HPLC using binary acetonitrile/water (75−100%) solvent system at a flow rate of 10 mL/min using dual UV detection at 214 and 220 nm. To check the purity, analytical HPLC was performed with a flow rate of 1 mL/min and a linear gradient of 50−100% in acetonitrile/water system. Analytical HPLC (Appendix, Fig. A3.1- A3.4) confirmed the >95% of purity of all peptides. All the purified peptides were characterized by ESI-MS (Appendix, Fig. A3.5-A3.8) and ^{1}H NMR (Appendix, Fig. A3.9-A3.12).

3.2.3. Gelation

The ability of all the four peptides to form organogels was studied by the simple heating-cooling method. Peptides were dissolved in 500 µL of solvent. Peptide solutions were heated at temperatures in between 90°-100° C for 10-15 min. Later, the heated peptide solutions were allowed to cool to room temperature. After cooling, the organogels were immediately formed which were further confirmed by the vial inversion test.

3.2.4. Phase selective gelation

All the three peptides were weighed at their MGC and a mixture of toluene and water (each 500 µL) was added to them. The solutions were properly vortexed and placed in a heating block at 90°-

100°C for 15 min. After cooling to room temperature selective gelation was observed in the organic layer in the presence of aqueous solvent.

3.2.5. Rheology

The mechanical strength of the organogels made from the three peptides in toluene was examined by conducting rheological experiments in an Anton Paar MCR102 Rheometer as discussed earlier in section **2.2.5 (**Chapter 2).

3.2.6. FESEM

Morphological studies of organogels were carried out with the help of FESEM on a Sigma Zeiss microscope. Firstly, the peptides were taken at their MGC and their solution in toluene was heated at 90 °C for 10-15 min. After that, 1-2 µL from the heated peptide solutions were cast on the silicon wafer and kept under the vacuum to dry properly before collecting images.

3.2.7. NMR

Nuclear magnetic resonance (NMR) experiments were conducted for the characterization of peptides on a 600 MHz Bruker NMR spectrometer. ^{1}H NMR experiments for all three peptides were performed in $CDCl_3$ solvent at ambient temperature.

3.2.8. PXRD

Wide angle X-ray diffraction analysis was carried out for xerogels prepared from the organogels in toluene for all the three peptides, by using a Rigaku Smartlab X-ray diffractometer (Cu-K α radiation, λ=1.540 Å).

3.2.9. Synthesis of quantum dots

3.2.9.1. Synthesis of Cadmium-Selenide core QDs

Highly fluorescent Cadmium-selenide QD core was synthesized by following a previously reported method with some modifications.[29] Briefly, 23 mg CdO, 200 mg stearic acid were taken in a 25 ml three necked flask and 7-8 ml of 1-octadecene was added to that flask. The mixture was heated at 220°C under argon atmosphere to obtain a colourless solution. Next, the solution was cooled at room temperature and ODA (1.5 g) and TOPO (0.6 g) were added to the flask and the mixture was again heated at 280°C under argon atmosphere. At this temperature, 1 mL of Selenium solution in TOPO (40 mg/mL) was quickly injected to the mixture. Then the emission of the mixture was thoroughly checked and reaction was quenched at the desired fluorescence emission. The reaction mixture was allowed to cool at room temperature and was purified using acetone-based precipitation-resuspension method. Most of the excess organic ligands were removed by using this method. Finally, these particles were dispersed in toluene. The particle concentration was measured by using its molar extinction coefficient (ε).

3.2.9.2. Synthesis of Cadmium Selenide Core-Zinc Sulphide shell QDs

Further shelling of these CdSe core QDs by zinc sulphide (ZnS) was done by following a previously reported method with some modifications.[30] Briefly, purified QD core was taken in a 25 ml three necked round bottomed flask and in that flask 1 g TOPO and 2.5 g ODA were added and the mixture was heated at 160°C under argon atmosphere. In other two vials, 224 mg of Zn-stearate and 14 mg Sulphur powder were dissolved in 4 mL 1-octadecence. These two solutions were injected alternatively to the reaction mixture at temperatures 160°C, 180°C, 190°C and 200°C. Finally, the reaction mixture was cooled down to room temperature and purified using acetone, chloroform and ethanol. These purified particles were dispersed in toluene.

3.2.10. Formation of QD-peptide hybrid gels

Both green and red QD core and core-shell nanoparticles were taken with a concentration of around 2.5 µM. The stock concentration of 10 µM was initially prepared for QDs in toluene, while on the other hand, the stock concentration of 10 mM was prepared for the peptide in toluene. Next, 250 µL of QD solution from stock was taken in a vial and 200 µL (for green QD core and core shell) and 200 µL (for red QD core and core shell) of peptide solutions were added to the respective vials. For green QD, the volume was made up to 1 mL by adding toluene. Hence, for the green QD core and core-shell, the final concentration of the peptide in the gel was 2 mM and the QD concentration was 2.5 µM. On the other hand, for the red QD core and core-shell, the final concentration of the peptide in the gel was 2 mM and the QD concentration was 2.5 µM. In order to make the gel, the mixtures were heated in a water bath/heating block at 90°-100° C for 10-15 min followed by cooling at room temperature.

3.2.11. Photophysical measurements

UV-visible spectra of the QDs and QD-peptide hybrid gels were measured in the Shimadzu UV-2550 spectrometer. Fluorescence spectra of the QDs and QD-peptide hybrid gels were recorded with excitation wavelength, λ=500 nm for the green QDs and λ=520 nm for the red QDs, in the PerkinElmer LS45 spectrometer. Fluorescence lifetimes were measured by time-correlated single photon counting (TCSPC) in solution (toluene) and gel state with a Horiba Jobin Yvon Fluoromax 3 spectrometer with magic angle with a 450 nm laser probe. The decay curves were fitted with a tri-exponential function for both QDs in solution and QD-peptide gels.

3.2.12. Quantum yield calculation

The quantum yields of the hybrid QD gels and QDs in solutions were measured in reference to Rhodamine 6G (QY = 94% at 500/520 nm excitation in ethanol). The calculations have been

completed by using the following equation:

$$(QY)_{Sm} = (QY)_{St} \times [(PL_{area}/OD)_{Sm}/ PL_{area}/OD)_{St}] \times \eta^2_{Sm}/\eta^2_{St,}$$

where Sm indicates the sample, St indicates the standard, η is the refractive index of the solvent, and PL area and OD are the fluorescence area and absorbance value, respectively.

3.2.13. Transmission electron microscopy

Morphological studies of QDs and QD encapsulated organogels were studied using FETEM under a Carl Zeiss microscope. QD samples were made by casting the QD solution on carbon-coated TEM copper grids and then allowing the TEM grids to dry under vacuum. On the other hand, for QD-peptide hybrid gel samples, peptide organogelator (2mg/ml) along with QDs were dissolved in toluene and heated for some time. The 1-2 µl of heated solution was casted on the TEM grid by using a micropipette and the grid was dried completely by keeping it in a desiccator under vacuum.

3.3. Results and discussions

3.3.1. Design of the peptides and their gelation studies

Considering the outstanding assembling ability of the FF moiety, we wanted to investigate the effect of the proximity of the Phe residues in the di-Phe unit, on its assembling nature and gelation ability, by designing three peptides where the two Phe units were spatially distal. We incorporated variable number of hydrophobic Leu amino acid residues as spacers in between the two Phe residues, to probe the effect of the length of spacers on the gelation abilities of the peptides. Use of single, di and tri Leu residues as spacers generated the peptides FLF, FLLF and FLLLF (Fig. 3.1 a). It is well-reported that FF dipeptide can form organogels in a range of aromatic solvents including toluene and chloroform. Here, the gelation ability of all three designed peptides was studied in a variety of aromatic and aliphatic solvents and confirmed by 'vial inversion test' (Fig.

3.1 b, c). It was observed that the three peptides were capable of forming a gel in different solvents like toluene and m-xylene upon heating-cooling, which was akin to the gelation of Boc-FF-OMe (Table 3.1).

The minimum gelation concentration of all the peptides obtained in a variety of solvents lied in between 0.2-0.45 % w/v (Table 3.1). The highest gelation efficiency for all the compounds was observed in toluene. Also, all the organogels showed a phase-selective gelation in the presence of water (Fig. 3.1 d). Thus, the gelation abilities of the three peptides seemed similar to each other and to the control peptide FF. This suggested that the gelation ability of the peptides was independent of the distance in between the two Phe residues of the di-Phe unit.

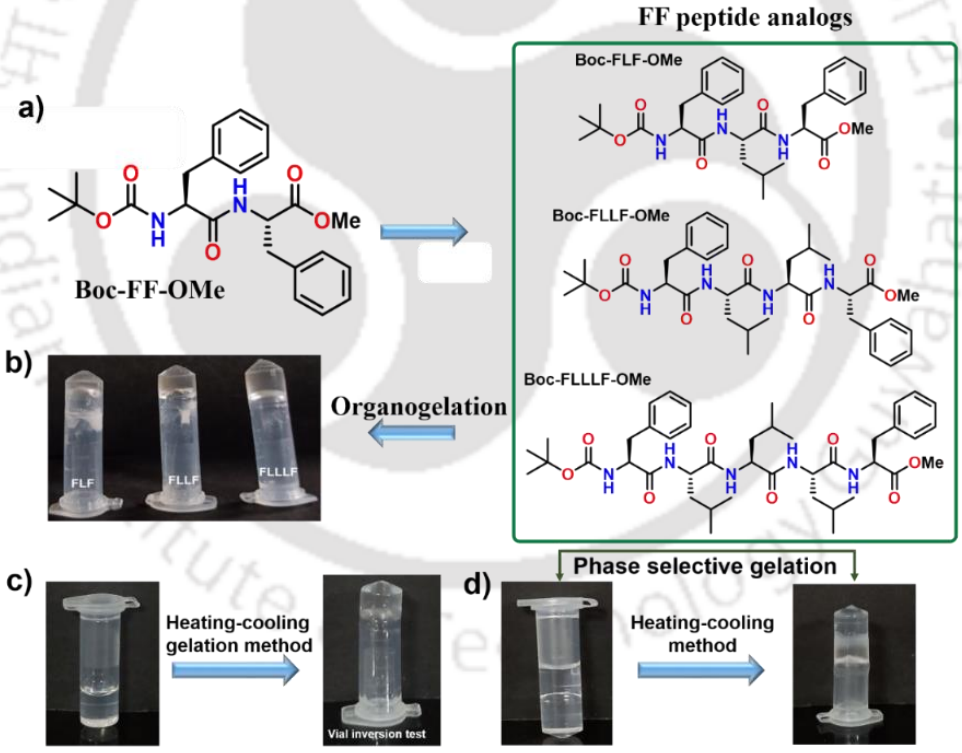

Fig. 3.1. (a) Chemical structures of peptide organogelators FLF, FLLF and FLLLF, (b) vial inversion test for all peptides, (c) gel formation by heating-cooling method, and (d) phase selective gelation in toluene in the presence of water.

Table 3.1. Gelation properties of the peptides in different solvents. Gelation state is described as: Soluble (S), Transparent gel (TG), Translucent gel (TLG) and Opaque gel (OG).

Solvents	**Temperature**	**FF/MGC (%wt/vol)**	**FLF/MGC (%wt/vol)**	**FLLF/MGC (%wt/vol)**	**FLLLF/MGC (%wt/vol)**
Chlorobenzene	100	TG/0.3	TG/0.3	TG/0.3	TG/0.4
Toluene	100	TLG/0.2	TLG/0.30	TLG/0.2	TLGG/0.2
m-xylene	100	TLG/0.3	TLG/0.3	TLG/0.3	TLG/0.3
DCB	100	TLG/0.3	TLG/0.4	TLG/0.5	TLG/0.45
Cyclohexane	100	OG/0.3	OG/0.3	OG/0.3	OOG/0.3
Hexane	100	OG/0.3	OG/0.3	OG/0.3	OG/0.3
Heptane	100	OG/0.3	OG/0.3	OG/0.3	OG/0.3
Methanol	100	S	S	S	S
Dioxane	100	S	S	S	S
ACN	S	S	S	S	S

3.3.2. Morphology

Morphological features of the organogels formed by the designed peptides in toluene at MGC have been studied by Field Emission Scanning Electron Microscopy (FESEM) (Fig. 3.2 a-d). FF appeared as a mixture of densely packed fibrous networks and nanorods while FLF, FLLF, and FLLLF appeared as densely packed fibrous networks.

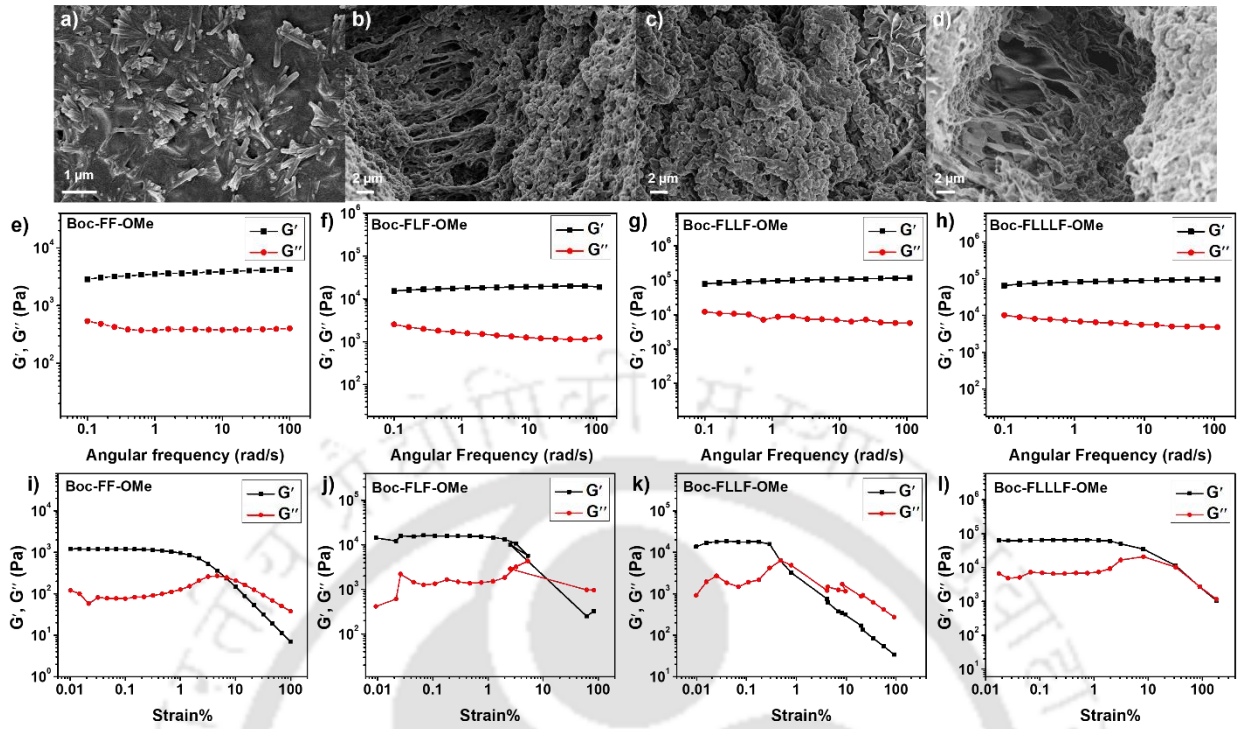

Fig. 3.2. FESEM images of the organogels formed by a) FF, b) FLF, c) FLLF and d) FLLLF in toluene at their MGC. Frequency dependence (e-h) of the dynamic storage moduli (G′) and the loss moduli (G″) of organogels at constant strain (0.1%) and strain dependence (i-l) of the dynamic storage modulus (G′) and the loss modulus (G″) of the organogels for FF, FLF**,** FLLF, and FLLLF in toluene at their respective MGC.

3.3.3. Rheology

Mechanical strength of all the four peptide organogels was studied using rheology. Here, organogels prepared in toluene at their MGC were subjected to an oscillatory frequency sweep experiment. In frequency sweep experiment, the variation of G′ and G″ was monitored as a function of angular frequency (ω) at a constant strain 0.1%. It was observed that for all three organogels, G′ was greater than G″ and was stable up to 100 rad/sec, confirming that all the peptides gave rise to stable organogels till a frequency of 100 rad/sec (Fig. 3.2 e-h). Also, the G′ values for all the FF analog peptide organogels were found to be of the order of $>10^4$ Pa, indicating considerable mechanical strength of all the organogels, which was slightly greater than Boc-FF-OMe organogel. In the strain sweep experiment, where the storage moduli (G′) and the loss moduli (G″) for all the

organogels were plotted as a function of % strain (Fig. 3.2 i-l), it was found that G′ was higher than G″ (of the order of 10^4 Pa) until a particular strain. Thus, all the three organogels had similar mechanical robustness and this was not dependent on the distance in between the two Phe residues.

3.3.4. PXRD study

To understand the process of self-assembly and conformation of the peptides, PXRD study was carried out. The recorded wide-angle PXRD patterns of xerogels of all three new peptides along with Boc-FF-OMe provided us with details about the molecular packing in their gel state (Table 3.2 and Fig. 3.3 a, b, c, d) An interplanar distance of ~4Å, confirmed the π-π interaction between the aromatic moieties present in the system.[31a, b] Interestingly, PXRD patterns of all the four xerogels looked almost identical, suggesting similar type of arrangement in their self-assembled state. This once again corroborated the fact that the length of the linker connecting the two Phe residues in these peptides had very little role to play in their self-assembly.

Table 3.2. Interplaner distances in the peptide organogels.

Xerogels	d spacing in Å (peak 1)	d spacing in Å (peak 2)	d spacing in Å (peak 3)	d spacing in Å (peak 4)
Boc-FF-OMe	6.14	5.10	4.62	3.96
Boc-FLF-OMe	6.23	5.15	4.75	4.03
Boc-FLLF-OMe	6.19	5.16	4.72	4.05
Boc-FLLLF-OMe	6.24	5.18	4.75	4.06

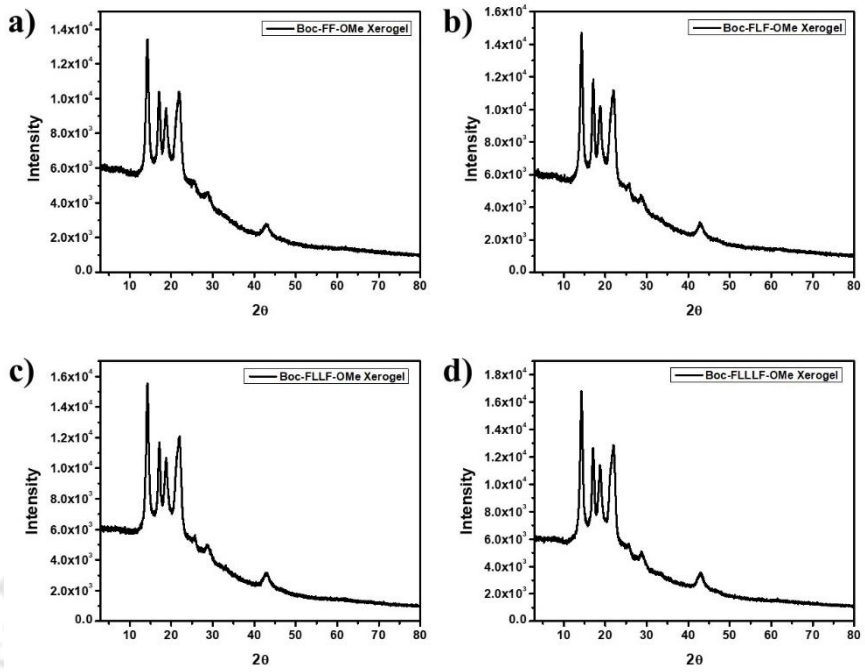

Fig. 3.3. Wide angle PXRD patterns of xerogels, a) FF, b) FLF, b) FLLF and d) FLLLF.

3.3.5. Immobilization of QDs

3.3.5.1. Selection of QD and peptide for making the composite

Literature suggested that inorganic nanocrystal composite gels could be used for applications like construction of electronic and optical devices.[32, 33] Fabrication of QD-peptide hybrid gel, needed several factors to be taken care of such as, (i) the compatibility of the solubility of both QDs and the peptide in a suitable solvent, so that a homogeneous mixture could be obtained, (ii) stability of both QDs and peptide under experimental conditions and (iii) absence of precipitation in the mixture containing both QD and peptide for complete optical transparency.[18]

In order to investigate if our designed peptide gels had the ability to encapsulate and stabilize the QDs, FLLF was chosen as the representative peptide, to carry out further investigations. Four different types of CdSe QDs (green core/ZnS core shell and red core/ ZnS core-shell) were chosen for in this study, as they were highly dispersed in toluene and FLLF peptide could form stable

organogel in toluene. The photophysical properties and the potential applications of QD are heavily based on the stability of the CdSe core of the QD. Both green core/core shell and red core/core-shell QDs were synthesized according to the well-established protocol with some modifications. Zinc sulphide (ZnS) was used to form the shell of the CdSe core QD. This shelling was reported to stabilize the core and enhance its fluorescence properties. Trioctylphosphonium Oxide (TOPO) and octadecylamine (ODA) were used for capping both core and core-shell QDs. Table 3.3 represents the compositions of the QD. The sizes of the QDs were within the range of 3-5 nm as confirmed by transmission electron microscope (TEM) (Fig. 3.4 a, b, c, d, e).

Table 3.3. QDs which were encapsulated in the FLLF organogel in this study.

Quantum Dots (QD)	Capping Agents	Sizes (nm)
Green QD core	TOPO, ODA	3-4
Green QD core shell	TOPO, ODA	4-5
Red QD core	TOPO, ODA	4-5
Red QD core shell	TOPO, ODA	4-5

TOPO: Trioctylphosphine oxide

ODA: Octadecyl amine

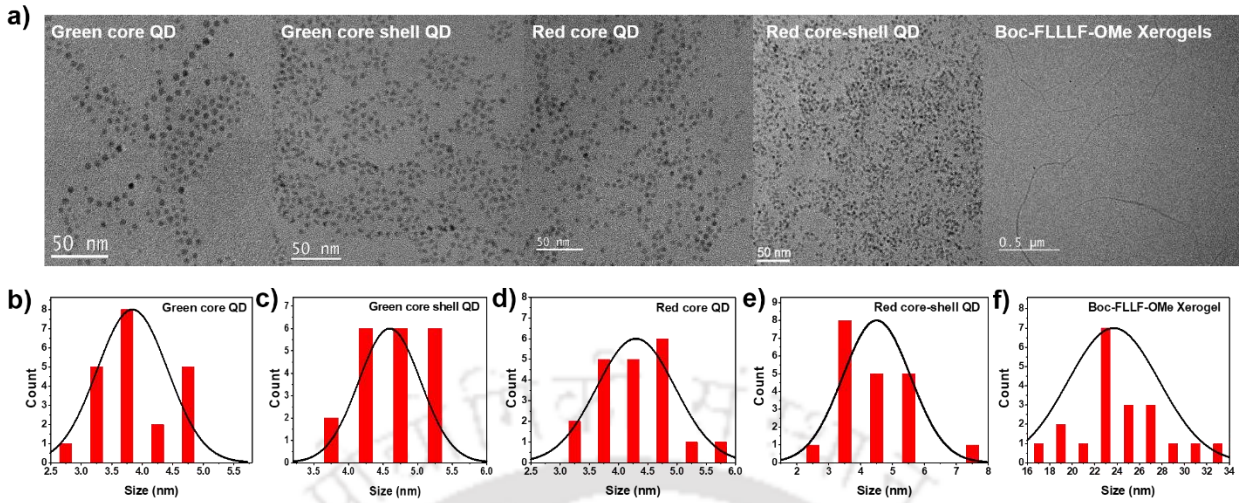

Fig. 3.4. a) TEM images of different QDs in toluene and FLLF xerogel, and b-f) their respective size distributions. b) Green core QD, c) green core-shell QD, d) red core QD e) red core-shell QD and f) FLLF xerogels.

3.3.5.2. Preparation of the QD-peptide hybrid organogel

In this study, we have used the heating-cooling method to prepare the QD-peptide hybrid organogel. Briefly, we have taken both QD and FLLF in toluene and heated the mixture in a water bath at around 90°-100° C for 10 min followed by cooling to room temperature. This process made translucent organogel embedded with QDs that was confirmed by vial inversion test. (Fig. 3.5) Toluene was used as the chosen solvent, since both the gelator peptide (FLLF) and the CdSe core QD/CdSe-ZnS core-shell QD were highly soluble/dispersible in it. The four resultant organogels were of pale yellow or reddish color, depending upon the nature of the embedded QD. (Fig. 3.5) These gels also emitted green/red emission upon irradiation with UV light (Fig. 3.5 a-d) indicating that the photophysical properties of the QDs were well-preserved in the QD-Peptide hybrid organogels. This could be attributed to the fact that once the QDs were embedded into the organogel matrix, interaction with aerial oxygen, which is well known to have strong fluorescence quenching effect via several mechanisms, was substantially reduced.

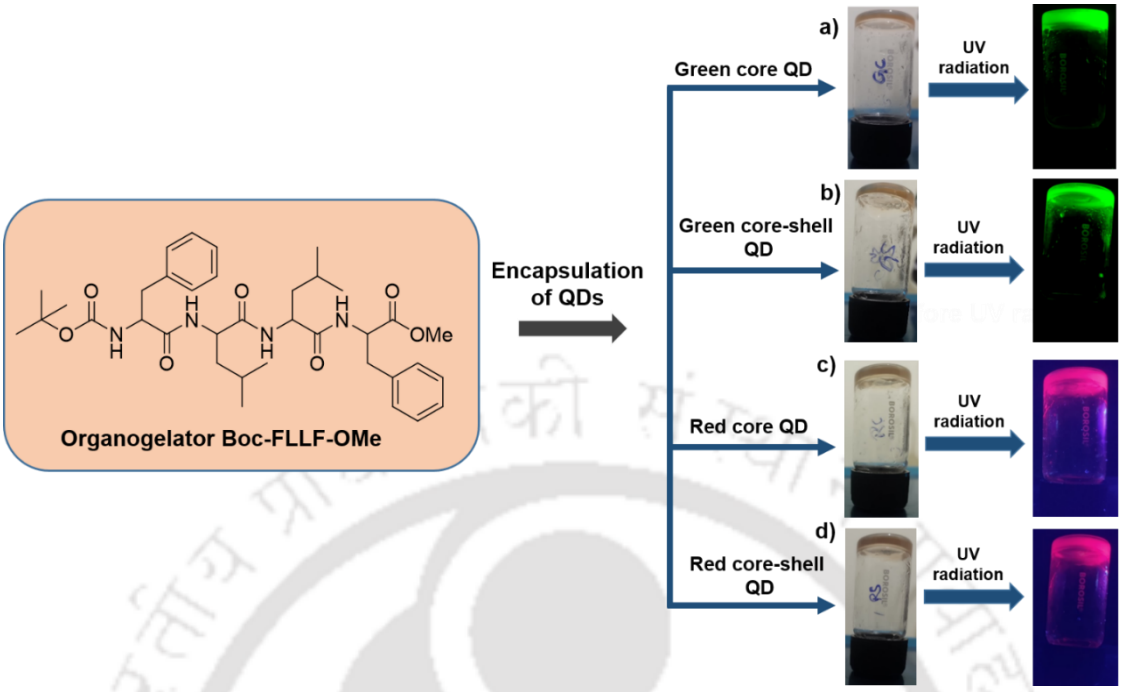

Fig. 3.5. Encapsulation of QDs in the gel matrix confirmed by vial inversion test. a) Green core QD-peptide gel, b) green core-shell QD-peptide gel, c) red core QD-peptide gel and d) red core-shell-peptide gel.

The strength and the stability of one of the representative hybrid QD-organogels (green core-peptide gel) was carried out through rheology measurements. The storage modulus, G′ was greater than loss modulus, G″ till 100 rad/sec, suggesting the formation of a stable gel (Fig. 3.6). The minimum gelation concentration (MGC) of the organogel remained unchanged before and after the embedding of QDs, suggesting that the QDs did not interfere in the organogelation process. Thus, the organogelation process and their stability remained unaltered in the hybrid gels.

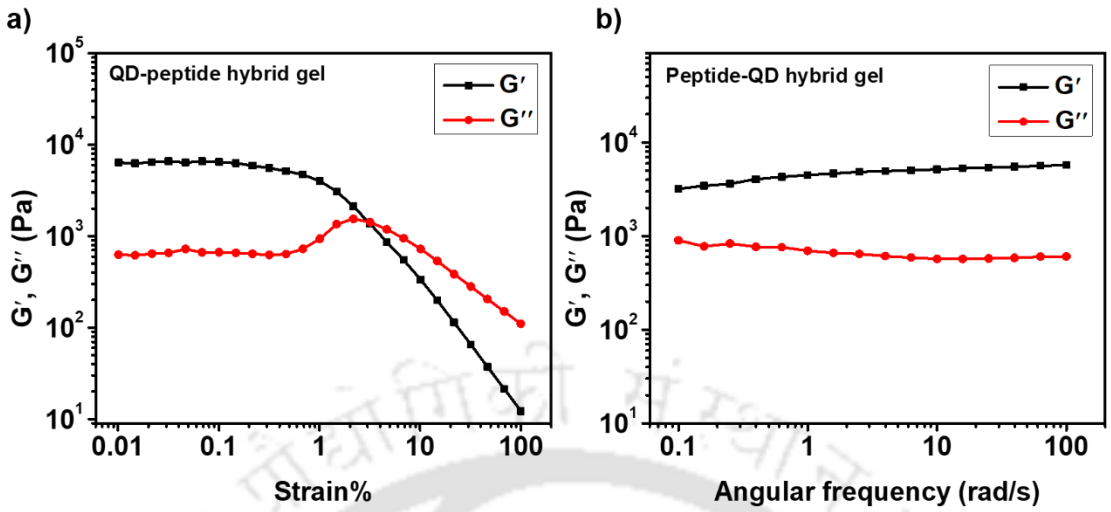

Fig. 3.6. Rheology profiles of green core QD-peptide hybrid organogel. a) Strain dependence and b) frequency dependence of the dynamic storage modulus (G′) and the loss modulus (G″).

3.3.6. Morphological studies

The morphologies of the green core/core-shell and red core-shell QD embedded FLLF organogels were examined by transmission electron microscopy (TEM) of the respective xerogels. The TEM images of the xerogel containing QDs showed an entangled 3D network consisting of bundles of fibres with QD stacked within them (Fig. 3.7 a-c). The morphology of the QD encapsulated xerogel was similar to that of the xerogel obtained in the absence of QD (Fig. 3.4 a), indicating that the encapsulation of QDs did not modify the microscopic organization of the supramolecular structure significantly. The dimensions of the fibers present in the xerogels before (Fig. 3.4 f) and after (Fig. 3.7 g-i) QD encapsulation remained almost identical. The TEM images allowed visualization of the nanoparticles stacked within the fibers of the peptide. Interestingly, the individual QDs were isolated and distributed along the superstructures formed by the organogelator. Also, individual QDs remained in their regular shapes and sizes (Fig. 3.4 a-e) upon entrapment in the gel fibers, with no significant QD aggregates (Fig. 3.7 a-f). Therefore, TEM measurements provided a strong

evidence that encapsulation of QDs in the organogels, had no significant morphological effect on the peptide fibrillar network or the nature of the QDs.

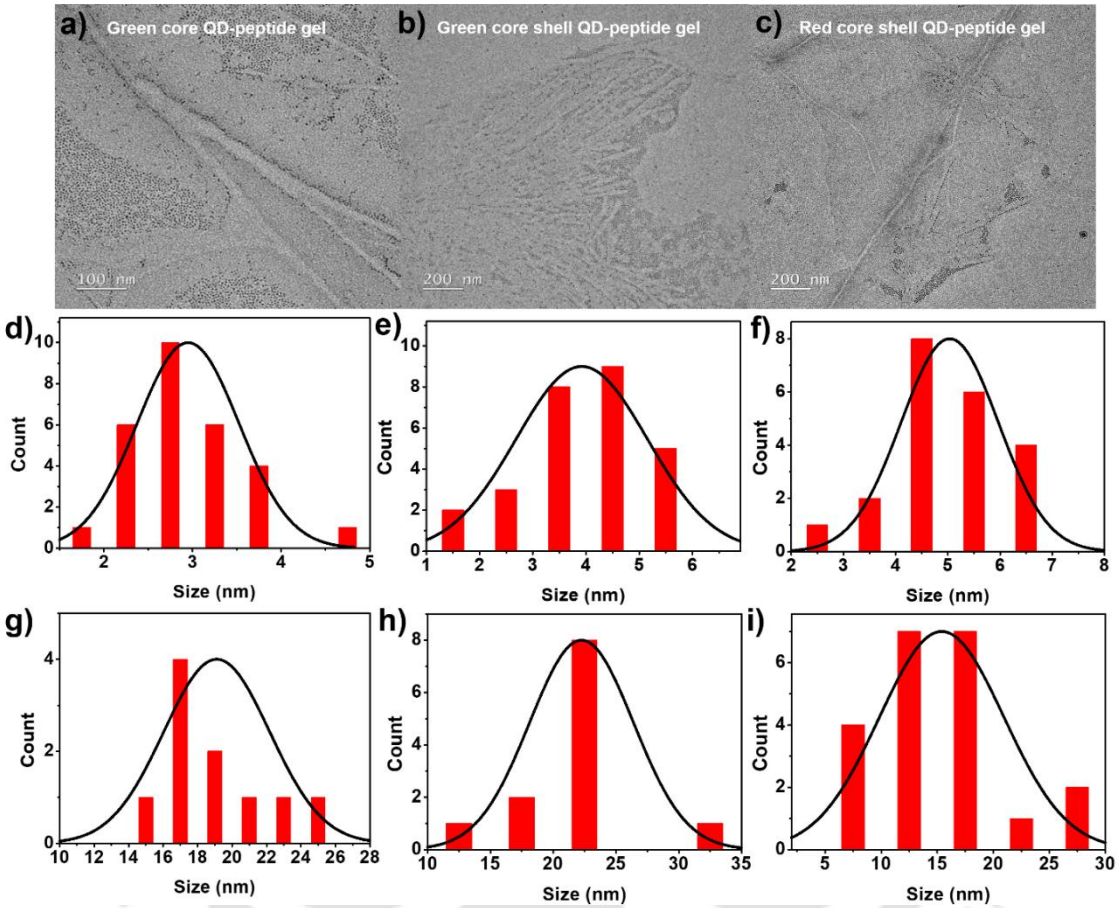

Fig. 3.7. Morphology of the QD encapsulated hybrid organogels. a) green core QD-peptide gel b) green core-shell QD-peptide gel and c) red core-shell QD-peptide gel. Size distribution of (d-f) QDs and (g-i) FLLF fibers in QD-peptide xerogels; d, g) green core, e, h) green core-shell and f, i) red core-shell.

3.3.7. Photophysical properties of the QD-peptide hybrid organogel:

After confirming the unaltered gelation properties of QD-peptide gel and the size/ shape of the encapsulated QDs, we compared the photophysical properties of the QD-doped hybrid organogels and free QDs. We recorded the UV-visible absorption spectra of QDs in toluene and QD-Peptide hybrid gel to determine the effect of organogelator on the absorption properties of the QDs.

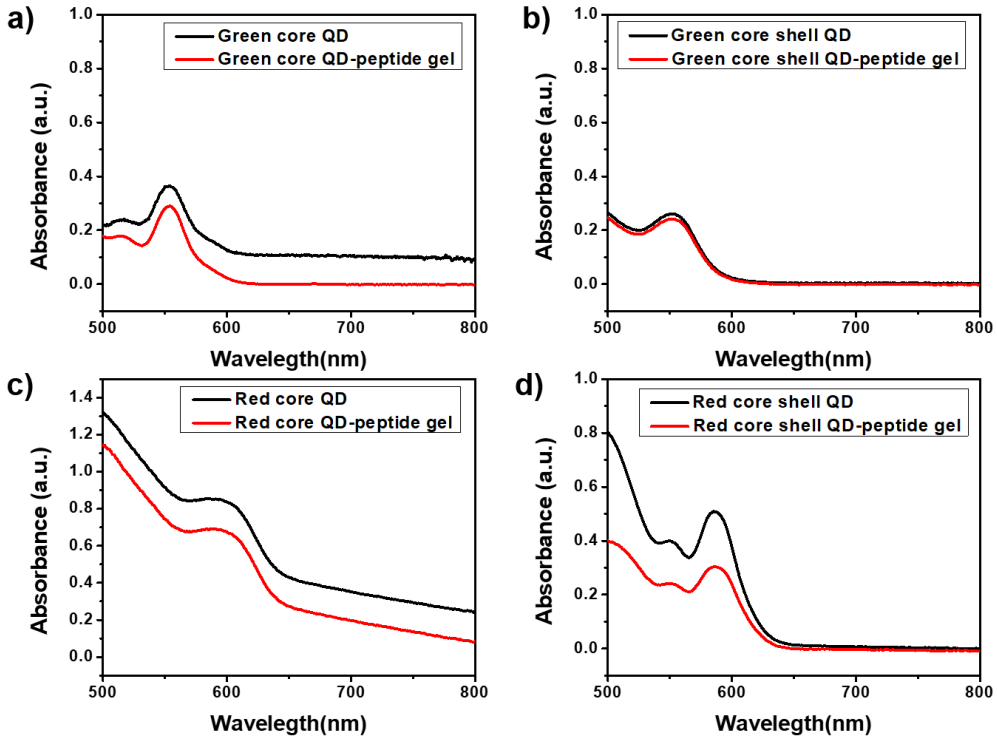

Fig. 3.8. Absorption spectra of different QDs in toluene and in the hybrid organogels: a) green core QD/green core QD-peptide gel b) green core-shell QD/ green core-shell QD-peptide gel c) red core QD/ red core QD-peptide gel and d) red core-shell QD/red core-shell-peptide gel.

From the Fig. 3.8 a-d, it can be observed that the absorption maxima (λ_{max}) of the QD and the QD doped organogels were identical and their absorption maxima were almost similar. This established that the proximity of peptide to the QDs had no adverse effect on their absorption properties. Additionally, unchanged absorption properties of the hybrid organogel, corroborated the results from FETEM, that embedding of the QDs in the hydrogel matrix did not cause any structural change of the QDs. Also, Fig. 3.9 a-d showed the unaltered fluorescence behavior of the QDs before and after gelation.

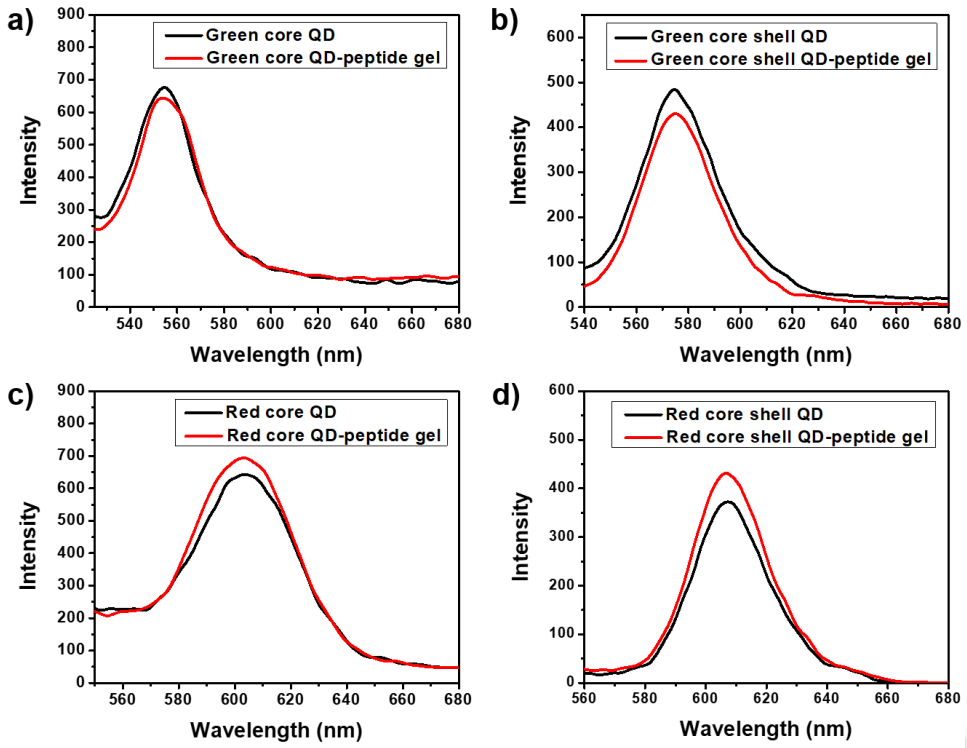

Fig. 3.9. Fluorescence emission spectra of different QDs in toluene and in the hybrid organogels: a) green core QD/green core QD-peptide gel b) green core-shell QD/ green core-shell QD-peptide gel c) red core QD/ red core QD-peptide gel and d) red core-shell QD/red core-shell-peptide gel.

3.3.8. Organogel stabilizes the fluorescence properties of the QDs

One of the main objectives of developing QD-peptide hybrid organogel was to stabilize the emission of the QDs and to protect the QDs from aerial oxidation. In order to check whether the peptide organogelator could protect the QDs from aerial oxidation, time-dependent fluorescence experiments were performed. Both free QD and the QD-embedded organogels were exposed to the open air and their fluorescence emission studied thereafter. Upon exposing both of these two variants under open air, the intensity of fluorescence emission of the free QD was substantially quenched, while that of the QD peptide hybrid organogel did not change at all, indicating successful stabilization of the QD in the peptide organogel system. Fig. 3.10 a-d shows that

fluorescence intensity of both green core/core shell and red core/core shell QD in the hybrid system remained constant till 5 h compared to free QD solutions.

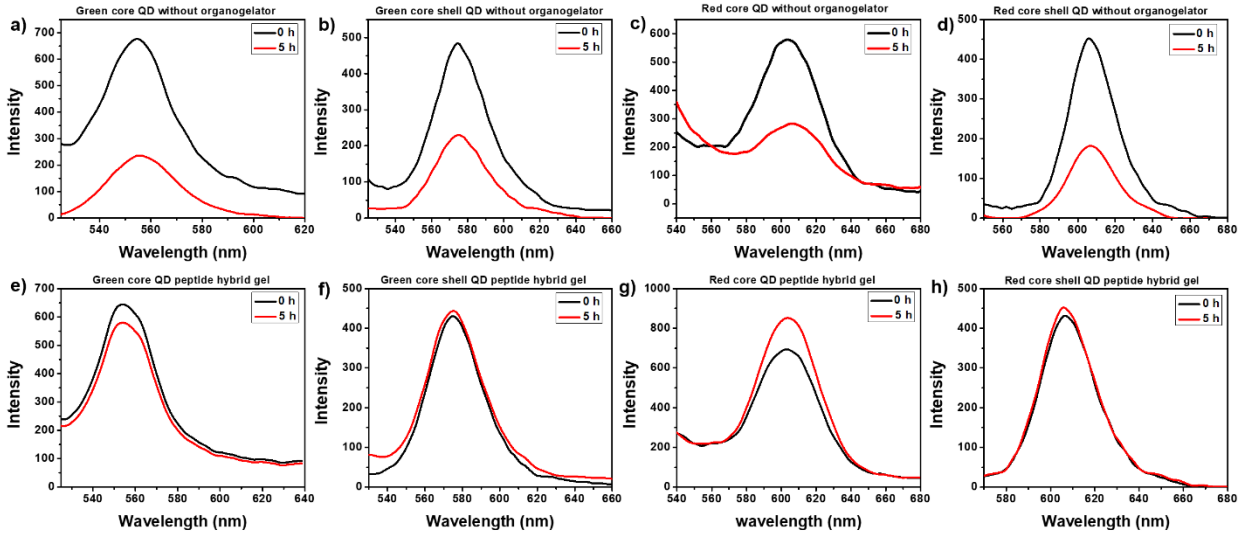

Fig. 3.10. Time-dependent fluorescence emission spectra of different QDs in toluene and QD-peptide hybrid organogel. a, e) Green core QD, Green core QD-peptide organogel; b, f) green core-shell QD, green core-shell QD-peptide organogel; c, g) red core QD, red core QD-peptide organogel and d, h) red core-shell QD, red core-shell QD-peptide organogel at 0 and 5 h.

We also quantified the lifetime of the excited state of the QDs before and after gelation through time resolved fluorescence studies by using time correlated single photon counting (TCSPC) method. Here, green and red core CdSe QDs in toluene solution and their respective QD-peptide gels have been selected. The fluorescence decay profiles were measured with an excitation/ emission wavelength of 450 nm/540 nm for green core and its hybrid gel and 450nm/580 nm for red core and its hybrid gel respectively. Also, the average fluorescence lifetime was calculated by using following equation[34]:

$\tau_{average} = \Sigma A_i \tau_i^2 / \Sigma A_i \tau_i$; i=1, 2, 3 ……(1) where τ_1, τ_2 and τ_3 are the decay time constants and A_1, A_2 and A_3 are the normalized amplitudes of the decay components.

The contribution of each fluorescence decay component (A1, A2, A3) for all samples towards the total lifetime are shown in Table 3.4. The average lifetime for green QD-peptide hybrid gel and red QD-peptide hybrid gel were observed to be almost similar with the green QD and red QD in the toluene solution without any significant change. (Fig. 3.11 a, c) The slight differences between them did not indicate any remarkable alteration in the lifetime of QD in gel form when compared to those in solution form.

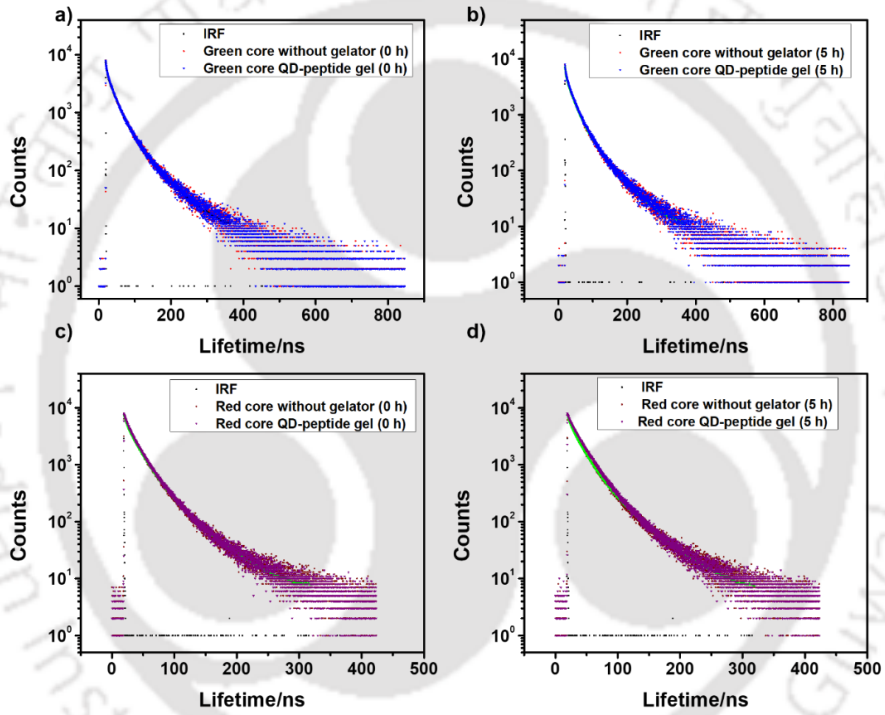

Fig. 3.11. Photoluminescence lifetime curves of CdSe QDs in toluene and hybrid gel-QD composite; green core QD at a) 0 h, b) 5 h; red core QD at c) 0 h and d) 5 h.

Further, to understand the time dependent fluorescence quenching for the QDs in solution which was observed previously, we repeated the time-resolved fluorescence studies for both green and red core QDs in toluene solution and in their respective hybrid gels after 5 h of time interval. All the component and time decay values are provided in the Table 3.5. Surprisingly, the green and red QD-peptide hybrid gels showed similar pattern and average lifetime values with the QDs in

solution without any significant differences even after 5 h (Fig. 3.11 b, d). This result suggested that the diminished fluorescence intensities were not attributed to the change in lifetime but might be possible due to static fluorescence quenching.[35] This was further corroborated by subsequent decrease in quantum yield values in reference to Rhodamine 6G. (Table 3.4 and Table 3.5)

Table 3.4. Fluorescence lifetime and quantum yield values of green and red CdSe core QDs in solutions and gel matrix at 0 h.

Samples (0 h)	τ1 (ns)	A1 (%)	τ2 (ns)	A2 (%)	τ3 (ns)	A3 (%)	Chi square	τ_{avr} (ns)	Fluorescence quantum yield (%)
Green core QD	21.506	45.04	3.124	45.31	62.51	9.65	1.16	34.42	23.14
Green core QD-peptide hybrid gel	21.139	43.68	2.897	46.31	60.95	10.01	1.07	34.24	33.32
Red core QD	4.156	30.81	19.56	59.82	48.70	9.37	1.13	26.01	32.98
Red core QD-peptide hybrid gel	5.499	28.24	20.405	62.55	50.69	9.21	1.08	26.63	37.33

Table 3.5. Fluorescence lifetime and quantum yield values of green and red CdSe core QDs in solutions and gel matrix at 5 h.

Samples (After 5 h)	τ1 (ns)	A1 (%)	τ2 (ns)	A2 (%)	τ3 (ns)	A3 (%)	Chi square	τ_{avr} (ns)	Fluorescence quantum yield (%)
Green core QD	2.832	42.90	21.31	46.68	61.50	10.42	1.17	34.69	1.28
Green core QD-peptide hybrid gel	21.46	47.21	3.081	42.59	62.03	10.2	1.14	34.59	29.71
Red core QD	5.3	30.81	20.4	59.82	52.33	9.37	1.17	27.44	7.33
Red core QD-peptide hybrid gel	5.73	18.89	22.14	73.08	54.09	8.03	1.09	27.74	33.57

3.3.9. Thermoreversibility of the QD peptide organogels

Thermoreversibility and the thermostability of the photophysical properties of the QD-peptide gels are important properties, crucial for their applications. To investigate this, several cycles of heating and cooling were applied to all QD-peptide hybrid gels. They were heated up to 90°-100°C and then cooled back to room temperature in subsequent cycles. While all the gels converted into sol upon heating, they returned to gel state upon cooling down in each subsequent cycle, establishing their thermo-reversible nature. The fluorescence emissions of the QD-hybrid peptide organogels after the fourth cycle of heating-cooling were found to be the same as the initial emissions. (Fig. 3.12 a-d) The unaltered absorption and fluorescence signals at the end of four cycles of heating and cooling, established the thermal stability of their photophysical characteristics.

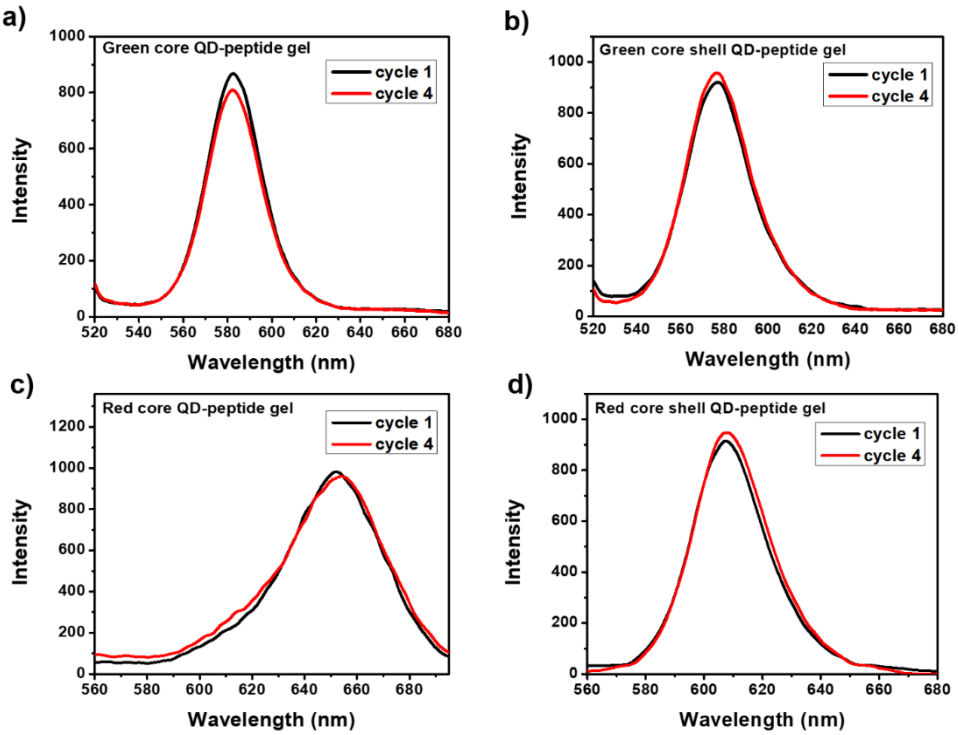

Fig. 3.12. Fluorescence emission spectra of QD-peptide hybrid organogels after the 1st and 4th cycles. a) Green core QD-peptide organogel, b) Green core-shell QD-peptide organogel, c) Red core QD-peptide organogel and d) Red core-shell QD-peptide organogel.

3.4. Conclusions

In this study, we have developed a series of FF dipeptide analogs FLF, FLLF and FLLLF, in which variable length of spacers (one two and three Leu residues) separated the Phe residues. With the help of extensive experimental investigations, we have conclusively established that the length of the spacers in between the Phe residues, had no effect on the gelation properties of these peptides. All the peptides were equally efficient in gelation, had similar mechanical strength and morphologies to the FF dipeptide. Thus, gelation ability of this class of peptides was independent of the physical proximity of the two Phe residues. We have used these robust organogels for stabilization of green and red core/core-ZnS shell CdSe QD through fabrication of hybrid QD-peptide organogels. We have demonstrated successfully that encapsulation of the QD in the organogel matrix, led to both retention and stabilization of their photophysical properties, by the prevention of aerial oxidation. Our developed hybrid organogels also

exhibited thermoreversibility and thermal stability of their photophysical properties. Such advanced soft materials would be of great impact in various applications in the future.

Overall, these organogels hold potential for device development due to their ability to stabilize various quantum dots. This opens up possibilities for creating LED-based devices for practical applications. In the future, we look forward to fabricating prototype devices as a proof of concept on the laboratory scale. However, translating this technology to industry will need to design of advanced devices with these organogels and establishment of their efficacy at a large scale.

3.5. References

1. Yan, X.; Zhu, P.; Li, J. Self-assembly and application of diphenylalanine-based nanostructures. *Chem. Soc. Rev.* **2010**, *39*, 1877-1890.
2. Mayans, E.; Alemán, C. Revisiting the self-assembly of highly aromatic phenylalanine homopeptides. *Molecules* **2020**, *25*, 6037.
3. Yan, X.; He, Q.; Wang, K.; Duan, L.; Cui, Y.; Li, J. Transition of cationic dipeptide nanotubes into vesicles and oligonucleotide delivery. *Angew. Chem. Int. Ed.* **2007**, *46*, 2431-2434.
4. Liu, X.; Danglad-Flores, J.; Eickelmann, S.; Sun, B.; Hao, J.; Riegler, H.; Li, J. Controlled-alignment patterns of dipeptide micro-and nanofibers. *ACS Nano* **2022**,*16*, 10372−10382.
5. 25. Yan, X.; Cui, Y.; Qi, W.; Su, Y.; Yang, Y.; He, Q.; Li, J. Self-assembly of peptide-based colloids containing lipophilic nanocrystals. *Small* **2008**, *4*, 1687-1693.
6. Arul, A.; Rana, P.; Das, K.; Pan, I.; Mandal, D.; Stewart, A.; Maity, B.; Ghosh, S.; Das, P. Fabrication of self-assembled nanostrcutures for intracellular drug delivery from diphenylalanune analogues with rigid or flexible chemical linkers. *Nanoscale Adv.* **2021**, *3*, 6176.
7. Huang, R.; Wang, Y.; Qi, W.; Su, R.; He, Z. Temperature-induced reversible self-assembly of diphenylalanine peptide and their structural transition from organogel to crystalline nanowires. *Nanoscale Res. Lett.* **2014**, *9*, 653.
8. Pramanik, A.; Paikar, A.; Maji, K.; Haldar, D. Photo-responsive modulation of hybrid peptide assembly, charge complex formation and gelation. *RSC Adv.* **2016**, *6*, 59891.
9. Nalluri, S. K. M.; Shivarova, N.; Kanibolotsky, A. L.; Zelzer, M.; Gupta, S.; Frederix, P. W. J. M.; Skabara, P. J.; Gleskova, H.; Ulijn, R. V. Conducting nanofibers and

organogels derived from the self-assembly of tetrathiafulvalene-appended dipeptides. *Langmuir* **2014**, *30*, 12429−12437.

10. Liu, X.; Fei, J.; Wang, A.; Cui, W.; Zhu, P.; Li, J. Transformation of dipeptide-based organogels into chiral crystals by cryogenic treatment. *Angew. Chem. Int. Ed*. **2017**, *56*, 2660 –2663.
11. Zhu, P.; Yan, X.; Su, Y.; Yang, Y.; Li, J. Solvent-induced structural transition of self-assembled dipeptide: from organogel to microcrystal. *Chem. Eur. J.* **2010**, *16*, 3176-3183.
12. Ibukun, O. J.; Gumtya, M.; Singh, S.; Shit, A.; Haldar, D. Effect of spacer on the structure and self-assembly of ff peptide mimetics. *Soft Matter* **2023**, *19*, 3215-3221.
13. Diaferia, C.; Roviello, V.; Moriello, G.; Accardo, A. Self-assembly of pegylated diphenylalanines into photoluminescent fibrillary aggregates. *ChemPhysChem* **2019**, *20*, 274-2782.
14. Petrov, S. A.; Machulkin, A. E.; Petrov, R. A.; Tavtorkin, A. N.; Bondarenko, G. N.; Legkov, S. A.; Nifant'ev, I. E.; Dolzhikova, V. D.; Zyk, N. V.; Majouga, A. G.; Beloglazkina, E. K. Synthesis and organogelating behaviour of urea- and fmoc-containing diphenylalanine based hexaamide. *J. Mol. Struct.* **2021**, *1234*, 130127.
15. Erdogan, H.; Sakalak, H.; Yavuz, M. S.; Demirel, G. Laser-triggered degelation control of gold nanoparticle embedded peptide organogels. *Langmuir* **2013**, *29*, 6975−6982.
16. Chakraborty, P.; Ji, W.; Rahmany, S.; Etgar, L.; Gazit, E. Formation of semiconducting supramolecular fullerene aggregates in a dipeptide organogel. *Adv. Mater. Technol.* **2020**, *5*, *1900829.*
17. Wadhavane, P. D.; Izquierdo, M. A.; Galindo, F.; Burguete, M. I.; Luis, S. V. Organogel-quantum dots hybrid materials displaying fluorescence sensitivity and structural stability towards nitric oxide. *Soft Matter* **2012**, *8*, 4373-4381.

18. Wadhavane, P. D.; Galian, R. E.; Izquierdo, M. A.; Aguilera-Sigalat, J.; Galindo, F.; Schmidt, L.; Burguete, M. I.; Pérez-Prieto, J.; Luis, S. V. Photoluminescence enhancement of cdse quantum dots: a case of organogel-nanoparticle symbiosis. *J. Am. Chem. Soc.* **2012**, *134*, 20554-20563.
19. Chan, W. C. W.; Nie, S. Quantum dot bioconjugates for ultrasensitive nonisotopic detection. *Science* **1998**, *281*, 2016-2018.
20. Smith, A. M.; Nie, S. Chemical analysis and cellular imaging with quantum dots. *Analyst* **2004**, *129*, 672-677.
21. Nga, P. T.; Chinh, V. D.; Hanh, V. T. H.; Nghia, N. X.; Dzung, P. T. Optical properties of normal and 'giant' multishell cdse quantum dots for potential application in material science. *Int. J. Nanotechnol.* **2011**, *8*, 347-359.
22. Hines, M. A.; Guyot-Sionnest, P. Synthesis and characterization of strongly luminescing zns-capped cdse nanocrystals. *J. Phys. Chem.* **1996**, *100*, 468-471.
23. Cheng, C.; Yan, H. Bandgap of the Core-Shell CdSe/ZnS nanocrystal within the temperature range 300-373 K. *Physica E* **2009**, *41*, 828-832.
24. Derfus, A. M.; Chan, W. C. W.; Bhatia, S. N. Probing the cytotoxicity of semiconductor quantum dots. *Nano Letters* **2004**, *4*, 11-18.
25. Chatterjee, S.; Kuppan, B.; Maitra, U. A self-assembled CdSe QD–organogel hybrid: photophysical and thermoresponsive properties. *Dalton Trans.* **2018**, *47*, 2522–2530.
26. Yan, X.; Cui, Y.; He, Q.; Wang, K.; Li, J. Organogels based on self-assembly of diphenylalanine peptides and their application to immobilize quantum dots. *Chem. Mater.* **2008**, *20*, 1522-1526.
27. Palui, G.; Nanda, J.; Ray, S.; Banerjee, A. Fabrication of luminescent cds nanoparticles on short-peptide-based hydrogel nanofibers: tuning of optoelectronic properties. *Chem. Eur. J.* **2009**, *15*, 6902-6909.

28. Misra, R.; Sharma, A.; Shiras, A.; Gopi, H. N. Backbone engineered γ-peptide amphitropic gels for immobilization of semiconductor quantum dots and 2d cell culture. *Langmuir* **2017**, *33*, 7762-7768.
29. Murray, C. B.; Norris, D. J.; Bawendi, M. G. Synthesis and characterization of nearly monodisperse CdE (E = S, Se, Te) semiconductor nanocrystallites. *J. Am. Chem. Soc.* **1993**, *115*, 8706-8715.
30. Dabbousi, B. O.; Rodriguez-Viejo, J.; Mikulec, F. V.; Heine, J. R.; Mattoussi, H.; Ober, R.; Jensen, K. F.; Bawendi, M. G. (CdSe)ZnS Core-shell quantum dots: synthesis and characterization of a size series of highly luminescent nanocrystallites. *J. Phys. Chem. B*. **1997**, *101*, 9463-9475.
31. a) Basak, S.; Nanda, J.; and Banerjee, A. A new aromatic amino acid based organogel for oil spill recovery. *J. Mater. Chem.* **2012**, *22*, 11658-11664. b) Hansda, B.; Majumder, J.; Mondal, B.; Chatterjee, A.; Das, S.; Kumar, S.; Gachhui, R.; Castelletto, V.; Hamley, I. W.; Sen, P. and Banerjee, A. Histidine-containing amphiphilic peptide-based non-cytotoxic hydrogelator with antibacterial activity and sustainable drug release. *Langmuir* **2023**, *39*, 7307-7316.
32. Li, L. S.; Stupp, S. I. One-dimensional assembly of lipophilic inorganic nanoparticles templated by peptide-based nanofibers with binding functionalities. *Angew. Chem. Int. Ed*. **2005**, *44*, 1833.
33. Kimura, M.; Kobayashi, S.; Kuroda, T.; Hanabusa, K.; Shirai, H. Assembly of gold nanoparticles into fibrous aggregates using thiol-terminated gelators. *AdV. Mater*. **2004**, *16*, 335-338.
34. Chatterjee, S.; Maitra, U. A novel strategy towards designing a CdSe quantum dot–metallohydrogel composite material. *Nanoscale* **2016**, *8*, 14979–14985.

35. Jha, A.; Shankar, H.; Kumar, S.; Sankar, M.; Kar, P. Efficient charge transfer from organometal lead halide perovskite nanocrystals to free base meso-tetraphenylporphyrins. *Nanoscale Adv*. **2022**, *4*, 1779–1785.

Chapter 4

Tuning of Hydrophobic-Hydrophilic Balance for the Development of a Salt-Tolerant and Protease-Resistant Lipopeptide AMP

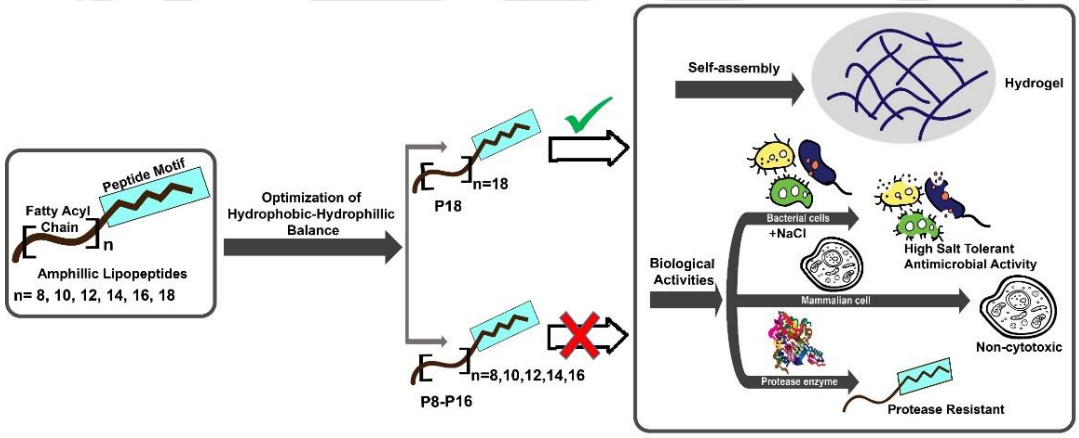

New J. Chem. **2024**, *48*, 2764-2777

4.1. Introduction

Rapidly growing antimicrobial resistance in the microbes against the arsenal of existing antibiotics/antimicrobials has been one of the greatest challenges faced by the human civilization in recent times.[1] Antimicrobial peptides (AMPs) have come up as an alternative potential class of therapeutic molecules to treat antibiotic-resistant infections, mainly owing to the delayed development of resistance in microbes against the AMPs.[2] The delayed resistance development against antibiotics can be attributed to the multiple modes of action of the AMPs against the microbes.[3] However, AMPs have achieved limited commercial success so far due to their short half-life, owing to protease degradability[3-4] and salt sensitivity of their antimicrobial potency.[5] Thus, the design principles of synthetic AMPs aim to a) increase the antimicrobial potency, b) increase the in *vivo* efficiency through salt tolerance of the activity and the resistance against proteolytic degradation, and c) decrease the cytotoxicity.[6–9] In this regard, lipidation is one of the well-known strategies that have been adopted for developing futuristic AMP therapeutics.[10] Lipopeptides are a class of amphiphilic AMPs that show high antimicrobial potency.[11] There are many naturally occurring lipopeptides, which are cyclic in nature and contain an N-terminal fatty acyl chain (daptomycin, polymyxin B and collistin)[12-14] or short N-terminal fatty acyl chains and C-terminal amino alcohol residues.[15] Along with that, synthetic lipopeptide-based AMPs are also available in the literature.[16-18] Lipidation (length and nature of the fatty acyl chain) modulates the antimicrobial efficacy, hydrophobicities, secondary structure and the self-assembling abilities of these peptides.[16,19-22] Lipidation is known to play an important role in the pharmacodynamic and pharmacokinetic behaviour of the AMPs in addition to enhancing their protease stability, membrane permeability, bioavailability and bioactivity.[23-24] Also, amphiphilic lipopeptides are known to exhibit strong self-assembling characteristics.[25-27]

In a quest to develop new AMP molecules, with improved therapeutic potential that overcomes

the well-known disadvantages of AMPs, in this work, we designed a library of six cationic amphiphilic lipopeptides, with varying hydrophobic-hydrophilic ratios (varied by changing the fatty acyl chain length from C_8 to C_{18}). Also, literature evidenced that the hydrophobic-hydrophilic balance[28] of the peptide is a very important attribute that can control several fundamental properties such as self-assembly,[29] membrane association and translocation,[30-31] and antimicrobial potency[32] of the peptide. Therefore, we investigated the effect of varying hydrophobic-hydrophilic ratios on several properties of the lipopeptides, starting from their assembly behaviour, gelation ability, antimicrobial potency and protease stability. We established that the properties of peptides are closely related to their hydrophobic–hydrophilic balance and can be tuned by controlling the same. The optimization of the hydrophobic-hydrophilic ratio of peptides led to the development of a highly potent, completely salt-tolerant, nontoxic, protease-resistant, non-resistance developing lipopeptide P18, which is active against several ESKAPE pathogens such as *P. aeruginosa*, *K. pneumoniae*, *S. aureus* and Methicillin-resistant *S. aureus* (MRSA).

4.2. Experimental section

4.2.1. Materials procured

Rink Amide MBHA resin (loading 0.7 mmol/g), all fluorenylmethyloxycarbonyl (Fmoc) protected amino acids, hydroxybenzotriazole (HOBt), and benzotriazole-1-yl-oxy-tris-pyrrolidino-phosphonium hexafluorophosphate (PyBOP) were purchased from G.L. Biochem. Piperidine, *N*, *N′* diisopropylethylamine (DIPEA), diethyl ether and pyridine were purchased from Merck. HPLC grade acetonitrile and dimethylformamide (DMF), dichloromethane (DCM) were obtained from Finar. Acetic anhydride was provided by the Department of Chemistry, IIT Guwahati. Thioflavin T (ThT) was purchased from Sigma-Aldrich.

Bacterial strains

Common laboratory strains of *P. aeruginosa* (ATCC 27853), *K. pneumoniae* (ATCC 13883), *S. aureus* (ATCC 25923) were obtained either from the American Type Tissue Culture Collection or the Microbial Type Tissue Culture Collection. MRSA strain was provided by Prof. Benu Dhawan, AIIMS, New Delhi and Prof. Kasturi Mukhopadhyay, JNU, New Delhi.

4.2.2. Synthesis and purification

Six peptides (P8, P10, P12, P14, P16 and P18) were synthesized by standard solid-phase peptide synthesis protocol using Fmoc Chemistry on rink amide MBHA resin (0.1 mM scale). Deprotection of the Fmoc group was achieved by 20% piperidine in DMF. The amino acids were coupled using HOBt and PyBOP as coupling reagents in DMF. After attaching all of the amino acids, peptides were cleaved from the resin using 95% trifluoroacetic acid (TFA) and were precipitated in cold diethyl ether. All the peptides were purified using reverse-phase High-Performance Liquid Chromatography (HPLC) on a C18 column using an acetonitrile/water gradient. After purification, the purity peptides were confirmed by analytical HPLC on a C18 column using acetonitrile/water as the solvent system with >95% purity. Further, they were characterized by MALDI-TOF Mass Spectrometry and ^{1}H Nuclear Magnetic Resonance (NMR) spectroscopy (600 MHz) (Appendix, Fig. A4.1-A4.18)

4.2.3. Formation of Hydrogel

1 mg of P18 peptide was taken in 500 µL (0.2% w/v, 2.23 mM) phosphate buffer saline (PBS) (pH 7.4) and then kept undisturbed at room temperature (RT) for one day. It resulted in the formation of hydrogel which was stable to inversion of the glass vial. Hydrogelation of P16 in PB (phosphate buffer pH 7.4) (1 mg/500 µL, 2.30 mM) was similarly studied. It was found that P16 was also capable of forming hydrogel under the similar condition. Here, for hydrogelation heat was not required. Also, it has been observed that, other four peptides P8, P10, P12 and P14 were non-gelators under the different experimental conditions that were tried.

4.2.4. Determination of the Gel-to-Sol Transition Temperature for the Hydrogel

The temperature at which the gel melts and starts to flow is called the Gel-Sol temperature (T_{gel}). To determine the T_{gel} for the hydrogels, vials containing the gels were placed in an oil bath, and then the temperature of the bath was slowly raised at the rate of 1° C per minute, with monitoring of the temperature.[33]

4.2.5. Field emission scanning electron microscopy (FESEM)

The morphology of the peptides in solution (1 mg/500 µL and 100 µM P18 in phosphate buffer system (7.4)) and in hydrogel form at their respective CGC (1 mg/500 µL) were obtained on a FESEM sigma 300 microscope. For morphology, a drop of the solution/hydrogel was cast on a silicon wafer, immediately after making the solutions/hydrogel and dried under vacuum before imaging.[33]

P. aeruginosa cells were pelleted down by centrifugation at 6000 rpm for 5 min, washed thrice and re-suspended in 10 mM sodium phosphate buffer at pH 7.4 to a final number of 10^5 cells/mL. The cell suspensions were incubated with P16 and P18 at 1X and 2X MIC values for 4 h at 310 K. Untreated cells were set as the control. After incubation, the cells were fixed with 2.5% glutaraldehyde for 1 h. at 277 K, then washed twice and re-suspended in 20 µL 10 mM sodium phosphate buffer. 10 µL cell suspension was spotted on a clean glass slide and the cells were allowed to dry overnight. Thereafter, the slides were washed with 50% and 80% ethanol each for 5 min. The samples were next air-dried, followed by gold coating and subsequently observed under the FESEM (Zesis, Model: Gemini).[34]

4.2.6. Fourier transform infrared (FT-IR) spectroscopy

The IR of all peptides was performed using a Perkin Elmer spectrometer. All FT-IR spectra were recorded in the region of 400−4000 cm^{-1}. All the peptides were in solid-state.

4.2.7. Rheology

In order to investigate the viscoelastic properties of P16 and P18 hydrogels, rheology experiments were performed with the use of an Anton Paar MCR 102 rheometer equipped with a 20 mm parallel plate (with 0.3 mm zero gap) measuring system at 25° C. Here, hydrogels were prepared in 10 mM PB/PBS (pH 7.4) at their CGC and kept at room temperature undisturbed for 24 h to form the hydrogels. After the formation of hydrogels, rheological measurements were performed to check their mechanical strength. First, strain sweep tests were carried out to identify the linear viscoelastic region (LVR) over a range from 0.01 to 1000% strain at a fixed oscillatory frequency of 1 rad/s. Then, frequency sweep tests were carried out under an appropriate strain (γ = 0.1%) with the frequency ranging from 0.1 to 100 rad/s at 25 °C. Further, a cyclic dynamic strain sweep experiment was conducted to explore the thixotropic properties of gels at their CGC. This experiment was completed at a constant angular frequency of 1 rad/s by applying a higher strain (γ = 100%) and a lower strain (γ = 0.1%) alternatively over a period of 2000 s and five successive cycles.[35]

4.2.8. ThT binding fluorescence assay

To study the mechanism of fibril formation of P16 and P18, we have performed ThT binding fluorescence assay. A stock solution of ThT with concentration 1 mM was prepared and diluted to 25 µM in phosphate buffer (7.4) for each fluorescence measurement. Various concentrations of the peptides, ranging from 10 µM to 140 µM were used. Emission spectra were recorded in between 455 nm and 700 nm for all the peptides, with an excitation wavelength of 440 nm using slit 5 nm on a Fluoromax-4 Horiba Fluorospectrometer.

4.2.9. Time kinetics of ThT fluorescence

The self-assembly pattern of peptide P18 was monitored by a time-dependent ThT fluorescence assay. To perform the experiment, concentration of P18 peptide and ThT were maintained at 100 µM (in PB, pH 7.4) and 25 µM respectively. The excitation wavelength for the fluorophore

was set at 440 nm and the emission was measured at 485 nm using slit width of 5 nm. Then, we monitored the fluorescence intensity of ThT, time upon being incubated with 100 μM P18 peptide, as a function of time.

4.2.10. Powder X-Ray diffraction (PXRD)

Wide-angle X-ray diffraction analysis was carried out on a Rigaku Smartlab X-ray diffractometer (Cu-Kα radiation with wavelength 1.540 Å) for all the powdered lipopeptide samples (P8–P18) (as obtained post-lyophilization).

4.2.11. Circular dichroism (CD) spectroscopy

Time-dependent CD spectra of P18 in the phosphate buffer system (pH 7.4) at 500 μM were recorded at 0 h, 24 h and 48 h by using a 200 μL quartz cuvette of 1 mm path length with a Jasco J-1500 spectropolarimeter at room temperature. Spectra were collected at a scan rate of 200 nm/min and 2 nm bandwidth from 190 to 290 nm with five scans for averaging. Before running the sample, respective solvent systems were run to correct the baseline.

4.2.12. Micro broth dilution assay

A standard micro broth dilution assay was used to study the antimicrobial activity of the lipopeptides.[36] All peptides were tested in solution forms. Overnight-grown cultures of respective microbes were used to obtain the mid-log-phase cultures of *P. aeruginosa*, *K. pneumoniae*, *S. aureus* and MRSA. The cell suspensions were centrifuged at 6000 rpm for 5 min. Cell pellets were washed thrice with 10 mM phosphate buffer of pH 7.4 alone or in the presence of PBS (10 mM, pH 7.4) and re-suspended in the same buffer to obtain a cell suspension containing 10^5 CFU/mL. The reaction was set in a 96 well plate, and 50 μL of the cell suspension was incubated with different concentrations of the lipopeptides (ranging from 1 to 200 μM), prepared from 1 mM peptide stock in phosphate buffer (pH 7.4) and incubated at 310 K for 4 h. A negative control containing only cell suspension and a positive control

containing 10 μM Polymyxin B with cell suspension was maintained. Absorbance of the culture was monitored at 630 nm to monitor microbial growth. The positive control polymyxin B was used to normalize all other readings. The peptide concentration at which 90% growth inhibition was observed, served as its $MIC_{99\%}$. All experiments were performed in triplicates.

4.2.13. Time course of bactericidal activity

Overnight grown culture of *P. aeruginosa* was centrifuged at 6000 rpm for 5 min and the pellet was washed thrice with 10 mM phosphate buffer (pH 7.4) and re-suspended to obtain 10^5 CFU/mL suspension of cells. 50 μL of bacterial cell suspension was incubated with the MIC of P16 and P18 and incubated at 310 K for different time intervals (5-120 min). After each incubation time, 5 μL aliquot was taken from each reaction volume, diluted in the same buffer and spread onto the NB agar plates for CFU counting after overnight incubation at 310 K. All experiments were performed in triplicate.[36]

4.2.14. Cell viability assay

Human dermal fibroblasts cells (HDF), Human cervical cancer cells (HeLa) and Human embryonic kidney cells (HEK 293) were plated into 96 well plate in triplicates at a density of $2x10^3$, $5x10^3$ and 10^4 cells/well respectively. After overnight incubation under normal cell culture conditions (37 °C with 5% CO_2 under humidified conditions), cells were treated with varying concentrations (from 0 μM to 160 μM) of each solubilized peptide for 24 h. All peptides were tested in solution forms.The peptides were removed, and subsequently, MTT (3-[4, 5-dimethylthiazol-2-yl]-2,5-diphenyltetrazolium bromide thiazolyl blue, Sigma-Aldrich, USA) (0.25 mg/mL) in DMEM was added and incubated with the cells for another 3 h. The formed formazan crystals were solubilized by adding 200 μL of DMSO (Himedia). Cell viability was calculated by measuring absorbance at 570 nm by using Multiskan GO spectrophotometer (Thermo Scientifc). Tests were performed in triplicates. The absorbance corresponded to the number of live cells in each well. Images of cells treated with varying

concentrations (from 0 µM to 160 µM) of each peptide were captured after 24 h, using ZOE™ fluorescent cell imager from Bio-Rad.

4.2.15. Haemolytic activity

Human blood was collected in an EDTA vial. 1 mL of the freshly collected cells were centrifuged at 1500 g for 5 min, and the supernatant or the serum obtained was discarded. The cell pellet was then washed with phosphate buffer saline of pH 7.4 for three consecutive times, and finally re-suspended in the same buffer. Peptide solutions of different concentrations were incubated with 10% of the blood cells for a period of 1 hr. Untreated blood cells were taken as the negative control, while the blood cells treated with 1% of Triton X was taken to be the positive control. Finally, the blood cells incubated with the peptides of various concentrations and 1% Triton X and the untreated cells were centrifuged post incubation period. The OD values of the supernatant obtained were measured at 540 nm. The untreated cells or the negative control was considered to have no hemolysis, while those treated with 1% of Triton X or the positive control was considered to have 100% haemolysis. The haemolytic percentages of the peptides at various concentrations, were determined from their respective OD values relative to the OD values obtained for the negative control and that of for the positive control. Experiment was performed in a set of triplicates.

4.2.16. Resistance development Assay

10 µL from overnight grown culture of MRSA (10^8 CFU/mL) was incubated with sub-MIC concentration of P18 (1.25 µM) in 6 mL of BHI media for 12 h at 37°C under shaking condition. This was repeated for 5 days. $MIC_{99\%}$ determination was done using the broth dilution method, as described earlier, at every 24 h time interval to check the development of resistance. $MIC_{99\%}$ was plotted as a function of number of generations of MRSA.[36 b]

The number of generations was calculated from the doubling time measurements,[36 c] which is discussed below:

Doubling Time

MRSA was grown in BHI media. Overnight grown culture was taken and 167 µl of 10^8 CFU/mL cells was sub-cultured in 100 mL (10 µL/6 mL) of BHI media. OD was monitored at every 2 h and plotted as a function of time (Appendix, Fig. A4.19)

Doubling time calculations:

$\mu = (\ln[X_2]-\ln[X_1])/(T_2-T_1)$; ($\mu$ = Specific Growth rate of cells)

$\mu = \ln(0.587)- \ln(0.1254)/(20-4)$

$\mu = -0.532+2.07/16$

$\mu = 0.096\ h^{-1}$

Doubling time (td)= ln2/ µ

td= 0.693/0.096

td= 7.2 h

Generation time calculations

Total growth cycle= 12 h

No. of generations (ng)= Total growth cycle/Doubling time

Ng= 12/7.2

Ng= 1.6 generations or 3.2 generations/day

4.2.17. Proteolytic stability assay

4.2.17.1. HPLC Experiment

To check the proteolytic stability, Proteinase K (0.1 mg/mL, 3.46 µM) was added to P16 and P18 (4 mM), and kept incubated at 37 °C for different time intervals between 30 min and 6 h. Post incubation, 50 µL of the reaction solution was quenched with 50 µL of acetonitrile and 1% TFA (at 4 °C, 15 min).[36] 20 µL was injected into the C18 reverse-phase column (Thermo-scientific, Biobasic-18, dimension: 250 X 4.6, particle size: 5 µ) for HPLC analysis. Samples were eluted by a linear gradient of 5–100% CH_3CN/H_2O in 0.1% TFA at a flow rate of 1

mL/min. The eluted peptides/fragments were detected at 214 nm. All the traces were acquired using an Agilent 1260 Infinity II analytic HPLC system (Agilent Technologies).

4.2.17.2. Mass spectrometry

In order to determine the chemical integrity of P16 and P18 upon protease degradation, a MALDI-TOF mass spectrometric analysis of the peptide-enzyme reaction mixture was carried out using MALDI-TOF spectrometer using Bruker Daltonics flex analysis.

4.3. Results and discussion

4.3.1. Rational design of lipopeptides

As lipidation is one of the strategies used to enhance the protease resistance of peptides, we based our design of effective antimicrobials on lipopeptides. We designed six cationic lipopeptides (P8, P10, P12, P14, P16 and P18) in this study (Fig. 4.1 a) and Table 4.1) and named them depending on the length of the fatty acyl chain present in them. The designed lipopeptides were amphiphilic in nature containing a positively charged C-terminal pentapeptide unit, ARKVR, and an N-terminal hydrophobic fatty acyl chain. The RKVR peptide motif was derived from the human lactoferrin protein, which is an iron-binding glycoprotein and important innate defense molecule with antimicrobial properties against a wide range of microbes.[37-38] The length of the fatty acyl chain was varied from C_8 to C_{18}, while keeping the peptide element of the lipopeptides unchanged. Thus, in going from P8 to P18, though the charge of the peptides remained the same (+3), the hydrophobicities increased proportionately with the length of the fatty acyl chain. This was evident from the increase in the retention times, observed for the lipopeptides in the analytical HPLC (Table 4.1). This systematically changed the hydrophobic-hydrophilic ratio of the lipopeptides. We explored various properties of these peptides, like self-assembly and the biological potency (salt tolerance of antimicrobial activity, cytotoxicity, protease resistance, etc.), and established a

direct link to their respective hydrophobic-hydrophilic ratios. All the designed peptides were synthesized, purified and characterized by analytical HPLC (Appendix, Fig. A4.1-A4.6) MALDI-MS (Appendix, Fig. A4.7-A4.12.) and ^{1}H NMR (Appendix, Fig. A4.13-A4.18).

4.3.2. Gelation studies

Amphiphilic lipopeptides are known to form hydrogels.[39a] Thus, we investigated the gelation property of our designed lipopeptides in water and buffer-based solvents. P16 and P18 formed homogeneous translucent hydrogels in a phosphate buffer system at pH 7.4 upon standing for 24 h (Fig. 4.1 b). The hydrogelation of P16 and P18 was tested using a simple vial inversion test. The minimum gelation concentrations of P16 and P18 were estimated to be 2 mg/ ml. The thermal stability of the hydrogels was determined using T_{gel}, which was estimated to be ~42 °C and ~46 °C for P16 and P18 hydrogels, respectively (Table 4.1). This suggested that the P18 hydrogel was slightly more thermally stable than the P16 hydrogel. This might be

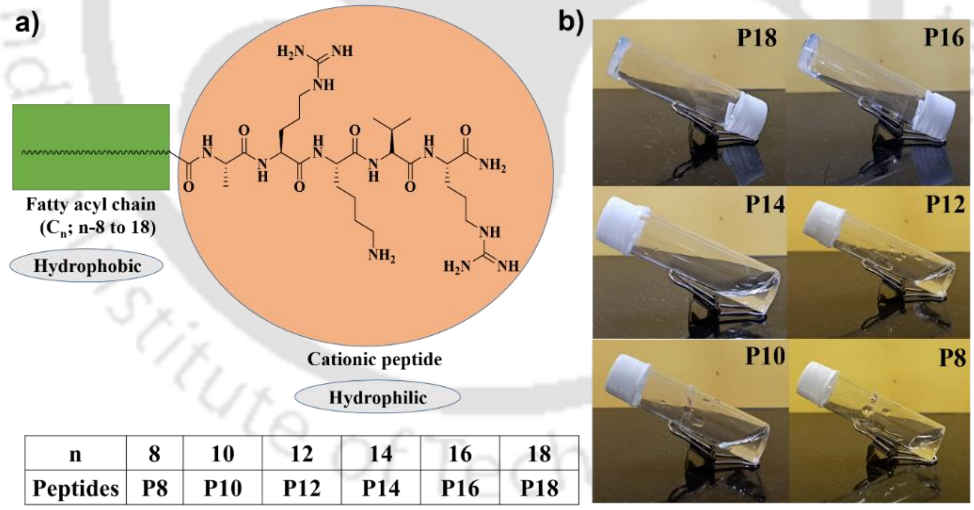

n	8	10	12	14	16	18
Peptides	P8	P10	P12	P14	P16	P18

Fig. 4.1. a) Chemical structures of the lipopeptides designed in this study. Designed lipopeptides are amphiphilic molecules containing a hydrophobic fatty acyl chain (of variable lengths, C_8-C_{18}) and a hydrophilic cationic peptide part. The peptide names indicate the length of the fatty acyl chains that they contain. b) Vial inversion test showing the hydrogelation ability of the lipopeptides. Of all the lipopeptides, only P16 and P18 formed hydrogels at 10 mM, phosphate buffer system, pH 7.4.

Table 4.1. Physico-chemical and gelation properties of the designed lipopeptides (P8-P18).

Peptides	Sequence	Charge	Gel/CMC/(% w/v)	T_{gel} (°C)	Molecular weight calculated/ observed $(M+H)^+$(Da)	Retention time (min)
P8	C_8-ARKVR-NH_2	+3	Not formed	-	754.979/ 755.048	12.16
P10	C_{10}-ARKVR-NH_2	+3	Not formed	-	782.565/ 783.183	12.93
P12	C_{12}-ARKVR-NH_2	+3	Not formed	-	810.596/ 810.663	13.63
P14	C_{14}-ARKVR-NH_2	+3	Not formed	-	838.628/ 840.262	14.72
P16	C_{16}-ARKVR-NH_2	+3	Translucent/ (2 mg/ml)/0.20	42	867.659/ 867.896	14.96
P18	C_{18}-ARKVR-NH_2	+3	Translucent/ (2 mg/ml)/0.20	46	894.690/ 895.885	16.95

attributed to the larger fatty acyl chain length of P18 compared to P16. None of the other lipopeptides with shorter fatty acyl chains formed hydrogels under the experimental conditions tested. Thus, the length of the fatty acyl chain, or in other words, the hydrophobic-hydrophilic balance of the lipopeptides, was a crucial determining factor in the gelation ability and stability of the hydrogels.

4.3.3. Secondary structure of the lipopeptides

The secondary structure of the lipopeptides was studied by FT-IR spectroscopy. The characteristic amide I band in the range of 1620-1630 cm^{-1} accompanied by the second peak at 1670-1680 cm^{-1} suggested the β-sheet conformational[39 b, c] preference for all the lipopeptides in general (Fig. 4.2).

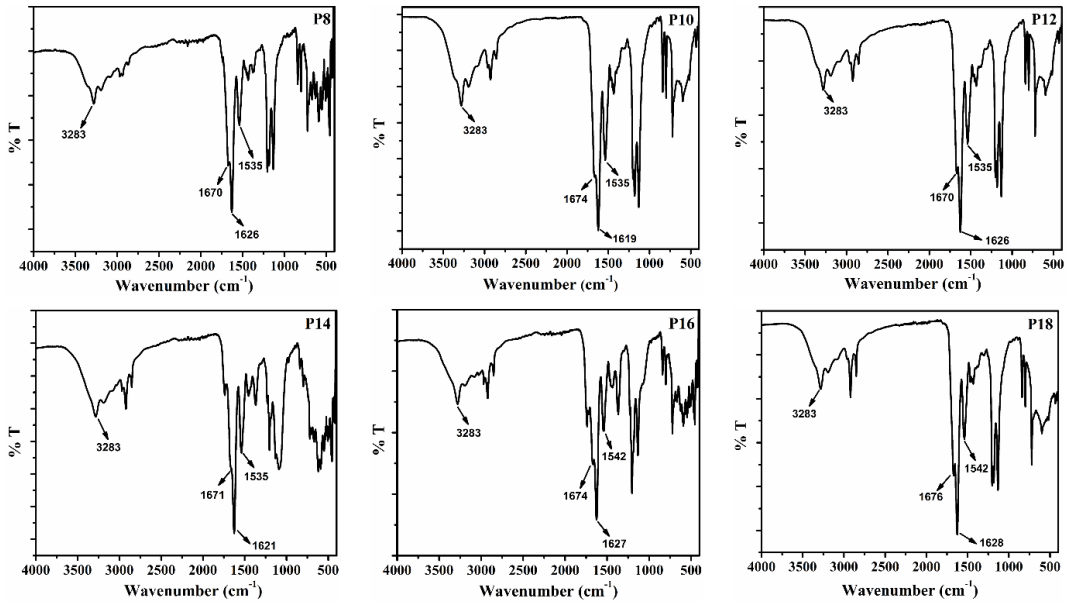

Fig. 4.2. FTIR spectra of P8-P18.

In order to look at the secondary structure of P18 in the hydrogel, FT-IR spectroscopy was performed for the corresponding xerogel (Fig. 4.3 a). The presence of the characteristic peaks in the range of ~1629 cm^{-1} and ~1677 cm^{-1} in the P18 xerogel proved the presence of β-sheet structures.

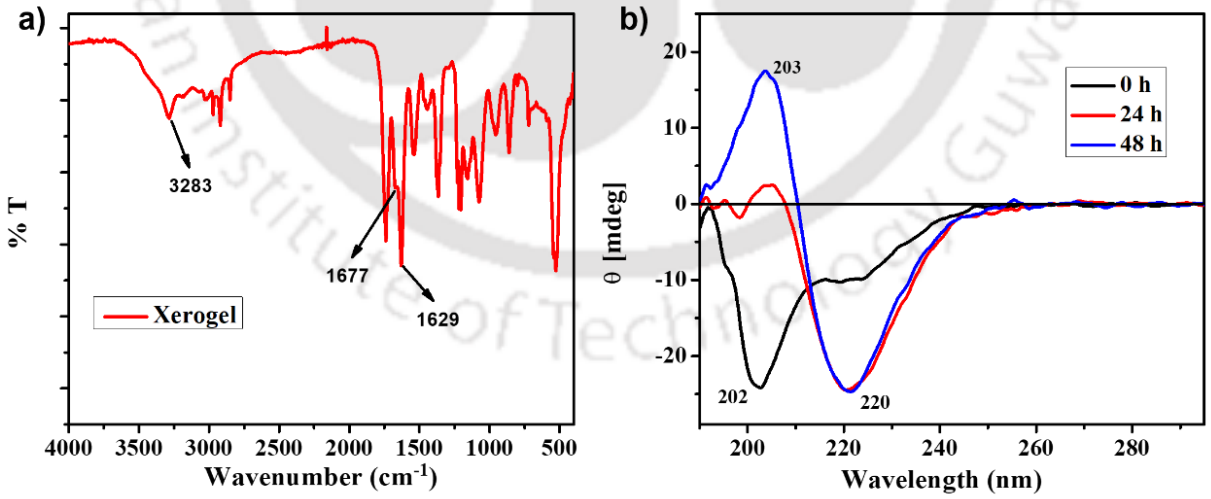

Fig. 4.3. Secondary structure of P18 in solution and gel state. a) IR spectra of P18 in xerogel state, b) CD spectra of P18 (500 μM) in 10 mM Phosphate buffer at 0 h, 24 h and 48 h of incubation.

Curious to learn about the secondary structure of P18 in the solution state, CD spectroscopy was performed. As the gelation required a long time, it was assumed that the fibril formation might be a relatively slow process for P18. To probe the time-dependent growth of the β-sheet structures, we performed a time-dependent CD spectroscopy experiment. Fig. 4.3 b shows the change in the molar ellipticity of P18 (500 μM) in the phosphate buffer, pH 7.4, upon incubation for 0, 24 and 48 h, respectively. P18 showed a negative cotton effect at ~202 nm at 0 h, suggesting a random coil-like conformation at the initial time. Later, upon incubation for 24 h, the negative cotton effect peak at 202 nm disappeared with the appearance of a new negative cotton effect peak at 220 nm. Peptides with the β-sheet structure give rise to a characteristic positive cotton effect peak at 195-200 nm and a negative peak at 220 nm.[39 d, e, f] The appearance of the negative cotton effect peak at 220 nm indicated the presence of β-sheet conformation of P18 upon incubation for 24 h. The absence of the positive cotton effect peak at 202 nm could be attributed to its cancellation with the negative cotton effect peak from the random coil conformation. It should be highlighted that the observed CD spectra was an additive spectra of various conformations present at any point of time in the solution. This suggested the presence of mixed populations of both random coils and β-sheets at 24 h. At 48 h, both the positive peak at 203 nm and the negative peak at 220 nm were observed, indicating that the entire population of the peptide had adopted β-sheet conformation. The above-mentioned CD study could clearly capture the time-dependent adoption of β-sheet conformation by P18, which led to the formation of β fibrils and its eventual hydrogelation. X-ray diffraction studies were carried out to obtain information about the molecular packing of the lipopeptides in the solid state. The XRD pattern of the lipopeptides in the wide-angle regions is shown in Fig. 4.4. For all the lipopeptides, a peak was observed in the range of 2θ = 20-23° which corresponded to a d-spacing of about 4.7-3.8 Å. A spacing of ~4 Å is typical for the inter-strand distance in the β-sheet structures (Fig. 4.4 and Table 4.2). It is noteworthy that

the d-spacings systematically decreased from P8 to P18, i.e., with the increase in the length of the fatty acyl chains. However, the tendency to form a β-sheet-like molecular packing increased upon lengthening the fatty acyl chain.

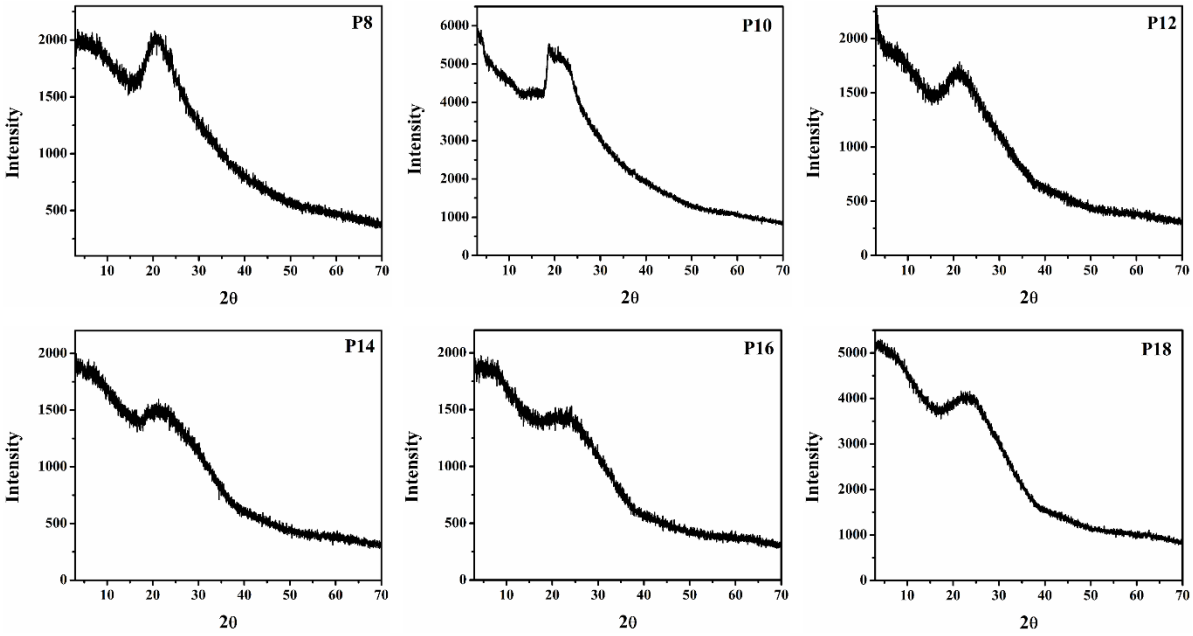

Fig. 4.4. PXRD spectra of P8-P18.

Table 4.2. 2θ and d-spacing values from PXRD.

Peptides	**P8**	**P10**	**P12**	**P14**	**P16**	**P18**
2θ	20.75	20.88	20.96	21.78	23.028	23.7
d spacing (Å)	4.27	4.24	4.241	4.07	3.85	3.8

4.3.4. Self-assembled morphology of the lipopeptides

FESEM was performed on the hydrogels of P16 and P18 at their CGC to investigate their morphology (Fig. 4.5 f and h). Both P16 and P18 hydrogels formed a uniform mesh-like fibrillar structure. The width of the fibrils was ~119 nm and ~63 nm in P18 and P16 hydrogels, respectively. It was interesting to note that the morphology of P18 in solutions (Fig. 4.5 g) at its CGC was distinctly different from that of the hydrogel. While in the hydrogel, the fibrous network was dense and homogeneously present, the fibrous structure was interspersed with irregular formations in the solution state. Additionally, the fibrils present in the gel state were

much more thicker (~119 nm) in contrast to the thinner fibrils (~50 nm) present in solutions. The morphology of P16 in solution, at its CGC (Fig. 4.5 e) and gel state, were somewhat similar composed of homogeneous fibrillar structures, though the hydrogel network contained thicker fibrils (~63 nm) in comparison to the fibrils present in solutions (~45 nm). It was also interesting to note that the fibrils present in the P18 hydrogel were thicker than those present in the P16 hydrogel. None of the other lipopeptides showed the presence of regular fibrillar structures and were mostly composed of irregular morphologies (Fig. 4.5 a-d). This clearly suggested that the hydrogel formation was directly dependent on the ability of the lipopeptides to form fibrils, and that the length of the fatty acyl chain determined the quality of the fibrils formed. In short, the self-assembling ability of the lipopeptides was directly related to their hydrophobic-hydrophilic balance.

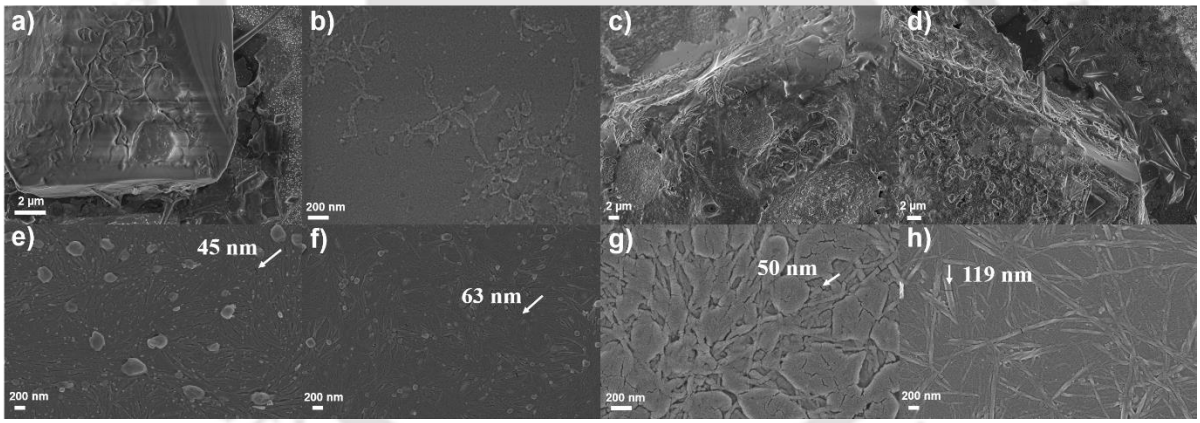

Fig. 4.5. FESEM images of solutions 0.2 % (w/v) of lipopeptides, a) P8 (2.65 mM), b) P10 (2.5 mM), c) P12 (2.47 mM), d) P14 (2.38 mM), e) P16 (2.3 mM) and g) P18 (2.23 mM). FESEM images of 0.2 % (w/v) hydrogels of f) P16 and h) P18 obtained from 10 mM phosphate buffer system 7.4. The arrows were pointing to the width of the fibrils.

4.3.5. Viscoelastic properties of the P16 and P18 hydrogels

The mechanical strength and stability of P16 and P18 hydrogels were studied by rheology. The storage modulus (G´) and loss modulus (G´´) were measured as a function of different parameters such as angular frequency and strain sweep. Gels formed from P16 and P18 at their respective CGC, in a 10 mM phosphate buffer system, pH 7.4, were used in this study. In the

angular frequency sweep experiment performed at a constant strain of 0.1% at 25 °C, G´ was found to be dominating over G´´ till about 100 rad/s (Fig. 4.6 a and d), for both the gels. Moreover, G´ and G´´ were found to be independent of angular frequency, in the region 1–100 rad/s, which indicated the formation of stable hydrogels. The storage moduli of both the hydrogels were of the order of ~10^2-10^3 Pa, in the frequency sweep experiment, which indicated a moderate mechanical strength for both the hydrogels. In a strain sweep experiment, where the storage moduli (G´) and the loss moduli (G´´) for both the hydrogels were plotted as a function of % strain (0.1-1000%) (Fig. 4.6 b and e), it was found that G´ was higher than G´´ (of the order of 10^2 Pa) till a particular strain (linear viscoelastic region (LVR), g = 0.1–0.5%) for P16 and P18 hydrogels. Next, in order to examine the thixotropicity of the hydrogels, a time-dependent step-strain rheological experiment was performed. First, when a low constant strain (g = 0.1%) was applied to the 0.20% (w/v) hydrogel, the G´ value was greater than G´´ value. This was followed by suddenly applying a higher strain (γ = 100%) (Fig. 4.6 c and f). This led to an increase in the G´´ value over the storage modulus G´. Such cycles of alternate reduced and increased strains were applied in a cyclic fashion for several times. In every cycle, upon increasing the strain, G´´ increased over G´, indicating a loss of the gel property, while the reduction in the strain led to an increase in G´ over G´´, indicating the restoration of the gel nature. The experiment was repeated over 5 cycles with 100% recovery of the gel property in each cycle. This experiment proved the thixotropic behaviour of both P16 and P18 hydrogels.

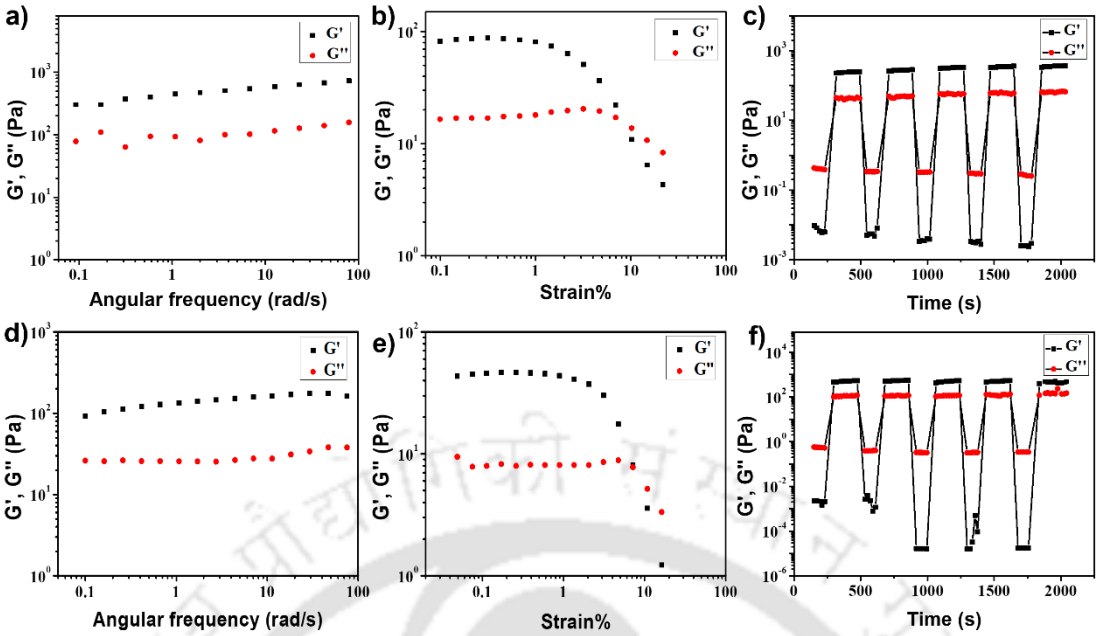

Fig. 4.6. Viscoelastic properties of P16 and P18 hydrogels. a, d) Frequency sweep rheology study, b, e) Strain sweep rheology study, and c, f) Step strain rheology study for 0.2% w/v P16 and P18 hydrogels, respectively.

4.3.6. Investigations of the fibril formation using ThT fluorescence

With the intention of probing the self-assembly process of P16 and P18 at the molecular level, we performed fluorescence experiments using the dye Thioflavin T (ThT). ThT is a nonfluorescent molecule in the free state, and it binds to β-sheet structures selectively, whereupon its fluorescence increases greatly. This enhancement in ThT fluorescence intensity is used to quantitate the extent of β-sheet formation. Fig. 4.7 a shows the increase in the fluorescence intensity of the dye upon incubation with different concentrations (10-140 μM) of various lipopeptides. An appreciable increase in the fluorescence intensity of ThT was observed upon incubation with P18 and P16 beyond 100 μM, though, to a comparably lesser extent for the later. This suggested that the β-sheet formation in these peptides started from around 100 μM concentration (Fig. 4.7 a and b). However, no increase in the fluorescence intensity was observed in the case of the other lipopeptides till 140 μM. This showed that P18 with the longest fatty acyl chain length had the greatest tendency of self-assembling to form β-

sheet structures followed by P16. Thus, it may be concluded that the self-assembling ability of the lipopeptides was related to their β-sheet forming abilities, which in turn depended on the length of the fatty acyl chain or on their hydrophobic-hydrophilic balance.

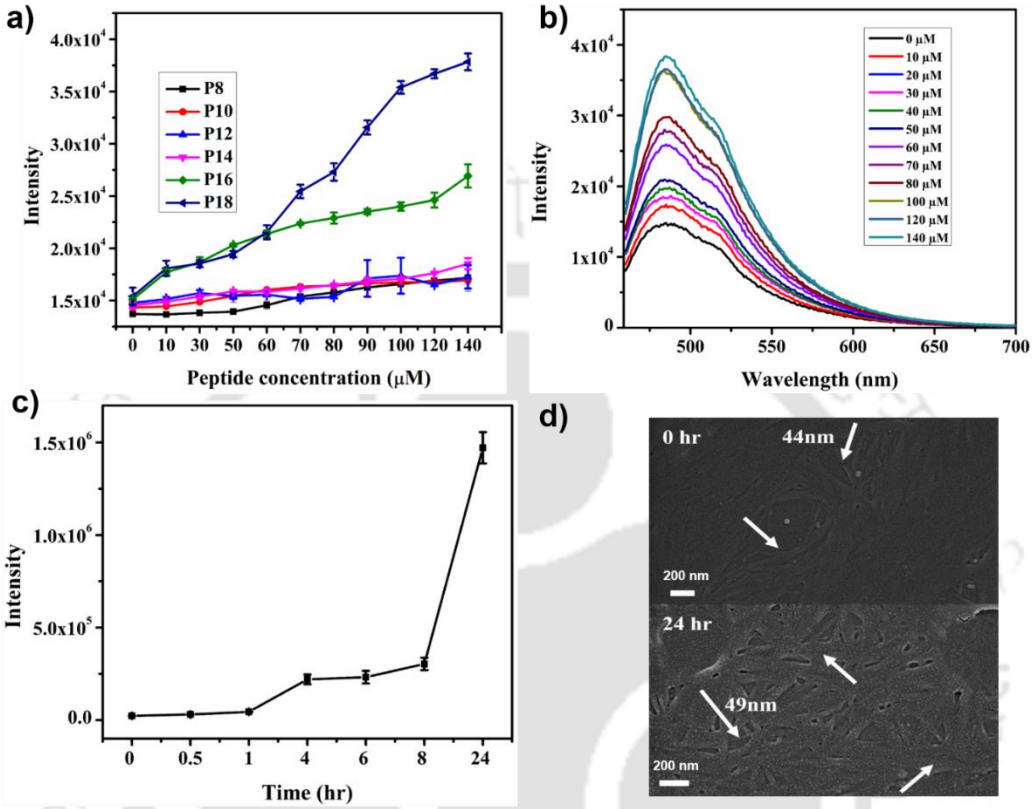

Fig. 4.7. ThT binding fluorescence studies: a) Plot of ThT fluorescence intensity as a function of the concentration of different lipopeptides at 485 nm. b) ThT fluorescence intensity at different concentrations of P18 in Phosphate buffer, pH 7.4. c) Time-dependent change in the fluorescence intensity of ThT, upon binding to P18 (100 μM). d) FESEM image of P18 at 100 μM concentration at 0 hr and 24 h. The arrows were pointing to the width of the fibrils.

4.3.7. Time-dependent growth of β-sheet fibrils

P18 required a significant time for gelation. In order to study the kinetics of β-sheet formation that subsequently led to the fibril formation at 100 μM, we monitored the ThT fluorescence as a function of time (Fig. 4.7 c). A significant increase in the ThT fluorescence intensity was observed after 8 h, suggesting a growth in the β-sheet formation after the said time point. This observation was also corroborated by the time-dependent CD spectroscopy experiments

described earlier, which clearly showed the slow development of fibrils over the time. Time-dependent change in the morphology of P18, at ~100 μM, where the β-sheet fibril formation just started, was studied by performing FESEM at 0 h and 24 h (Fig. 4.7 d). P18 adopted fibrillar network morphology at 100 μM, which corroborated the presence of β-sheet structures, as detected from the ThT fluorescence studies. The aging of the sample for 24 h did not show any change in the morphology, suggesting that this self-assembly was thermodynamically governed. The fibrils were ~44 nm in width at time zero and became ~49 nm upon aging for 24 h, supporting the growth of β-sheet structures with time.

4.3.8. Mechanism of the self-assembly of lipopeptides

Of the different lipopeptides designed, only P16 and P18 were capable of forming hydrogels. The hydrogels were formed from the fibrillar network that was constituted by β-sheet-like structures. The length of the fatty acyl chain, or in other words, the hydrophobic–hydrophilic balance determined the β-sheet formation ability of the lipopeptides. P18 had the best β-sheet formation ability among all the lipopeptides and, hence, gave rise to gels composed of the sturdier fibrils in comparison to the P16 hydrogel. The P18 hydrogel had slightly greater thermal stability, as shown earlier. Gelation of P16 and P18 was driven by hydrogen bonding in between the peptide segments of the molecule and hydrophobic interaction between the hydrophobic fatty acyl chains (Fig. 4.8). As the peptides were positively charged, the self-assembly was not possible in water, owing to the electrostatic repulsion between the individual peptide molecules. In the presence of PBS buffer (pH = 7.4), the counter anions helped in neutralizing the repulsion between the positive charges, thereby promoting the self-assembly process. The growth of the self-assembled structures was hierarchical and relatively slow. This led to a longer gelation time for both P18 and P16. Initially formed thinner fibrils subsequently led to the formation of thicker fibrils that finally gave rise to the hydrogels.

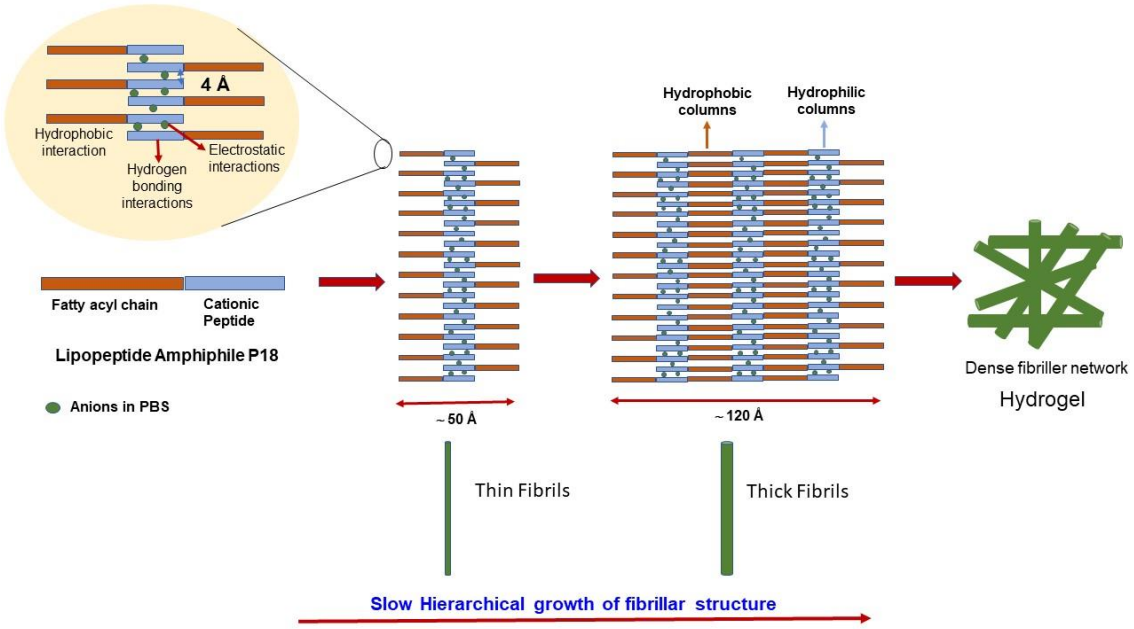

Fig. 4.8. Mechanism of hydrogelation in the AMP **P18**: time-dependent growth of dense fibrillar hydrogel network driven by hydrogen bonding and hydrophobic interactions in the presence of salt.

4.3.9. Antimicrobial properties of lipopeptides

The antimicrobial activities of all the designed lipopeptides were tested against Gram-positive (*S. aureus*) and Gram-negative (*P. aeruginosa* and *K. pneumoniae*) ESKAPE pathogens (Table 4.3 and Fig. 4.9). Peptide P18 showed very good activity against both the Gram-positive and Gram-negative bacterial strains, while P16 and P14 showed a better activity towards Gram-negative strains than that of the Gram-positive strain. Gram-positive bacteria are easier to kill than the Gram-negative bacteria, due to the presence of the protective outer covering of the later.

Table 4.3. $MIC_{99\%}$ values for the lipopeptides in µM concentration against a) *P. aeruginosa*, *K. pneumoniae* and *S. aureus* in the presence and absence of salt. ND = Not done (we did not perform antimicrobial activity tests in the presence of salts for all the lipopeptides; we only considered the most potent ones, specifically P18 and P16).

Microbes	***P. aeruginosa*** **($MIC_{99\%}$) (μM)**		***K. pneumoniae*** **($MIC_{99\%}$) (μM)**		***S. aureus*** **($MIC_{99\%}$) (μM)**	
Peptides	**Absence of salts**	**Presence of salts**	**Absence of salts**	**Presence of salts**	**Absence of salts**	**Presence of salts**
Polymyxin B (positive control)	**10**	**10**	**10**	**10**	**10**	**10**
P8	**>200**	**ND**	**>200**	**ND**	**>200**	**ND**
P10	**100**	**ND**	**>200**	**ND**	**60**	**ND**
P12	**80**	**ND**	**200**	**ND**	**20**	**ND**
P14	**10**	**ND**	**10**	**ND**	**20**	**ND**
P16	**10**	**10**	**10**	**20**	**20**	**20**
P18	**10**	**10**	**10**	**20**	**10**	**10**

P18 showed remarkable activity against *P. aeruginosa*, a nosocomial bacterial pathogen that has extracellular alginate capsules on its outer membrane preventing the entry of antimicrobials, thus making them ineffective.[40] P18 also showed a very good activity against opportunistic Gram-negative pathogen *K. pneumonia*, that is known to cause lethal infections including pneumonia, bloodstream infections and meningitis. P12 was selectively active against Gram-positive *S. aureus*, while P10 and P8 showed no activity against any of the tested pathogens (Fig. 4.9 and Table 4.3). In short, lipopeptides containing longer fatty acyl chains possessed higher antimicrobial potency, which diminished proportionately with the decrease in the length of the fatty acyl chain. Or in other words, an optimum hydrophobic–hydrophilic balance was crucial for good antimicrobial activity. The most potent peptide P18 had comparable potency to the standard antibiotic Polymixin B, used as a positive control. It was interesting to note that P18 lost its activity partially at higher concentrations (~100–200 μM). This might be attributed to the self-assembly of P18 at higher concentrations (Fig. 4.9).

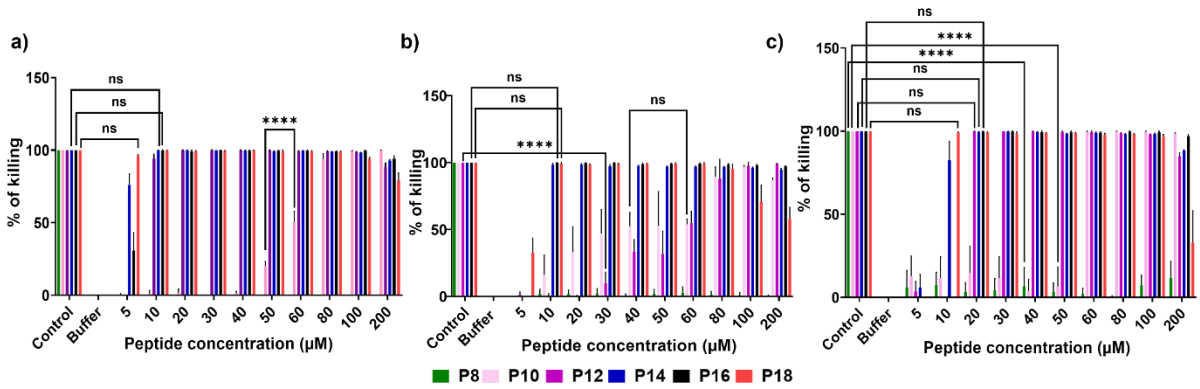

Fig. 4.9. $MIC_{99\%}$ of P8-P18 against a) *P. aeruginosa*, b) *K. pneumonia*, c) *S. aureus* in the absence of salt by Micro broth dilution assay. 10 μM Polymixin B and buffer were taken as positive and negative controls respectively. The data represents the mean of N=3 experiments (*p< 0.05, **p< 0.01, ***p< 0.001, ****p< 0.0001) via two-way analysis of variance (ANOVA) with and Turkey's multiple comparison test).

The molecular association of P18 led to a decrease in the concentration of the free molecular form of the peptide responsible for its antimicrobial potency, thereby decreasing the activity at higher concentrations.

4.3.10. Salt tolerance of antimicrobial properties

Most of the AMPs are rendered inactive at physiological salt concentrations and this is one of the major drawbacks that limit the therapeutic potential of the AMPs. Though the reason for this inactivation is not understood properly in detail, it is grossly attributed to the electrostatic reasons. Several strategies such as increasing the tryptophan content, changing the stereochemistry of amino acid residues, use of bulky unnatural amino acid residues and dimerization have been adopted to impart salt sensitivity to synthetic AMPs.[41] Thus, we wanted to study the salt tolerance of our most active lipopeptides (P16 and P18) at physiological concentrations of salt. Both P16 and P18 showed remarkable salt tolerance of their activity against *P. aeruginosa* and *S. aureus* (Fig. 4.10 and Table 4.3). The activity of both P16 and P18 was slightly compromised against *K. pneumonia* in the presence of salt.

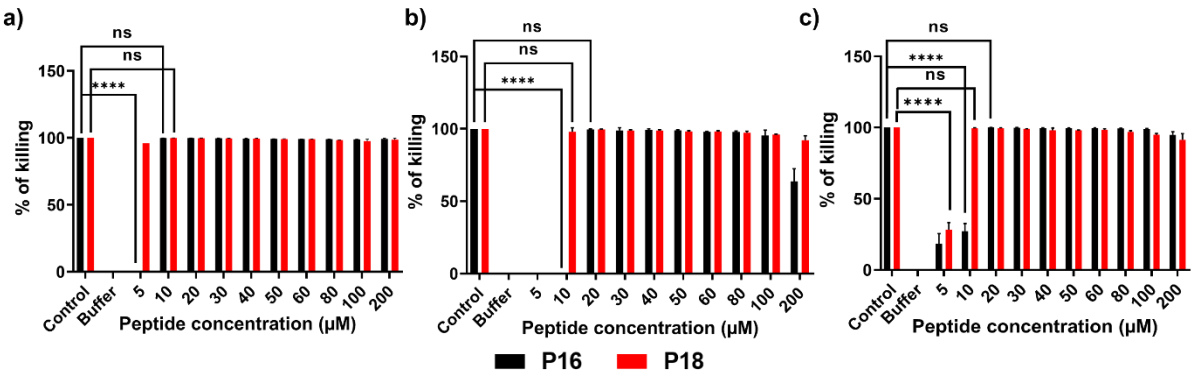

Fig. 4.10. $MIC_{99\%}$ of P16 and P18 against a) *P. aeruginosa*, b) *K. pneumonia*, c) *S. aureus* in the presence of salt by Micro broth dilution assay. 10 μM polymixin B and buffer were taken as positive and negative controls respectively. The data represents the mean of N=3 experiments (*p< 0.05, **p< 0.01, ***p< 0.001, ****p< 0.0001) via two-way analysis of variance (ANOVA) with and Turkey's multiple comparison test).

4.3.11. Activity against Methicillin-resistant *S. aureus* (MRSA)

The activities of P16 and P18 were tested against Methicillin-resistant *S. aureus* (MRSA) obtained from clinical isolates, both in the absence and in the presence of salts. Both the peptides showed high salt-tolerant antimicrobial activity ($MIC_{99\%}$ ~10 μM) (Fig. 4.11 a and b).

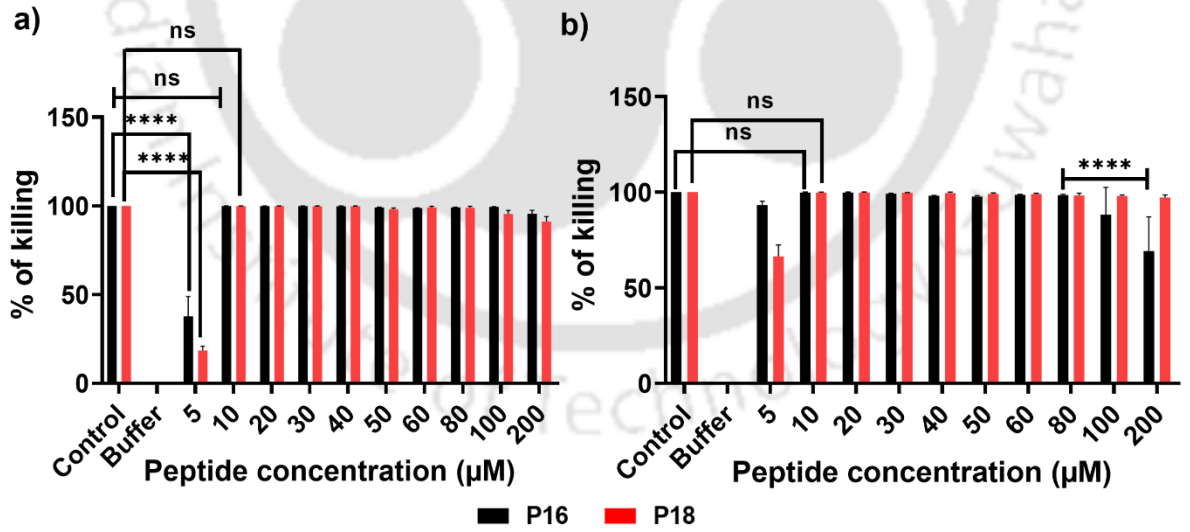

Fig. 4.11. $MIC_{99\%}$ of P16 and P18 against Methicillin-Resistant *S. aureus* (MRSA) in the a) absence and b) presence of physiological concentration (150 mM) of NaCl, estimated by Micro broth dilution assay. The data represents the mean of N=3 experiments (*p< 0.05, **p< 0.01, ***p< 0.001, ****p< 0.0001) via two-way analysis of variance (ANOVA) with and Turkey's multiple comparison test).

4.3.12. Time kinetics of the bactericidal activity of P16 and P18

To determine the time needed by P16 and P18 to express their bactericidal activity against *P. aeruginosa* at their respective $MIC_{99\%,}$ a time-course experiment was performed (Fig. 4.12). Cells incubated with the standard antibiotic Polymixin B (10 µM) (positive control), P16 and P18 at their respective $MIC_{99\%}$ for different time spans, were spread onto NB agar plates.

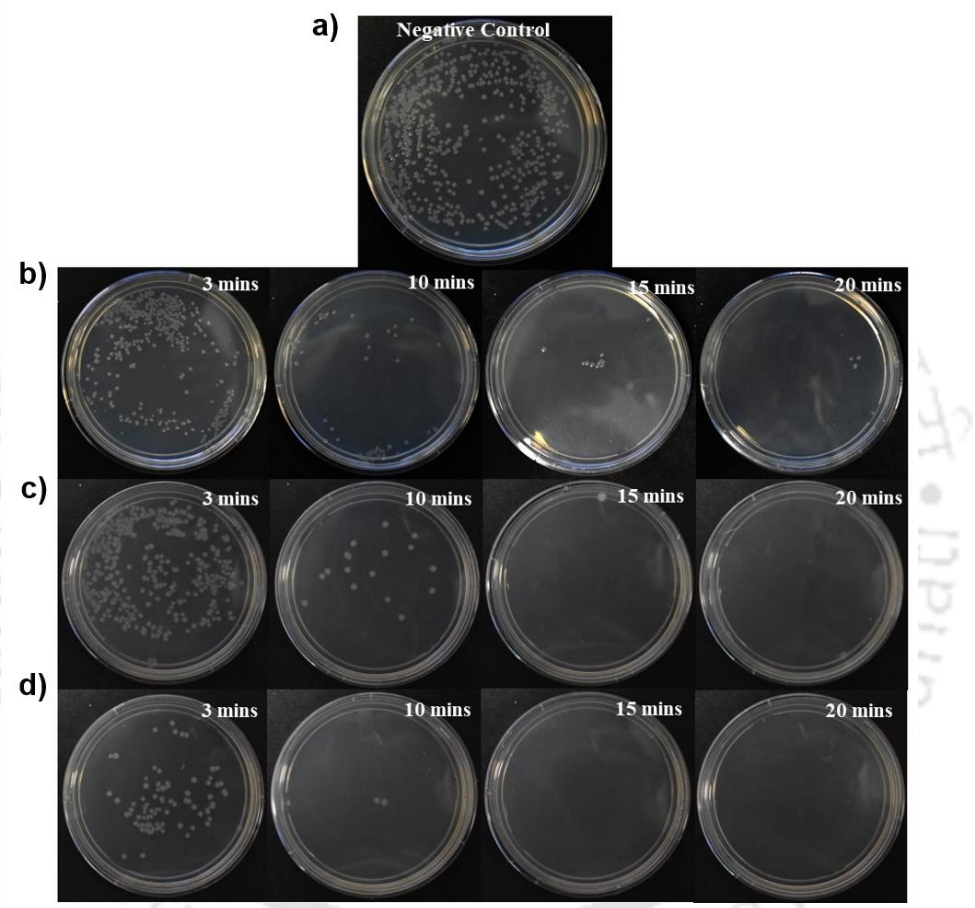

Fig. 4.12. Time kinetics of the bactericidal activity of P16 and P18 at their respective MIC99% against *P. aeruginosa* cells. *P. aeruginosa* cells were treated with P16 and P18 for different time intervals and cells were spread on NA plate for CFU count after overnight incubation at 37 °C. Bacterial killing percentage was calculated from CFU count of the plate in comparison to the control plate. (a) Negative control plate(no peptides added), (b) positive control plate (10 µM Polymyxin B treated cells), (c) plates treated with P16 at time points 3, 10, 15 and 20 min, respectively and (d) plates treated with P18 at time points 3, 10, 15 and 20 min, respectively.

After overnight incubation of the agar plate, the number of viable cells was calculated through CFU counting. There was a considerable decrease in the colony count at 10 min for both the

peptides, with almost complete killing of *P. aeruginosa* cells within 15 min for P18 (Fig. 4.12. c) and within 20 min for P16 (Fig. 4.12 b). Upon plotting the CFU counts as a function of time (Fig. 4.13 a), P18 evidently showed a faster bactericidal effect than P16 against *P. aeruginosa*. Both P16 and P18 were faster acting than the conventional antibiotic Polymixin B, which took around 45 min for complete killing of the *P. aeruginosa* cells.

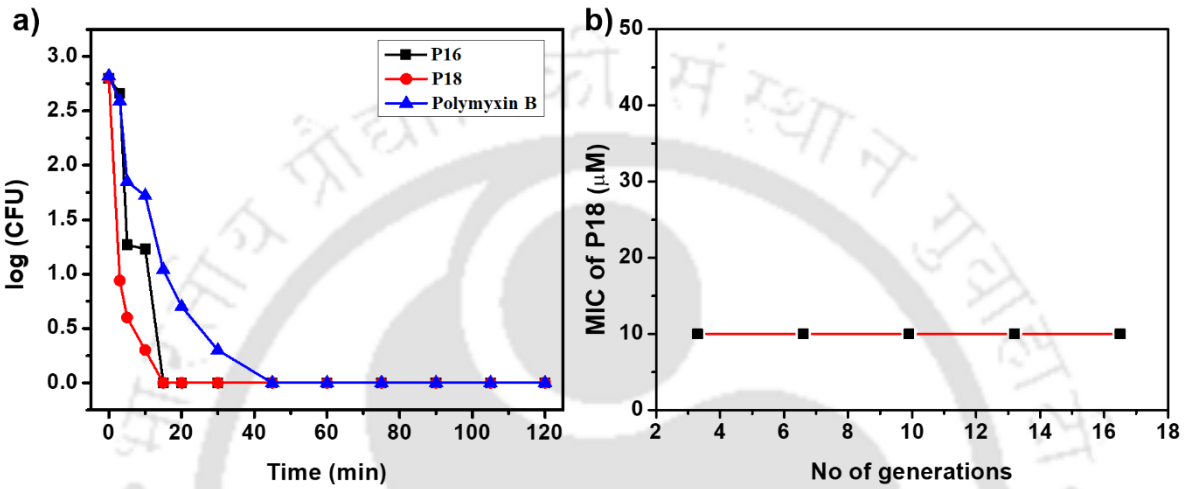

Fig. 4.13. Plot of a) percentage killing of *P. aeruginosa* at different time points, plotted from the CFU count for P16 and P18, b) $MIC_{99\%}$ of P18 against MRSA plotted as a function of the number of generations, showing no development of resistance in MRSA against P18.

4.3.13. Resistance development against P18 in MRSA

Rapid resistance development in microbes against antibiotics is one of their major shortcomings. We investigated if AMP P18 induced resistance against itself in MRSA. MRSA cells were treated with sub-MIC concentrations of AMP and allowed overnight growth at 37 °C with constant shaking. The OD was monitored regularly and the $MIC_{99\%}$ value calculated after every 24 h. The $MIC_{99\%}$ value remained constant at 10 μM over 7 days or ~16 generations. Thus, it may be concluded that there was no development of resistance against P18 in the MRSA cells till 16 generations (Fig. 4.13 b).

4.3.14. Cytotoxicity

For being a good therapeutic agent, the AMPs must be non-cytotoxic towards the mammalian cells. It is reported in some studies in the literature that increasing the length of the fatty acyl chain, increases the cytotoxicity of the peptides.[42-44] Some other studies report that the cytotoxicity depends on the peptide sequence as well and not on the length of the fatty acyl chain alone.[45a] As our lead active peptides contained long fatty acyl chains of C_{18} and C_{16},

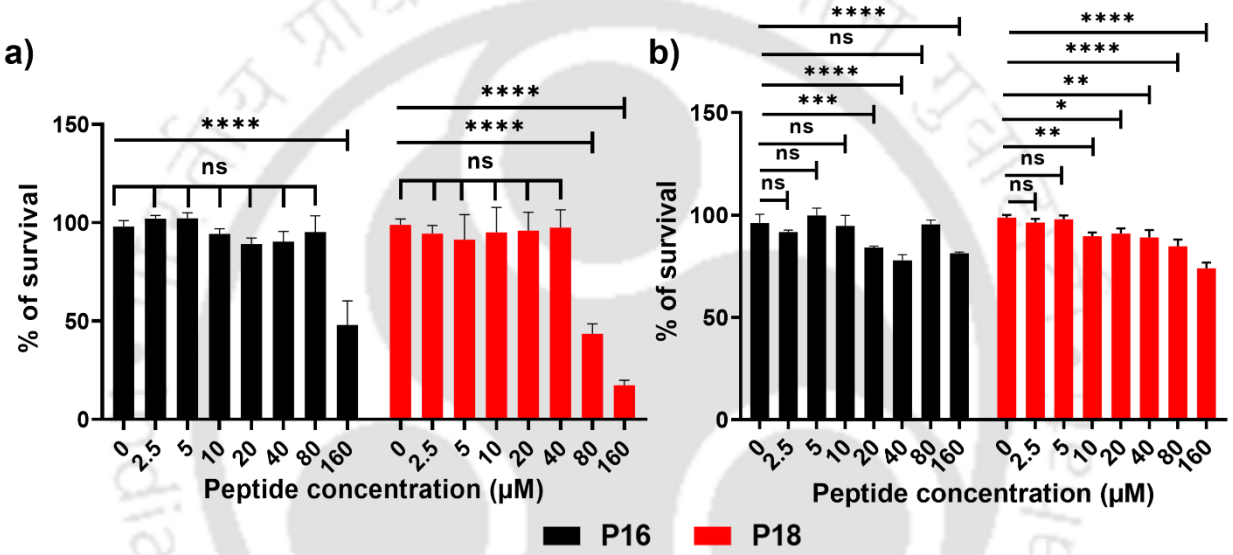

Fig. 4.14. MTT assay of P16 and P18 on a) HEK 293 and b) HDF cells. Cell were treated with increasing concentrations of peptides and their viability was measured by monitoring the absorbance at 570 nm. All the experiments were performed in triplicates. The data represents the mean of N=3 experiments (*p< 0.05, **p< 0.01, ***p< 0.001, ****p< 0.0001) via two way analysis of variance (ANOVA) with and Turkey's multiple comparison test).

we wanted to investigate their cytotoxicity towards mammalian cells. MTT assay was performed to investigate the cytotoxicity of P16 and P18 on HEK 293 cells (Fig. 4.14 a), and on Human Dermal Fibroblast (HDF) cells (Fig. 4.14 b). As evident from Fig. 4.14, both P16 and P18 exhibited cell viability of >90% against both HEK 293 and HDF cells till 40 μM concentration, which was much higher than their biologically active concentration (~10-20

μM). The microscopy images (Fig. 4.15) of lipopeptide treated HEK 293 cells attested the MTT results.

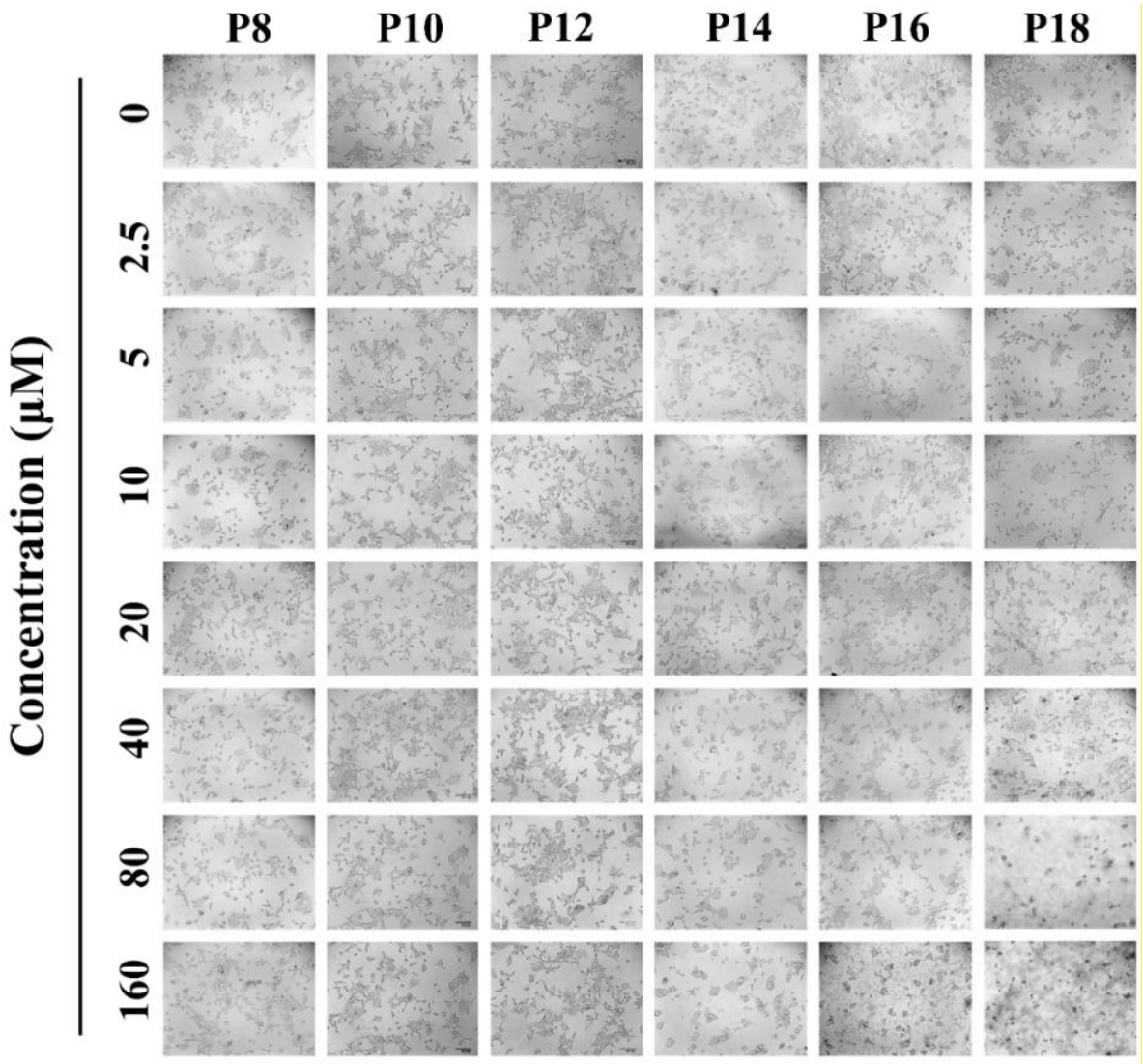

Fig. 4.15. Microscopy images of HEK 293 cells treated with incremental concentrations (0-160 μM) of different lipopeptides P8-P18 (Scale bar: 100 μm).

HEK 293 cells maintained their regular morphology and were viable up to a concentration of 40 μM for both P16 and P18 lipopeptides. P8-P14 were all non-cytotoxic (viability > 90%) against HEK293 cells, till 160 μM, the highest concentration tested. P16 and more prominently P18 became relatively cytotoxic at higher concentrations of 160 μM and 80 μM respectively. This suggested that the cytotoxicity of the lipopeptides against HEK 293 cells increased with

the increasing hydrophobicity of the peptides, accompanied by the increasing length of the fatty acyl chain. The cytotoxicity was tested against HDF, only for P16 and P18. Against HDF cells, both P16 and P18 remained non-cytotoxic even till 160 μM concentration. Thus, the cytotoxicity of the lipidated peptides, not only depended on the length of the fatty acyl chain and the peptide sequence in question, but also on the cell lines that were used in the experiment. MTT assay was performed to investigate the cytotoxicity of other designed lipopeptides on HEK 293 cells (Fig. 4.16 a), showing non-cytoxic nature. P16 and P18 had no striking anticancer activity as seen from the cell viability against the HeLa cells (Fig. 4.16. b).

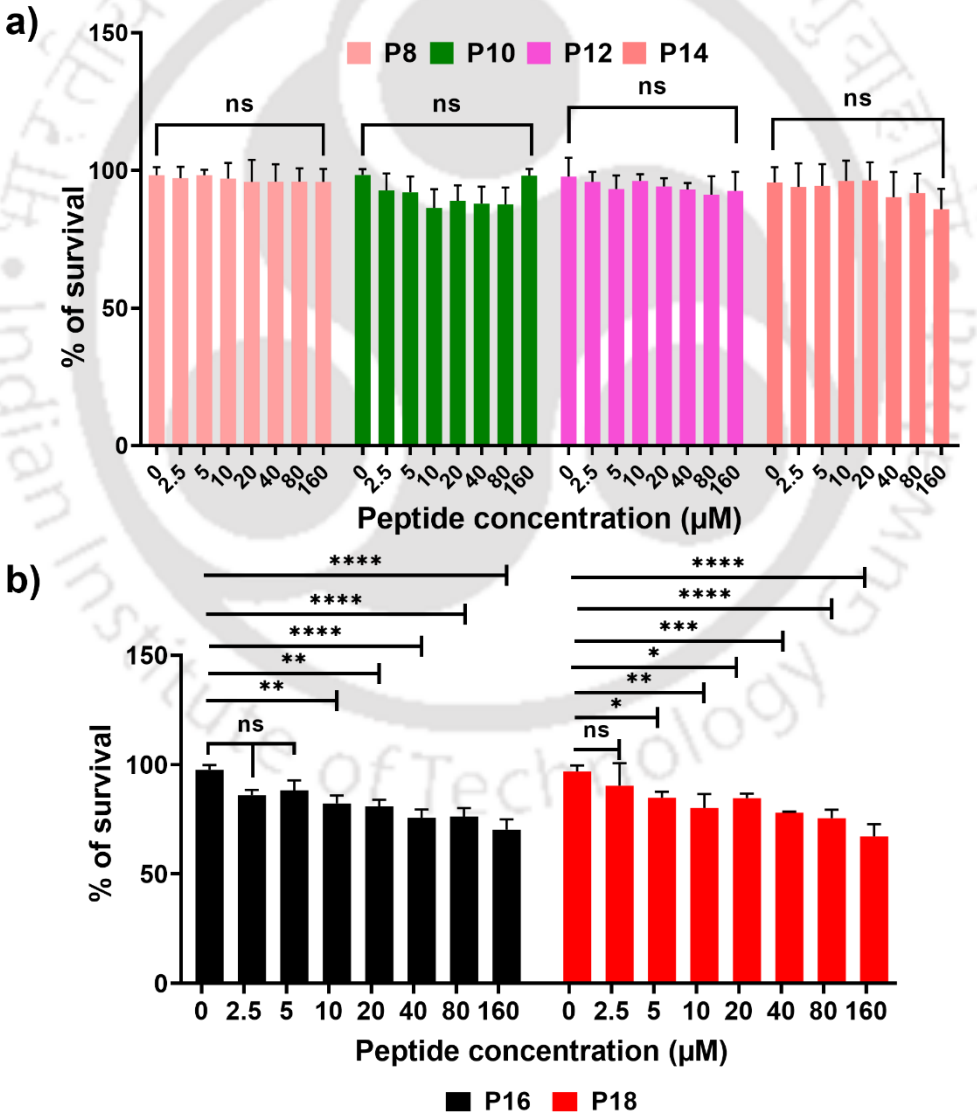

Fig. 4.16. MTT assay of a) P8, P10, P12 and P14 on HEK293 cell line and b) P16 and P18 on HeLa cell line. Cells were treated with increasing concentrations of peptides and their viability

was measured by monitoring the absorbance at 570 nm. All the experiments were performed in triplicates. The data represents the mean of N=3 experiments (*p< 0.05, **p< 0.01, ***p< 0.001, ****p< 0.0001) via two way analysis of variance (ANOVA) with and Turkey's multiple comparison test).

4.3.15. Haemolytic activity

The haemolytic ability of P16 and P18 were determined both qualitatively and quantitatively (Fig. 4.17). First, 1% RBCs were incubated with different concentrations of peptides for an h. Post centrifugation, percentage hemolysis was checked by measuring the absorbance of the supernatant at 414 nm and comparing the values with the untreated and 1% Triton-X treated cells. Both the peptides were almost non-haemolytic (≤2%) at their biologically relevant concentrations (10 µM), as shown in Fig. 4.17. Both P16 and P18 became haemolytic at higher concentrations, with the effect more pronounced for the later. Thus, it may be concluded that the haemolytic ability of the lipopeptides was also connected to their hydrophobic-hydrophilic balance.

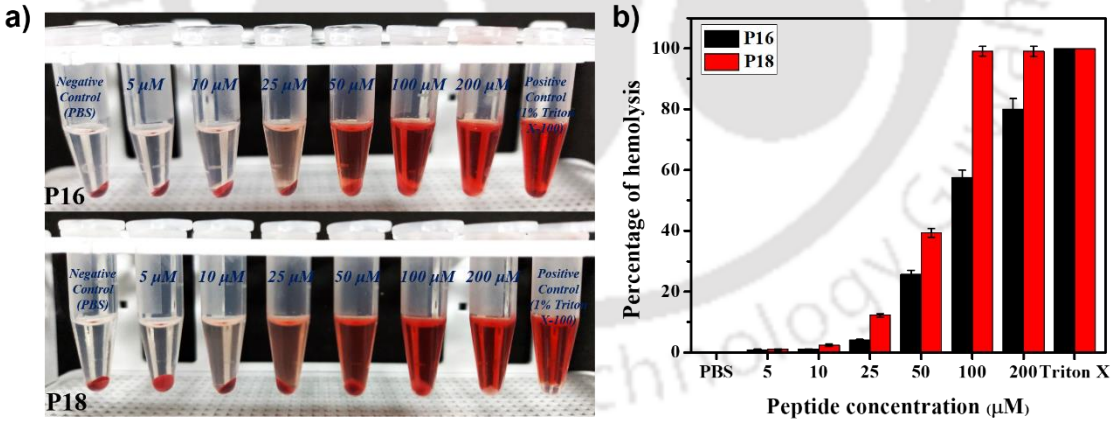

Fig. 4.17. a) Digital images represent haemolytic assay for P16 and P18 against human RBC at different peptide concentrations (5, 10, 25, 50, 100, 200 µM), b) Bar diagram showing the % haemolysis for P16 and P18 against different concentrations of the peptides. Buffer and Triton-X 100 treated as negative and positive control.

However, hemolytic assay is a very tricky assay because there are several limitations linked up with this hemolytic assay due to various factors that can create the possibility of showing

false results. Therefore, addressing those limitations is very crucial for a clean hemolytic assay and results with high accuracy. Reports available in the literature revealed that the species origin of blood used for hemolysis assays could influence the hemolytic response to a considerable degree. Therefore, this assay necessitates multiple blood samples from different healthy humans to perform the same experiment to avoid possible errors.[45b] Also, including distilled water is important for this assay as it causes hemolysis through osmotic shock and is often used as the positive control in hemolysis assays.[45c,d] Additionally, the effect of tested samples on the hemolysis of erythrocytes depends strongly on the osmolarity of the solution, which demands this assay to be performed in different solutions like hypotonic, isotonic, and hypertonic with different osmotic pressures.[45e] Moreover, other factors like erythrocyte concentration, sample transport and/or storage type of detergent and concentration used for positive controls, and incubation time also have the ability to affect the calculated hemolysis ratios.[45f,b] Therefore, it is very important to consider all the key parameters while performing a hemolytic assay for proper results. In our study also, we have got this result by performing it in a regular simple method; however, to be more precise and sure about this data, we would like to say that this experiment may be explored further by considering all possible factors as they affect the hemolytic assay and may give a false result.

4.3.16. Protease resistance

Another great challenge that limits the commercialization of the AMPs is their short systemic half-life, owing to their protease degradability. To investigate if our lead lipopeptides P16 and P18 were resistant to protease degradation, we monitored their chemical integrity upon incubation with proteinase K, by analytical HPLC (Fig. 4.18) and MALDI-MS (Fig. 4.19 and 4.20). P16 remained protease resistant until an h of incubation with the enzyme, after which it started degrading, as evidenced by the appearance of several new peaks in the chromatogram (Fig. 4.18 a-d).

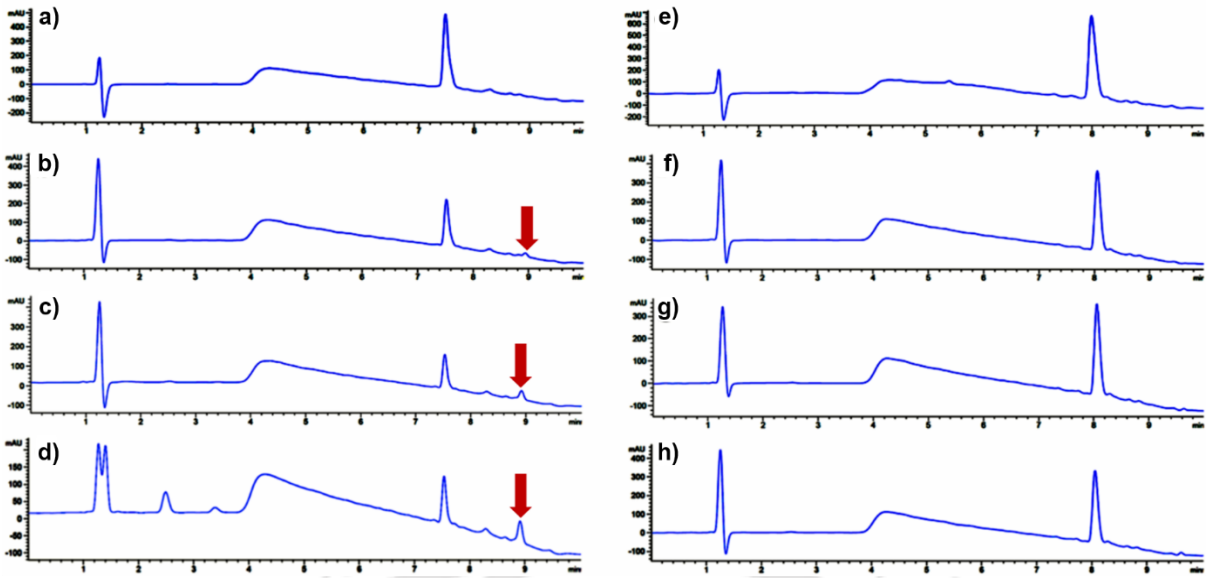

Fig. 4.18. Protease resistance of P16 and P18. Analytical HPLC traces of P16 (left panel) and P18 (right panel), after incubation with enzyme proteinase K for different time intervals. Chromatogram of P16 and P18: (a) and (e) in the absence of enzymes and in the presence of enzyme after (b), (f) 1 h, (c), (g) 3 h and (d) and (h) 6 h of incubation with proteinase K.

However, P18 maintained its retention time when injected into the analytical HPLC, even after incubation with enzyme proteinase K till 6 h, suggesting its robustness to the protease degradation (Fig. 4.18 e-h). MALDI-MS analysis of the reaction mixtures post incubation with the enzyme corroborated the analytical HPLC results. The MALDI-MS spectra contained only intact P18 (differently ionized, Fig. 4.20) peaks in contrast to a mixture of intact and truncated peptides for P16 (Fig. 4.19).

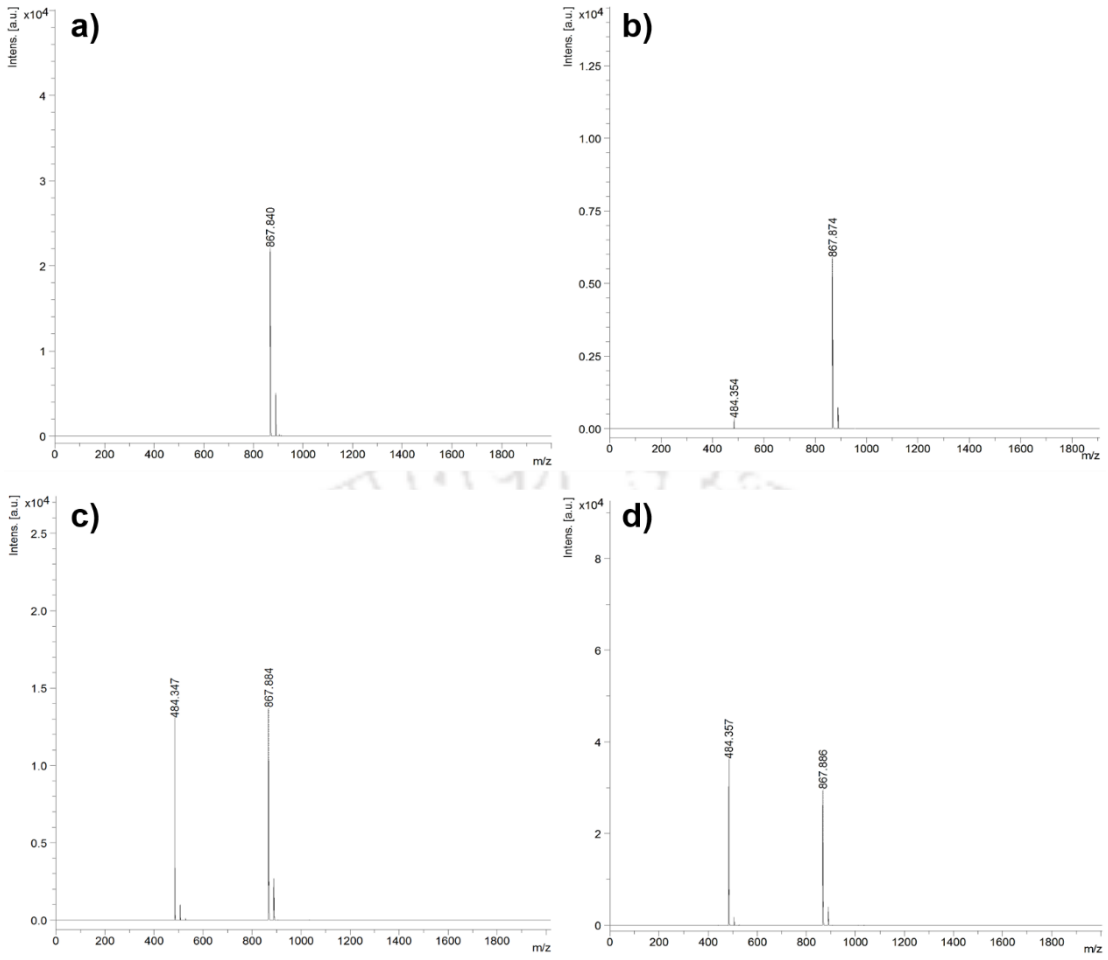

Fig. 4.19 MALDI-TOF mass spectra for studying enzymatic action on P16. a) Untreated P16 Calc. $(M+H)^+$ = 867.6589 Da; Obs. $(M+H)^+$ = 867.840 Da. b) P16 in presence of proteinase K at 1 h. Calc. $(M+H)^+$ = 867.6589 Da; Obs. $(M+H)^+$ = 867.874 Da. m/z 484.357 corresponds to $(M+2H^+)$ of the fragment C_{16}-AR. c) P16 in presence proteinase K at 3 h. Calc. $(M+H)^+$ = 867.6589 Da; Obs. $(M+H)^+$ = 867.884 Da. m/z 484.347 corresponds to $(M+2H^+)$ of the fragment C_{16}-AR. d) P16 in presence of proteinase K at 6 h. Calc. $(M+H)^+$ = 867.6589 Da; Obs. $(M+H)^+$ = 867.886 Da. m/z = 484.357 corresponds to $(M+2H^+)$ of the fragment C_{16}-AR.

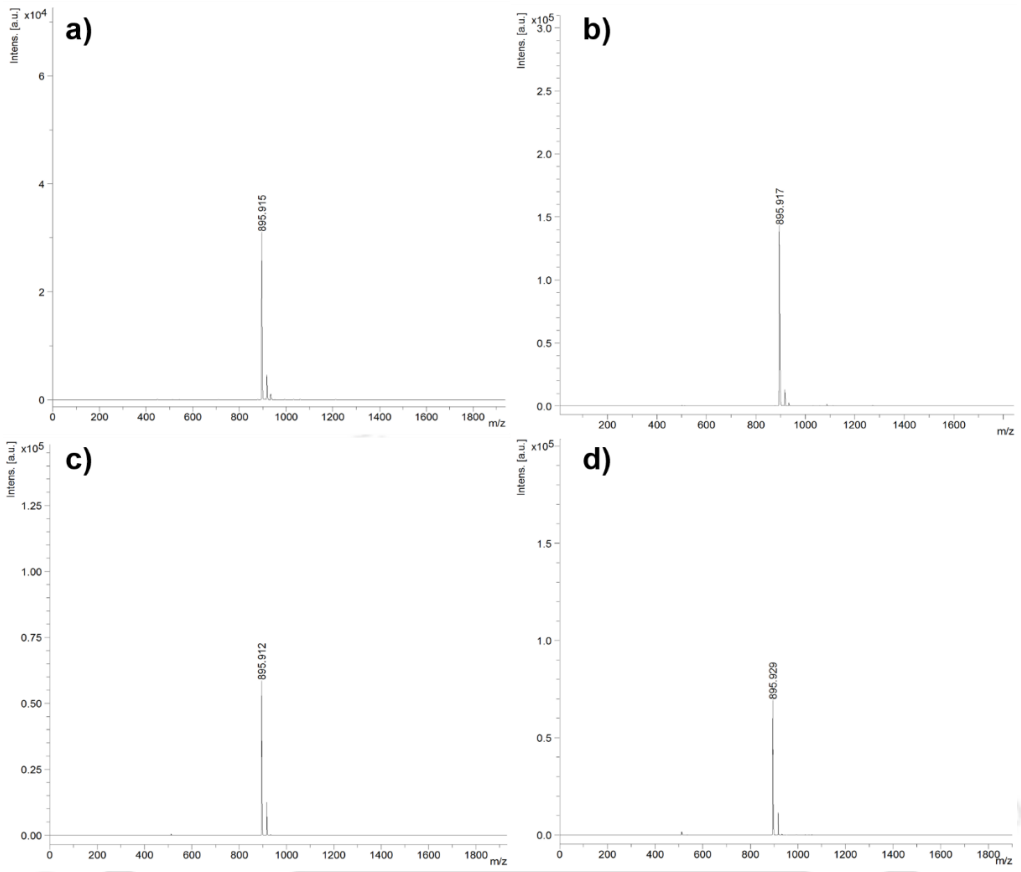

Fig. 4.20. MALDI-TOF mass spectra for studying enzymatic action on P18. a) untreated P18 for enzymatic action study. Calc. $(M+2H)^+$ = 895.6902 Da; Obs. $(M+2H)^+$ = 895.915 Da. b) MALDI-TOF mass spectra of P18 in presence of proteinase K at 1 h. Calc. $(M+2H)^+$ = 895.6902 Da; Obs. $(M+2H)^+$ = 895.917 Da. c) MALDI-TOF mass spectra of P18 in presence of proteinase K at 3 h. Calc. $(M+2H)^+$ = 895.6902 Da; Obs. $(M+2H)^+$ = 895.912 Da. d) MALDI-TOF mass spectra of P18 in presence of proteinase K at 6 h. Calc. $(M+2H)^+$ = 895.6902 Da; Obs. $(M+2H)^+$ = 895.929 Da.

The above-mentioned results conclusively proved better resistance of P18 towards enzymatic degradation, than P16, which might be related to the difference in their constituent fatty acyl chain lengths. Thus, the hydrophobic-hydrophilic balance also played a crucial role in conferring protease resistance to the lipopeptides. This made P18 a better choice as an antimicrobial therapeutic peptide than P16.

4.3.17. Mechanism of action

Cationic AMPs are generally known to be membrane-active molecules manifesting their activity through membrane lysis.[3] In order to visualize the effect of cationic AMPs P16 and P18 on the membrane integrity and morphology of live *P. aeruginosa* cells, we performed FESEM. Live cells were incubated with P18 at its 1× and 2× MIC concentrations. While the

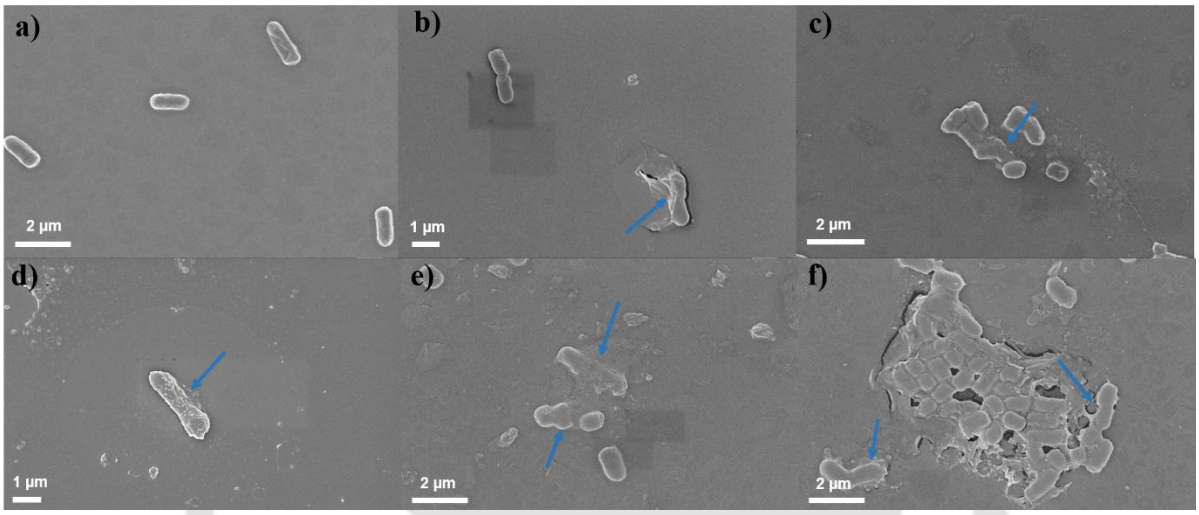

Fig. 4.21. Field Emission Scanning Electron Microscopic (FESEM) images of *P. aeruginosa* cells in the absence and presence of P16 and P18. a) Negative control and d) positive control in presence of Polymyxin B. Considerable deformation in cellular morphology was observed upon incubation of cells with (b, e) 1X MIC and (c, f) 2X MIC of P16 and P18, respectively.

Cells treated with Triton X (positive control) for 4 h showed complete disruption of the cellular morphology and the presence of cell debris, untreated cells retained their healthy morphology with a smooth outer membrane (Fig. 4.21 d and a). Upon addition of 1× and 2× MIC concentrations of P16 and P18 to the *P. aeruginosa* cells, cellular morphology was severely deformed, accompanied by the disruption of the cell membrane[46] (Fig. 4.21 b, c, e, and f). This conclusively proved that P16 and P18 had membranolytic mode of action.

4.4. Conclusions

We have designed a library of lipopeptides varying in their hydrophobic-hydrophilic balance in a quest to develop antimicrobial peptides with enhanced therapeutic potentials. On the one

hand, we have established that important properties of the peptides such as secondary structure, self-assembly (morphology, kinetics, stability), antimicrobial properties (potency, killing kinetics, salt tolerance of the antimicrobial activity) and protease resistance depend on their hydrophobic-hydrophilic balance, while on the other hand, we have developed an extremely potent, non-cytotoxic, salt-tolerant and protease-resistant AMP P18, against ESKAPE pathogens such as *P. aeruginosa*, *K. pneumonia*, *S. aureus* and MRSA. Our study established the fact that the properties of peptides might be tuned to suit any desired function, by controlling the hydrophobic-hydrophilic balance. This fundamental know-how might be exploited for the directed design of custom-made functional peptides in the future.

However, despite the excellent outcomes of our designed lipopeptide P18, in vivo studies are essential for real-world applicability. Additionally, some other factors need to be explored, such as the stability of peptides in the presence of other proteolytic enzymes, their activity against various bacterial as well as fungal strains, including clinically isolated variants, and long-term resistance development studies. Our long-term goal will be to conduct animal model studies and work on the scalability of P18 for its industrial translation.

4.5. References

1. Hawkey, P. M. The growing burden of antimicrobial resistance. *J. Antimicrob. Chemother*. **2008**, *62*, i1–i9.

2. Mahlapuu, M.; Håkansson, J.; Ringstad, L.; Björn, C. Antimicrobial peptides: an emerging category of therapeutic agents. *Front. Cell. Infect. Microbiol.* **2016**, *6*, DOI: 10.3389/fcimb.2016.00194.

3. Sarkar, T.; Chetia, M.; Chatterjee, S. Antimicrobial peptides and proteins: from nature's reservoir to the laboratory and beyond. *Front. Chem.* **2021**, *9*, DOI: 10.3389/fchem.2021.691532.

4. Wang, J.; Song, J.; Yang, Z.; He, S.; Yang, Y.; Feng, X.; Dou, X.; Shan, A. Antimicrobial peptides with high proteolytic resistance for combating Gram-negative bacteria. *J. Med. Chem.* **2019**, *62*, 2286-2304.

5. Yu, H. Y.; Tu, C. H.; Yip, B. S.; Chen, H. L.; Cheng, H. T.; Huang, K. C.; Lo, H. J.; Cheng, J. W. Easy strategy to increase salt resistance of antimicrobial peptides. *Antimicrob. Agents Chemother.* **2011**, *55*, 4918-4921.

6. Li, J.; Koh, J.-J.; Liu, S.; Lakshminarayanan, R.; Verma, C. S.; Beuerman, R. W. Membrane active antimicrobial peptides: translating mechanistic insights to design. *Front. Neurosci*. **2017**, *11*, 73.

7. Huan, Y.; Kong, Q.; Mou, H.; Yi, H. Antimicrobial peptides: classification, design, application and research progress in multiple fields. *Front. Microbiol*. **2020**, *11*, 582779.

8. Han, Y.; Zhang, M.; Lai, R.; Zhang, Z. Chemical modifications to increase the therapeutic potential of antimicrobial peptides. *Peptides* **2021**, *146*,170666.

9. Saravanan, R.; Li, X.; Lim, K.; Mohanram, H.; Peng, L.; Mishra, B.; Basu, A. Lee, J.-M.; Bhattacharjya, S.; Leong, S. S. J. Design of short membrane selective antimicrobial peptides

containing tryptophan and arginine residues for improved activity, salt-resistance, and biocompatibility. *Biotechnol. Bioeng.* **2014**, *111*, 37-49.

10. Rounds, T.; Straus, S. K. Lipidation of antimicrobial peptides as a design strategy for future alternatives to antibiotics. *Int. J. Mol. Sci.* **2020**, *21*, 9692.

11. Laverty, G.; McLaughlin, M.; Shaw, C.; Gorman, S. P.; Gilmore, B. F. Antimicrobial activity of short, synthetic cationic lipopeptides. *Chem. Biol. Drug Des.* **2010**, *75*, 563-569.

12. Pokorny, A.; Almeida, P. F. The antibiotic peptide daptomycin functions by reorganizing the membrane. *J. Membr. Biol.* **2021**, *254*, 97-108.

13. Trimble, M. J.; Mlynárčik, P.; Kolář, M.; Hancock, R. E. W. Polymyxin: alternative mechanisms of action and resistance. *Cold Spring Horbor Perspect. Med.* **2016**, *6*, a025288.

14. Li, J.; Nation, R. L.; Milne, R. W.; Turnidge, J. D.; Coulthard, K. Evaluation of colistin as an agent against multi-resistant Gram-negative bacteria. *Int. J. Antimicrob. Agents* **2005**, *25*, 11-25.

15. Toniolo, C.; Crisma, M.; Formaggio, F.; Peggion, C.; Epand, R. F.; Epand, R. M. Lipopeptaibols, a novel family of membrane active, antimicrobial peptides. *Cell. Mol. Life Sci.* **2001**, *58*, 1179-1188.

16. Wiman, E.; Zattarin, E.; Aili, D.; Bengtsson, T.; Selegård, R.; Khalaf, H.; Development of novel broad-spectrum antimicrobial lipopeptides derived from plantaricin NC8 β. *Sci. Rep.* **2023**, *13*, 4104.

17. Armas, S. Pacor, Ferrari, E.; Guida, F.; Pertinhez, T. A.; Romani, A. A.; Scocchi, M.; Benincasa, M. Design, antimicrobial activity and mechanism of action of Arg-rich ultra-short cationic lipopeptides. *PLoS One* **2019**, *14*, e0212447.

18. Makovitzki, A.; Avrahami, D.; Shai, Y. Ultrashort antibacterial and antifungal lipopeptides. *Proc. Natl. Acad. Sci. U.S.A.* **2006**, *103*, 15997-16002.

19. Mangoni, M. L.; Shai, Y. Short native antimicrobial peptides and engineered ultrashort lipopeptides: similarities and differences in cell specificities and modes of action. *Cell. Mol. Life Sci.* **2011**, *68*, 2267-2280.

20. Rounds, T.; Straus, S. K. Lipidation of antimicrobial peptides as a design strategy for future alternatives to antibiotics. *Int. J. Mol. Sci.* **2020**, *21*, 9692.

21. Mak, P.; Pohl, J.; Dubin, A.; Reed, M. S.; Bowers, S. E.; Fallon, M. T.; Shafer, W. M. The increased bactericidal activity of a fatty acid-modified synthetic antimicrobial peptide of human cathepsin G correlates with its enhanced capacity to interact with model membranes. *Int. J. Antimicrob. Agents* **2003**, *21*, 13-19.

22. Liu, K.; Yang, L.; Peng, X.; Wang, J.; Lu, J. R.; Xu, H. Modulation of Antimicrobial Peptide Conformation and Aggregation by Terminal Lipidation and Surfactants. *Langmuir* **2020**, *36*, 1737-1744.

23. Chionis, K.; Krikorian, D.; Koukkou, A. I.; Sakarellos-Daitsiotis, M.; Panou-Pomonis, E. Synthesis and biological activity of lipophilic analogs of the cationic antimicrobial active peptide anoplin. *J. Pept. Sci.* **2016**, *22*, 731-736.

24. Guo, L.; Wang, C.; Broos. J.; Kuipers, O. P. Lipidated variants of the antimicrobial peptide nisin produced via incorporation of methionine analogs for click chemistry show improved bioactivity. *J. Biol. Chem.* **2023**, *299*, 104845.

25. Forns, P.; Lauer-Fields, J. L.; Gao, S.; Fields, G. B. Induction of protein-like molecular architecture by monoalkyl hydrocarbon chains. *Biopolymers* **2000**, *54*, 531-546.

26. Dehsorkhi, A.; Castelletto, V.; Hamley, I. W. Self-assembling amphiphilic peptides. *J. Pept. Sci.* **2014**, *20*, 453-467.

27. Tsutsumi, N.; Ito, A.; Ishigamori, A.; Ikeda, M.; Izumi, M.; Ochi, R. Synthesis and self-assembly properties of bola-amphiphilic glycosylated lipopeptide-type supramolecular

hydrogels showing colour changes along with gel-sol transition. *Int. J. Mol, Sci.* **2021**, *22*, 1860.

28. Hollmann, A.; Martínez, M.; Noguera, M. E.; Augusto, M. T.; Disalvo, A.; Santos, N. C.; Semorile, L.; Maffía, P. C. Role of amphipathicity and hydrophobicity in the balance between hemolysis and peptide-membrane interactions of three related antimicrobial peptides. *Coloids Surf, B* **2016**, *141*, 528-536.

29. Ihsan, A. B.; Nargis, M.; Koyama, Y. Effects of the hydrophilic-lipophilic balance of alternating peptides on self-assembly and thermo-responsive behaviors. *Int. J. Mol. Sci.* **2019**, *20*, 4604.

30. Zhao, H.; Mattila, J. P.; Holopainen, J. M.; Kinnunen, K. J. Comparison of the membrane association of two antimicrobial peptides, magainin 2 and indolicidin. *Biophys. J.* **2001**, *81*, 2979-2991.

31. Matsuzaki, K.; Murase, O.; Fujji, N.; Miyajima, K. Translocation of a channel-forming antimicrobial peptide, magainin 2, across lipid bilayers by forming a pore. *Biochemistry* **1995**, *34*, 6521-6526.

32. Lv, S.; Wang, J.; You, R.; Liu, S.; Ding, Y.; Hadianamrei, R.; Tomeh, M. A.; Pan, F.; Cai, Z.; Zhao, X. Highly selective performance of rationally designed antimicrobial peptides based on ponericin-W1. *Biomater. Sci.* **2022**, *10*, 4848.

33. Roy, K.; Pandit, G.; Chetia, M.; Sarkar, A. K.; Chowdhuri, S.; Bidkar, A. P.; Chatterjee, S. Peptide hydrogels as platforms for sustained release of antimicrobial and antitumor drugs and proteins. *ACS Appl. Bio Mater.* **2020**, *3*, 6251-6262.

34. Pandit, G.; Chowdhury, N.; Mohid, S. A.; Bidkar, A. P.; Bhunia, A.; Chatterjee, S. Effect of secondary structure and side chain length of hydrophobic amino acid residues on the antimicrobial activity and toxicity of 14-residue-long de novo AMPs. *Chem. Med. Chem* **2020**, *16*, 355-367.

35. Roy, K.; Chetia, M.; Sarkar, A. K.; Chatterjee, S.; Co-assembly of charge complementary peptides and their applications as organic dye/heavy metal ion (Pb^{2+}, Hg^{2+}) absorbents and arsenic(iii/v) detectors. *RSC Adv.* **2020**, *10*, 42062-42075.

36. a) Pandit, G.; Sarkar, T.; Vignesh, S. R.; Debnath, S.; Satpati, P.; Chatterjee, S. Delineating the mechanism of action of a protease resistant and salt tolerant synthetic antimicrobial peptide against *Pseudomonas aeruginosa*. *ACS Omega* **2022**, *7*, 15951-15968. b) Thappeta, K. R. V.; Vikhe, Y. S.; Yong, A. M. H.; Chan-Park, M. B.; Kline, K. A. Combined efficacy of an antimicrobial cationic peptide polymer with conventional antibiotics to combat multidrug-resistant pathogens. *ACS Infect. Dis.* **2020**, *6*, 1228−1237.

c) Bhattacharjee, B.; Das, A.; Das, G.; and Ramesh, A. Urea-based ligand as an efflux pump inhibitor: warhead to counter ciprofloxacin resistance and inhibit collagen adhesion by MRSA. *ACS Appl. Bio Mater*. **2022**, *5*, 1710−1720.

37. Bruni, N.; Capucchio, M. T.; Biasibetti, E.; Pessione, E.; Cirrincione, S.; Giraudo, L.; Corona, A.; Dosio, F. Antimicrobial activity of lactoferrin-related peptides and applications in human and veterinary medicine. *Molecules* **2016**, *21*, 752.

38. Farnaud, S.; Evans, R. W. Lactoferrin-a multifunctional protein with antimicrobial properties. *Mol. Immunol.* **2003**, *4*0, 395-405.

39. a) Adak, A.; Ghosh, Gupta, V.; Ghosh, S. Biocompatible lipopeptide-based antibacterial hydrogel. *Biomacromolecules* **2019**, *20*, 1889–1898.

b) Cobb, J. S.; Zai-Rose, V.; Correia, J. J. and Janorkar, A. V. FT-IR spectroscopic analysis of the secondary structures present during the desiccation induced aggregation of elastin-like polypeptide on silica. *ACS Omega* **2020**, *5*, 8403−8413.

c) Sanii, B.; Martinez-Avila, O.; Simpliciano, C.; Zuckermann, R. N.; and Habelitz. S. Matching 4.7-Å XRD spacing in amelogenin nanoribbons and enamel matrix. *J Dent Res.* **2014**, *93*, 918-922.

d) Toniolo, C.; Polese, A.; Formaggio, F.; Crisma, M.; Kamphuis, J. Circular Dichroism Spectrum of a Peptide 3_{10}-Helix. *J. Am. Chem. Soc.***1996**, *118*, 2744−2745.

e) Greenfield, N. J.; Fasman, G. D. Computed circular dichroism spectra for the evaluation of protein conformation. *Biochemistry* **1969**, 8, 4108−4116.

f) Yang, J. J.; Pitkeathly, M.; and Radford, S. E. Far-UV Circular dichroism reveals a conformational switch in a peptide fragment from the /3-sheet of hen lysozyme1. *Biochemistry* **1994**, *33*, 7345-7353.

g) Hamley, I. W.; Dehsorkhi, A.; Castelletto, V.; Seitsonen, J.; Ruokolainen, J.; and Iatrou, H. Self-assembly of a model amphiphilic oligopeptide incorporating an arginine head group. *Soft Matter* **2013**, *9*, 4794–4801.

40. Pandit, G.; Ilyas, H.; Ghosh, S.; Bidkar, A. P.; Mohid, S. A.; Bhunia, A.; Satpati, P.; Chatterjee, S. Insights into the mechanism of antimicrobial activity of seven-residue peptides. *J. Med. Chem.* **2018**, *61*, 7614-7629.

41. B. H. Gan, J. Gaynord, S. M. Rowe, T. Deingruber and D. R. Spring, The multifaceted nature of antimicrobial peptides: current synthetic chemistry approaches and future directions. *Chem. Soc. Rev.* 2021, **50**, 7820-7880.

42. Kamysz, E.; Sikorska, E.; Ja´skiewicz, M.; Bauer, M.; Neubauer, D.; Bartoszewska, S.; Baranska-Rybak, W.; Kamysz, W. Lipidated analogs of the ll-37-derived peptide fragment kr12-structural analysis, surface-active properties and antimicrobial activity. *Int. J. Mol. Sci*. **2020**, *21*, 887.

43. Armas, F.; Stasi, A. D.; Mardirossian, M.; Romani, A. A.; Benincasa, M.; Scocchi, M. Effects of lipidation on a proline-rich antibacterial peptide. *Int. J. Mol. Sci*. **2021**, *22*, 7959.

44. Lin, B.; Hung, A.; Singleton, W.; Darmawan, K. K.; Moses, R.; Yao, B.; Wu, H.; Barlow, A.; Sani, M.-A.; Sloan, A. J.; Hossain, M. A.; Wade, J. D.; Hong, Y.; O'Brien-Simpson, N.

M.; Li, W. The effect of tailing lipidation on the bioactivity of antimicrobial peptides and their aggregation tendency. *Aggregate*. **2023**, *4*, e329.

45. a) Zhang, P.; Jian, C.; Jian, S.; Zhang, Q.; Sun, X.; Nie, L.; Liu, B.; Li, F.; Li, J.; M. Liu, M.; Liang, S.; Zeng, Y.; Liu, Z. Position effect of fatty acid modification on the cytotoxicity and antimetastasis potential of the cytotoxic peptide lycosin-I. *J. Med. Chem.* **2019**, *62*, 11108-11118.

b) Ingvill Pedersen Sæbø, I. P.; Magnar Bjørås, M.; Henrik Franzyk, H.; Helgesen, E.; Booth, J. A. Optimization of the hemolysis assay for the assessment of cytotoxicity. *Int. J. Mol. Sci.* **2023**, *24*, 2914.

c) Salehi, N.; Moosavi-Movahedi, A.A.; Fotouhi, L.; Yousefinejad, S.; Shourian, M.; Hosseinzadeh, R.; Sheibani, N.; Habibi-Rezaei, M. Hemedegradation upon production of endogenous hydrogen peroxide via interaction of hemoglobin with sodium dodecyl sulfate. *J. Photochem. Photobiol. B Biol.* **2014**, *133*, 11–17.

d) Chen, Z.; Duan, H.; Tong, X.; Hsu, P.; Han, L.; Morris-Natschke, S.L.; Yang, S.; Liu, W.; Lee, K.-H. Cytotoxicity, hemolytic toxicity, and mechanism of action of pulsatilla saponin d and its synthetic derivatives. *J. Nat. Prod*. **2018**, *81*, 465–474.

e) Paarvanova, B.; Tacheva, B.; Savova, G.; Karabaliev, M.; Georgieva, R. Haemolysis by saponin is accelerated at hypertonic conditions. *Molecules* **2023**, *28*, 7096.

f) Masafumi Koga, M.; Toshika Okumiya, T.; Midori Ishibashi, M. Sample transport and/or storage can cause falsely low HbA1c levels in blood cells measured by enzymatic assay. *Diabetol. Int.* **2020**, *11*, 155-157.

46. a) Dosunmu, E.; Chaudhari. A. A.; R Singh, S. R.; Dennis, V. A.; Pillai, S. R. Silver-coated carbon nanotubes downregulate the expression of *Pseudomonas aeruginosa* virulence genes: a potential mechanism for their antimicrobial effect. *Int. J. Nanomedicine* **2015**, *10*, 5025–5034.

b) Otis, G.; Bhattacharya, S.; Malka, O.; Kolusheva, S.; Bolel, P.; Porgador, A.; Jelinek, R. Selective labeling and growth inhibition of *Pseudomonas aeruginosa* by amino guanidine carbon dots. *ACS Infect. Dis.* **2019**, *5*, 292–302.

Chapter 5

Combinatorial Hydrogels from Antimicrobial Peptide P18 and Ciprofloxacin for Inhibition of MRSA Biofilms

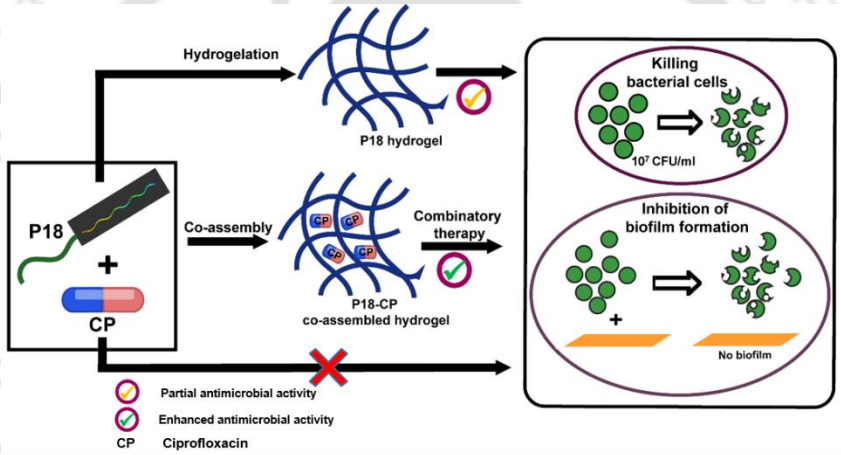

5.1. Introduction

The emergence of antimicrobial resistance has obstructed treatments offered by several therapeutic antibiotics against bacterial infections, entailing severe threats to human society.[1] Most conventional antibiotics work on the intracellular targets of the bacterial pathogens, which can be modified over time by the bacteria themselves through spontaneous mutation.[2-3] Such target modifications are one of the leading causes of microbial resistance. This has been further fuelled by overuse, clinical misuse, poor quality, and ease of availability of antibiotics.[4] *Staphylococcus aureus* is a Gram-positive bacteria, linked to a plethora of clinical infections such as endocarditis, blood-stream infections, pulmonary infections like pneumonia, bone and joint infections, skin and soft-tissue infections, and device-related infections.[5-6] Rapid increase in the development of antibiotic resistance in this microbe has seen the rise of the Methicilin-resistant *Staphylococcus aureus* (MRSA) in epidemic proportions, resulting in a high rate of morbidity and mortality.[7-9a] Also, the development of resistance in MRSA involves various mechanisms including production of penicillin binding protein, PBP 2, an enzyme that has low affinity for beta-lactam antibiotics or efflux pumps that antibiotics out of the bacterial cell.[9b] It has emerged as one of the unavoidable causes for both community and hospital-acquired infections, mostly connected with soft tissue infections and osteomyelitis.[10-11] Moreover, the development of inflammatory injuries due to immune response against MRSA infections, results in the tissue necrosis and slow healing rates.[12-13] Studies revealed that MRSA can survive on dry surfaces for months.[14] Besides, their ability to form biofilm has further exacerbated the microbial infection-related complications.[15-16] A biofilm is an assemblage of bacterial communities that affix to a living or non-living surface, including living tissues, indwelling medical devices, industrial or potable water system piping, or natural aquatic systems in which the cells are covered by a protective matrix comprising of extra-cellular polymeric substance (EPS) and other macro molecules like DNA, proteins, and

polysaccharides.[17-20] The matrix not only protects the bacterial cells from the host-immune response but also make them less susceptible to antibiotics.[21-23] MRSA is also known to develop resistance against a number of known antibiotics, including all available penicillins and most of the β-lactam drugs.[1, 24] Thus, there is a pressing need to develop new classes of therapeutic molecules to deal with the situation. Among many others,[25-27] antimicrobial peptides (AMP) have been found to be one of the most promising choices in the race for antimicrobial agents against both Gram-positive and Gram-negative bacteria as well as fungi.[28-29] Delayed resistance development and low immunogenicity make AMPs potential alternate therapeutics.[30-32] Synthetic approaches have led to the development of salt-resistant and protease-stable AMPs with better therapeutic potentials.[33] AMPs are capable of not only combating the planktonic microbes, but also mitigating their biofilms.[34-35] AMPs also act as adjuvants in restoring the lost activity of several antibiotics against the resistant microbial strains,[36] in the combination therapy. AMPs, in combination with the conventional antibiotics are known to inhibit the MRSA biofilms.[37] Some AMPs can form supramolecular hydrogels, through various non-covalent interactions, and retain their antimicrobial activity.[38-39] Biocompatibility, responsiveness, and controllability are the attributes that make antimicrobial hydrogels unique and prominent biomaterials. Interestingly, antimicrobial hydrogels loaded with antibiotics or other molecules, possessing a precise and controllable release of either of the components, have been found to be more effective due to synergistic effects.[40-42]

5.2. Experimental section

5.2.1. Materials procured

Materials Procured: Rink Amide MBHA resin (loading 0.7 mmol/g), all fluorenylmethyloxycarbonyl (Fmoc)-protected amino acids, hydroxybenzotriazole (HOBt), and benzotriazole-1-yl-oxy-tris-pyrrolidino-phosphonium hexafluorophosphate (PyBOP) were purchased from G.L. Biochem. Piperidine, *N, N′* diisopropylethylamine (DIPEA), diethyl ether

and pyridine were purchased from Merck. HPLC-grade acetonitrile and dimethylformamide (DMF), dichloromethane (DCM) were obtained from Finar. Acetic anhydride was provided by the Department of Chemistry, IIT Guwahati. ciprofloxacin, vancomyacin and BHI media were obtained from HiMedia. Crystal violet was purchased from spectrochem.

Bacterial strains: Common laboratory strains of *P. aeruginosa* (ATCC 27853) was obtained either from the American Type Tissue Culture Collection or the Microbial Type Tissue Culture Collection. MRSA strain was provided by Prof. Benu Dhawan, AIIMS, New Delhi and Prof. Kasturi Mukhopadhyay, JNU, New Delhi.

5.2.2. Synthesis and purification

P18 peptide was synthesized using a standard solid-phase peptide synthesis protocol with Fmoc Chemistry on rink amide MBHA resin (0.1 mM scale). Purification and characterization were carried out following the protocol described earlier (see section **4.2.2** of chapter 4).

5.2.3. Formation of co-assembled hydrogel(s)

1 mg of P18 peptide was taken in (0.2% w/v, 2.23 mM) phosphate buffer saline (PBS) (pH=7.4), CP was added to the solution, and the final volume was made up to 500 µl. The solution was then kept undisturbed overnight at room temperature (RT). This resulted in the formation of hydrogel, which was stable to the inversion of the glass vial. Co-assembled hydrogels with different compositions of CP were prepared by varying the concentrations of CP in P18 solutions of PBS 7.4 (1mg/500 µl, 2.23 mM).

5.2.4. Field emission scanning electron microscopy (FESEM)

To capture the FESEM image of P18-CP(50) hydrogel, a drop of the solution of CP (50 µM) and peptide at its CGC concentration (1 mg/500 µl) in 10 mM PBS (7.4) buffer, was cast on a silicon wafer immediately after making solution. Hydrogel formed on the wafer was dried under vacuum before imaging.

Samples for bacterial cell imaging were made by using the protocol described earlier (Chapter 4). All the samples were next air-dried, followed by gold coating and subsequently observed under the FESEM (Zeiss, Model: Gemini).

5.2.5. Rheology

To investigate the viscoelastic properties of the co-assembled P18-CP(50) hydrogel, rheological experiments were performed using the methods reported in section **4.2.6** of chapter 4.

5.2.6. Drug release study

The CP release efficiency of the co-assembled P18-CP(50) hydrogel was studied by monitoring the UV absorbance of the release medium at 272 nm. 500 µl of PBS solution (as a release medium) was added to the preformed co-assembled hydrogel. The absorbance of the supernatant solution was measured at different time intervals up to 96 h. The concentration of the drug released was determined from a standard curve (Appendix, Fig. A5.1) obtained from the known concentrations of CP alone in PBS. CP release was studied by the same strategy for all the different composition hydrogels. The amount of drug released from the co-assembled hydrogels was calculated from the below-mentioned formula

release (%) = (released concentration/ loaded concentration) ×100

5.2.7. Antimicrobial activity of P18 hydrogel/CP co-assembled gels against MRSA

The mid-log-phase cultures of MRSA were obtained from overnight-grown cultures. The cell suspensions were centrifuged at 6000 rpm for 6 min. Cell pellets were washed thrice with 10 mM phosphate buffer (pH 7.4). Thereafter, the cell pellets were re-suspended in the same buffers to obtain a cell suspension of 10^6 CFU/ml. The reaction was performed in a 96-well plate, where 50 µl of the cell suspension was incubated with several doses of P18 hydrogel/co-assembled hydrogel. The final cell count was maintained at 10^5 CFU/ml. The reaction was

incubated at 310 K for 4 h. A negative control containing only cell suspension and a positive control containing 10 µM Vancomycin with cell suspensions were maintained. Next, a sufficient volume of BHI medium was added to each well to make a final volume of 200 µl, and the reaction was incubated overnight with constant shaking at 310 K temperature. The absorbance of the culture was monitored at 630 nm to monitor microbial growth. The well where bacterial growth was inhibited served as MIC of hydrogel. For determining the activity of P18 hydrogel against a high number of cell counts, the same protocol was used by maintaining final cell counts of 10^6 CFU/ml and 10^7 CFU/ml.

The MIC experiment was performed in two ways. The 5 µL of the gel that was used for accessing the activity was either formed at a different place and injected into the 96 well plate with a micropipette or the gel was casted in the 96 well plate itself.[43 a, b, c] Appendix, Fig. A5.2 shows that the antimicrobial activity of the gel is independent of the way in which the gel is taken for the experiment.

5.2.8. MRSA biofilm inhibition by P18 Hydrogel / CP Co-assembled gels

The biofilm formation assay was performed as described for the MIC assay with some alterations.[43 d, e] Plates containing hydrogels (preformed) and bacteria were incubated for 48 h at 37 °C without agitation, to allow biofilm formation. Unattached bacteria were then washed from plates, and the plates stained with 0.1% CV. This was followed by absorbance measurements at OD590 using a microplate auto reader. Data are presented as a percentage of the biofilm biomass compared to biofilm formed by untreated bacteria.

5.2.9. Cell viability assay

In order to study the bio-compatibility of our hydrogel, co-assembled hydrogels, we performed an MTT assay. Briefly, HT22 and KB cells were cultured in DMEM media supplemented with 10% fetal bovine serum (FBS) and 1% penicillin-streptomycin antibiotic in a humidified

atmosphere (37°C) and 5% CO_2. Next, cells were sub-cultured in 24 well cell culture plates overnight. The next day, samples were treated to the cells and were incubated for 24 h. Next, cells were washed with fresh PBS buffer, followed by the addition of fresh DMEM. Finally, cell viability was observed using an MTT assay. Formation of violet-coloured formazan crystal was observed. These crystals were dissolved in SDS solution (1:1 water-DMF). The absorbance of the solutions was taken at 570 nm. Cells without any sample treatment were considered to be 100% viable.[43 f]

5.2.10. Time kill kinetics of the hydrogels

MRSA cells at 10^5 CFU/ml were incubated with P18 and P18-CP(50) hydrogels at their MIC in a 96-well plate. A 10µl aliquot from the solution was taken at different intervals of time (5 min, 15 min, 45 min, 60 min) and spread on NB agar plates. The plates were left to incubate for 24 h and colony counting was done. Untreated cells and Vancomycin-treated cells were treated as negative and positive controls.

5.2.11. Resistance development

The MIC of P18 and P18-CP(50) hydrogels were determined against 10^5 CFU/ml MRSA cells using the broth dilution method. Ciprofloxacin was used as a control. Bacterial samples from the well at sub-MIC of the hydrogels were withdrawn to make a bacterial dilution for subsequent testing. These bacterial solutions were then transferred to a fresh 96-well plate with new dilutions of the hydrogels and the control. Following an overnight incubation at 37°C, any variation in MIC values was assessed. This cycle was repeated daily for a total of 48 generations (15 days).

5.3. Results and discussion

5.3.1. Antimicrobial activity of P18 hydrogel

In the present work, we have employed a lipopeptide hydrogel (P18 hydrogel, Fig. 5.1) and its ciprofloxacin (CP) co-assembled analog (P18-CP hydrogel) in the inhibition of planktonic MRSA and MRSA biofilms.

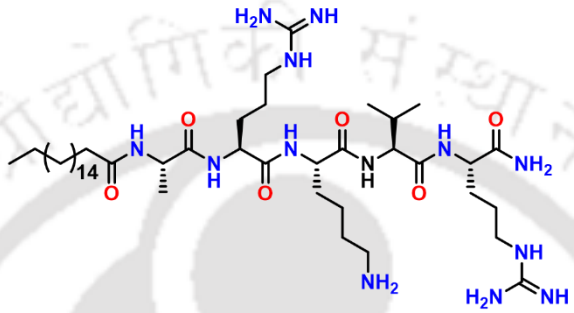

Fig. 5.1. Chemical structure of the hydrogelator AMP P18.

In the previous study from our group (Chapter 4), we reported a cationic non-cytotoxic and protease stable lipopeptide P18, that possessed high salt-tolerant antimicrobial activity against several ESKAPE pathogens (Gram-negative bacteria *P. aeruginosa*, *K. pneumoniae* and Gram-positive bacteria *S. aureus*, Methicillin-resistant *S. aureus* (MRSA), along with the ability to self-assemble and form the hydrogel. The ability of P18 to form gel at pH 7.4, in addition to its excellent antimicrobial potency, tempted us to test the antimicrobial potency of the P18 hydrogel.

As seen from Fig. 5.2 a, P18 hydrogel (5 µl, 0.2 % wt/vol) retained almost 95% of P18's (in solution) activity against 10^5 cells of MRSA and *P. aeruginosa*, respectively. Since, P18 hydrogel was very effective against MRSA; thus, we decided to continue our further studies with P18 hydrogel, against MRSA. P18 hydrogel (5 µl, 0.2% wt/vol) retained about 75% and 60% of its activity against a final concentration of 10^6 and 10^7 MRSA cells (Fig. 5.2 b).

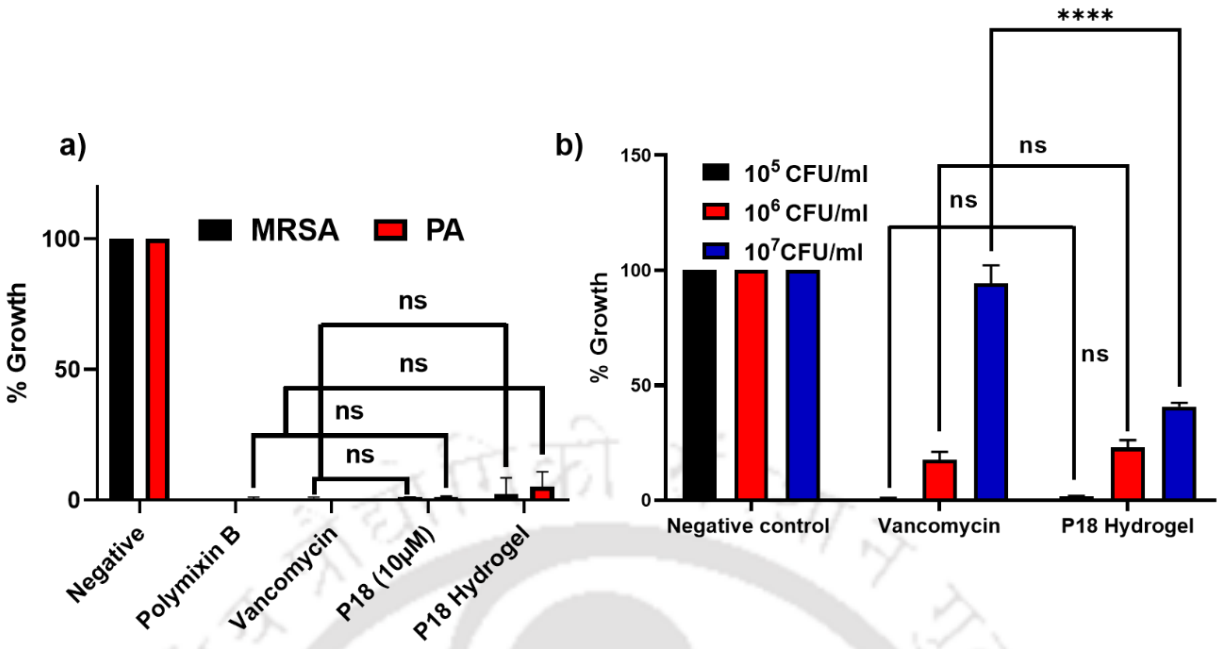

Fig. 5.2. Antimicrobial potency of a) P18 (in solution with 10 μM concentration and as a hydrogel) against Methicillin-resistant *S. aureus* (MRSA; vancomycin as control for MRSA) and *P. aeruginosa* (PA; polymixin B as control for PA); b) P18 hydrogel against different cell counts of MRSA as studied from micro broth dilution assay. The data represents the mean of N=3 experiments (*p< 0.05, **p< 0.01, ***p< 0.001, ****p< 0.0001) via two way analysis of variance (ANOVA) with Sidak's multiple comparison test for plot a) and Turkey's multiple comparision test for plot b).

10 μM vancomycin which was used as a positive control against 10^5 MRSA cells, also lost ~20% of its activity against 10^6 cells and almost complete activity against 10^7 MRSA cells, respectively. Thus, P18 hydrogel was a stronger antimicrobial agent with respect to vancomycin (10 μM) against 10^7 MRSA cells. MRSA has been reported to have developed antimicrobial resistance against several standard antibiotics. There are studies in the literature of combination therapy of antibiotics and AMPs, leading to very efficient potency against the microbes at their respective synergistic combinations.[42] AMPs have also been employed in the potentiation of antibiotics against resistant microbes.[44] We tested the activity of antibiotic CP against the MRSA strain (Fig. 5.3) to find that ~85% of 10^5 cells, ~50% of 10^6 of cells and only 5% of 10^7 cells of MRSA, were killed by 200 μM CP.

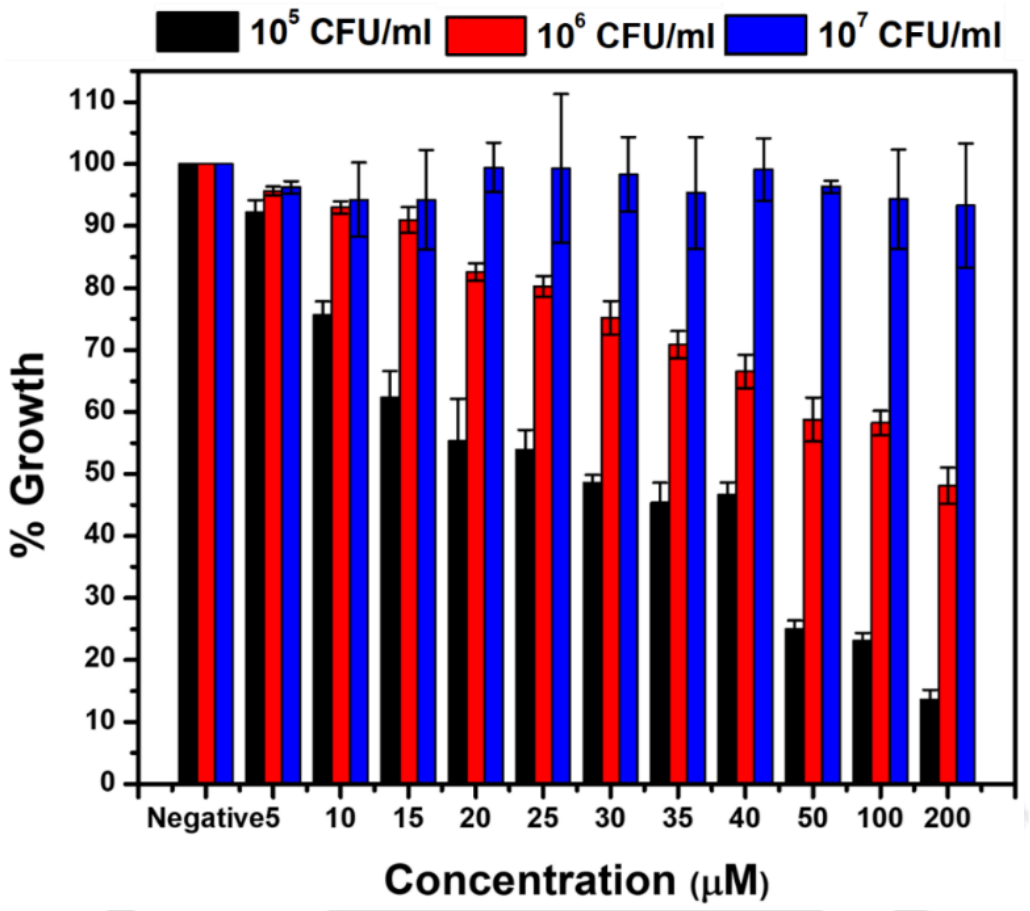

Fig. 5.3. Antimicrobial activity of CP against 10^5, 10^6 and 10^7 no. of MRSA cells.

5.3.2. Formation of co-assembled hydrogel and characterization

With the intention of investigating if the activity of CP against the MRSA could be improved in combination with the P18 hydrogel, we prepared co-assembled hydrogels of CP and P18. 50 μM CP readily formed a translucent hydrogel, P18-CP(50), with P18, as confirmed from the vial inversion test (Fig. 5.4 a and b). FESEM investigations of P18-CP(50) revealed the co-existence of two distinct fibre-like and mesh-like morphologies, suggesting a plausible orthogonal mechanism of co-assembly (Fig. 5.4 c).

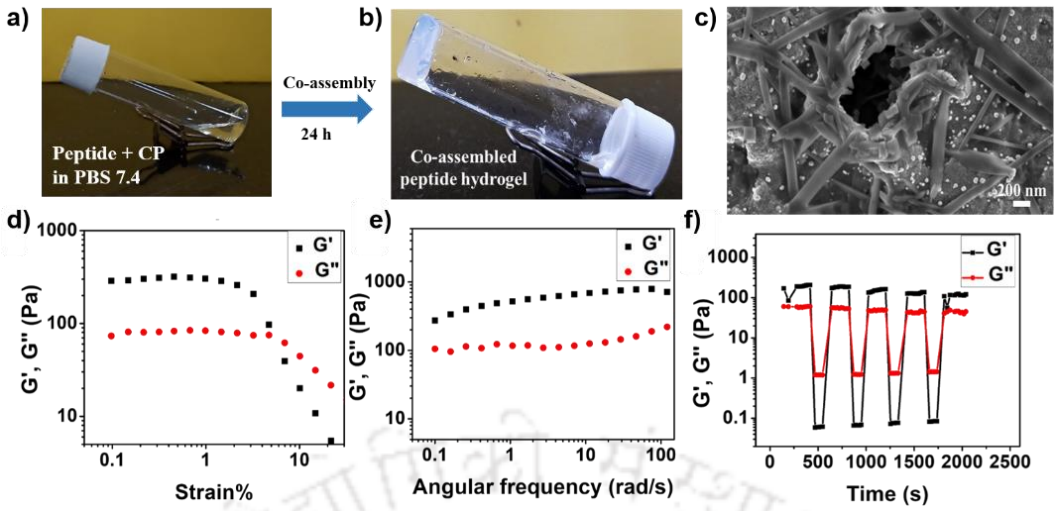

Fig. 5.4. Co-assembled hydrogel P18-CP(50). a), b) Formation and gel inversion test of P18-CP(50). c) Morphological behaviour, d), e) rheological profile as a function of strain and angular frequency and f) step-strain rheological analysis of P18-CP(50).

Viscoelastic properties of the gel were investigated via rheological studies. The co- assembled hydrogel was subjected to an oscillatory frequency sweep and strain dependence experiment. In the strain sweep experiment, G′ was found higher than G″ till a particular strain, beyond which the two crossed each other indicating destabilization of the gel state (Fig. 5.4 d). In an angular frequency sweep experiment, at a constant strain, the G′ was found to be greater than G″ till about 100 rad/s (Fig. 5.4 e), indicating a considerable mechanical strength of co-assembled P18-CP(50) hydrogel. A time-dependent step-strain experiment was performed by varying the applied strains, keeping angular frequency constant at 1 rad/s, to evaluate the thixotropicity of P18-CP(50) hydrogel. Fig. 5.4 f confirmed that P18-CP(50) retained its gel nature at lower strain (γ = 0.1%), where the G′ value was greater than G″, and lost its gel property at higher strain (γ = 100%), where the G″ value was greater than G′. The gel state was restored upon lowering the applied strain. This cyclic interconversion in between the gel and the sol state, in response to the changing strain, established the thixotropicity of P18-CP(50).

5.3.3. Antibiotic release study from the co-assembled hydrogel

The release ability of the antibiotic CP from the co-assembled gel was studied by monitoring the absorbance of the supernatant release medium over time (Fig. 5.5 a). About 80% of CP was released steadily over a span of 72 h from P18-CP(50) hydrogel.

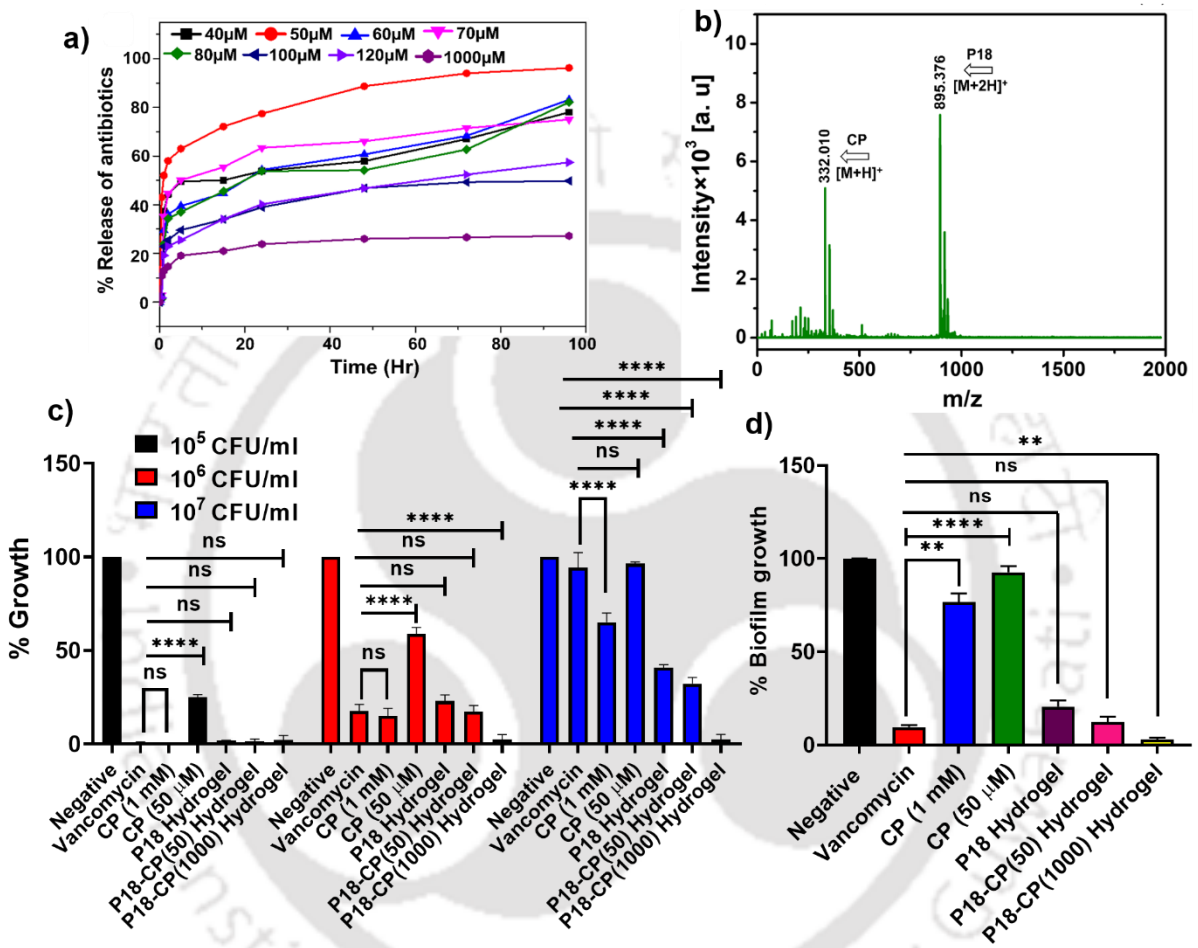

Fig. 5.5. a) Release study of CP from the various co-assembled hydrogels at different time intervals at pH 7.4, b) MALDI-TOF analysis of the release media of co-assembled hydrogel P18-CP(50) for release of CP and AMP P18. Antimicrobial potency of P18 hydrogel and co-assembled hydrogel against Methicillin-resistant *S. aureus* (MRSA); c) Planktonic cells with 10^5, 10^6 and 10^7 no. of MRSA cells; d) Inhibition of biofilm formation. The data represents the mean of N=3 experiments (*p< 0.05, **p< 0.01, ***p< 0.001, ****p< 0.0001) two-way analysis of variance (ANOVA) via Turkey's multiple comparison test for plot c) and Welch analysis of variance (ANOVA) with Brown-Forsyth test for plot d).

To check the loading ability of P18 hydrogel with CP, different concentrations of CP were co-assembled with P18 to generate a host of various compositions of P18-CP hydrogels (Table

5.1). Though CP could be released from all the co-assembled hydrogels, the greatest % efficiency (95%) of release was obtained from the P18-CP(50) hydrogel (Fig. 5.5 a, Table 5.1) over 96 h. The % release efficiency of the antibiotic decreased with the increase of the concentration of the co-assembled antibiotic in the gels. Greatest amount (in wt.) of CP was released from the P18-CP(1000) hydrogel, though the % release of the drug was the most inefficient in this case (Table 5.1). For combination therapy, the release of P18 molecules from the co-assembled hydrogel, was of utmost importance. To investigate if the P18 was also released alongside the antibiotic, we performed a MALDI analysis of the supernatant release media. Fig. 5.5 b shows the MALDI spectra of the release media, which confirmed the presence of both P18 and the antibiotic in it.

Table 5.1. Drug released from co-assembled hydrogels of different composition, at different time intervals (numbers in parentheses in the names of the gels indicate the final concentrations of the CP in μM).

Hydrogels	**P18-CP (40)**	**P18-CP (50)**	**P18-CP (60)**	**P18-CP (70)**	**P18-CP (80)**	**P18-CP (90)**	**P18-CP (120)**	**P18-CP (1000)**
Conc. of CP (μM)	**40**	**50**	**60**	**70**	**80**	**100**	**120**	**1000**
Amount of CP (μg)	**7.7**	**9.62**	**11.55**	**13.47**	**15.4**	**19.25**	**23.1**	**192.5**
% Drug release (96 h)	**79**	**96.2**	**83.1**	**75.0**	**82.1**	**49.8**	**57.4**	**27.2**
Amount of drug released (96 h, μg)	**6.08**	**9.26**	**9.6**	**10.10**	**12.65**	**9.60**	**13.26**	**52.39**

5.3.4. Investigation of antimicrobial potency of co-assemble hydrogels

After having developed the co-assembled hydrogels, we decided to check their antimicrobial activity against 10^5, 10^6 and 10^7 planktonic MRSA cells and their efficiency in the inhibition of MRSA biofilms. We chose to study the activities of two compositions of co-assembled hydrogels: a) the P18-CP(50) with the highest % release of CP and b) the P18-CP(1000) hydrogel with the greatest quantity of CP release. Fig. 5.5 c represents the percentage growth of MRSA cells in the presence of P18 hydrogel and the co-assembled P18 hydrogels. While P18 hydrogel and both the co-assembled P18-CP hydrogels were capable of substantially preventing the growth of 10^5 MRSA cells, activity of the co-assembled gels were clearly better than the P18 hydrogel against greater number of cells (10^6 and 10^7). Thus, while P18 hydrogel prevented ~ 80% and 60% of cell growth for 10^6 and 10^7 cells, P18-CP(50) prevented ~85% and 75% of cell growth and P18-CP(1000) hydrogels prevented >95% of cell growth for both 10^6 and 10^7 MRSA cells. 50 μM CP prevented 75%, 40% and 5% cell growth and 1 mM CP prevented >95%, ~82% and ~35% cell growth for 10^5, 10^6 and 10^7 cells, respectively. Thus, the improved activity of the co-assembled hydrogel might be attributed to the combination effect of AMP P18 and antibiotic CP. As mentioned earlier, inhibition of biofilms of MRSA is far more challenging than the prevention of the planktonic cells. P18 hydrogel inhibited biofilm growth by 80%, while P18-CP(50) and P18-CP(1000) inhibited biofilm growth to a greater extent of ~88% and ~99%, respectively (Fig. 5.5 d). 50 μM CP and 1mM CP inhibited only ~6-8% and 20% of MRSA biofilms, respectively. Thus, the enhanced activity of the co-assembled gels could only be accounted for by the combination effect of the AMP and CP.

5.3.5. Cytotoxicity

To utilize P18 hydrogel and co-assembled hydrogels for therapeutic purposes, it was important for them to be non-cytotoxic in nature. To investigate this, we performed an MTT assay against

two mammalian cell lines, HT22 and KB. (Fig. 5.6) Results suggested that P18 hydrogel and P18-CP(50) hydrogel have a non-cytotoxic effect on HT22 and KB cell lines with more than 90% viable cells at their active concentrations, suggesting biocompatibility towards mammalian cells. On the other hand, P18-CP(1000) co-assembled hydrogel was found to be slightly cytotoxic compared to P18 hydrogel and P18-CP(50) hydrogel, which limited its applicability despite having very good activity against both planktonic MRSA with high cell counts and biofilm formation.

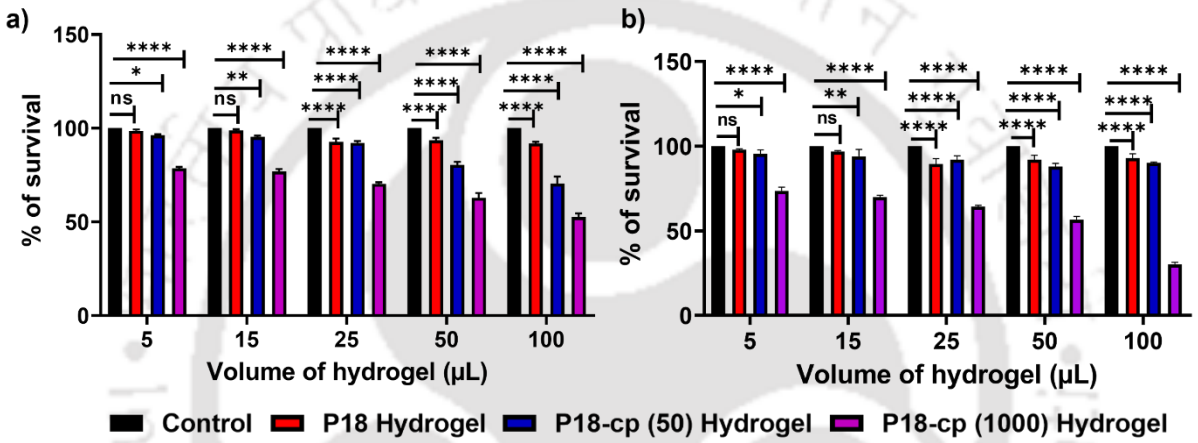

Fig. 5.6. MTT assay of the hydrogels in mammalian cells; a) HT22 cells and b) KB cells. Control indicates cells without any sample treatment. The data represents the mean of N=3 experiments (*p< 0.05, **p< 0.01, ***p< 0.001, ****p< 0.0001) via two-way analysis of variance (ANOVA) with Turkey's multiple comparison test).

5.3.6. Time kill kinetics and resistance development experiment

Further, to evaluate the amount of time required to exhibit the bactericidal activity, bacterial killing kinetics was performed for both P18 hydrogel and P18-CP(50) hydrogels. MRSA bacterial cells (10^5 CFU/ml) were incubated with both the hydrogels at their respective MIC concentrations for 0, 5, 15, 15, and 60 min and then cultured on NB agar plates (Fig. 5.7).

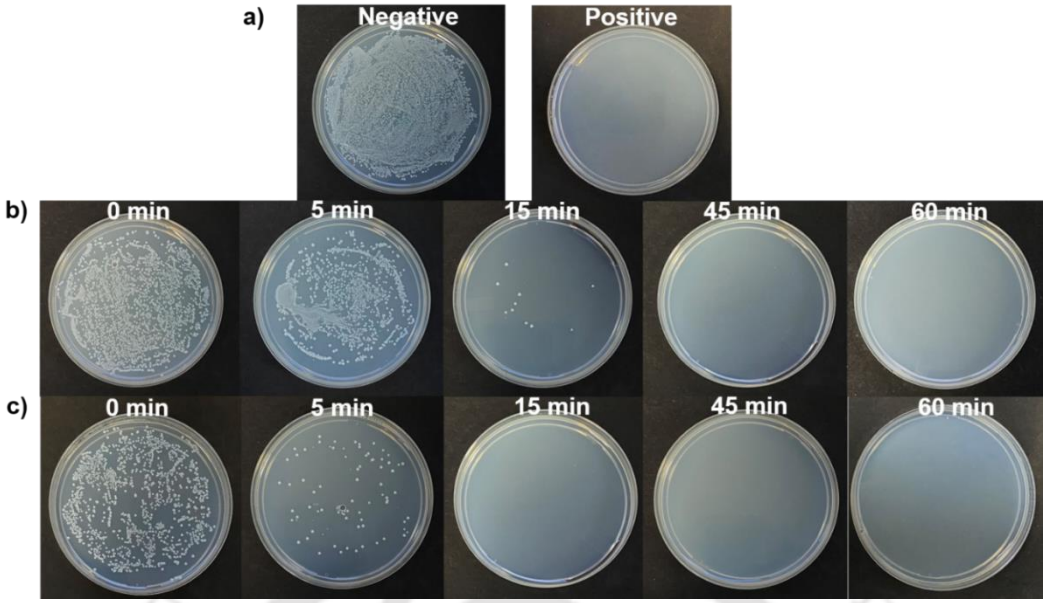

Fig. 5.7. Time kinetics of the bactericidal activity of P18 hydrogel and P18-CP(50) hydrogel against MRSA cells. MRSA cells were treated with hydrogels for different time intervals and cells were spread on Agar plate for CFU count after overnight incubation at 37 °C. Bacterial killing percentage was calculated from CFU count of the plate in comparison to the control plate. (a) Negative control (untreated cells) plate and positive control plate (10 μM vancomycin treated cells). Plates treated with (b) P18 hydrogel and (c) P18-CP(50) hydrogel at time points 3, 10, 15 and 20 min, respectively.

Plotting of CFU counts as a function of time (Fig. 5.8 a) evidenced that P18 hydrogel required almost 45 min to show the complete killing activity, while P18-CP(50) needed 15 min to kill the microbes. This result proved the enhancement of the antimicrobial activity and the faster bactericidal effect of drug-loaded P18-CP(50) hydrogel compared to P18 hydrogel. Next, we examined the resistance development ability of the MRSA bacteria against P18 hydrogel and co-assembled P18-CP(50) hydrogel along with CP. Fig. 5.8 b demonstrated that the bacteria developed no resistance against P18 hydrogel and co-assembled P18-CP(50) hydrogel till 48 generations. But, at the same time, multiple folds of increment in the MIC of CP were observed.

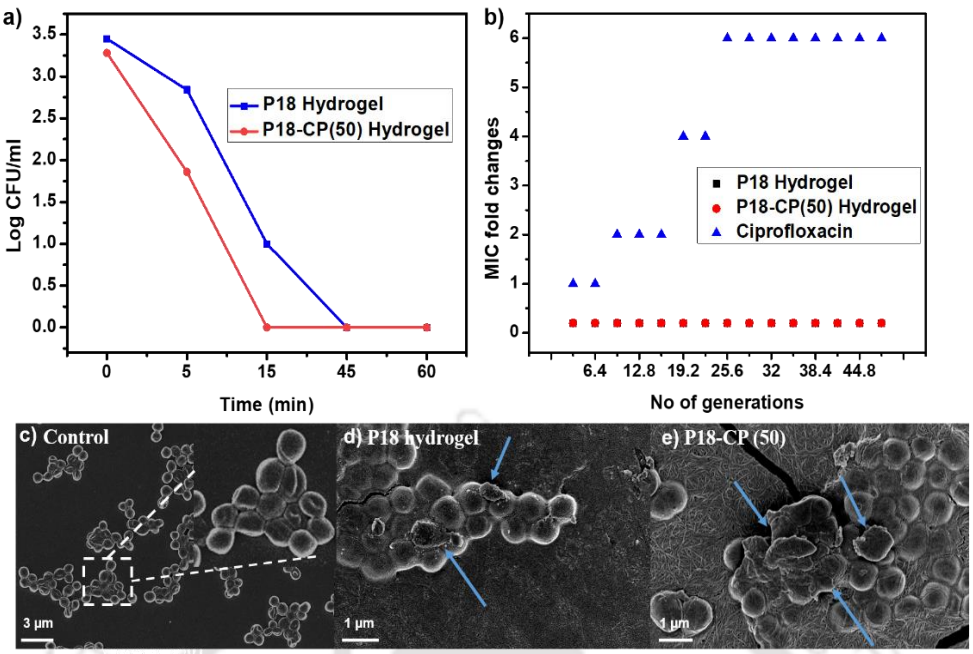

Fig. 5.8. a) Plot of percentage killing of MRSA at different time points, plotted from the CFU count, for P18 hydrogel and P18-CP(50) hydrogel; b) Change in MIC of P18 hydrogel, P18-CP(50) hydrogel and CP against MRSA plotted as a function of the number of generations, showing no development of resistance in MRSA against hydrogels; FESEM images of MRSA cells in the absence and presence of hydrogels: c) negative control, d) P18 hydrogel and e) P18-CP(50) hydrogel showing considerable deformation in cellular morphology.

5.3.7. Effect of hydrogels on bacterial cell morphology

A FESEM experiment was also conducted to visualize the effect of the P18 hydrogel and drug-loaded P18-CP(50) hydrogel on the morphology of MRSA cells (10^6 CFU/ml). The control untreated cells showed the distinct spherical shape of MRSA bacterial cells with intact morphology (Fig. 5.8 c). In contrast, the bacterial cells treated with P18 hydrogel and P18-CP(50) hydrogel (Fig. 5.8 d and e) displayed visible deformations of the membrane, implying a membranolytic mode of action.

5.4. Conclusion

In this study, we have been able to develop antimicrobial hydrogels effective in combating MRSA both in its planktonic and biofilms forms. Antibiotic co-assembled antimicrobial hydrogels (AMP P18+CP) were more effective than the AMP hydrogel P18. Of the different

compositions of antibiotic-loaded antimicrobial hydrogels studied here, P18-CP(1000) was the most effective and could completely prevent MRSA (10^5, 10^6, and 10^7) cell growth and biofilm formation, but showed slight cytotoxicity. P18-CP(50) hydrogel was the best overall therapeutic material developed in this study with enhanced antimicrobial efficacy and faster killing kinetics against MRSA, inhibitory activity towards MRSA biofilm formation, non-cytotoxicity against mammalian cells and no development of antibiotic resistance against MRSA upto 48 generations. Such antimicrobial hydrogels are extremely promising therapeutic biomaterials that might help in combating MRSA biofilm related complications in the future.

Overall, this study introduced combinatorial antimicrobial hydrogels of P18 and CP, demonstrating excellent results against MRSA, The present study only involves a single antibiotic and its efficacy against a single microbe. This study can be taken ahead in the future by testing combinations of P18 with various other antibiotics as well as different microbial strains (Bacterial and fungal). Moreover, in vivo studies are crucial for real life applications. Our future studies will be directed towards animal model studies and development of non-cytotoxic synergistic combinations."

5.5. References

1. Narayanan, K. B.; Park, G. T.; Han, S. S. Biocompatible, antibacterial, polymeric hydrogels active against multidrug-resistant *Staphylococcus aureus* strains for food packaging applications. *Food Control* **2021**, *123*, 107695.

2. Ng, V. W. L.; Chan, J. M. W.; Sardon, H.; Ono, R. J.; García, J. M.; Yang, Y. Y.; Hedrick. J. L. Antimicrobial hydrogels: A new weapon in the arsenal against multidrug-resistant infections. *Adv. Drug Deliv. Rev*. **2014**, *78*, 46–62.

3. Salam, M. A.; Al-Amin, M. Y.; Salam, M. T.; Pawar, J. S.; Akhte, N.; Rabaan, A. A.; Alqumber, M. A. A. Antimicrobial resistance: a growing serious threat for global public health. *Healthcare*, **2023**, *11*, 1946.

4. Chokshi, A.; Sifri, Z.; Cennimo, D.; Horng, H. Global contributors to antibiotic resistance. *J. Glob. Infect. Dis*. **2019**, *11*, 36-42.

5. Tuon, F. F.; Suss, P. H.; Telles, J. P.; Dantas, L. R.; Borges, N. H.; Ribeiro, V. S. T. Antimicrobial treatment of *Staphylococcus aureus* biofilms. *Antibiotics* **2023**, *12*, 87.

6. Tong, S. Y. C.; Davis, J. S.; Eichenberger, E.; Holland, T. L.; Fowler Jr., V. G. *Staphylococcus aureus* infections: epidemiology, pathophysiology, clinical manifestations, and management. *Clin. Microbiol. Rev*. **2015**, *28*, DOI: 10.1128/CMR.00134-14.

7. Vestergaard, M.; Frees, D.; Ingmer, H. Antibiotic resistance and the MRSA problem. *Microbiol. Spectr*. **2019**, *7*, DOI: 10.1128/microbiolspec.gpp3-0057-2018.

8. Lee, A. S.; de Lencastre, H.; Garau, J.; Kluytmans, J.; Malhotra-Kumar, S.; Peschel, A.; Harbarth, S. Methicillin-resistant *Staphylococcus aureus*. *Nat. Rev. Dis. Primers* **2018**, *4*, 18033.

9. a) Enright, M. C.; Robinson, D. A.; Randle, G.; Feil, E. J.; Grundmann, H.; Spratt, B. G. The evolutionary history of Methicillin-resistant *Staphylococcus aureus* (MRSA)

Proc. Natl. Acad. Sci. **2002**, *99*, 7687- 7692. b) Llarrull, L. I.; Fisher, J. F.; Mobashery, S. Molecular basis and phenotype of methicillin resistance in *Staphylococcus aureus* and insights into new-lactams that meet the challenge. *Antimicrob. Agents Chemother.* **2009**, *53*, 4051–4063.

10. Wu, H.; Wei, M.; Hu, S.; Cheng, P.; Shi, S.; Xia, F.; Xu, L.; Yin, L.; Liang, G.; Li, F.; Ling, D. A Photomodulable bacteriophage-spike nanozyme enables dually enhanced biofilm penetration and bacterial capture for photothermal-boosted catalytic therapy of MRSA infections. *Adv. Sci*. **2023**, *10*, 2301694.

11. Turner, N. A.; Sharma-Kuinkel, B. K.; Maskarinec, S. A.; Eichenberger, E. M.; Shah, P. P.; Carugati, M.; Holland, T. L.; Fowler Jr, V. G. Methicillin-resistant *Staphylococcus aureus*: an overview of basic and clinical research. *Nat. Rev Microbiol*. **2019**, *17*, 203-218.

12. Liu, Y.; Gong, H.; Wang, Z.; Yuan, C.; Lu, J.; Yan, X. Treatment of superbug infection through a membrane-disruption and immune-regulation cascade effect based on supramolecular peptide hydrogels. *Adv. Funct. Mater*. **2023**, *33*, 2305726.

13. Diep, B. A.; Otto, M. The role of virulence determinants in community-associated MRSA pathogenesis. *Trends Microbiol*. **2008**, *16*, 361.

14. Kramer, A.; Schwebke, I.; Kampf, G. How long do nosocomial pathogens persist on inanimate surfaces? A systematic review. *BMC Infect. Dis*. **2006**, *6*, 130.

15. Deusenbery, C.; Carneiro, O.; Oberkfell, C.; Shukla, A. Synergy of antibiotics and antibiofilm agents against Methicillin-Resistant *Staphylococcus aureus* biofilms. *ACS Infect. Dis*. **2023**, *9*, 1949-1963.

16. Schilcher, K.; Horswill, A. R. Staphylococcal biofilm development: structure, regulation, and treatment strategies. *Microbiol. Mol. Biol. Rev*. **2020**, *84*, e00026-19.

17. Donlan, R. M. Biofilms: microbial life on surfaces. *Emerging Infect. Dis*. **2002**, *8*, 881-890.

18. Liu, X.; Ren, Y.; Fan, D.; Huang, S.; Ma, Y.; Ding, J.; Luo, Z.; Chen, F.; Zeng, W. Shining light on multidrug-resistant bacterial infections: rational design of multifunctional organosilver-based aiegen probes as light-activated theranostics for combating biofilms and liver abscesses. *Adv. Funct. Mater*. **2023**, *33*, 2304974.

19. Zeng, J.; Wang, Y.; Sun, Z.; Chang, H.; Cao, M.; Zhao, J.; Lin, K.; Xie, Y. A novel biocompatible PDA/IR820/DAP coating for antibiotic/photodynamic/photothermal triple therapy to inhibit and eliminate *Staphylococcus aureus* biofilm. *Chem. Eng. J.* **2020**, *394*, 125017.

20. Koo, H.; Allan, R. N.; Howlin, R. P.; Stoodley, P.; Hall-Stoodley, L. Targeting microbial biofilms: current and prospective therapeutic strategies. *Nat. Rev. Microbiol*. **2017**, *15*, 740-755.

21. Hu, J.; Ding, Y.; Tao, B.; Yuan, Z.; Yang, Y.; Xu, K.; Li, X.; liu. P.; Cai. K. Surface modification of titanium substrate via combining photothermal therapy and quorum-sensing-inhibition strategy for improving osseointegration and treating biofilm-associated bacterial infection. *Bioactive Materials*. **2022**, *18*, 228-241.

22. Yelin, I.; Kishony, R. Antibiotic resistance. *Cell* **2018**, *172*, 1136.

23. Donlan, R. M.; Costerton, J. W. Biofilms: survival mechanisms of clinically relevant microorganisms. *Clin. Microbiol. Rev*. **2002**, *15*, 167-93.

24. Ovchinnikov, K. V.; Kranjec, C.; Telke, A.; Kjos, M.; Thorstensen, T.; Scherer, S.; Carlsen, H.; Diep, D. B. A Strong synergy between the thiopeptide bacteriocin micrococcin p1 and rifampicin against MRSA in a murine skin infection model. *Front. Immunol*. **2012**, *12*, DOI:10.3389/fimmu.2021.676534.

25. Tang, S.; Zheng, J. Antibacterial activity of silver nanoparticles: structural effects. *Adv. Healthc. Mater*. **2018**, *7*, e1701503.

26. Chen, H.; Wang, R.; Zhang, J.; Hua, H.; Zhu, M. Synthesis of core-shell structured ZnO@m-SiO_2 with excellent reinforcing effect and antimicrobial activity for dental resin composites. *Dent. Mater*. **2018**, *34*, 1846-1855.

27. Duncan, M. J.; Wheatley, P. S.; Coghill, E. M.; Vornholt, S. M.; Warrender, S. J.; Megson, I. L.; Morris, R. E. Antibacterial efficacy from NO-releasing MOF–polymer films. *Mater. Adv*. **2020**, *1*, 2509-2519.

28. Wang, J.; Song, J.; Yang, Z.; He, S.; Yang, Y.; Feng, X.; Dou, X.; Shan, A. Antimicrobial peptides with high proteolytic resistance for combating Gram-negative bacteria. *J. Med. Chem*. **2019**, *62*, 2286-2304.

29. Malanovic, N.; Lohner, K. Antimicrobial peptides targeting Gram-positive bacteria. *Pharmaceuticals* **2016**, *9*, 59.

30. Papo, N.; Shai, Y. Can we predict biological activity of antimicrobial peptides from their interactions with model phospholipid membranes? *Peptides* **2003**, *24*, 1693-1703.

31. Sarkar, T.; Chetia, M.; Chatterjee, S.; Antimicrobial peptides and proteins: from nature's reservoir to the laboratory and beyond. *Front. Chem*. **2021**, *9*, DOI: 10.3389/fchem.2021.691532.

32. Mabrouk, D. M. Antimicrobial peptides: features, applications and the potential use against covid-19. *Mol. Biol. Rep*. **2022**, *49*, 10039-10050.

33. Pandit, G.; Sarkar, T.; Vignesh, S. R.; Debnath, S.; Satpati, P.; Chatterjee, S. Delineating the mechanism of action of a protease resistant and salt tolerant synthetic antimicrobial peptide against *Pseudomonas aeruginosa*. *ACS Omega*, **2022**, *7*, 15951-15968.

34. Yasir, M.; Willcox, M. D. P.; Dutta, D. Action of antimicrobial peptides against bacterial biofilms. *Materials* **2018**, *11*, 2468.

35. Patra, A.; Das, J.; Agarwal, N. R.; Kushwaha, G. S.; Ghosh, M.; Son, Y. O. Marine antimicrobial peptides-based strategies for tackling bacterial biofilm and biofouling challenges. *Molecules* **2022**, *27*, 7546.

36. Chen, C.; Shi, J.; Wang, D.; Kong, P.; Wang, Z.; Liu, Y. Antimicrobial peptides as promising antibiotic adjuvants to combat drug-resistant pathogens. *Crit. Rev. Microbiol*. **2023**, DOI: 10.1080/1040841X.2023.2186215.

37. Mataraci, E.; Dosler, S. In vitro activities of antibiotics and antimicrobial cationic peptides alone and in combination against methicillin-resistant Staphylococcus aureus biofilms. *Antimicrob. Agents Chemother*. **2012**, *56*, 6366-71.

38. Zhou, J.; Zhang, H.; Fareed, M. S.; He, Y.; Lu, Y.; Yang, C.; Wang, Z.; Su, J.; Wang, P.; Yan, W.; Wang, K. An Injectable peptide hydrogel constructed of natural antimicrobial peptide j-1 and adp shows anti-infection, hemostasis, and antiadhesion efficacy. *ACS Nano* **2022**, *16*, 7636-7650.

39. Hu, B.; Owh, C.; Chee, P. L.; Leow, W. R.; Liu, X.; Wu, Y. L.; Guo, P.; Loh, X. J. Chen. X. Supramolecular hydrogels for antimicrobial therapy. *Chem. Soc. Rev*. **2018**, *47*, 6917-6929.

40. Wang, J.; Chen, X. Y.; Zhao, Y.; Yang, Y.; Wang, W.; Wu, C.; Yang, B.; Zhang, Z.; Zhang, L.; Liu, Y.; Du, X.; Li, W.; Qiu, L.; Jiang, P.; Mou, X. Z.; Li, Y. Q. pH-switchable antimicrobial nanofiber networks of hydrogel eradicate biofilm and rescue stalled healing in chronic wounds. *ACS Nano* **2019**, *13*, 11686-11697.

41. Yang, K.; Han, Q.; Chen, B.; Zheng, Y.; Zhang, K.; Li, Q.; Wang, Antimicrobial hydrogels: promising materials for medical application. J. *Int. J. Nanomed.* **2018**, *13*, 2217-2263.

42. Wu, S.; Yang, Y.; Wang, S.; Dong, C.; Zhang, X.; Zhang, R.; Yang, L. Dextran and peptide-based pH-sensitive hydrogel boosts healing process in multidrug-resistant

bacteria-infected wounds. *Carbohydr. Polym*. **2022**, *278*, 118994.

43. a) Liu, Y.; Yang, Y.; Wang, C.; and Zhao, X. Stimuli-responsive self-assembling peptides made from antibacterial peptides. *Nanoscale* **2013**, *5*, 6413-6421.

b) Veiga, A. S.; Sinthuvanich, C.; Gaspar, D.; Franquelim, H. G.; Castanho, M. A. R. B.; Schneider, J. P. Arginine-rich self-assembling peptides as potent antibacterial gels. *Biomaterials* **2012**, *33*, 8907-8916.

c) Salick, D. A.; Kretsinger, J. K.; Pochan, D. J. and Schneider, J. P. Inherent antibacterial activity of a peptide-based β-hairpin hydrogel. *J. Am. Chem. Soc*. **2007**, *129*, 14793-14799.

d) Haney, E. F.; Trimble, M. J.; Hancock, R. E. W. Microtiter plate assays to assess anti biofilm activity against bacteria. *Nat. Protoc*. **2021**, *16*, 2615–2632.

e) Haney, E., Trimble, M., Cheng, J., Vallé, Q. & Hancock, R. Critical assessment of methods to quantify biofilm growth and evaluate anti biofilm activity of host defence peptides. *Biomolecules* **2018**, *8*, 29.

f) Kumar, P.; Nagarajan, A.; and Uchil, P. D. Analysis of cell viability by the MTT Assay.*Cold Spring Harb Protoc*. **2018**, 469-471.

44. Rishi, P.; Vij, S.; Maurya, I. K.; Kaur, U. J.; Bharati, S.; Tewari, R. Peptides as adjuvants for ampicillin and oxacillin against Methicillin-resistant *Staphylococcus aureus* (MRSA). *Microb. Pathog.* **2018**, *124*, 11-20.

Chapter 6

Thesis Overview and Future Prospects

6.1. Thesis Overview

In this thesis, we have designed a library of low molecular weight peptide-based gelator molecules capable of forming organogels/hydrogels under the influence of non-covalent interactions, and explored some of their possible applications in both biomedical and non-biomedical fields of research. We have also investigated their self-assembly mechanism to understand the gelation process with the help of several experimental techniques. Chapter 2 detailed the development of phase-selective, thermo-reversible, mechanically robust organogels formed by low molecular weight dipeptides that were rich in aromatic moieties through aromatic π-π stacking and hydrophobic interactions. Their phase-selective gelation ability rendered them as potential materials for controlling marine oil spills. Also, they were found to be useful as excellent dye absorbents in water purification and matrices for making conducting hybrid material by incorporation of RGO into them.

In Chapter 3, a series of FF dipeptide analogs, FLF, FLLF, and FLLLF, was studied by incorporating a variable number of leucine amino acid residues as spacers in between the two Phe residues. With the help of extensive experimental investigations, we have conclusively established that distance in between the Phe residues, had no effect on the gelation properties of these peptides. All the peptides with variable length of the spacers were found to be equally efficient in gelation, and had similar mechanical strength and morphologies. Further, these organogels were utilized in the encapsulation of green and red core/core-ZnS shell CdSe QDs into their gel matrix with both retention and stabilization of their photo-physical properties, by the prevention of aerial oxidation.

Chapter 4 dealt with a library of lipopeptides, varying in their hydrophobic-hydrophilic balance. We established that hydrophobic-hydrophilic balance of the peptides was pivotal in controlling several properties like secondary structure, self-assembly (morphology, kinetics, stability), antimicrobial properties (potency, killing kinetics, salt tolerance of the antimicrobial

activity) and protease resistance. Based on that, we have developed an extremely potent, non-cytotoxic, salt tolerant and protease resistant AMP P18, against ESKAPE pathogens like *P. aeruginosa*, *K. pneumonia*, *S. aureus* and MRSA.

In Chapter 5, P18 hydrogel was further explored for the development of hybrid antimicrobial hydrogels effective in combating MRSA both in its planktonic and biofilm forms by using the idea of combination therapy. Our study revealed that the new co-assembled hybrid antimicrobial hydrogels (AMP P18-CP(X)) were more effective with faster bactericidal effect against MRSA (10^5, 10^6 and 10^7) cell growth and the biofilm formation than the AMP hydrogel P18 and the antibiotic alone. Moreover, MRSA microbes were found to develop no resistance against these antimicrobial hydrogels, unlike ciprofloxacin. Such antimicrobial hydrogels are extremely promising therapeutic biomaterials that might help in combating MRSA biofilm-related complications.

6.2. Future Prospects

Peptide-based supramolecular gels emerge as one of the most fascinating soft materials with diverse applications in biomedical and non-biomedical research. We believe that the insights gained from our studies will guide us to design peptides rationally and to understand the role of various driving forces along with other stimuli that are involved in gelation for the development of advanced peptide biomaterials with specific functions. However, we understand the practical applicability of any material necessitates addressing several factors like large manufacturing, greener synthesis methods with environmental sustainability, and real-world testing outside the laboratory. For industrial translation, it is essential to develop environmentally friendly synthesis procedures with high yield, using greener coupling reagents and replacing DMF with less hazardous solvents. Additionally, ensuring the efficiency of these materials for large-scale use is crucial. In the future, we aim to develop peptide gel-based

biomaterials by addressing the limitations of our current methods, thereby improving their quality and applicability.

Some other approaches for betterment of our systems are underway. We are working on the improvement of the viscoelastic properties of the gels by introducing covalent cross-linkings and controlling the gelation rates. Stimuli responsiveness is another attractive property of gel materials, which we are trying to introduce into our systems.

Apart from that, we also want to develop therapeutically important AMP-based materials with high potency, salt tolerance of antimicrobial activity, protease resistance, and non-cytotoxicity. Though our AMPs and their gels are very potent against both Gram-positive and Gram-negative microbes, further in *vivo* studies involving animal models are necessary to establish their practical efficiency. Additionally, though we have incorporated combinatorial therapy in our studies, its full potential remains unexplored. Due to time constraints and limited availability of the facility, we could only perform combination therapy for only one antibiotic and against a single microbial strain. We intend to explore combination therapy with other available antibiotics to get improved potency against multi-drug resistant superbugs in both planktonic state and biofilm forms. Finally, we plan to apply our developed combination therapy in the in *vivo* animal infection models and wound healing models, which would provide them a possibility for pharmaceutical applications. Therefore, we look forward to introducing the above-mentioned features to our gels to create more advanced and tunable soft materials.

CHAPTER 2: APPENDIX

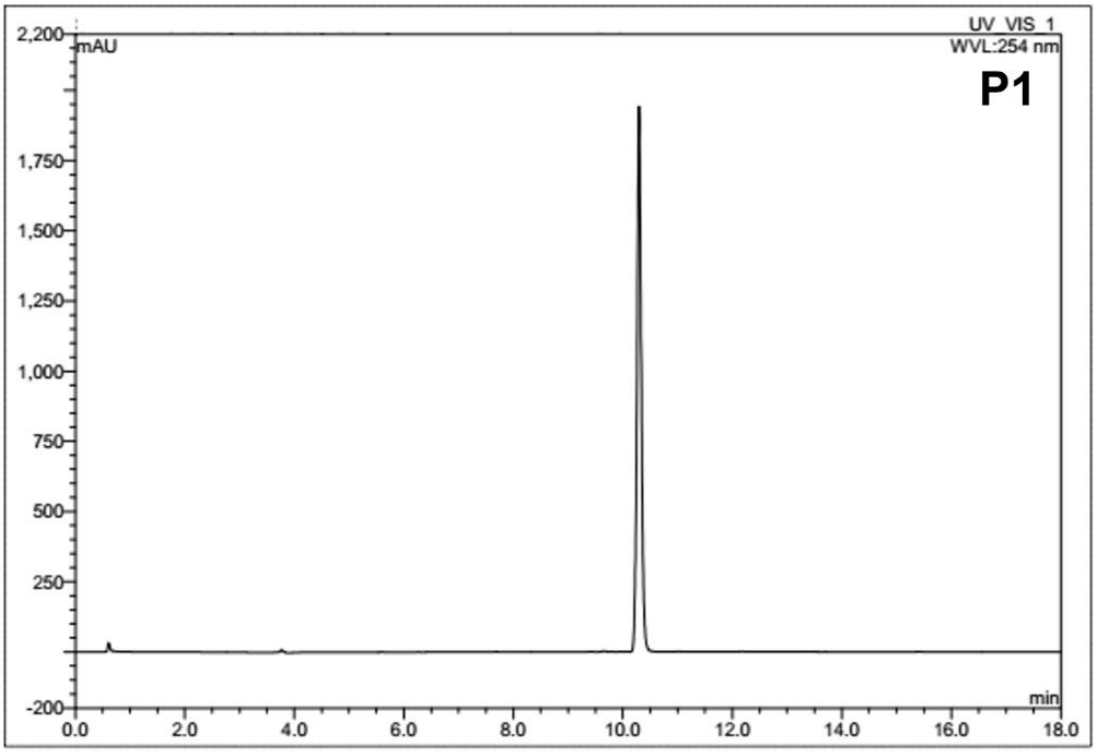

Fig. A2.1. Analytical HPLC trace of the peptides P1.

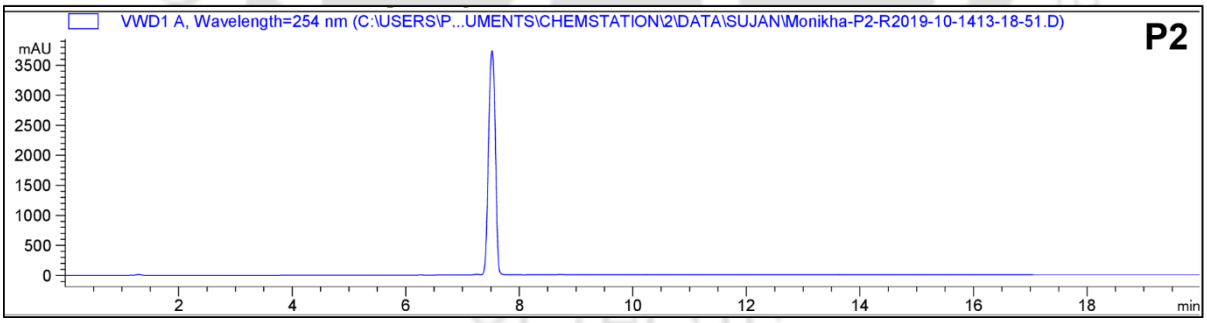

Fig. A2.2. Analytical HPLC trace of the peptides P2.

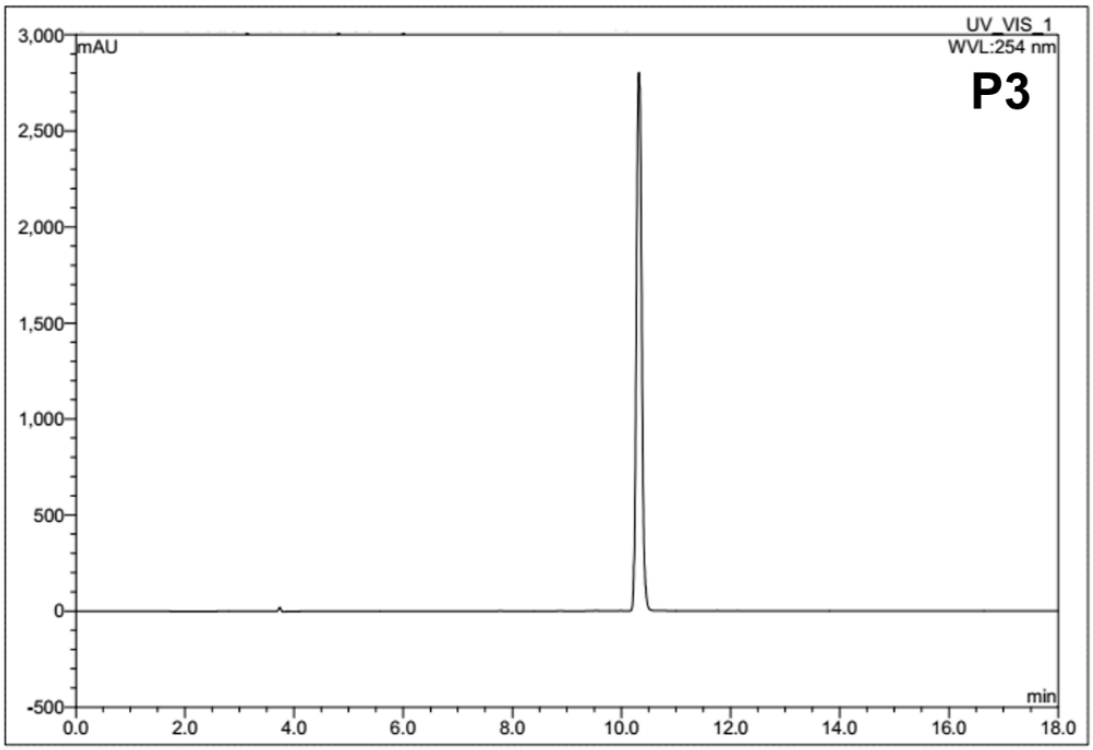

Fig. A2.3. Analytical HPLC trace of the peptides P3.

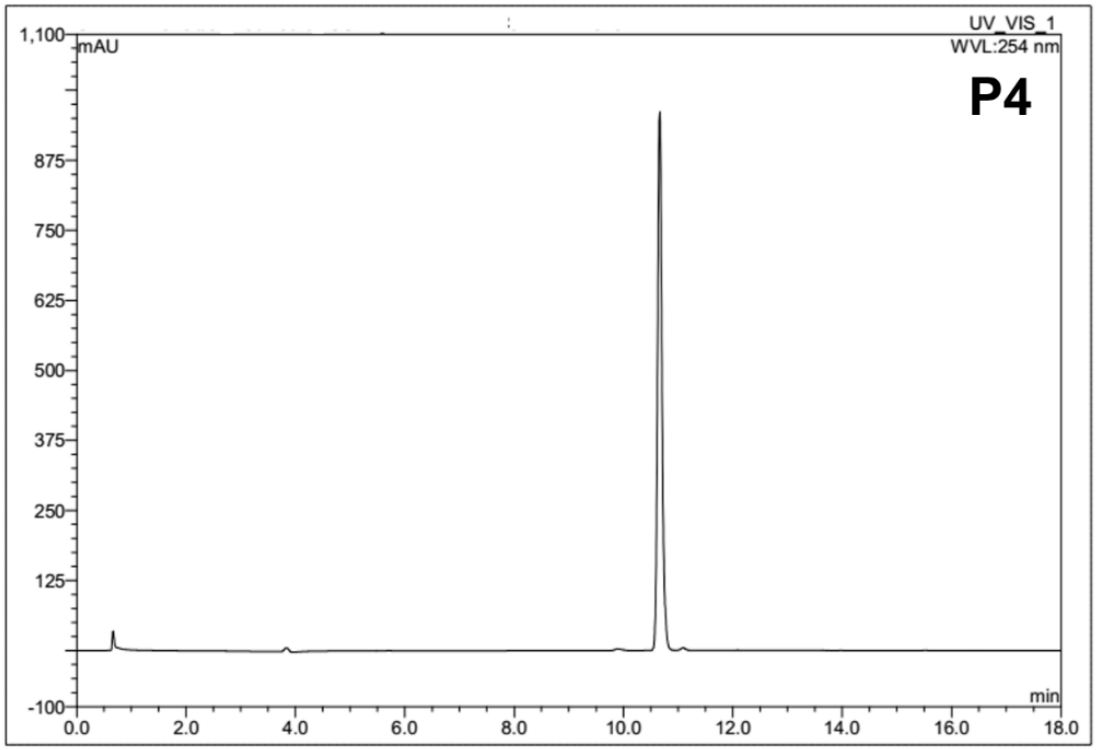

Fig. **A2.4.** Analytical HPLC trace of the peptides P4

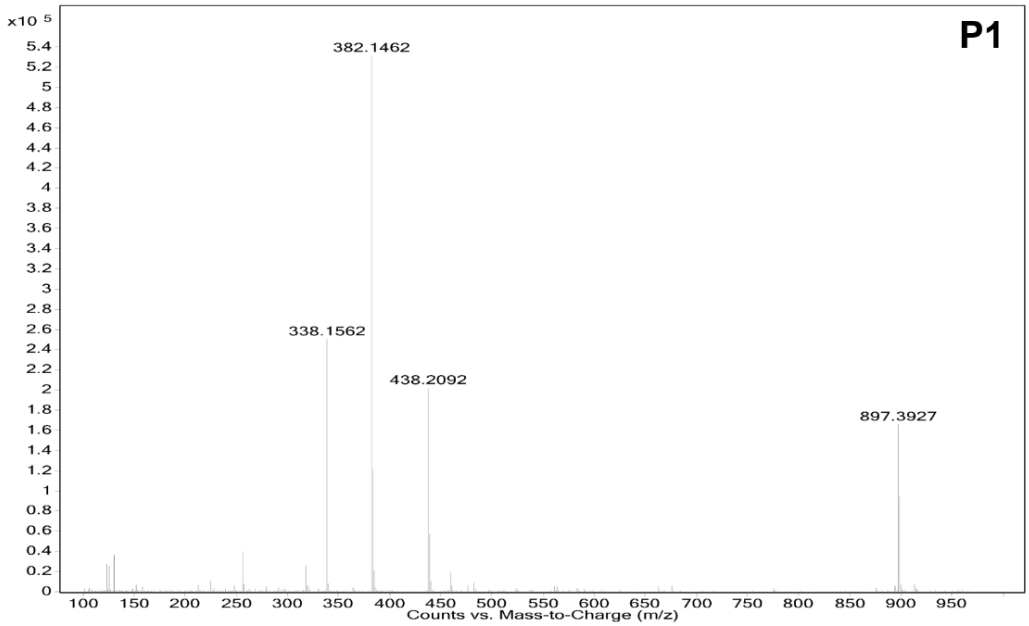

Fig. A2.5. ESI-MS of P1. Mass calc. for P1: $(M+H)^+$ =438.208 Da; Mass Obs.: $(M+H)^+$=438.2092 Da.

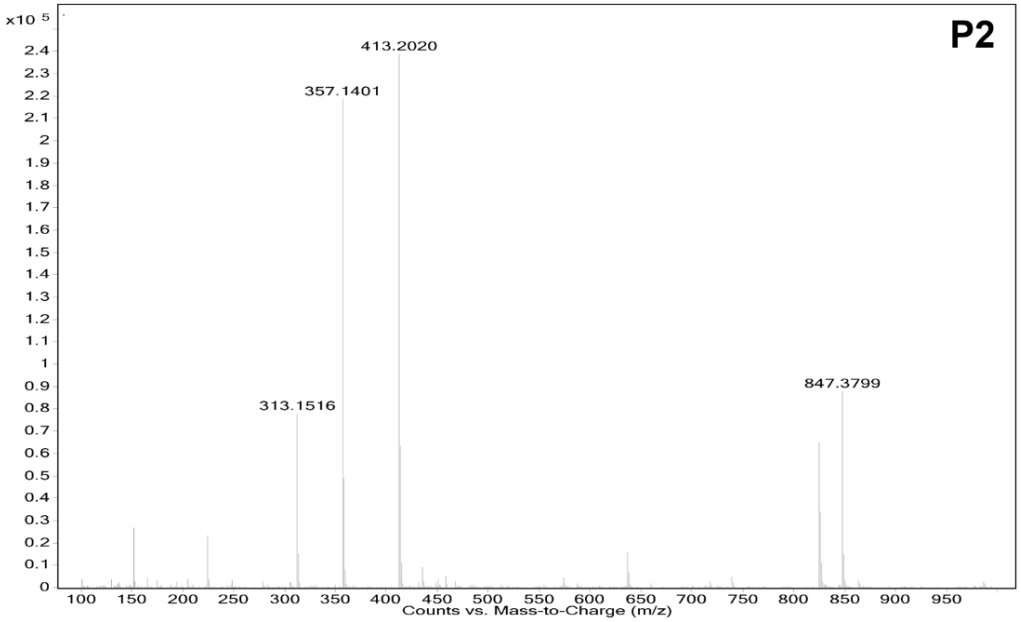

Fig. A2.6. ESI-MS of P2. Mass calc. for P2: $(M+H)^+$ =413.208 Da; Mass Obs.: $(M+H)^+$=413.2020 Da.

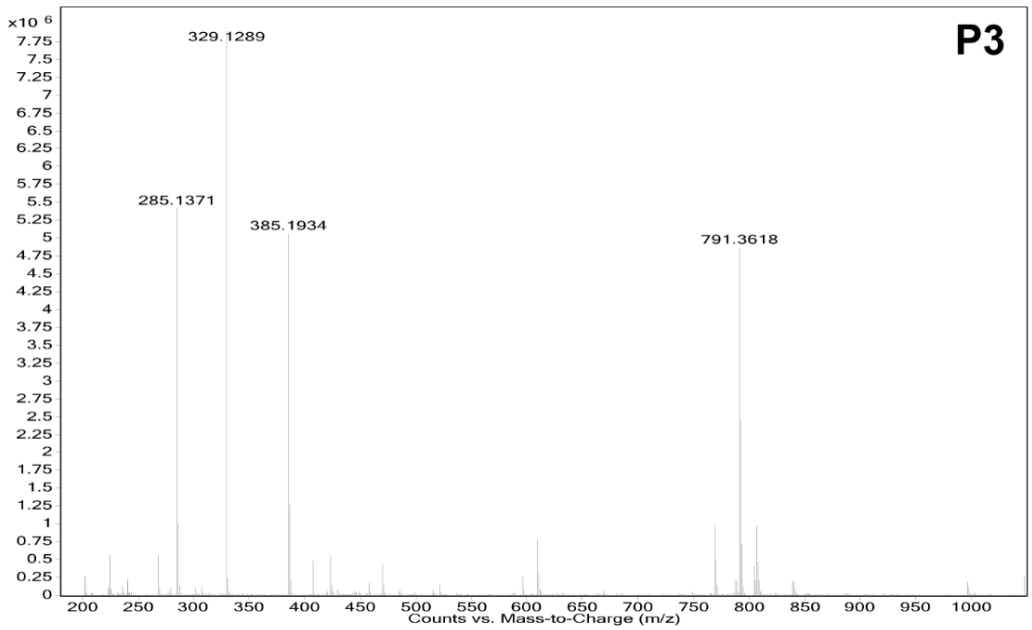

Fig. A2.7. ESI-MS of P3. Mass calc. for P3: $(M+H)^+$ =385.178 Da; Mass Obs.: $(M+H)^+$=385.1934 Da.

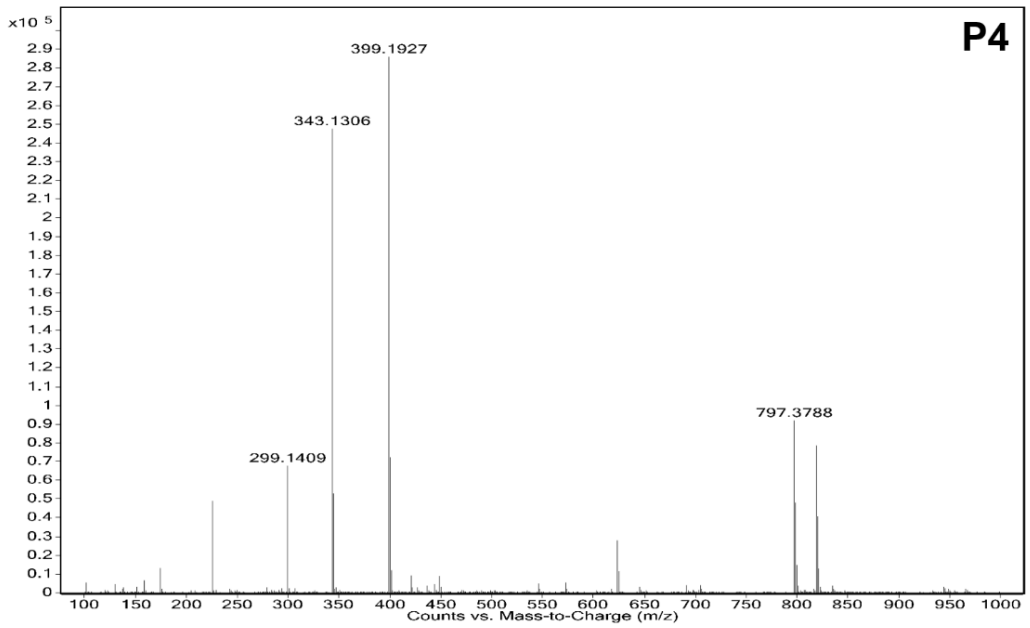

Fig. A2.8. ESI-MS of P4. Mass calc. for P4: $(M+H)^+$ =399.188 Da; Mass Obs.: $(M+H)^+$=399.1927 Da.

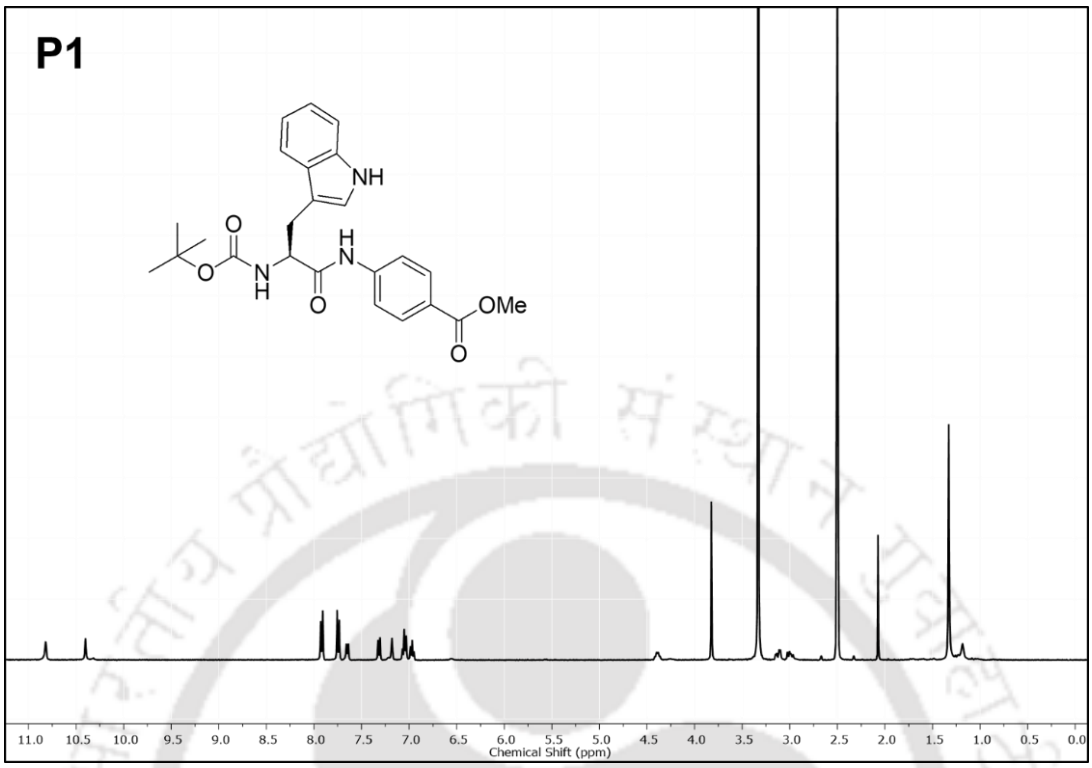

Fig. A2.9. 400 MHz ^{1}H NMR spectra of P1 recorded in DMSO-d_6 at room temperature. (400 MHz, DMSO-d_6) δ 10.82 (s, 1H, NH of indole ring), 10.40 (s, 1H, NH of backbone), 7.92 (d, J = 8.5 Hz, 2H, Aromatic ring Hs), 7.75 (d, J = 8.6 Hz, 2H, Aromatic ring Hs), 7.65 (d, J = 7.9 Hz, 1H, Aromatic ring H),7.32 (d, J = 8.1 Hz, 1H, NH of Boc group), 7.18 (s, 1H, H of Aromatc ring),7.05 (t, J = 7.7 Hz, 2H, Aromatic ring Hs), 6.97 (t, J = 7.4 Hz, 1H, H of Aromatic ring), 4.39 (d, J = 6.7 Hz, 1H, H of alpha -CH), 3.82 (s, 3H, Hs of -CH_3 group), 3.12 (dd, J = 14.6, 5.3 Hz, 1H, H of beta -CH_2), 3.00 (dd, J = 14.5, 9.0 Hz, 1H, H of beta -CH_2), 1.33 (s, 9H, Hs of Boc group).

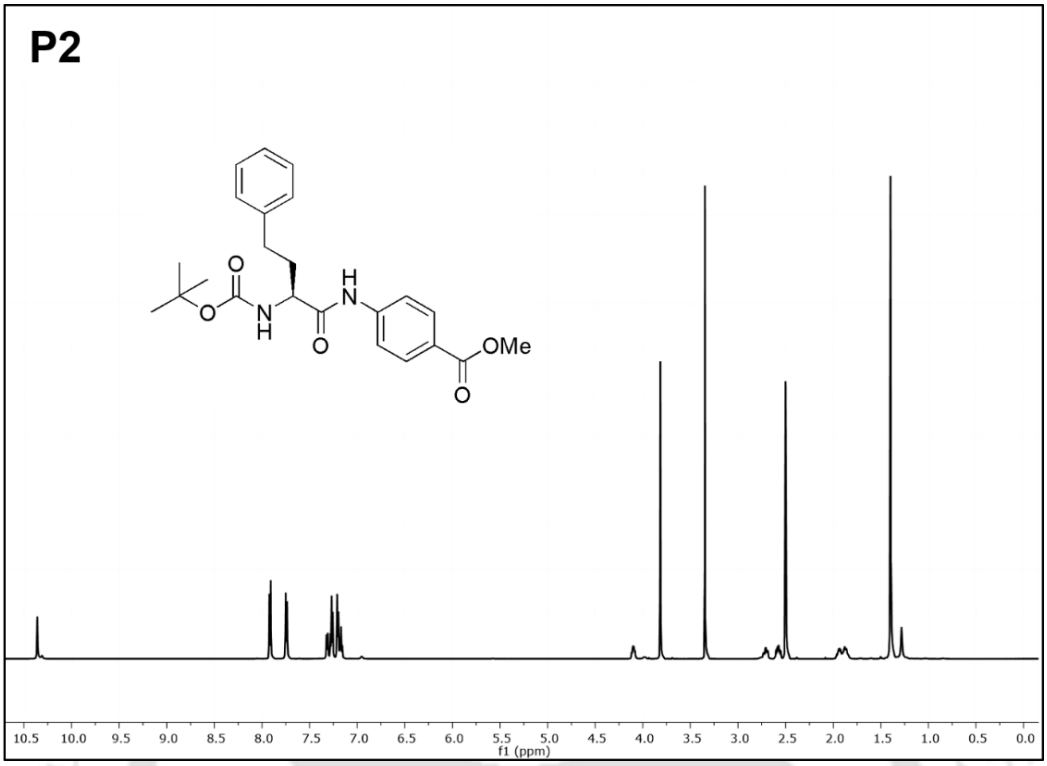

Fig. A2.10. 400 MHz ^{1}H NMR spectra of P2 recorded in DMSO-*d6* at room temperature. ^{1}H NMR (600 MHz, DMSO-d_6) δ 10.36 (s, 1H, NH of backbone), 7.93 – 7.89 (m, 2H, Hs of Aromatic ring), 7.74 (d, *J* = 8.8 Hz, 2H, Hs of Aromatic ring), 7.32 (d, *J* = 7.6 Hz, 1H, NH of Boc group), 7.27 (t, *J* = 7.5 Hz, 2H, Hs of Aromatic ring), 7.24 – 7.19 (m, 2H, Hs of Aromatic ring), 7.19 – 7.15 (m, 1H, H of Aromatic ring), 4.10 (ddd, *J* = 9.5, 7.5, 4.7 Hz, 1H, H of alpha -CH group), 3.82 (s, 3H, Hs of -CH_3 group), 2.71 (ddd, *J* = 13.3, 10.8, 5.0 Hz, 1H, H of beta -CH_2 group), 2.58 (ddd, *J* = 13.5, 10.8, 5.9 Hz, 1H, H of beta CH_2), 1.97 – 1.83 (m, 2H, Hs of gamma -CH_2 group), 1.40 (s, 9H, Hs of Boc group).

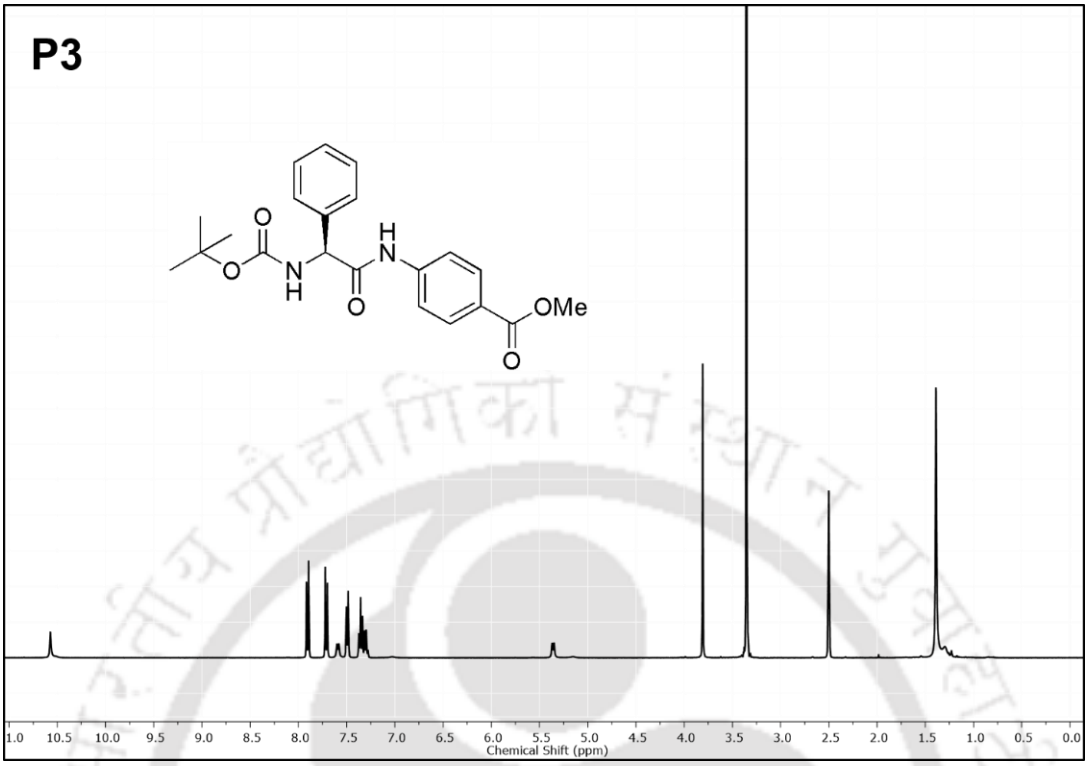

Fig. A2.11. 400 MHz ^{1}H NMR spectra of P3 recorded in DMSO-d_6 recorded at room temperature. ^{1}H NMR (400 MHz, DMSO-d_6) δ 10.57 (s, 1H, H of backbone NH), 7.93 – 7.88 (m, 2H, Hs of Aromatic ring), 7.74 – 7.68 (m, 2H, Hs Of Aromatic ring), 7.59 (d, J = 8.1 Hz, 1H, NH of Boc group), 7.52 – 7.47 (m, 2H, Hs of Aromatic ring), 7.38 – 7.27 (m, 3H, Hs of Aromatic ring), 5.36 (d, J = 8.1 Hz, 1H, H of alpha -CH), 3.81 (s, 3H, Hs of -CH_3), 1.39 (s, 9H, Hs of Boc group).

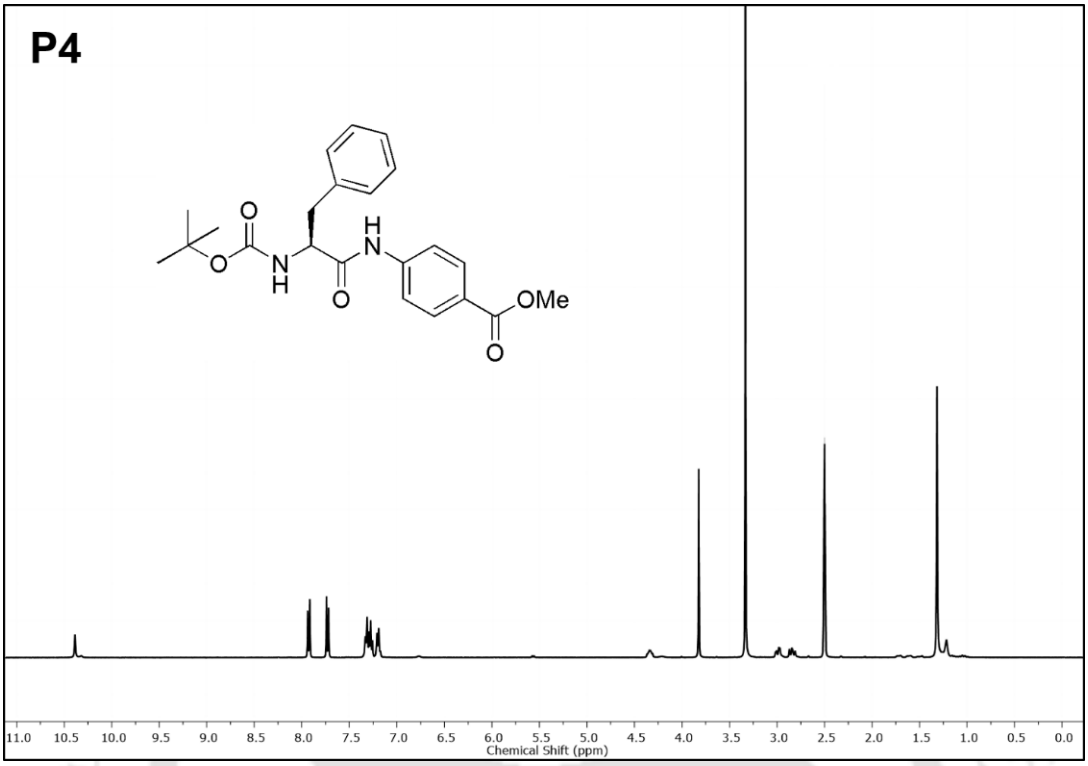

Fig. A2.12. 400 MHz ^{1}H NMR spectra of P4 recorded in DMSO-d_6 at room temperature. ^{1}H NMR (400 MHz, DMSO-d_6) δ 10.39 (s, 1H, NH of backbone), 7.96 – 7.90 (m, 2H, Hs of Aromatic ring), 7.77 – 7.69 (m, 2H, Hs of Aromatic ring), 7.29 (dt, J = 14.8, 7.5 Hz, 4H, Hs of Aromatic ring and NH of Boc group), 7.20 (d, J = 7.7 Hz, 2H, Hs of Aromatc ring), 4.44 – 4.16 (m, 1H, H of alpha -CH), 3.82 (s, 3H, Hs of -CH_3 group), 2.99 (dd, J = 13.7, 4.7 Hz, 1H, H of beta -CH_2), 2.84 (dd, J = 13.7, 10.1 Hz, 1H, H of beta -CH_2), 1.32 (s, 9H, Hs of Boc group).

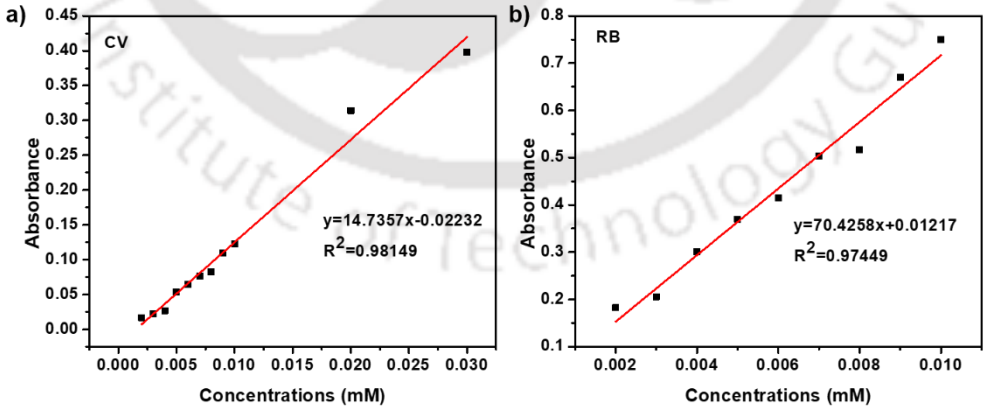

Fig. A2.13. Calibration curve for a) CV and b) RB.

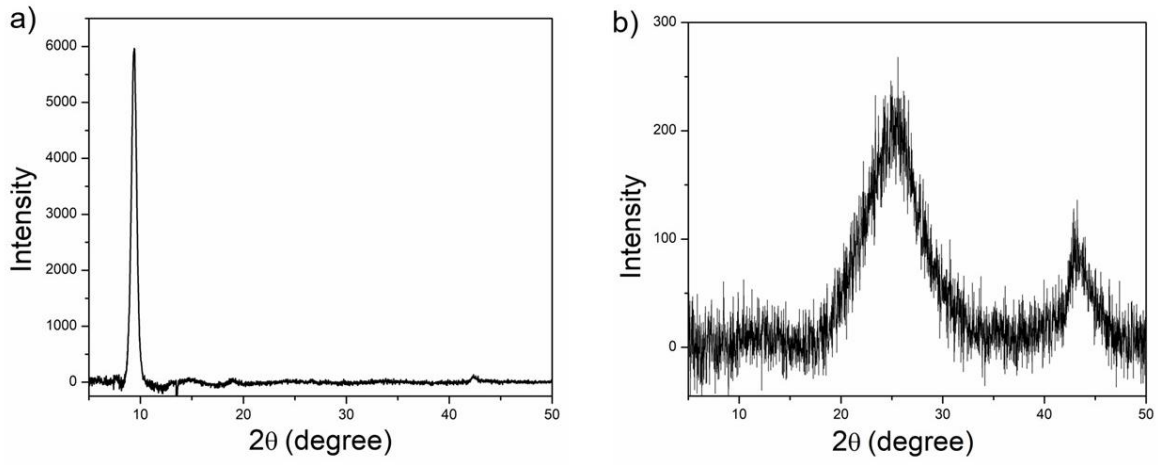

Fig. A2.14. PXRD of a) graphene oxide and b) RGO incorporated into the hybrid organogels. a) TEM of RGO and b) Raman spectroscopy of GO and RGO.

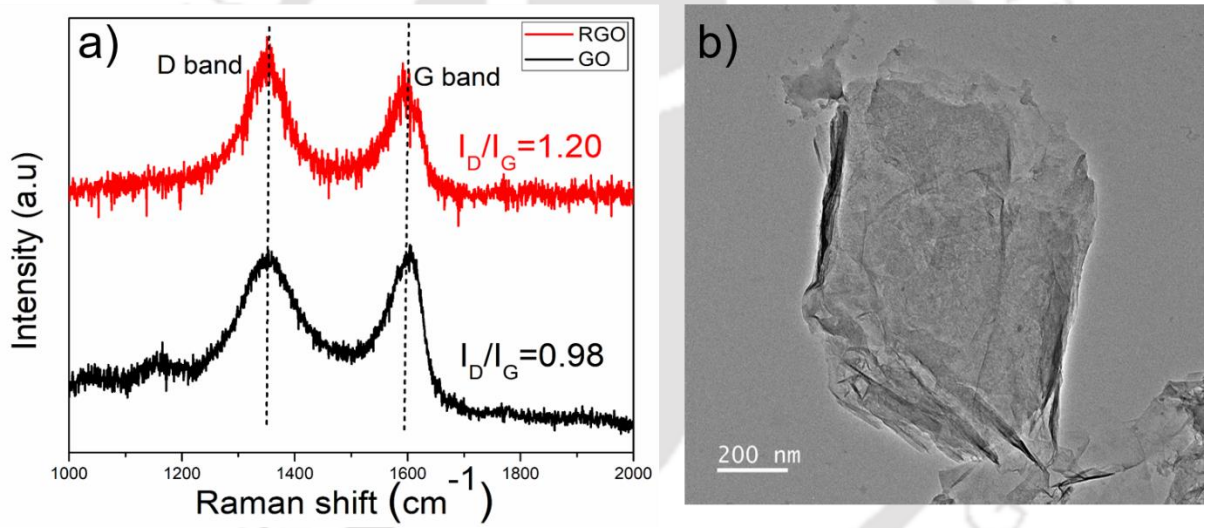

Fig. A2.15. a) Raman spectra of GO and RGO. b) TEM image of RGO.(Raman analysis of GO and RGO was done by using a laser micro-raman (Horiba Jobin Vvon LabRam HR) with 514 nm laser excitation).

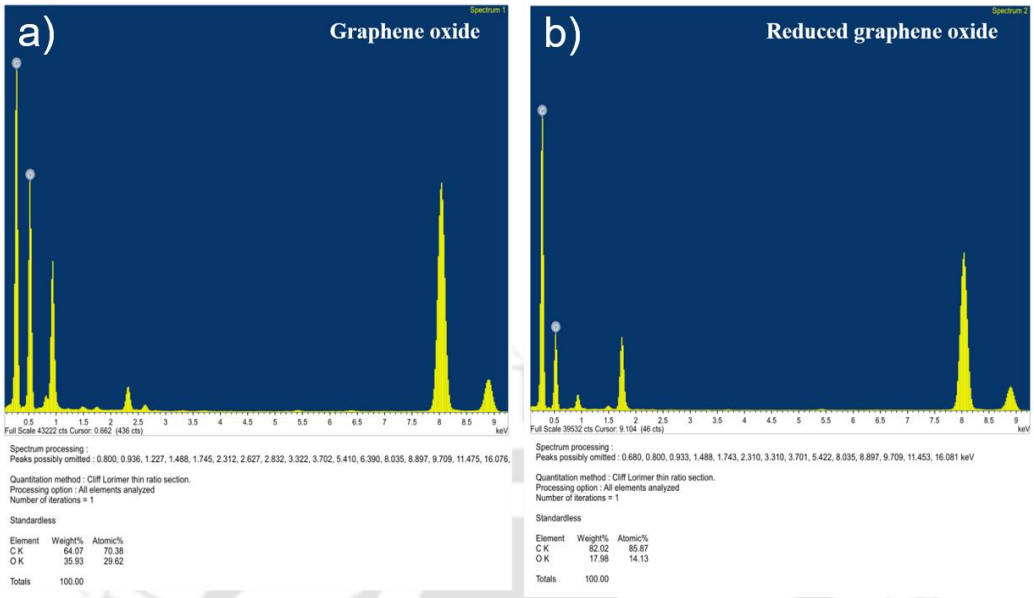

Fig. A2.16. a) EDX analysis of GO and b) EDX analysis of RGO.(EDX analysis of graphene oxide and reduced graphene oxide has been done to estimate the wt% of Carbon and oxygen in the samples. While the C and O % were 64.07%. and 35.93% for graphene oxide, it was 82.02% and 17.98% for RGO).

CHAPTER 3: APPENDIX

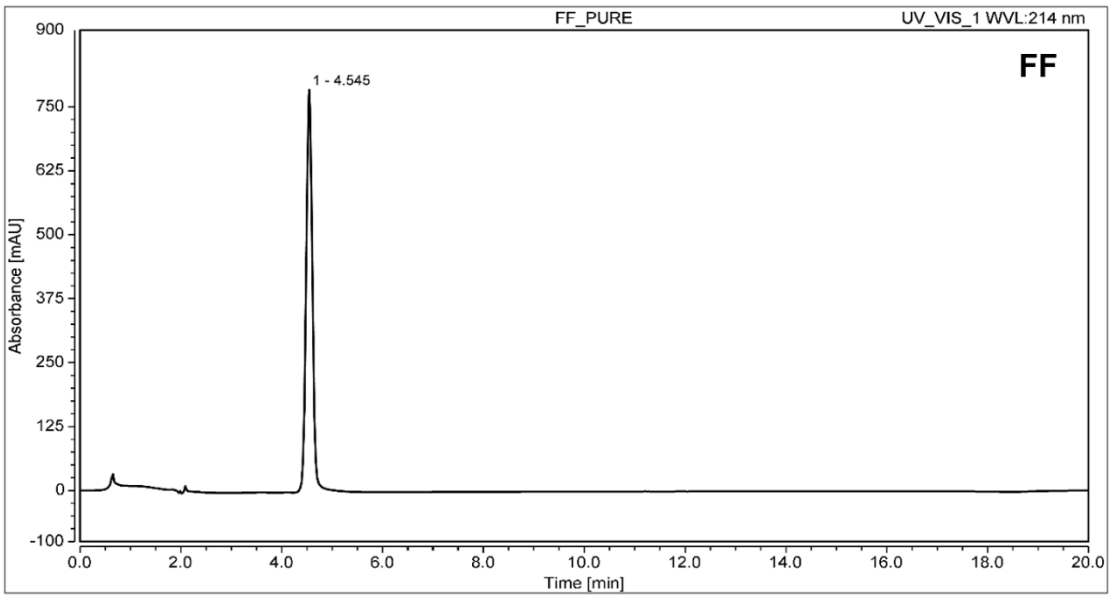

Fig. A3.1. Analytical HPLC trace of Boc-FF-OMe in ACN/H_2O.

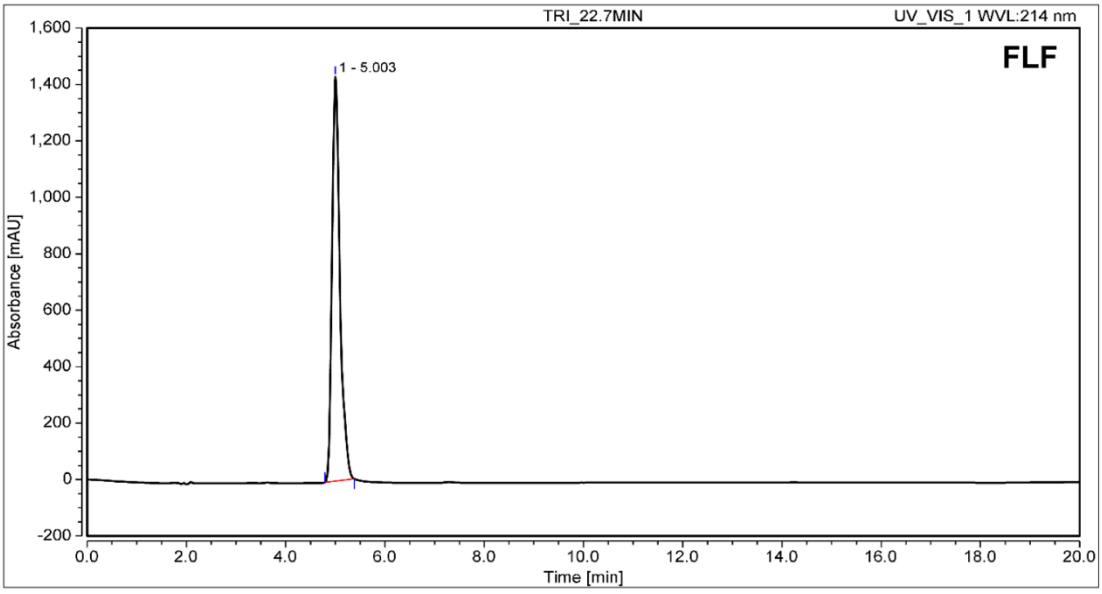

Fig. A3.2. Analytical HPLC trace of Boc-FLF-OMe in ACN/H_2O.

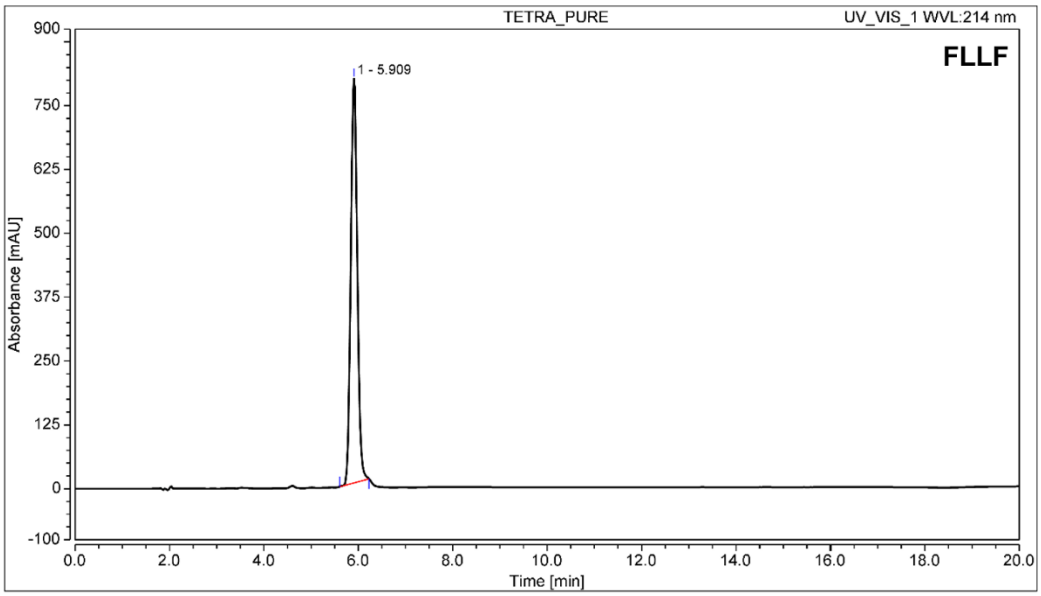

Fig. A3.3. Analytical HPLC trace of Boc-FLLF-OMe in ACN/H_2O.

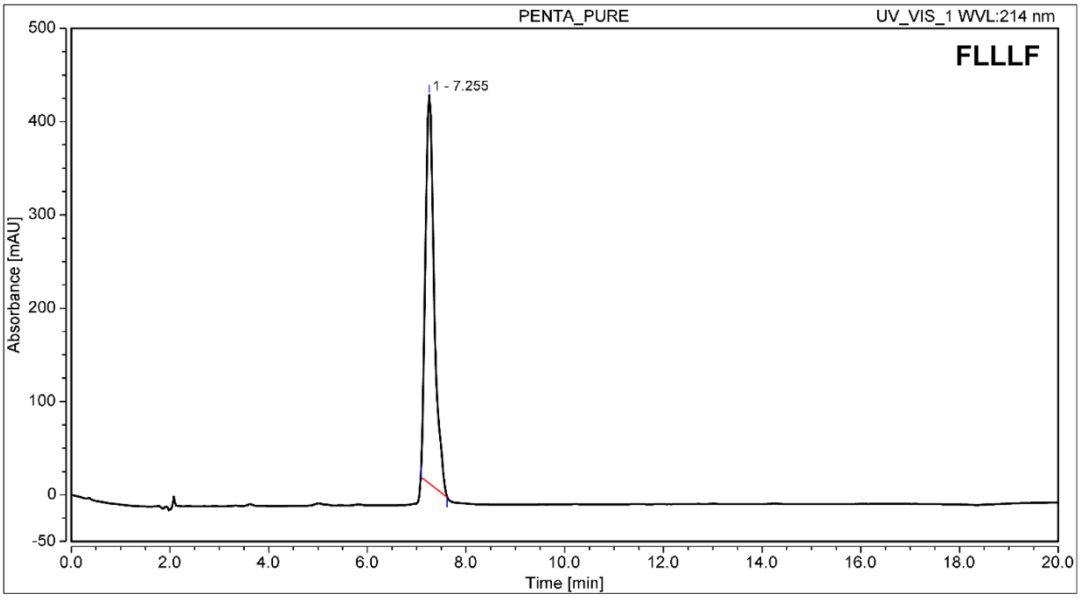

Fig. A3.4. Analytical HPLC trace of Boc-FLLLF-OMe in ACN/H_2O.

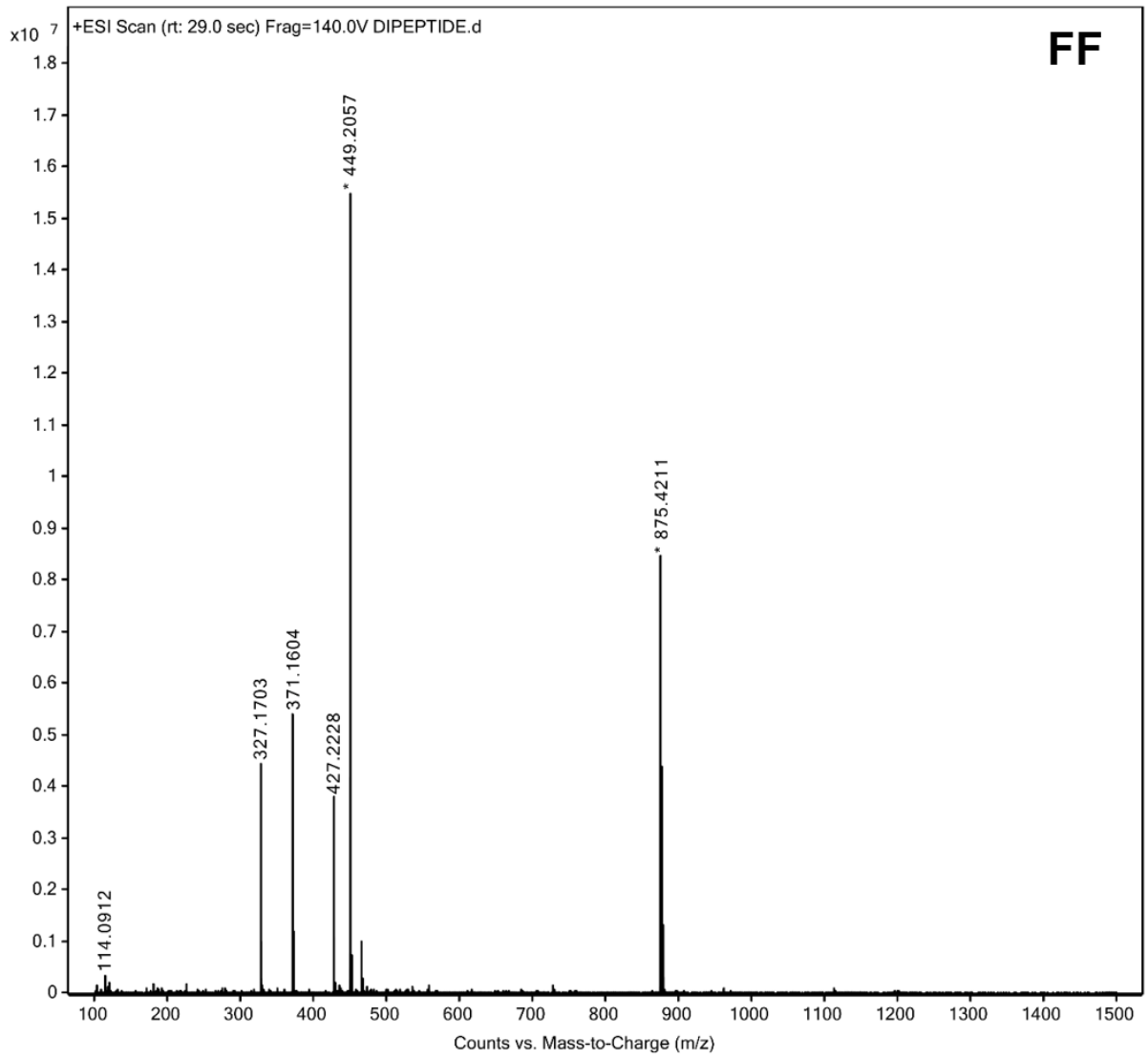

Fig. A3.5. ESI-MS (m/z) of Boc-FF-OMe. Calc. for $(M+H)^+$ $C_{24}H_{30}N_2O_5$ = 427.2188 Da; Obs. for $(M+H)^+$ = 427.2228 Da, $(M+Na)^+$ = 449.2057 Da, $(2M+Na)^+$ = 875.4211 Da.

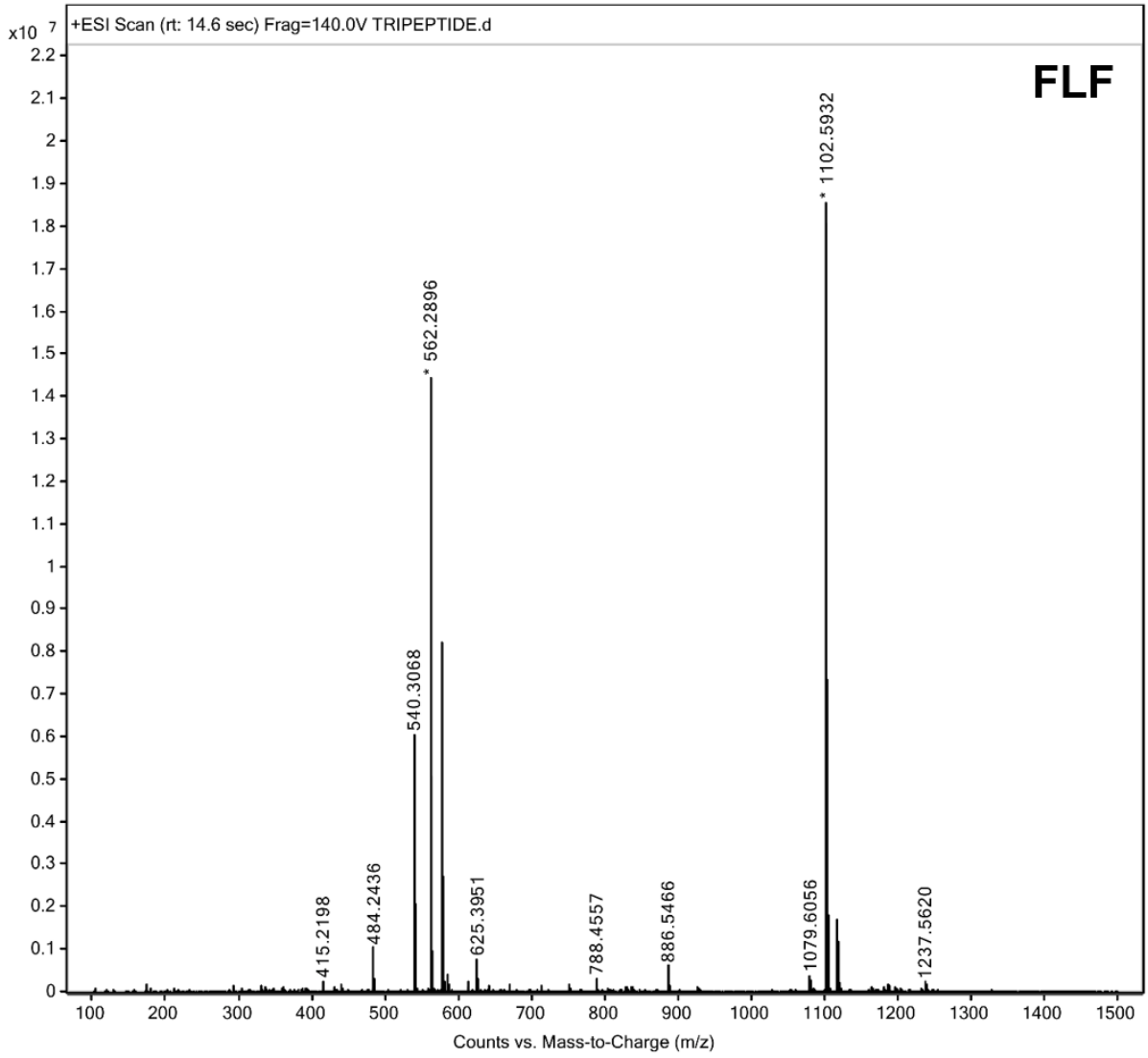

Fig. A3.6. ESI-MS (m/z) of Boc-FLF-OMe. Calc. for $(M+H)^+$ $C_{30}H_{41}N_3O_6$ = 540.3029 Da; Obs. for $(M+H)^+$ = 540.3068 Da, $(M+Na)^+$ = 562.2896, $(2M+Na)^+$ = 1102.5932 Da.

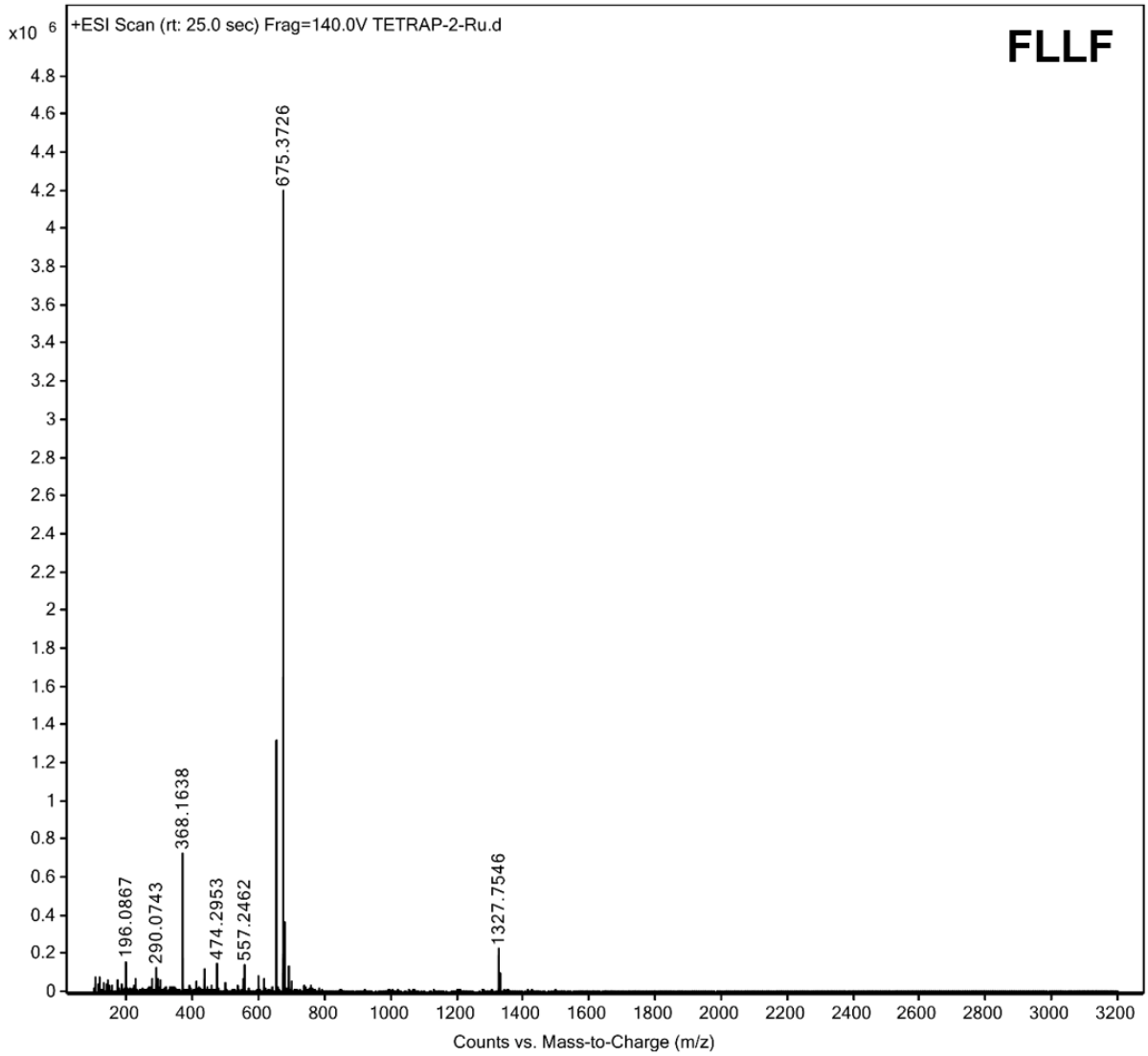

Fig. A3.7. ESI-MS (m/z) of Boc-FLLF-OMe. Calc. for $(M+Na)^+$ $C_{36}H_{52}N_4O_7$ = 675.3734 Da; Obs. for $(M+Na)^+$ = 675.3726, $(2M+Na)^+$ = 1327.7546 Da.

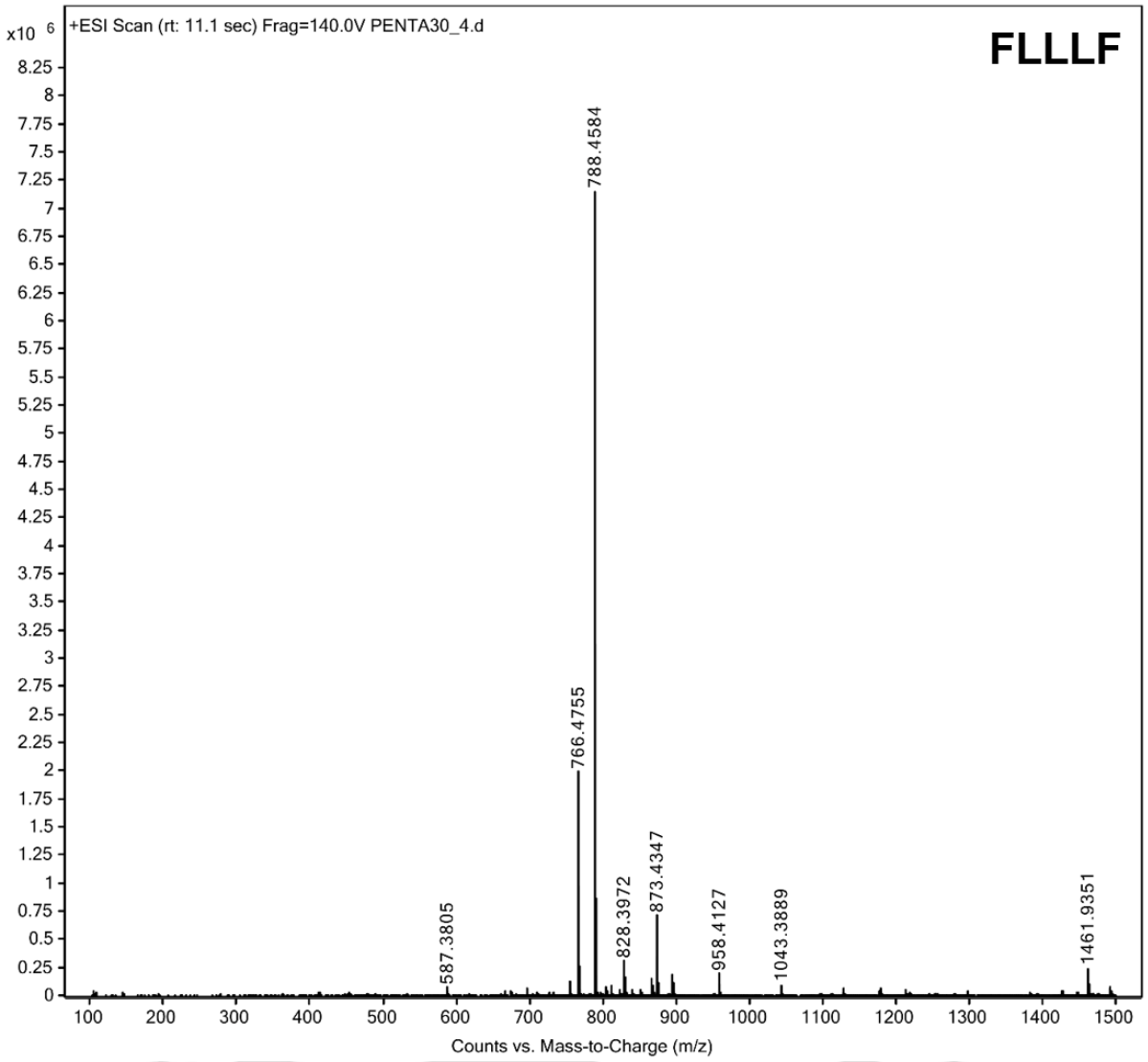

Fig. A3.8. ESI-MS (m/z) of Boc-FLLLF-OMe. Calc. for (M+H)+ $C_{42}H_{63}N_5O_8$ = 766.4710 Da; Obs. for (M+H)+ = 766.4755 Da, (M+Na)+ = 788.4584 Da.

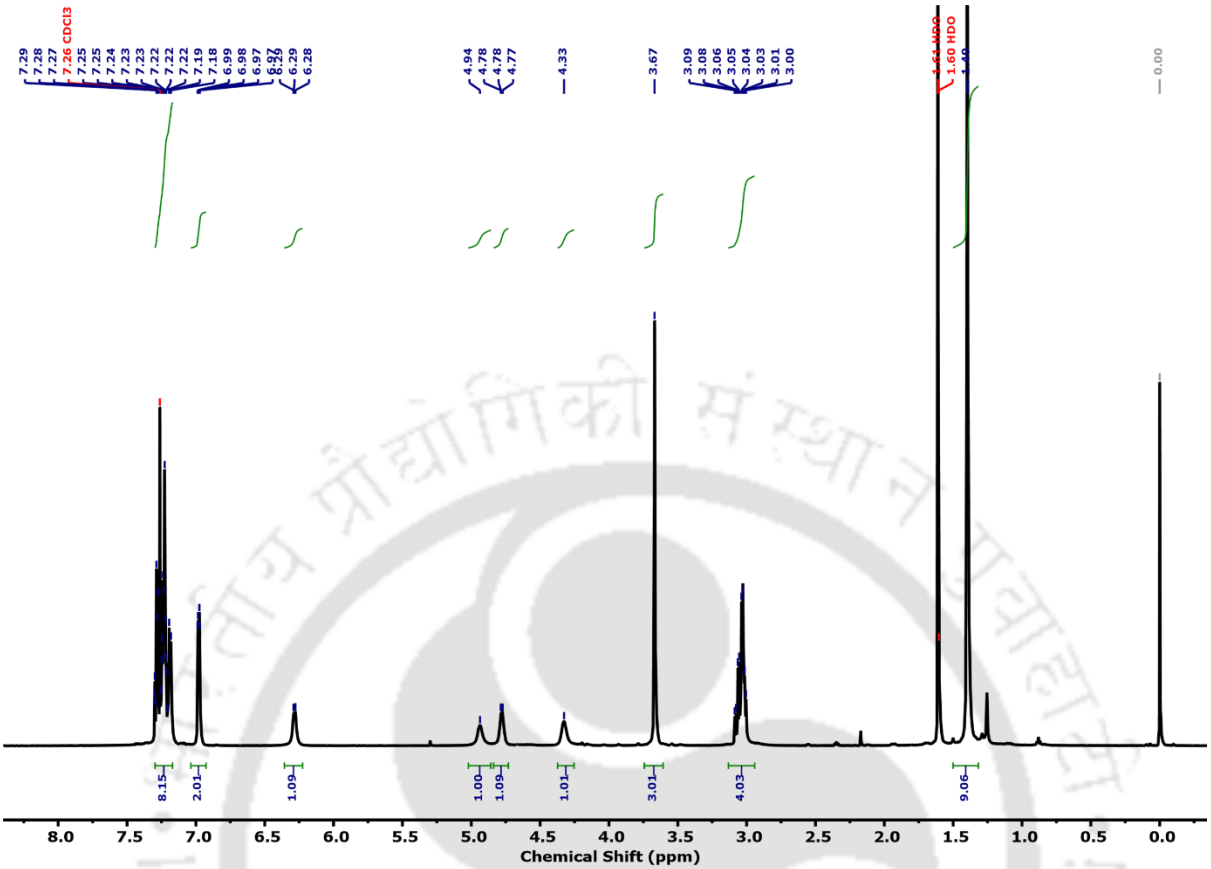

Fig. A3.9. 600 MHz ^{1}H NMR spectrum of Boc-FF-OMe recorded at 5 mM concentration in $CDCl_3$ at at room temperature. ^{1}H NMR (600 MHz, Chloroform-*d*) (Figure S9): ^{1}H NMR (600 MHz, Chloroform-*d*) δ 7.30 – 7.17 (m, 8H), 7.04 – 6.93 (m, 2H), 6.29 (b, 1H), 4.94 (b, 1H), 4.84 – 4.73 (m, 1H), 4.33 (b, 1H), 3.67 (s, 3H), 3.13 – 2.94 (m, 4H), 1.40 (s, 9H).

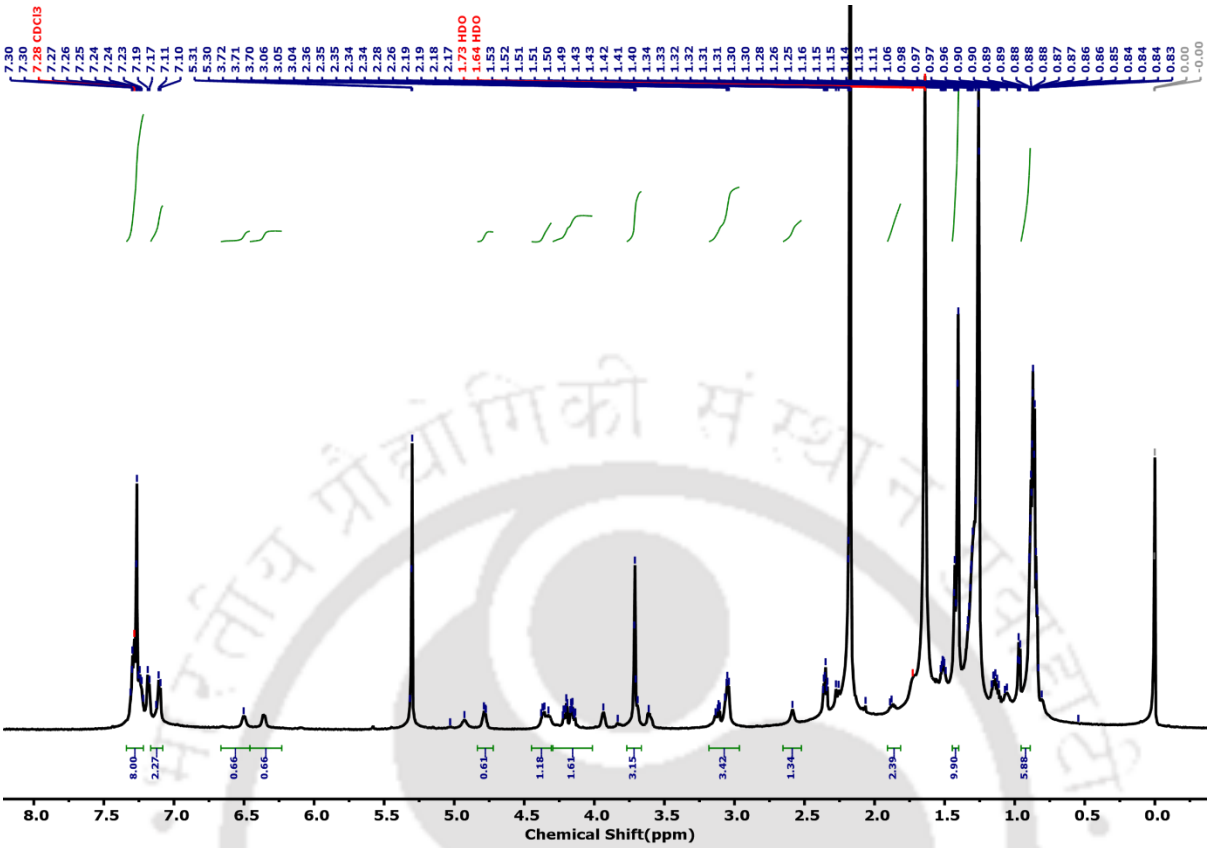

Fig. A3.10. 600 MHz ^{1}H NMR spectrum of Boc-FLF-OMe recorded at 5 mM concentration in $CDCl_3$ at at room temperature. ^{1}H NMR (600 MHz, Chloroform-*d*) (Figure S10): δ 7.34 – 7.22 (m, 8H), 7.11 (t, J = 9.3 Hz, 2H), 6.50 (s, 1H), 6.36 (s, 1H), 4.84 – 4.72 (m, 1H), 4.45 – 4.31 (m, 1H), 4.30 – 4.01 (m, 2H), 3.71 (d, J = 3.0 Hz, 3H), 3.18 – 2.96 (m, 3H), 2.59 (s, 1H), 1.87 (dd, J = 14.1, 6.8 Hz, 2H), 1.42 (dd, J = 15.0, 2.9 Hz, 10H), 0.95 – 0.89 (m, 6H).

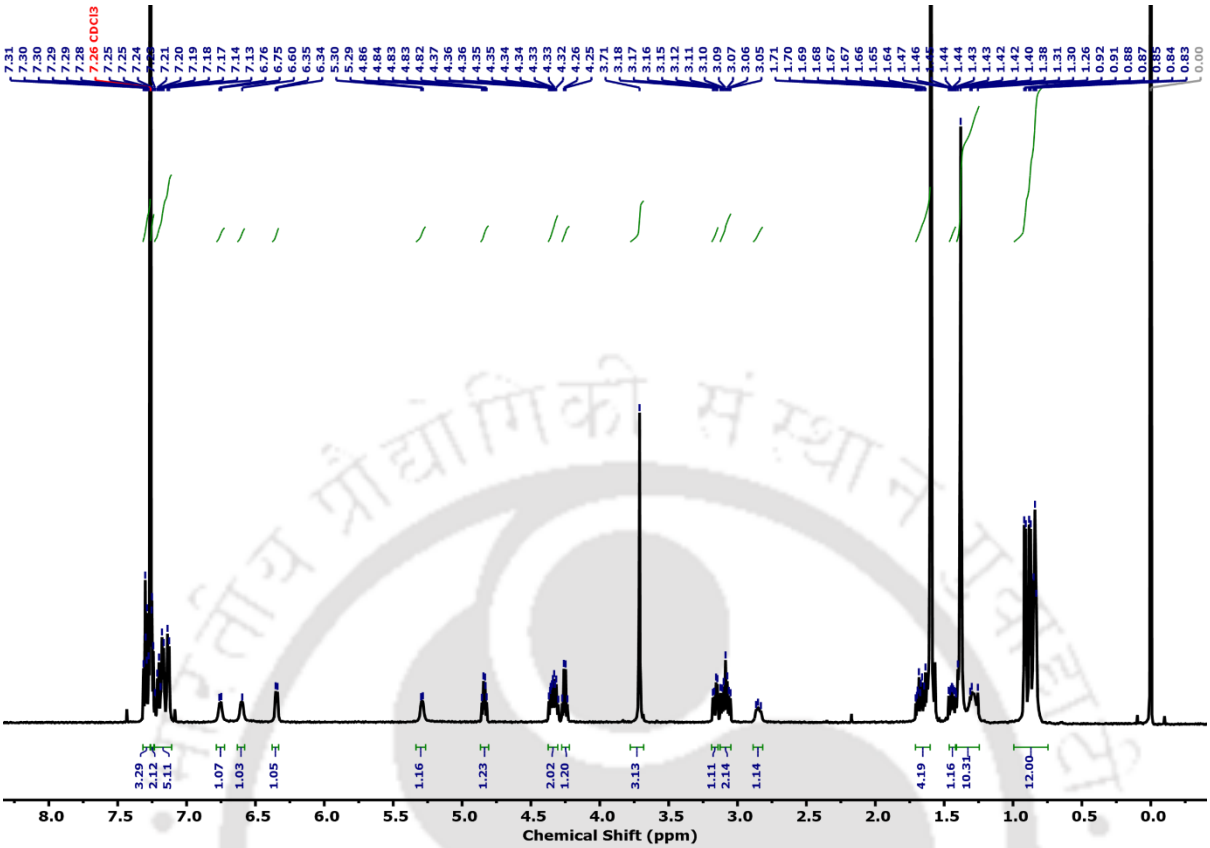

Fig. A3.11. 600 MHz ^{1}H NMR spectrum of Boc-FLLF-OMe recorded at 5 mM concentration in $CDCl_3$ at at room temperature. 1H NMR (600 MHz, Chloroform-d) (Figure S11): δ 7.33 – 7.27 (m, J = 7.1 Hz, 3H), 7.26 – 7.24 (m, 2H), 7.23 – 7.11 (m, 5H), 6.76 (b, 1H), 6.60 (b, 1H), 6.35 (d, J = 8.1 Hz, 1H), 5.29 (d, J = 6.9 Hz, 1H), 4.84 (q, J = 7.0 Hz, 1H), 4.37 – 4.31 (m, 2H), 4.25 (q, J = 7.5 Hz, 1H), 3.71 (s, 3H), 3.16 (dd, J = 13.9, 5.8 Hz, 1H), 3.09 (ddd, J = 21.4, 13.9, 7.1 Hz, 2H), 2.89 – 2.82 (m, 1H), 1.71 – 1.60 (m, 4H), 1.46 – 1.42 (m, 1H), 1.41 – 1.25 (m, 10H), 0.99 – 0.75 (m, 12H).

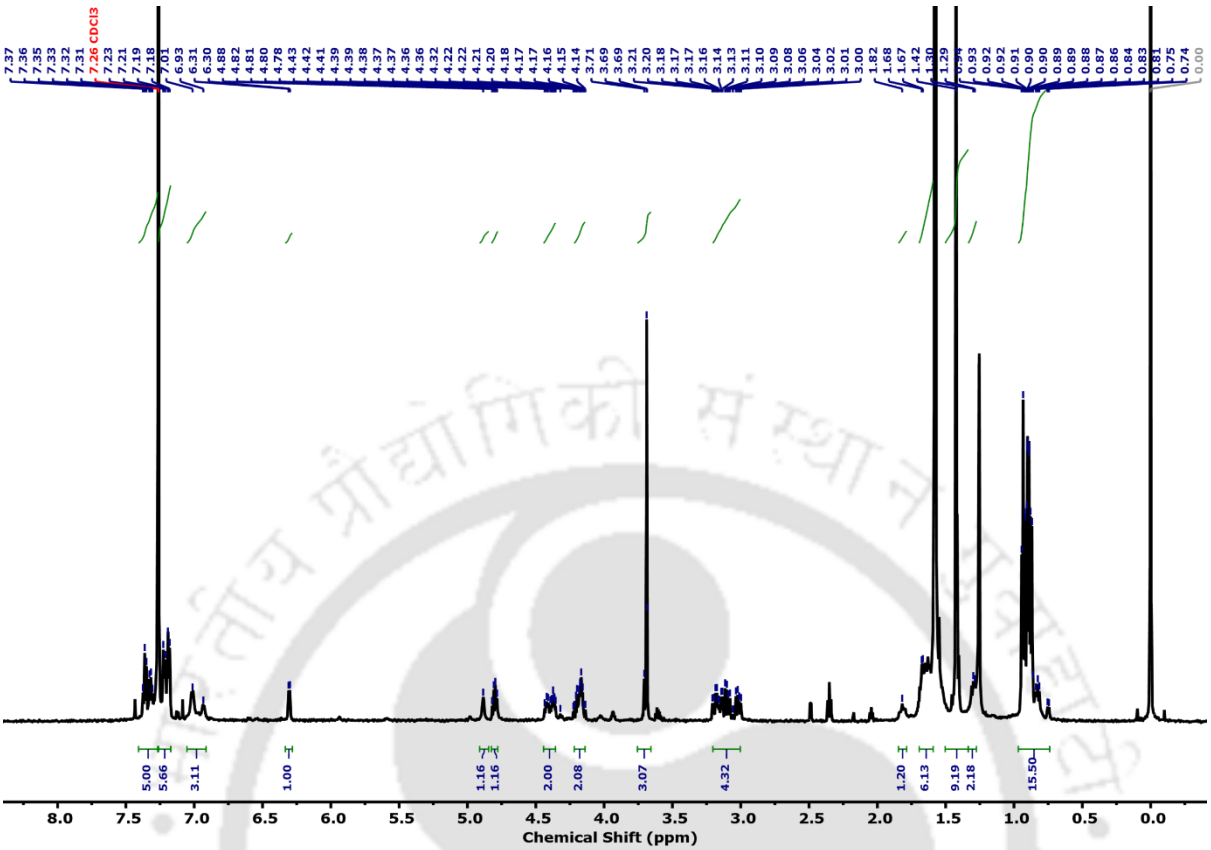

Fig. A3.12. 600 MHz ^{1}H NMR spectrum of Boc-FLLLF-OMe recorded at 5 mM concentration in $CDCl_3$ at room temperature. ^{1}H NMR (600 MHz, Chloroform-*d*) (Figure S12): δ 7.40 – 7.27 (m, 5H), 7.26 – 7.18 (m, 5H), 6.97 (b, 3H), 6.30 (d, *J* = 5.4 Hz, 1H), 4.88 (s, 1H), 4.80 (q, *J* = 7.4 Hz, 1H), 4.44 – 4.36 (m, 2H), 4.22 – 4.14 (m, 2H), 3.69 (s, 3H), 3.20 – 3.00 (m, 4H), 1.82 (s, 1H), 1.70 – 1.60 (m, *J* = 5.0 Hz, 6H), 1.42 (s, 9H), 1.33 – 1.28 (m, 2H), 0.97 – 0.74 (m, 15H).

CHAPTER 4: APPENDIX

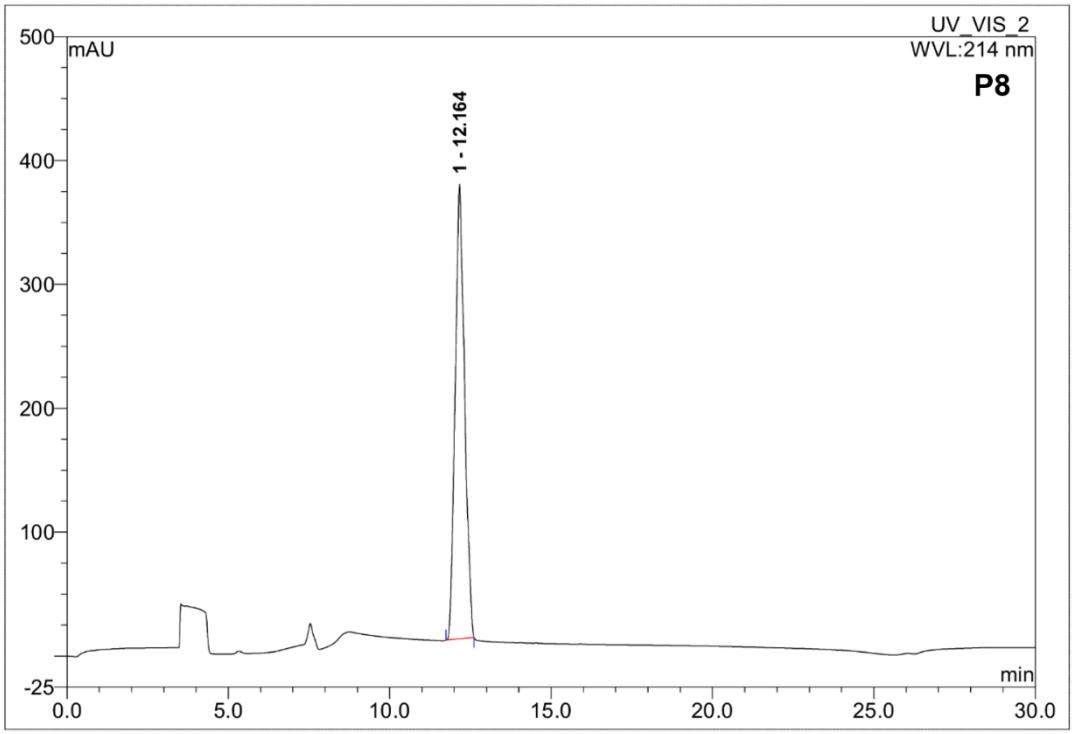

Fig. A4.1. Analytical HPLC trace for **P8.**

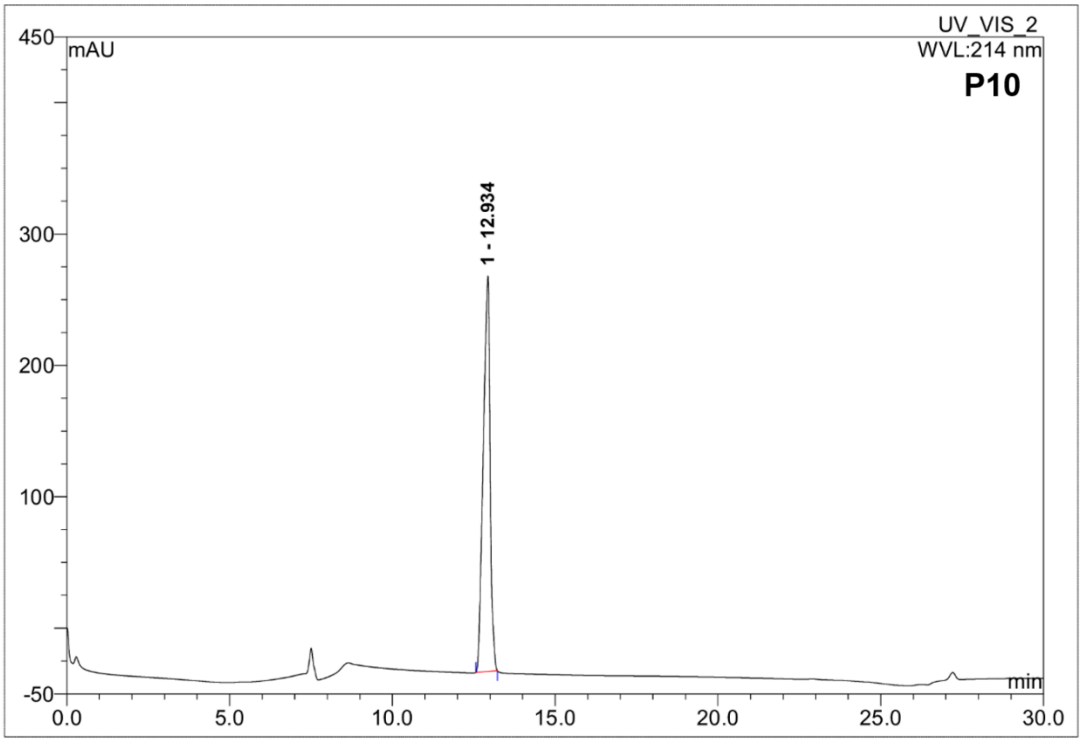

Fig. A4.2. Analytical HPLC trace for **P1**

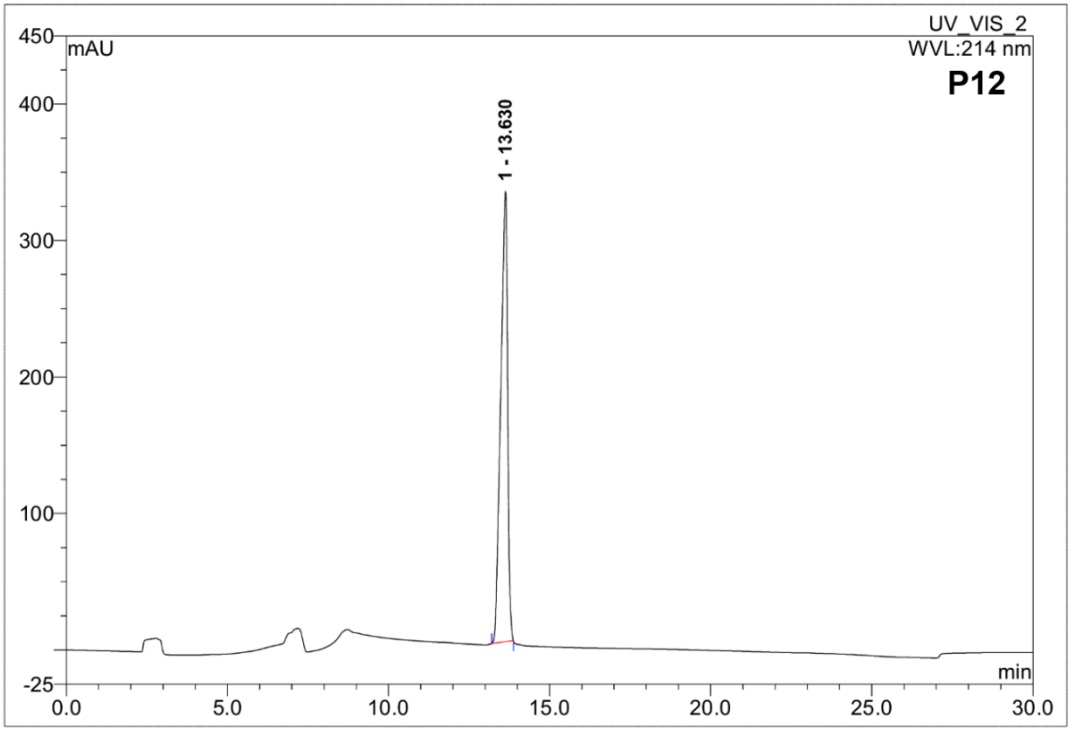

Fig. A4.3. Analytical HPLC trace for **P12.**

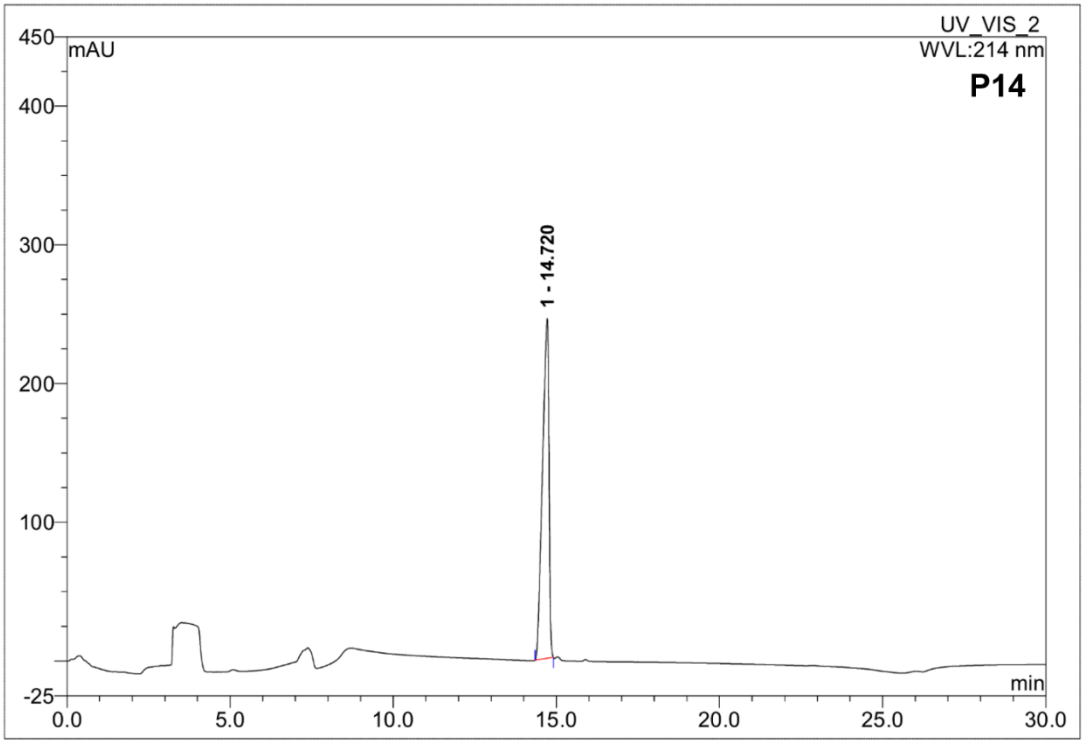

Fig. A4.4. Analytical HPLC trace for **P14**

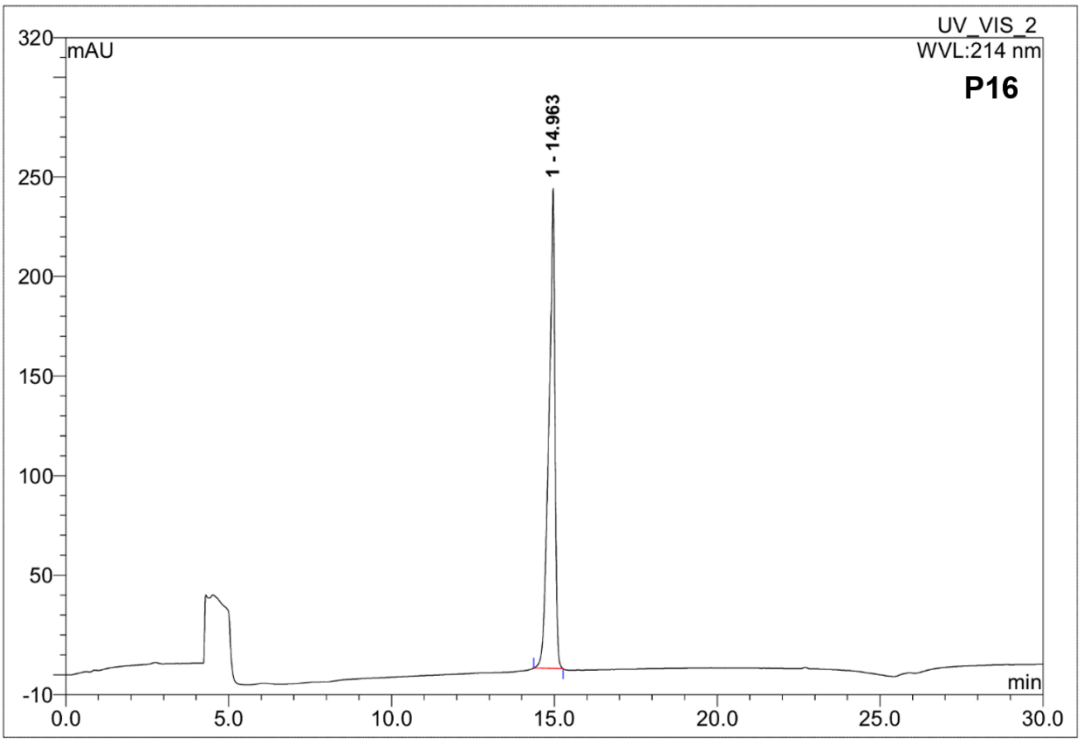

Fig. A4.5. Analytical HPLC trace for **P16.**

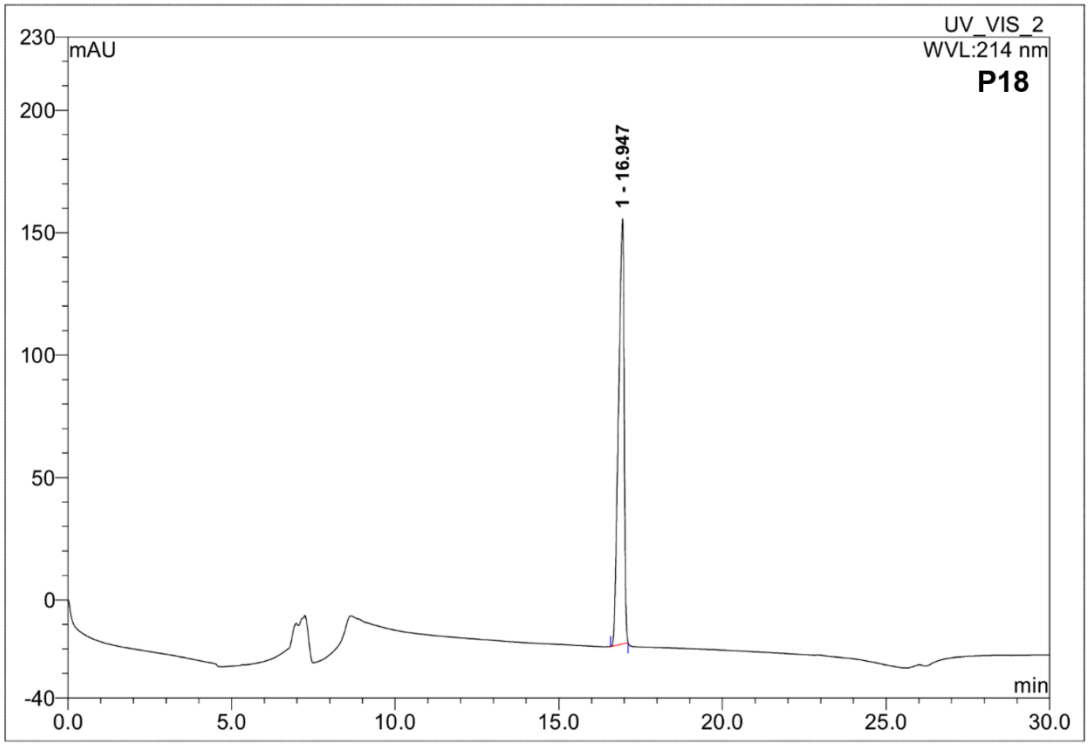

Fig. A4.6. Analytical HPLC trace for **P18**

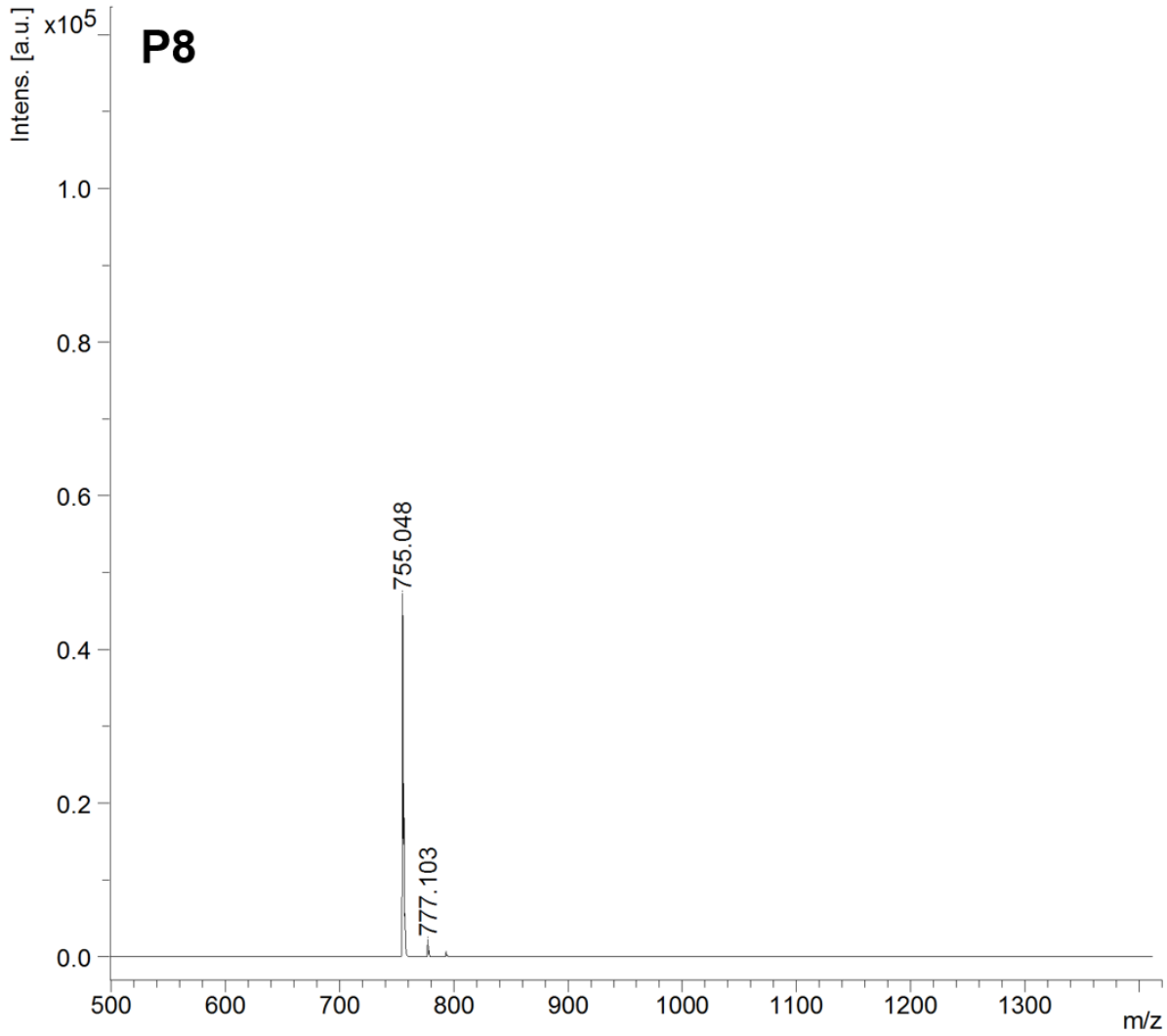

Fig. A4.7. MALDI-TOF mass spectra of **P8**. Calc. $(M+H)^+$ = 754.9793 Da; Obs. $(M+H)^+$ = 755.048 Da.

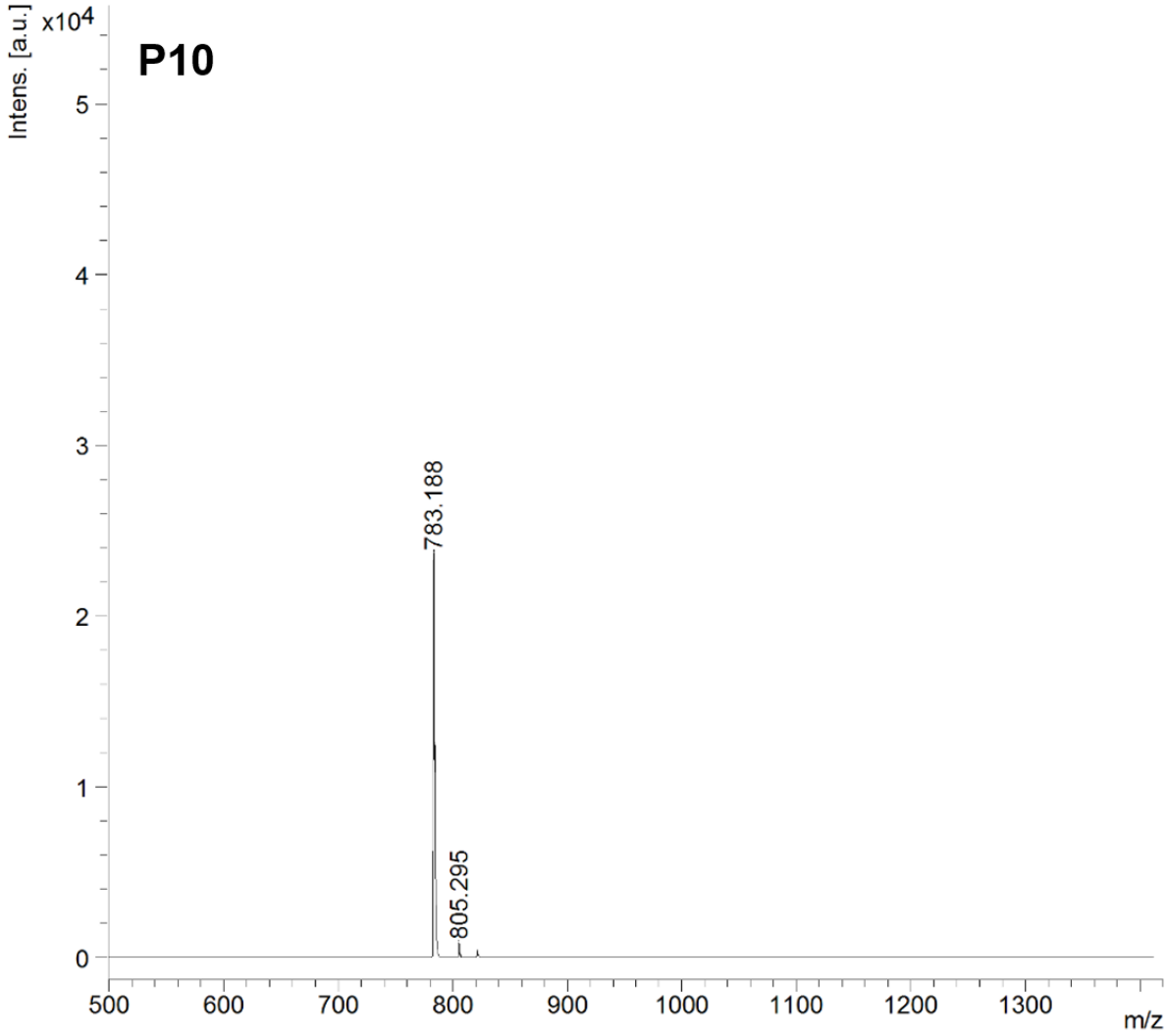

Fig. A4.8. MALDI-TOF mass spectra of **P10**. Calc. $(M+H)^+$ = 782.5650 Da; Obs. $(M+H)^+$ = 783.188 Da, $(M+Na)^+$ =805.295 Da.

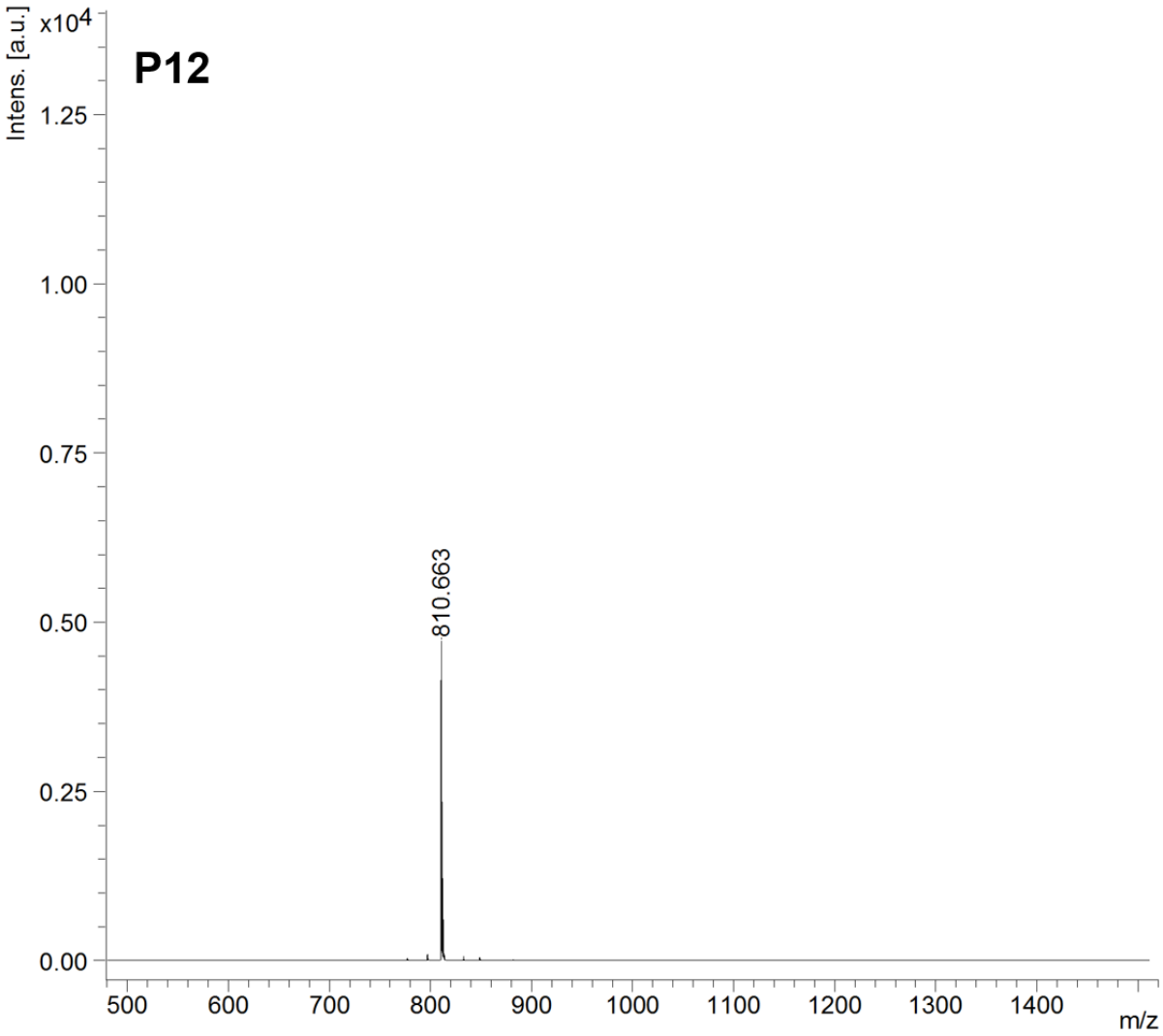

Fig. A4.9. MALDI-TOF mass spectra of **P12**. Calc. $(M+H)^+$= 810.5963 Da; Obs. $(M+H)^+$ =810.663 Da.

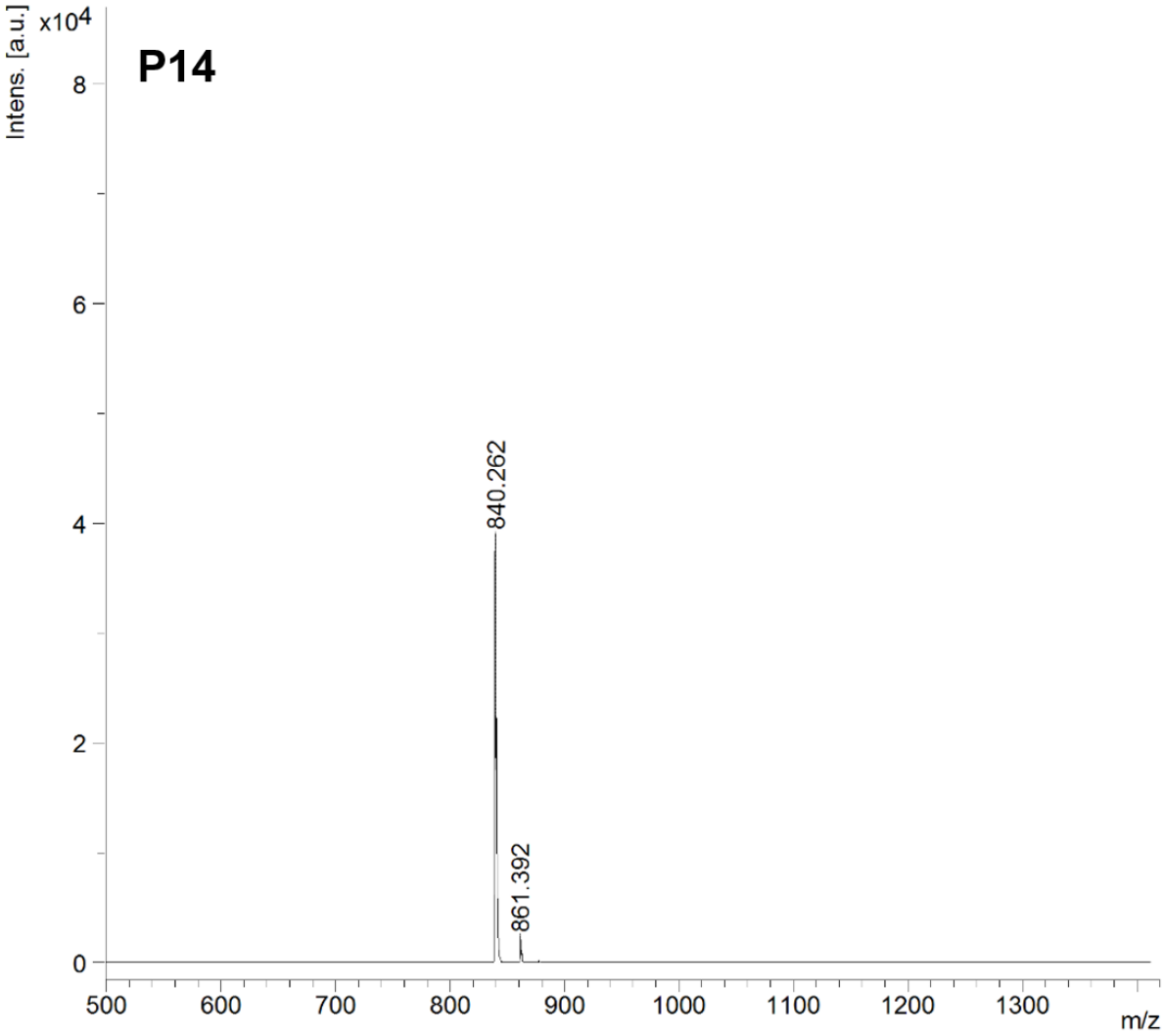

Fig. A4.10. MALDI-TOF mass spectra of **P14**. Calc. $(M+H)^+$ = 838.6276 Da; Obs. $(M+2H)^+$ =840.262 Da, $(M+Na)^+$ =861.392 Da.

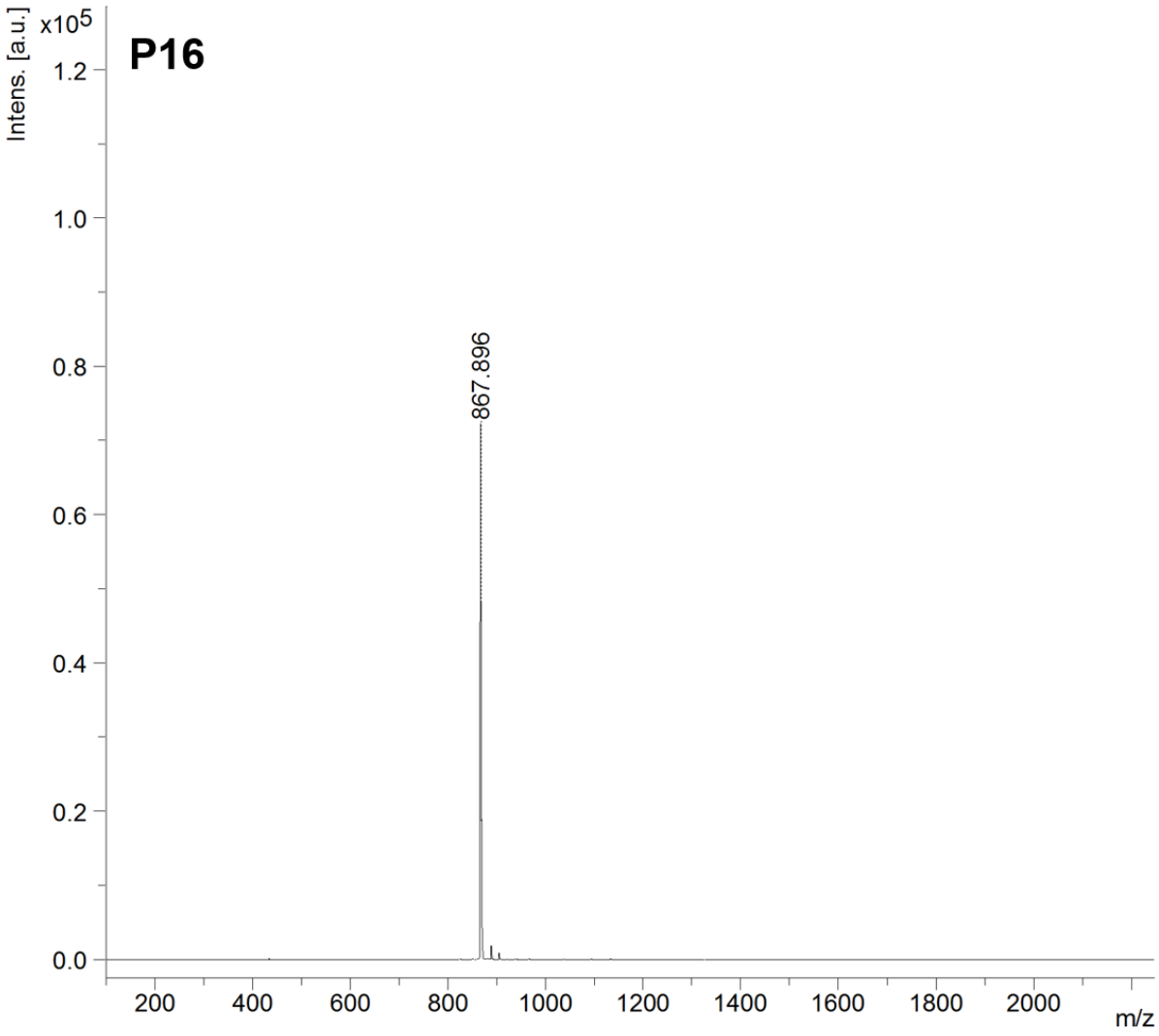

Fig. A4.11. MALDI-TOF mass spectra of **P16**. Calc. $(M+H)^+$ = 867.6589 Da; Obs. $(M+H)^+$ = 867.896 Da.

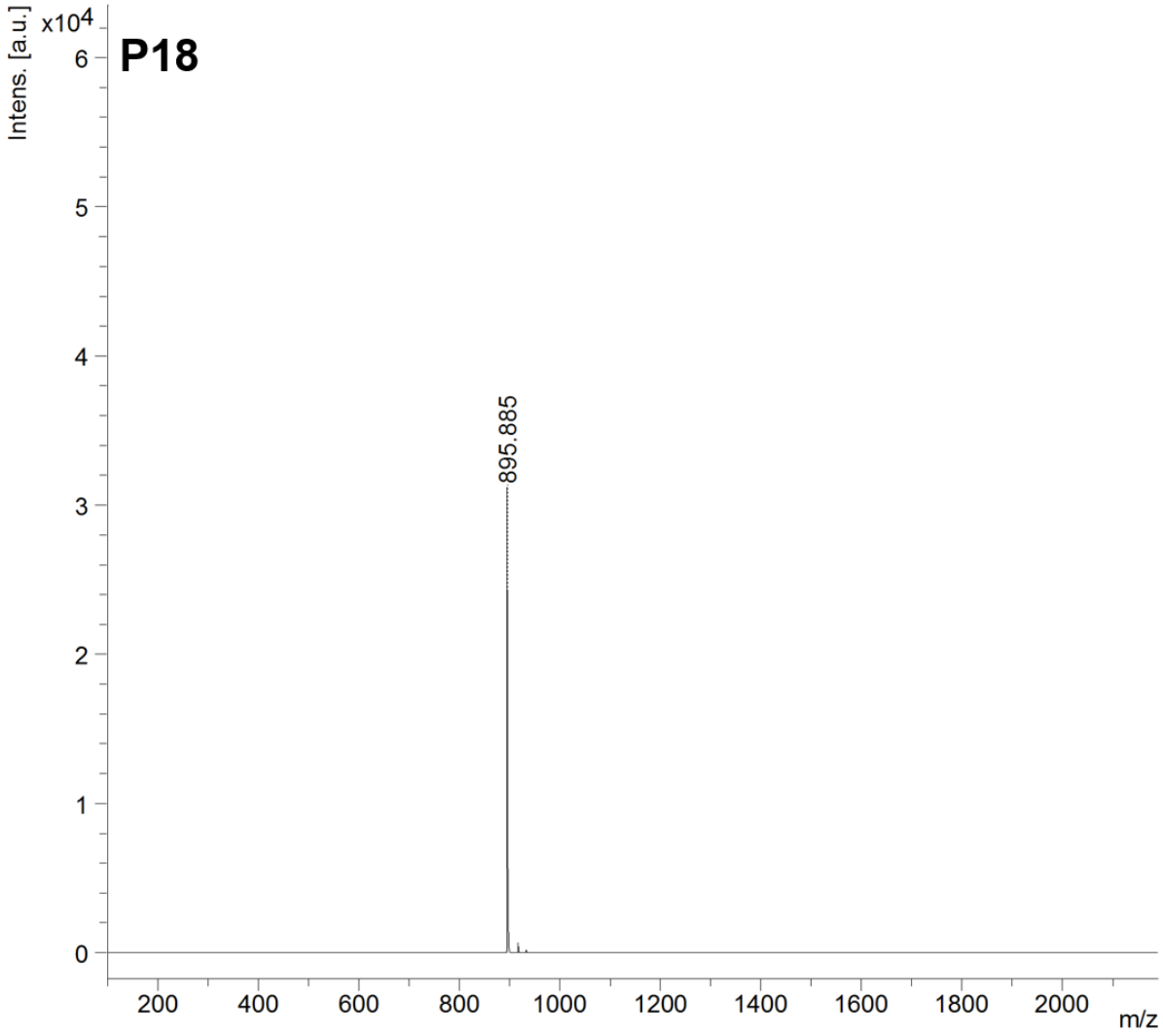

Fig. A4.12. MALDI-TOF mass spectra of **P18**. Calc. $(M+H)^+$ = 894.6902 Da; Obs. $(M+2H)^+$ = 895.885 Da.

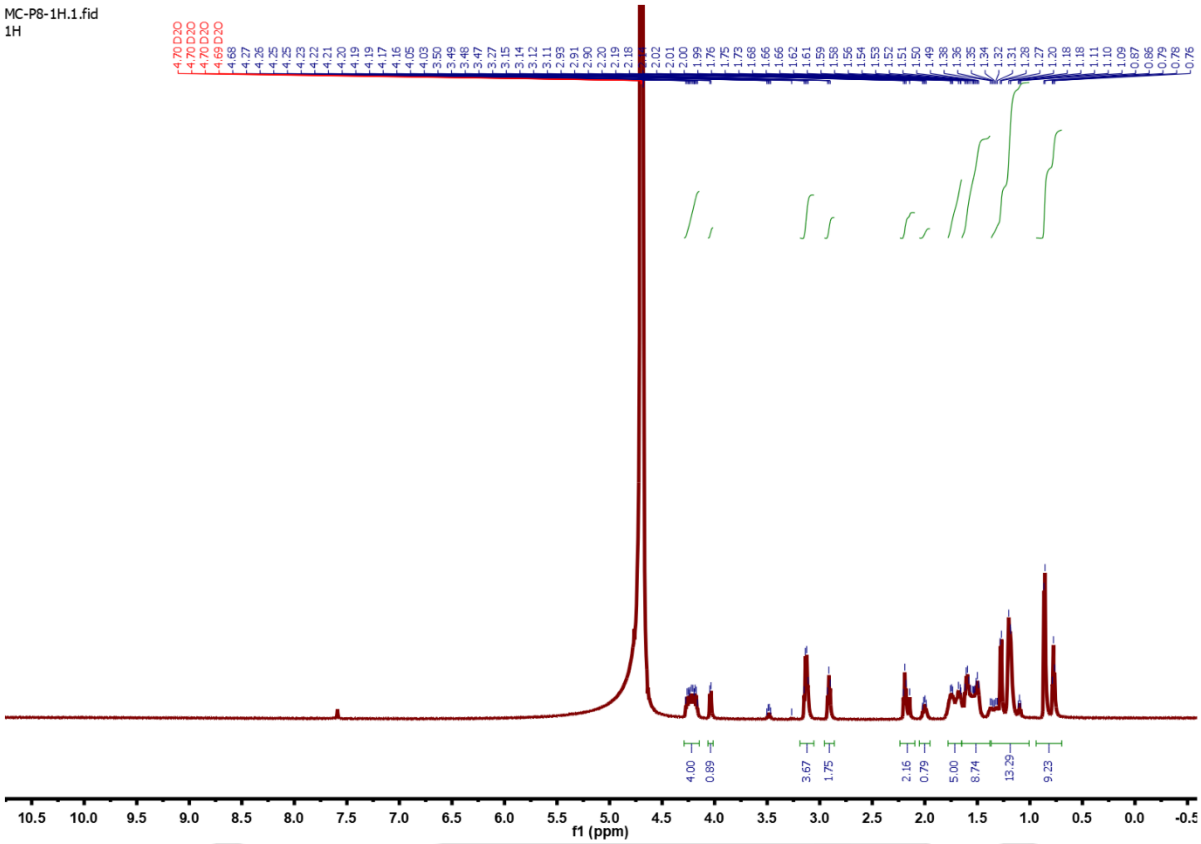

Fig. A4.13. 600 MHz ^{1}H NMR of **P8** recorded in D_2O at room temperature. ^{1}H NMR (600 MHz, D_2O). 0.79-0.90 (9Hs: 3Hs from long-chain -CH_3 and 6Hs from two -CH_3 of Val), 1.2-1.4 (13 Hs: 10Hs from long-chain, 3Hs from -CH_3 of Ala), 1.6-1.8 (14 Hs: 8Hs from Arg, 4Hs from Lys, 2H from long-chain), 2.05-2.2 (3Hs: 1Hs from Val, 2Hs from K), 2.9-3.1 (6Hs: 4Hs from Arg, 2Hs from Lys), 4.06-4.2 (5Hs, 5 αH).

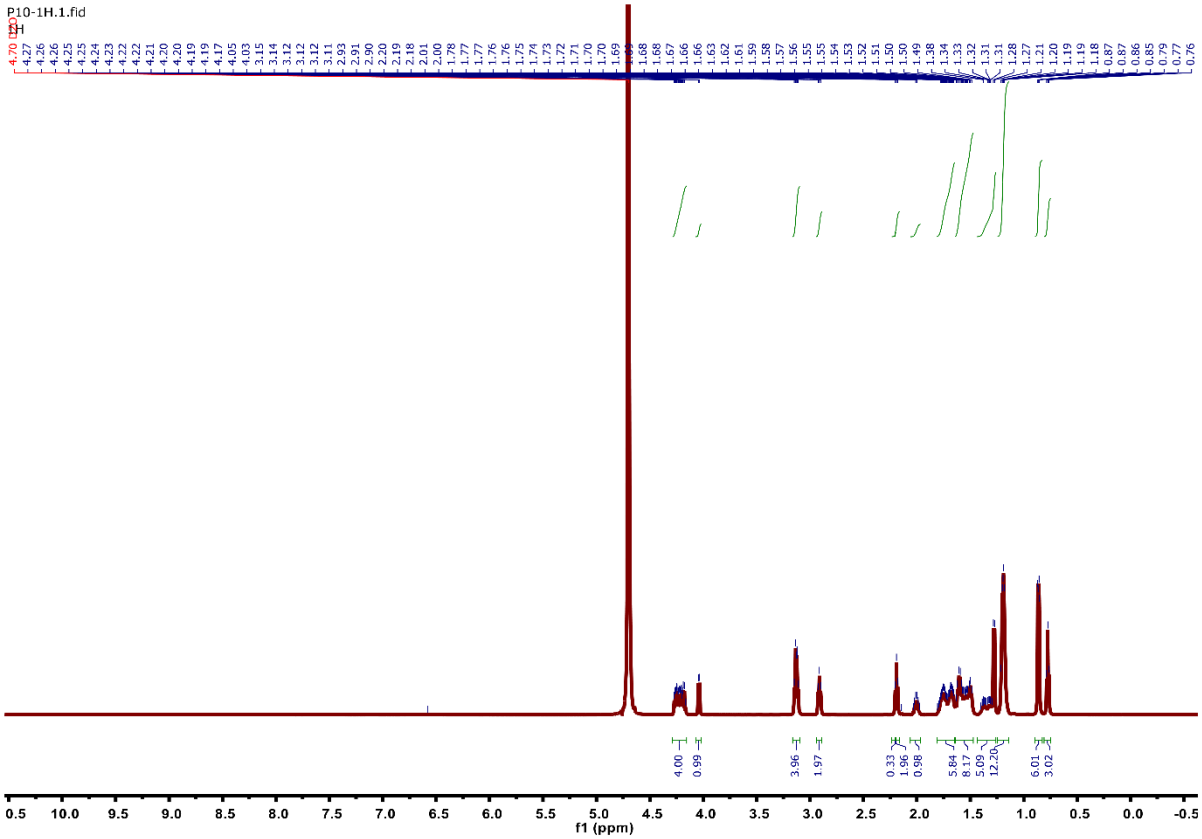

Fig. A4.14. 600 MHz ^{1}H NMR of **P10** recorded in D_2O at room temperature. ^{1}H NMR (600 MHz, D_2O). 0.8-0.89 (9Hs: 3Hs from long-chain -CH_3 and 6Hs from two -CH_3 of Val), 1.2-1.4 (17 Hs: 14Hs from long-chain, 3Hs from -CH_3 of Ala), 1.6-1.8 (14 Hs: 8Hs from Arg, 4Hs from Lys, 2H from long-chain), 2.06-2.2 (3Hs: 1Hs from Val, 2Hs from K), 2.9-3.1 (6Hs: 4Hs from Arg, 2Hs from Lys), 4.07-4.2 (5Hs, 5 αH).

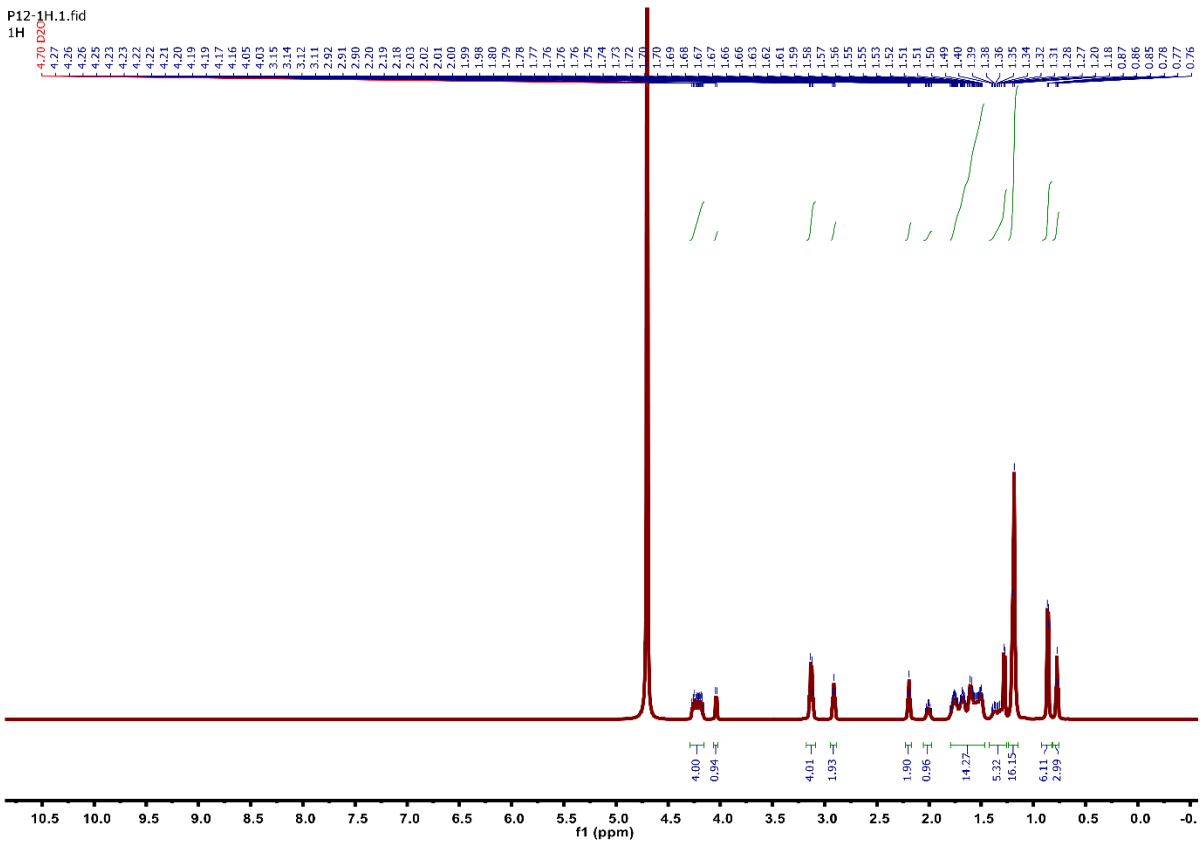

Fig. A4.15. 600 MHz ^{1}H NMR of **P12** recorded in D_2O at room temperature. ^{1}H NMR (600 MHz, D_2O). 0.8-0.92 (9Hs: 3Hs from long-chain -CH_3 and 6Hs from two -CH_3 of Val), 1.2-1.4 (21 Hs: 18Hs from long-chain, 3Hs from -CH_3 of Ala), 1.7 (14 Hs: 8Hs from Arg, 4Hs from Lys, 2H from long-chain), 2.05-2.2 (3Hs: 1Hs from Val, 2Hs from K), 2.9-3.1 (6Hs: 4Hs from Arg, 2Hs from Lys), 4.06-4.2 (5Hs, 5 αH).

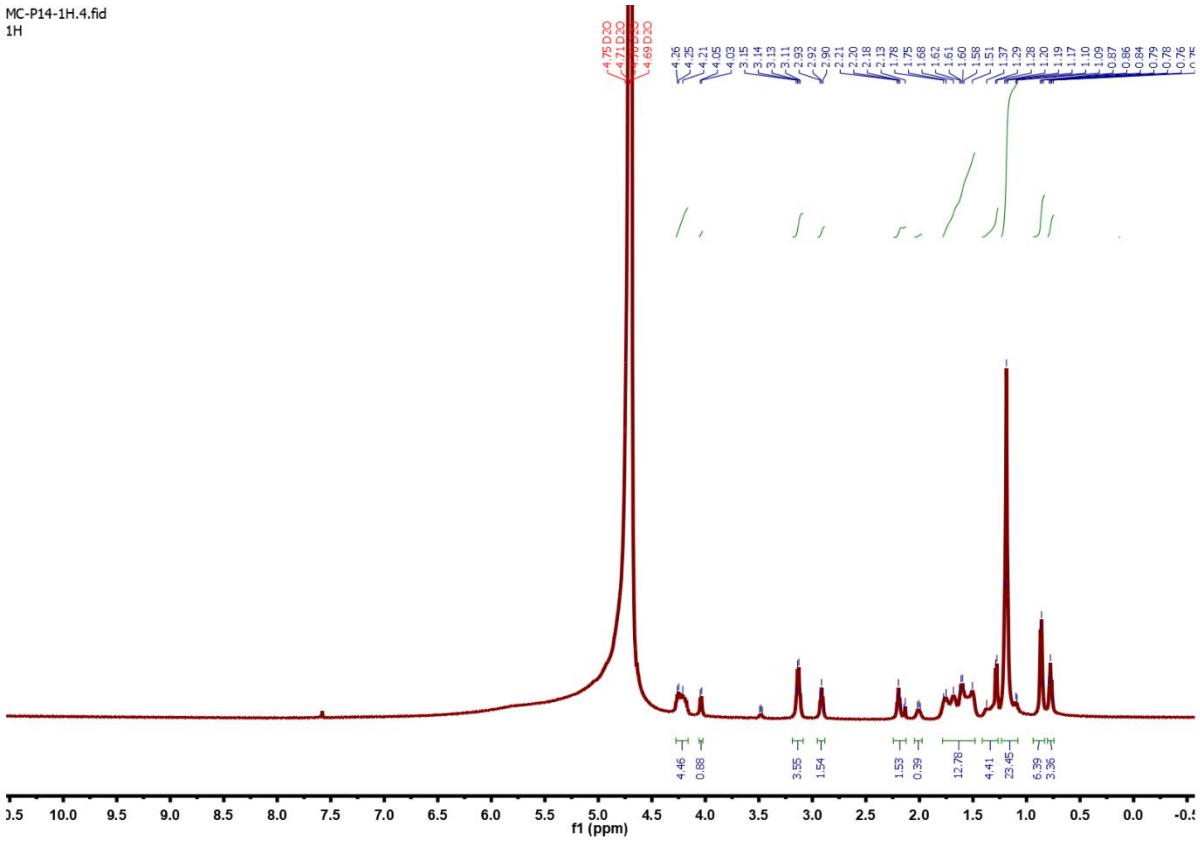

Fig. A4.16. 600 MHz ^{1}H NMR of **P14** recorded in D_2O at room temperature. ^{1}H NMR (600 MHz, D_2O). 0.83-0.93 (9Hs: 3Hs from long-chain -CH_3 and 6Hs from two -CH_3 of Val), 1.2-1.4 (27 Hs: 24Hs from long-chain, 3Hs from -CH_3 of Ala), 1.7 (13 Hs: 8Hs from Arg, 4Hs from Lys, 1H from Val,), 2.05-2.2 (2Hs: 2Hs from K), 2.9-3.1 (6Hs: 4Hs from Arg, 2Hs from Lys), 4.1-4.3 (5Hs, 5 αH).

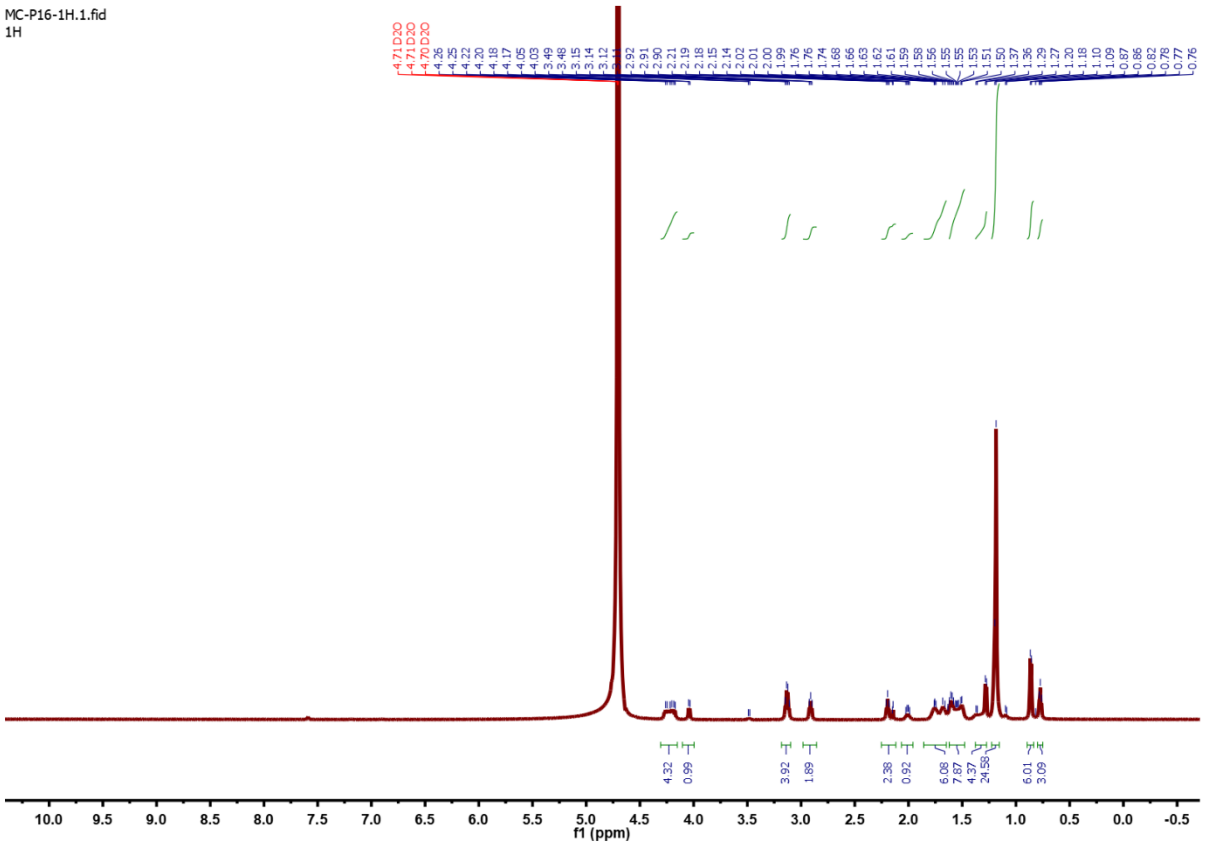

Fig. A4.17. 600 MHz ^{1}H NMR of **P16** in D_2O at room temperature. ^{1}H NMR (600 MHz, D_2O). 0.79-0.89 (9Hs: 3Hs from long-chain -CH_3 and 6Hs from two -CH_3 of Val), 1.22-1.3 (29 Hs: 26Hs from long-chain, 3Hs from -CH_3 of Ala), 1.6-1.8 (14 Hs: 8Hs from Arg, 4Hs from Lys, 2H from long-chain), 2.06-2.25 (3Hs: 1Hs from Val, 2Hs from K), 2.9-3.18 (6Hs: 4Hs from Arg, 2Hs from Lys), 4.1-4.3 (5Hs, 5 αH).

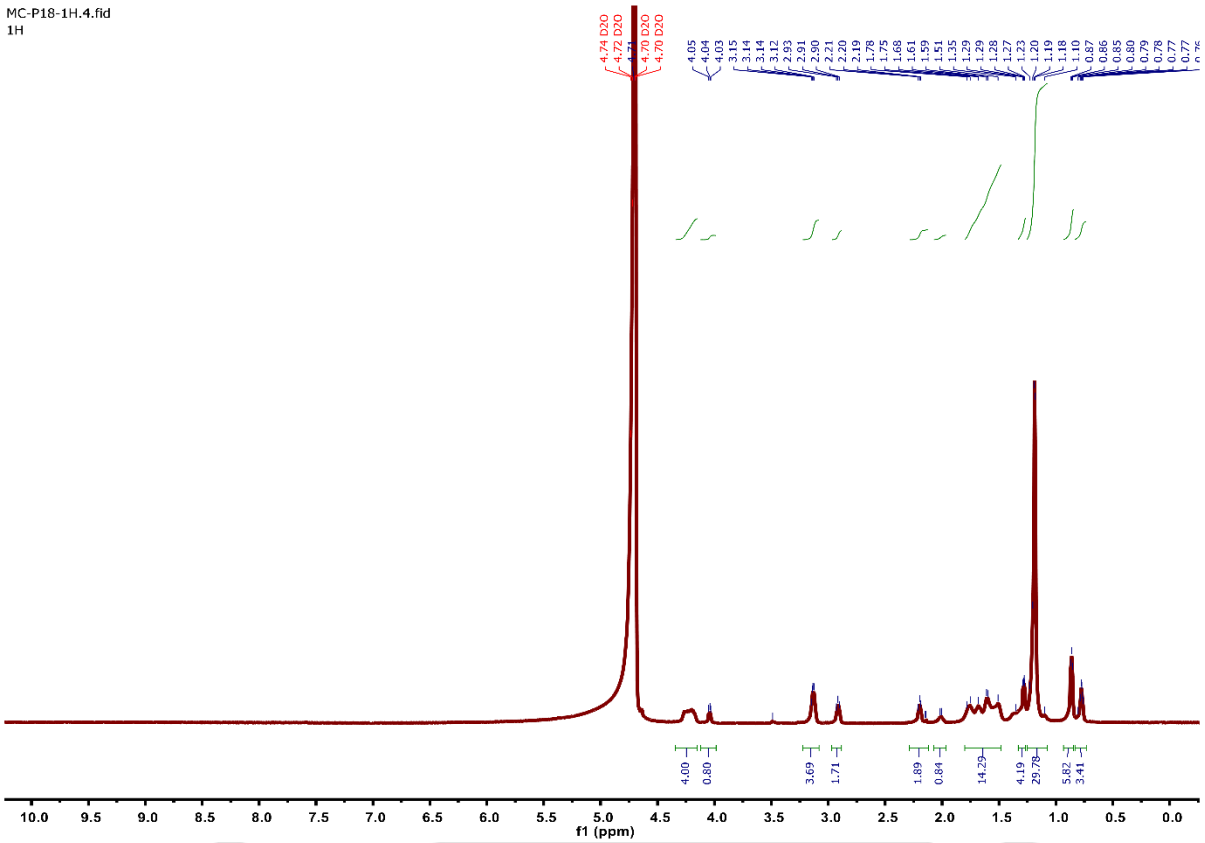

Fig. A4.18. 600 MHz ^{1}H NMR of **P18** recorded in D_2O at room temperature. ^{1}H NMR (600 MHz, D_2O). 0.83-0.93 (9Hs: 3Hs from long-chain -CH_3 and 6Hs from two -CH_3 of Val), 1.25-1.3 (33 Hs: 30Hs from long-chain, 3Hs from -CH_3 of Ala), 1.8 (14 Hs: 8Hs from Arg, 4Hs from Lys, 2H from long-chain), 2.07-2.2 (3Hs: 1Hs from Val, 2Hs from K), 2.9-3.2 (6Hs: 4Hs from Arg, 2Hs from Lys), 4.1-4.3 (5Hs, 5 αH).

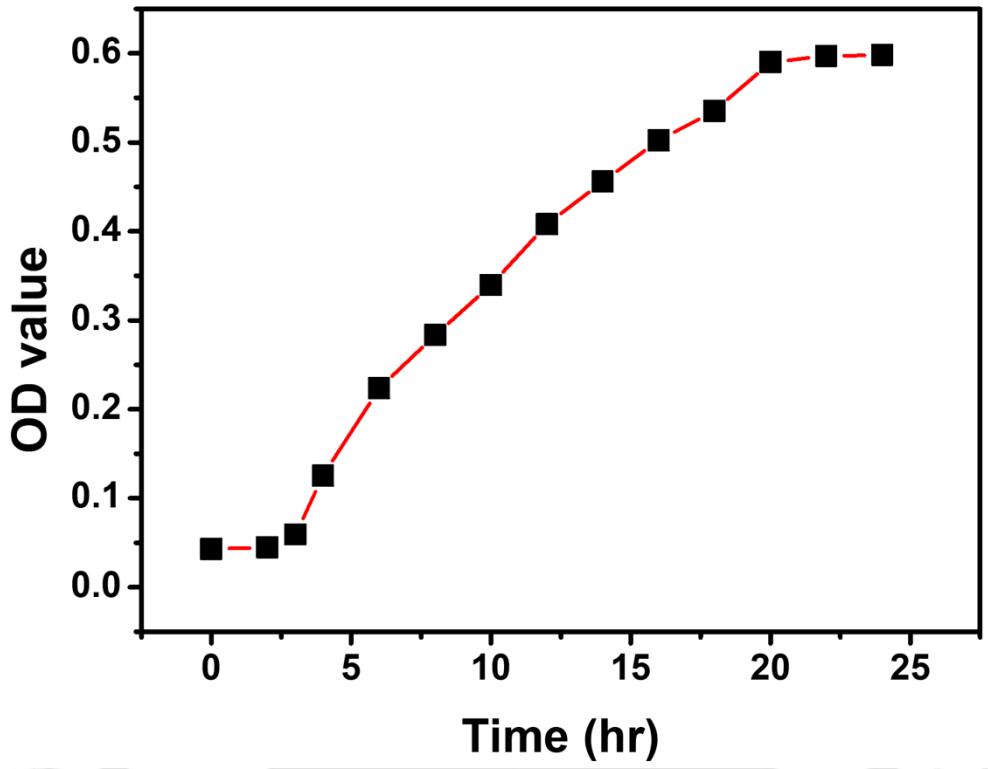

Fig. A.4.19. Growth curve of MRSA bacterial strain

CHAPTER 5: APPENDIX

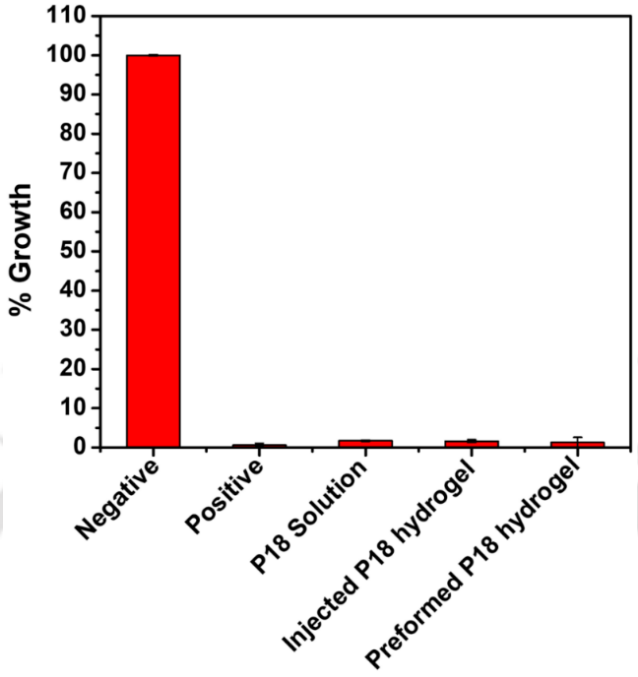

Fig. A5.1. Antimicrobial potency of P18 hydrogel. Microbial cell viability (in % growth) of Methicillin-resistant *S. aureus* (MRSA) with 10^5 CFU/ml cell counts.

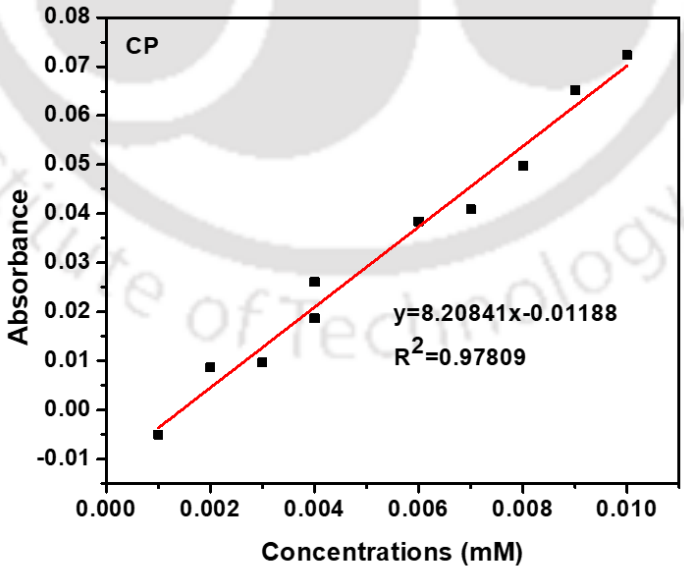

Fig. A5.2. Calibration curve of ciprofloxacin

List of Publications

1. ***Chetia, M.**; Sarkar, T.; Yadav, M.; Dey, C.; Sundaravadivelu, P. K.; Thummer, R. P.; Chatterjee, S. Tuning of hydrophobic-hydrophilic balance for the development of a salt-tolerant and protease-resistant lipopeptide AMP. *New J. Chem.* **2024**, *48*, 2764-2777.

2. Sarkar, T.; **Chetia, M.**; Chatterjee, S. Antimicrobial peptides and proteins: from nature's reservoir to the laboratory and beyond. *Front. in Chem.* **2021**, *9*, 691532.

3. Roy, K.; **Chetia, M.**; Sarkar, A. K.; Chatterjee, S. Co-assembly of charge complementary peptides and their applications as organic dye/heavy metal ion (Pb^{2+}, Hg^{2+}) absorbents and arsenic (III/V) detectors. *RSC Adv.* **2020**, *10*, 42062-42075.

4. Roy, K; Pandit, G.; **Chetia, M.**; Sarkar, A. K.; Chowdhuri, S.; Bidkar, A. P.; Chatterjee, S. Peptide hydrogels as platforms for sustained release of antimicrobial and antitumor drugs and proteins. *ACS Appl. Bio Mater*. **2020**, *3*, 6251–6262.

5. ***Chetia, M.**; Debnath, S.; Chowdhury, S.; Chatterjee, S. Self-assembly and multifunctionality of peptide organogels: oil spill recovery, dye absorption and synthesis of conducting biomaterials. *RSC Adv*. **2020**, *10*, 5220-5233.

6. Roy, K.; Ghosh, S.; **Chetia, M.**; Satpati, P.; Chatterjee, S. Dicyclohexylurea derivatives of amino acids as dye absorbent organogels and anion sensors. *Org. Biomol. Chem*. **2019**, *17*, 3026-3039.

7. Das, S. K.; Deka, P.; **Chetia, M.**; Deka, R. C.; Bharali, P.; Bora, U. Spherical CuO Nanoparticles as catalyst for Chan–Lam cross-coupling reaction under base free condition. **2018**, *148*, 547–554.

*** Marked Publications are included in this Doctoral dissertation**